INVESTIGATION OF A MULTI-AXIS PRECISION MACHINE PLATFORM FOR ULTRAPRECISION MANUFACTURING: AN INTEGRATED APPROACH COMBINING MULTISCALE MODELLING AND DIGITAL TWIN AND ITS IMPLEMENTATION PERSPECTIVES

A thesis submitted for the degree of Doctor of Philosophy

By

Ning Gou

College of Engineering, Design and Physical Sciences

Brunel University London

October 2023

Abstract

This thesis initially presents a scientific approach for investigating aerostatic bearings design, the simulation approach combined with aerostatic bearing slideway design and development is initially presented for modelling and analysis of the static and dynamic performance of single-axis linear motion system. The modelling is developed and implemented by using COMSOL™ MULTIPHYSICS computational environment integrated with MATLAB programming as needed. The work described is fundamental and essential as a basic part of the efforts for developing the simulation-based virtual machine platform and its digital twin.

The improved control algorithms are further investigated and developed in this doctoral research, which aims to enhance the scientific understanding of the multi-axis integrated motion control process for precision machine platform design and its industrial UPM application.

In this doctoral research, micro cutting mechanics analysis and tool path generation are integrated to support the establishment of the digital twin in a multiscale multiphysics manner. The method is used to evaluate and predict the key parameters of the UPM machine platform in real time. Furthermore, experimental trials for freeform surface machining based on single point diamond turning (SPDT) system are carried out to evaluate and validate the competence and accuracy of motion control algorithms developed working with DT.

Industrial case studies on using CFD simulations and integrated design approach for aerostatic bearing slideway and rotary table design and development are further undertaken to generate the aerostatic bearing products design protocols, which also evaluate and validate the aerostatic bearings design modelling and analysis method and the precision of design simulation and analysis tools developed. Shop floor metrology measurements on the precision machine platform are conducted to validate the developed design and simulations against industrial requirements. There are good agreements between the results of simulations and experimental trials, which are further supported by industrial manufacturing data. The effects of air bearing design variables and control system characteristics are investigated by analysing the results from both the industrial trials and simulations.

Acknowledgement

Table of Contents

List of Figures

List of Tables

Nomenclature

c = viscous friction coefficient

C = the constant for damping (kg/s)

c_1 = damping ratio

D_P = pitch circle diameter (mm)

D_0 = orifice diameter (mm)

f = Force(N)

F(t)= the force vector variation at step time (N/s)

F_f = disturbance forces in the direction of motion (N)

F_m = magnetic thrust force (N)

h = fluid film thickness (mm)

i_q = electric current (A)

K = the stiffness constant (N/m)

K' = motion part elasticity coefficient

K_e = motor potential coefficient

K_f = magnetic thrust coefficient

L = inductance (H)

m = motion part mass (kg)

M = inertia matrix

Mü = mass acceleration at step time (m/s^2)

N= number of bodies in system

P_A = ambient atmospheric pressure (Pa)

P_S = gauge pressure (Pa)

p = fluid film pressure (Pa)

ρ = air density (kg/m^3)

Q = generalised vectors of forces

R = armature resistance (Ω)

t= time (s)

u(t)= the vector for displacement at step time (m)

ů (t)= represents the vector for velocity at step time (m/s)

ü (t)= represents the vector for acceleration at step time (m/s^2)

u_q= input voltage (V)

v= velocity (m/s)

u, v, w= velocity of air in x, y, z directions (m/s)

μ= dynamic viscosity (Pa/s)

ω_n= free oscillation frequency (Hz)

x, y= bearing width and length (mm)

θ= angle between the tangent line through the point and the axis (°)

$\boldsymbol{\Phi_q}$= the Jacobian matrix constraint equations

λ= the Lagrange multiplier vector

Abbreviations

ADAMS	Automated Dynamics Analysis of Mechanical Systems
AE	Acoustic Emission
CAD	Computer Aided Design
CAM	Computer Aided Manufacturing
CCC	Cross-Coupling-Control
CFD	Computational Fluid Dynamics
CMM	Coordinate Measuring Machine
CNC	Computer Numerical Control
CPS	Cyber-Physical System
DADS	Dynamic Analysis and Design System
DT	Digital Twin
FEA	Finite Element Analysis
FEM	Finite Element Method
FSI	Fluid-Structure Interaction
FSO	Full Scale Output
FTS	Fast Tool Servo
GUI	Graphical User Interface
HUD	Head Up Display
ICT	Information and Communications Technology
IPC	Industrial Personal Computer
LiDAR	Light Detection & Ranging
NS	Navier-Stokes Equation
NURBS	Non-Uniform Rational B-Spline

PAL   Progressive Addition Lenses

PCD   Pitch Circle Diameter

PID   Proportional-Integral-Derivative

R&D   Research and Development

SCD   single crystal diamond

SEM   Scanning Electron Microscope

SPDT   Single Point Diamond Turning

STS   Slow Tool Servo

UPM   Ultraprecision Manufacturing

Chapter 1   Introduction

1.1   Background and significance of the research

Ultraprecision manufacturing (UPM) technology is defined as the ultimate capability of a manufacturing process in which the materials removal or addition at the nanometric and/or even lower scale (e.g., atomic scale) is achieved, the difference between machining accuracies during specific time periods is shown in Figure 1.1. Within this process, conventional cutting tools do not have the cutting-edge sharpness nor the hardness to cope with the high specific cutting energy and thus tool wear, while UPM uses single crystal diamond (SCD) tools for ultraprecision cutting, grinding, or polishing[1].
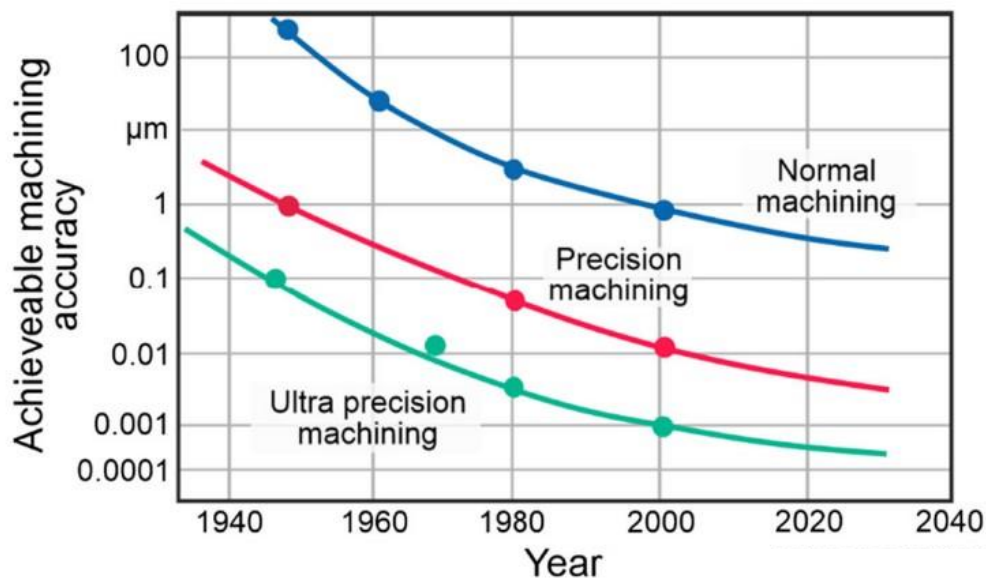
Figure 1.1 Evolution of the achievable machining accuracy for machining processes[2]

In the late 1950s, under the demands from aerospace and defense industries, the United States pioneered the development of UPM by using the single point diamond turning (SPDT) technology in the scenario of the manufacture for gyroscope components and high precision spherical and aspheric parts. To date, UPM technology has evolved as a high precision machining related technology developed

to meet the manufacturing requirements of high-end cutting-edge and/or high throughput products including nuclear energy producers, ultra-large-scale integrated circuits, freeform optics such as vari-focal lenses, information and communications technology (ICT) hardware, head up display (HUD) and light detection & ranging (LiDAR) devices for automotive industry, space optics for SpaceX. In specific, UPM techniques can often be categorized as ultraprecision cutting (diamond turning, diamond milling), ultraprecision grinding, ultraprecision polishing, and ultraprecision non-traditional machining (e.g., electron beam and ion beam cutting)[3]. Based on the integration of power electronics, direct drives, sensors, and control technologies, the UPM machines and machining systems aim to continually achieve the higher machining accuracy in an industrial competitive manner.

1.2 Design and development of ultraprecision machine platform

The fluid (gas, liquid) bearing and electromagnetic direct drive based machine platform is a new type of ultraprecision motion mechanism, which overcomes the shortcomings of traditional servo motor and rolling-screw driven positioning system, e.g., numerous transmission links, large response delay and obvious friction. Thus, it has large wide range of applications in lithography equipment, precision measurement and biomedical fields. Due to the complex and non-linear fluid dynamic effects, traditional modelling and analysis methods are not able to solve and simulate the problems regarding system static and dynamic performance, and positioning control.

As a zero pollution and non-friction load/lubricate material of fluid bearing product, air is widely applied as the ideal lubricate media in UPM machine components like slideway, support pad, spindle or rotary table. The methods of design and analysis for air bearing based UPM machine platform have been derived over several decades. For instance, using CFD and Finite Element Analysis (FEA) to assistance the mechanical structure and performance design. Using transfer function or state space modeling method to establish and/or simulate control system. As time progresses, existing design and analysis methods have matured in terms of computing and simulation capabilities. Scientifically, there are several mature solutions for physical and mathematical modelling method for different industrial engineering problem.

Regarding the design and development of ultraprecision machine platform, the factors and features from the machine itself, the component metalogical surface or tolerance, and the machine assembly clearance in multiple scales and physical fields will have effects not only on themselves, but also collectively on the performance of the entire machine. Therefore, as the demand of machine performance and motion precision are ever increasing, it is essentially important to develop a multiscale multiphysics modelling and analysis-based approach for design and development of high precision mechanics, particularly for overcoming the limitations in design and building of the machine systems for generating nanometric surfaces on an industrial scale. Furthermore, under the backdrop of the Fourth Industrial Revolution (Industry 4.0), the enhancement of precision machining equipment performance through intelligent means is a noteworthy subject. The convergence of the Industry 4.0 concept with UPM is a prevailing trend.

1.3 Aim and objectives of the research

This PhD project as a whole, aims to investigate an integrated scientific approach, by combining multiscale modelling and digital twin, developing multi-axis precision machine platform for UPM and its implementation perspectives, particularly in the context of industrial scale UPM and the industry 4.0.

To address the major challenges in UPM machine platform, it is essential to develop a highly effective and efficient engineering approach, thus this research will integrate the multiscale multiphysics modelling, design and analysis methods on mechanical frame structure, electrical direct drive system, control logic and advanced algorithm. It is specifically involved with the key enabling approach of digital twin technology in industrial manner.

The distinct objectives of the research are to:
- Critically review the state-of-the-art in design and development of precision machine platforms and clarify the underlying technological and scientific challenges, and identify the research and knowledge gaps.
- Investigate the multiscale modelling and analysis-based approach to design of aerostatic bearing supported slideways, against its stringent design specifications as required by the industrial partner.

- Explore and investigate the modelling and control algorithms for 2/3-axis air-bearing slideways and their simultaneous tuning simulations and implementation protocols.
- Investigate the fundamentals of the precision machine platform design, including the relevant design methodologies, modularity analysis, connectivity, reconfigurability and the associated implementation perspectives.
- Develop digital twin-based simulations on 2-axis air-bearing slideways and their extended application to the multi-axis precision machine platform.
- Undertake relevant industrial application case studies of the investigation and development above, and in-depth analysis of case study and experiment results.

The research above also aims to develop the industrial-feasible precision engineering design and analysis methods for aerostatic bearing products for engineering researchers and practitioners in either industrial and/or academic background.

1.4   Scope of the thesis

As illustrated in Figure 1.2, the thesis is presented with eight chapters in the precision engineering logic flow.
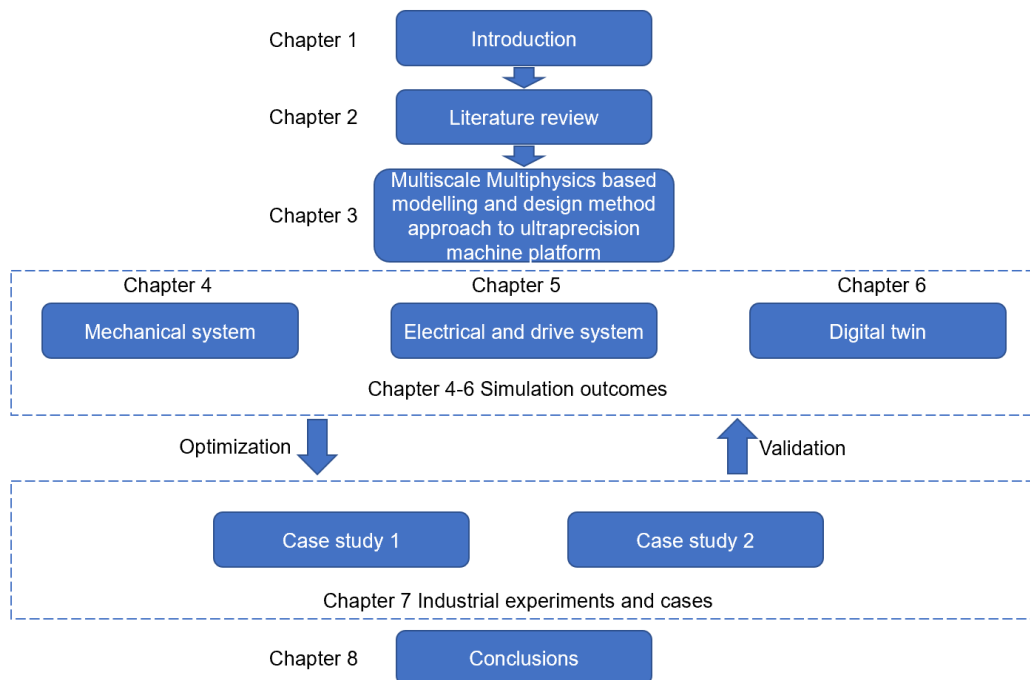
Figure 1.2 Research scope and chapter plan of this thesis

Chapter 1 explains the motivation and objectives of this work.

Chapter 2 reviews the UPM related technologies, including machine tools and machining processes, design and analysis method for aerostatic bearing components and the digital twin approach. The literature survey shows that the investigation of a multiscale multiphysics modelling and analysis method is essential in order to provide an effective design method and to further obtain a scientific understanding of the generation of high precision multi-axis machine platform.

Chapter 3 critically summarise the development of modelling and simulation approach used in this research, and introduce how these simulations linked with each other and collaborated as the whole multiscale multiphysics modelling and design method.

Chapter 4 specifically introduce how the modelling and simulation predict the static/dynamic performance of single axis aerostatic bearing slideway. With the collaboration of COMSOL^{TM} MULTIPHYSICS, which is an advanced engineering software based on CFD simulation and Computer Aided Design (CAD) modelling method, a simplified Reynolds' equation is introduced in the chapter which aims to predict the air pressure distribution. The simulation result is further integrated into a digital twin, the discussion of related model, functional benefit, and limitation are also included.

Chapter 5 describes the methodology and simulation used in predicting and modelling the control system of ultraprecision machine platform. Transfer function and PID tuning method are used with the collaboration of software MATLAB SIMULINK, and the approach of cross-coupling-controller with variable gains are implemented to integrate the data transport between multiple axis, thus to realize integrated tuning of the whole machine platform.

Chapter 6 illustrates the method of building a digital twin system for ultraprecision diamond turning process of freeform surface, with the implement of kinematic, dynamic and mathematic model, the 'In-process' data retrieval from the machining system can be realized with the function of prediction and monitoring the processing status in real time.

Chapter 7 presents the simulation establishment, experimental setup and results of different industrial cases based on ultraprecision machine platform and its components design. A discussion on the simulations of experimental trails and the evaluation and validation process are also included.

Chapter 8 concludes the results of this investigation. Recommendations are made for future work.

Chapter 2　　Literature Review

2.1　Introduction

UPM technology constitutes a cornerstone for modern high-tech industries and development of big science and technologies, and represents the orientation of advancement for modern engineering science. Nevertheless, the experimental basis and implementation perspectives for modern science and technologies require almost exclusively the support of ultraprecision technologies and the associated equipment/facilities for fulfilling their application purposes. The transition from macro-manufacturing to micro-manufacturing is proved to be a prevailing trend in the development of the manufacturing industry. Presently, UPM aims to maintain the physical properties of the workpiece material while achieving extreme precision in shape accuracy, dimension accuracy, surface roughness, and surface integrity, with minimal surface damage such as micro-cracks, residual stresses, and microstructural changes[4].

As the key enabling tool of the UPM, the modeling, design, and analysis methods for ultraprecision machines and components have been a research hotspot for manufacturers and national laboratories worldwide. In 2005, Altintas provided a detailed review and analysis of the state-of-the-art and future trends in virtual machine tool technology, addressing issues such as machine tool statics, structural dynamics, and control strategy integration in simulation environments[5]. In 2010, the mechanical engineering journal, "International Journal of Machine Tools and Manufacture," published a special issue which systematic review of the research achievements and development trends in ultraprecision machine tool technology worldwide[6], it explicitly pointed out that complex integrated design methods are one of the key technologies for ultraprecision machines. Integrated design and simulation analysis are important means of achieving the comprehensive design and improving the overall design performance of ultraprecision machine systems. These reviews showed that the establishment of integrated design methods and the development of design models and guidelines are fundamental scientific issues that urgently need to be addressed.

The difficulty of integrated design for ultraprecision machine and component lies in their unique structures compared to traditional machine tools. Ultraprecision machine

systems extensively utilize structures with microscale dimensions, such as hydro- and/or aero-static spindles and motion components, by which fluid media forms pressure films with a certain stiffness and load-carrying capacity between fixed and moving components, thus, minor changes in the combined interfaces between dynamic and static structural components during the machining process result in significant changes in the performance of rigidity, stability, precision, and other characteristics at various points in the working space, directly affecting the overall performance. Due to the high sensitivity to microstructural changes in the structure and its combined interfaces, the design and analysis of ultraprecision machine components require comprehensive considerations, e.g., the characteristics of multiscale structures and combined interfaces in the system. Although precision machine manufacturers and research institutions have designed various ultraprecision products and solutions and conducted machine tool design analyses for specific applications[7][8], the lack of mapping relationships between the characteristics of multiscale multiphysics and the overall system performance in the design methods has led to a lack of seamless analysis and optimized design for the overall system performance. Thus, in ultraprecision machine tool development, it is urgent to establish a modelling and design method system that addresses the multiscale multiphysics influence factors, transitioning from empirical-driven design and isolated analysis of key components to design-driven system-level performance analysis and integrated overall design.

Based on the demand for surface roughness, contouring accuracy, precision motion of UPM process, the rotary and linear motion control in precision engineering has reached sub-micron or even nano level. In this industrial context, aerostatic bearings, as the key enabling components of the ultraprecision technology, and their design modeling and analysis and design methodology are becoming essentially important and crucial, particularly for addressing the increasingly stringent demands in their design and manufacturing at an industrial scale as well[9].

As one of the core technologies for precision and ultraprecision machining equipment, aerostatic bearing has been widely applied in UPM mechanical components like spindles, rotary tables and slideways over the last 1-2 decades in particular[10]. Compared with conventional bearing products, aerostatic bearings on the basis of sacrificing a certain load-bearing capacity and stiffness, can greatly reduce the friction so that to increase the motion accuracy, moving smoothness, maintenance and life

cycle of the machine components[11]. The typical structures of aerostatic bearing products for specific application scenarios are illustrated in Figure 2.1 with specific examples.

(a)

(b)

1—Linear Motor Stator of X Direction
2—Linear Motor Slider of X Direction
&Motor Stator of Y Direction
3—Linear Motor Slider of Y direction
4、5、6、7—Air Bearing

(c)
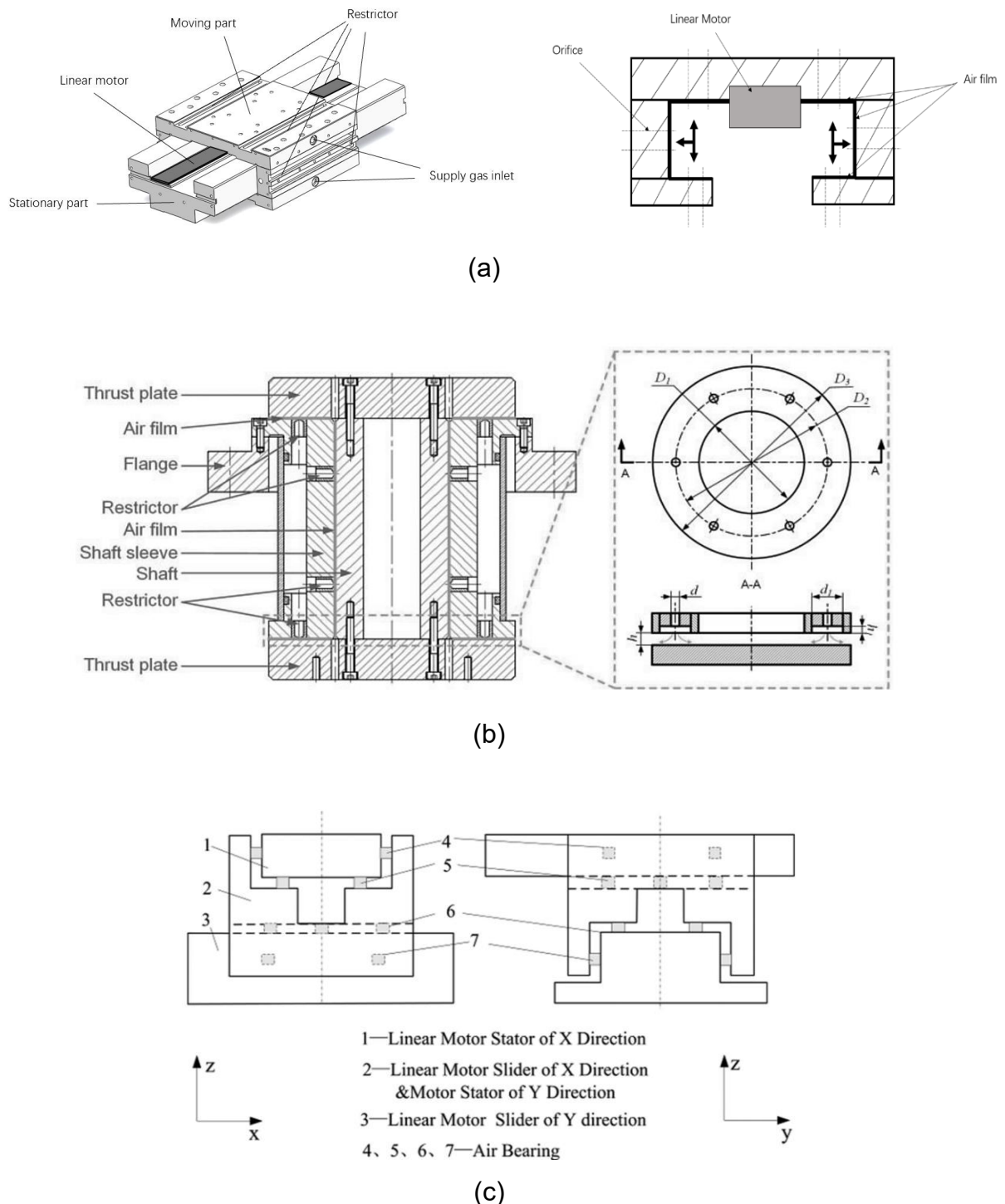
Figure 2.1. Examples of the key components and schematic illustration of aerostatic bearing products: (a) slideway[12]; (b) spindle[13]; (c) rotary table[14].

As the key components of high precision machines and equipment, aerostatic bearing

products rely on an external source of high-pressure air to generate the lubricating air film with appropriate thickness normally at the micrometre level[15]. To provide enough load capacity and stiffness, therefore, these air films act as the lubricating media during the relative motions through appropriate constrained design and analysis particularly on air orifices or restrictors and air film clearances. As shown in Figure 2.1, there are numerous restrictors in every direction on the bearing surface, pressured air is output by a compressor passing through these restrictors so that to form such stable and rigid air film. Regarding this, Gao et.al[13][16]discussed the advantages and disadvantages of various mainstream types of restrictors including annular orifice, or simple orifice, or slot-entry, or groove, or porosity. Tsheir review article is focused on perspectives of load capacity, stiffness, stability, air consumption and manufacture difficulty of air bearings, which can provide guidelines for aerostatic bearing design and analysis.

The main advantages in lubricating with compressed air are the extremely low friction of the air films, which is almost zero at low speed, although the static performance such as load capacity and stiffness of air films is normally lower in comparison with other lubrication materials such as oil, it generates lower heat and surface adhesions at the same time and thus provides the bearings with an extremely long service life and low damping ratio. Many researchers have demonstrated the technological advantages of aerostatic bearings, one of the examples is from Wardle's research study[15] showing that aerostatic bearings can produce the lowest motion errors of any bearing type in industrial applications and enable them to compete very favourably with other bearing types in high precision machine applications, where high dimensional/form precision and surface quality being required.

The methods for design and analysis of aerostatic bearings have been derived over several decades. Before the maturity of computer aided design and analysis, early research on air bearings design and analysis was mainly based on experimental methods. One of the earliest experimental demonstrations of air lubrication technology was carried out by Willis [17], he roughly studied the state of air flow between two parallel planes, which is considered as the embryonic form of modern air bearing technology. After that, Kingsbury [18] experimentally investigated the support characteristics of air bearing spindle at the end of the 19th century. Several decades later, the aerostatic bearings related research attempted to be focused on physical and mathematical fundamentals rather than only on experimental works[19][20][21]. As time progressing, more and more research studies began to focus on the solution

to Navier Stokes equation and Reynolds equation based on differential equations with the aid of finite difference method (FDM), finite volume method (FVM), finite element method (FEM), and also the modern finite element analysis method (FEA) and computational fluid dynamics (CFD) analysis. Simulation tools, such as Ansys, Abaqus and COMSOL™ MULTIPHYSICS[22], are also developed and applied using the above- mentioned methods but with much more convenient user-interface and customizable functions [22-28]. In recent years, an increasing number of researchers have been starting to consider the performance of aerostatic bearings under the combined influences of multiple physics phenomena in multi-scale (i.e. macro-meso-micro-nano scales and/or combined as well), and thus investigated design modelling and analysis and simulations of air bearings from multiscale and multiphysics perspectives[12][30]. Overall, the underlying philosophy of developing the above-mentioned aerostatic bearings design and analysis methods is to achieve the scientific understanding of aerostatic bearings design in precision engineering science context, on which therefore to design and manufacture the high-quality aerostatic bearing products in a truly competitive industrial scale, although the industrial requirements for air-bearings performance are increasing constantly as it progresses. Figure 2.2 provides a summative illustration on the development of design and analysis methods for aerostatic bearings, the timeline is approximately indicated in the decade, by which the design and analysis methods are developed and began to be widely applied.
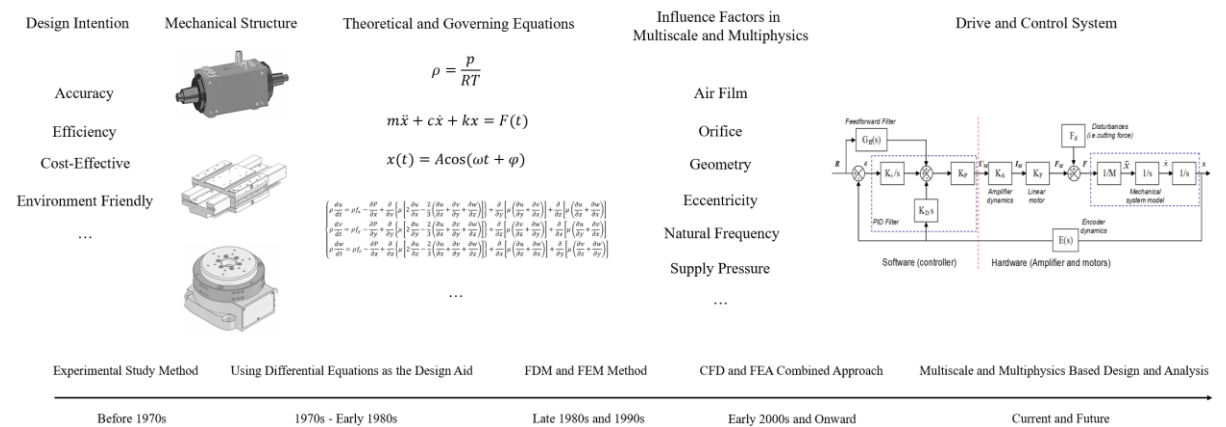
Figure 2.2. Development for design and analysis methods of aerostatic bearings.

This chapter aims to present a comprehensive and critical review on design and analysis methods for the components of ultraprecision machine platform by analysing and summarizing existing literature in past decades, and thus provide a

comprehensive snapshot of the development and evolution paths for the methodology, on-going research and challenges, and the future research and development trends. The state of UPM is described at the very first step, then the industrial application of aerostatic bearings and their associated products is also reviewed subsequently on the main product form as spindle, rotary table and slideway, which are increasingly applied for high-tech industries including semiconductors manufacturing and optics manufacturing. The fundamentals of aerostatic bearings from mathematical governing equations, underlying mechanics and physics, and technological perspectives including manufacturing aspect are discussed with in-depth details. Furthermore, the design and analysis methods for aerostatic bearings are reviewed. Finally, this chapter is also concluded with the further discussion on the multiscale based approach, and its implementation perspectives and potentials.

2.2 State of the art of UPM

The development of UPM has undergone four distinctive stages:
- The first stage, spanning from the 1950s to the 1980s, was a period characterized by a technological breakthrough. During this time, the United States pioneered the field by introducing the single-point diamond cutting technique, also referred to as "micro-inch technology," with diamond cutting tools[31]. This innovative technology facilitated the production of large spherical and non-spherical components, which were used in critical applications such as laser fusion mirrors, tactical missiles, and manned spacecraft. Notably, Union Carbide Corporation, Philips Corporation, and Lawrence Livermore National Laboratory successively introduced their ultraprecision diamond turning lathes, which were mainly employed for experimental research in a few large corporations and research institutions for defense or scientific research purposes. Although diamond turning lathes were primarily used for the processing of soft metals such as copper and aluminum and for the machining of axisymmetric shapes such as aspheric mirrors, their application was restricted during this period.
- The second stage, spanning from the 1980s to the 1990s, marked the commencement of civilian industrial applications. In this period, several research groups and companies were encouraged by the government to commercialize

ultraprecision machining equipment, Some of the representative studies include the review of ultraprecision machining by Taniguchi on 1983[32] and the prediction of cutting force by Lee, in 1990[33]. However, ultraprecision machining equipment was still costly and rare, primarily in the form of custom-made machines. During this period, ultraprecision diamond grinding, which could machine hard and brittle materials, was developed, as presented by McKeown et. al[34], supplementing diamond turning lathes used for processing soft metals. However, its machining efficiency and mechanism complexity could not match that of diamond turning lathes. In the late 1980s, the large optics diamond turning machine (LODTM) developed by the Lawrence Livermore National Laboratory in the US is a classic example in the history of ultraprecision machining[4].

- The period from the 1990s to the 2010s represents the maturity of civilian industrial applications. Since 1990, the demand for UPM equipment has sharply increased due to the rapid development of industries such as automotive, energy, medical equipment, information, optoelectronics, and communications. The industrial applications of UPM equipment during this period include non-spherical optical lenses, Fresnel lenses, ultraprecision molds, magnetic disk drive heads, magnetic disk substrates, and semiconductor wafer cutting, among others. During this period, significant studies of ultraprecision machining equipment, have emerged and prompt the related technology gradually matured, making UPM equipment a common production tool in the industry. In addition to diamond turning lathes and ultraprecision grinding, ultraprecision multi-axis milling[35] and fly cutting[36] technologies have also been developed, which can machine non-axisymmetric non-spherical optical lenses.

- From 2010s to date, with the rapid development of computer, communication, and consumer electronics (3C) technologies, UPM has gradually evolved from a form that relies primarily on mechanical equipment as the main technological carrier to an integrated and complex electromechanical system. More and more researchers start to discuss the UPM related technology from an interdisciplinary perspective.
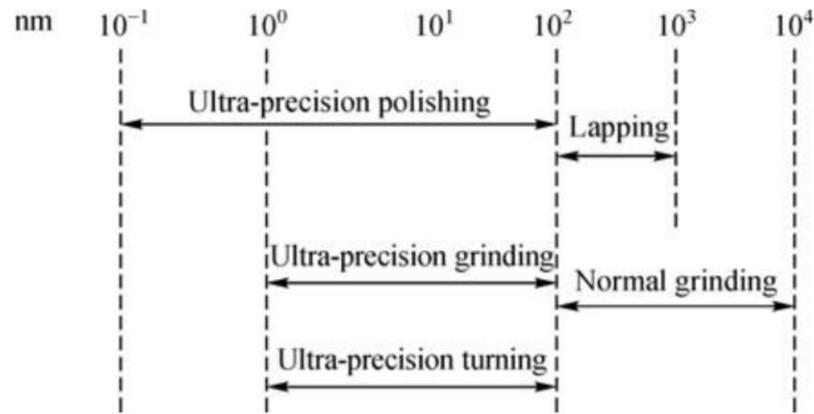
Figure 2.3.The machining accuracy of ultraprecision machining methods[15]

The modern machining accuracy of UPM are shown in Figure 2.3, it can be seen that several ultraprecision machining methods like polishing, grinding or turning has already reached nanometric or sub-nanometric level. Although ultraprecision machining technology has been continuously updated and machining accuracy has been continuously improved with the changing times, the factors that promote the development of ultraprecision machining equipment are essentially the same: the pursuit of high quality, high performance, high reliability, and miniaturization of products.

2.3 Aerostatic bearing technology and its implementation in UPM machine platform

Air bearing technology was first proposed in 1850s, but it was not until more than 40 years later that Kingsbury developed the first air lubricated radial bearing. Unfortunately, due to the relatively low manufacturing ability at that time, this new technology did not receive sufficient application[18]. In 1913, British researcher Harrison derived the Reynolds equation for gas under isothermal conditions, which established a solid theoretical basis for gas lubrication technology [37]. After the 1950s, due to the urgent needs of aerospace, military industry, and others, air bearing technology gradually gained popularity and developed rapidly. Among these years, noteworthy study including: Ro and Kim proposed a slideway preloading technology based on gas lubrication, which provides a good solution for high-precision motion and positioning accuracy by achieving excellent linearity and extremely low motion control

error for the air bearing slideway[38]. Stanev, Wardle, and Corbett proposed that the aerostatic groove has a significant impact on the air bearing film, it can enhance the bearing stiffness, stability, and ultimate speed of ultra-high-speed spindles. However, in practical laboratory studies, the ultimate speed is often limited due to the influence of the driving device, which may deviate from the simulation results of computer modelling[39]. Yoshimoto established a model of air bearing film using fluid simulation software and applied certain boundary conditions. The results showed that the pressure distribution was very close to the experimental measurements, verifying the accuracy of the simulation method[40]. In summary, air bearing technology has a solid research foundation in theoretical methods, simulation methods, and experimental testing, including preload technology, vibration control and bearing capacity research, design of orifice structure parameters, air film stiffness research, as well as the collaborative research of dynamics. This lays a foundation for the in-depth study of modelling and simulation, design and analysis methods of aerostatic bearing machine components.

The air bearing machine platform, as the foundation of precision measurement and ultraprecision machining equipment, has established a solid research foundation in related technology. In recent years, significant progress has been made in the structure, materials, driving, control, and measurement aspects of air bearing platform applied in three-dimensional precision measurement or other fields of research, enabling the positioning platform to advance towards high precision, high speed, and large stroke. The ultraprecision machine platform is an essential key component of high-precision measuring machines, which directly affects the measuring accuracy and efficiency that can be achieved by the measuring machine.

2.4 Design and development of aerostatic bearing associated products applied in UPM

2.4.1 Aerostatic bearings: applications and products

As a key component of ultraprecision machine tools, the superior properties of aerostatic bearing products compared to conventional contact bearings, aerodynamic bearings and also liquid pressurized bearings have been proved by many studies since 1950s[41][42], such as negligible friction and wear, longer life cycle, extremely

high speed and accuracy of motion, and unique environment-friendly properties. These advantages also result in aerostatic bearing products being widely applied in many industrial fields.

Before 1960, the applications of aerostatic bearing products were restricted to two specialized areas: gyroscopes for inertial navigation and gas circulators in nuclear reactors[43]. In the next one or two decades, the application of aerostatic bearings in manufacturing industry was mainly limited by manufacturing accuracy and ability of material treatment and was also only applied in a small scale[44]. Due to the rapid development of manufacturing technology and high-performance computers in the past few decades, the performance and applicability of aerostatic bearings have also been improved, following are some application examples for the classic approaches of aerostatic bearings and the benefits they can bring:

- For the food processing, medical device and textile industries: Because it's lubricant material (air) has no adverse environmental impact and also generate very low noise during working, aerostatic bearing slideways and rotary tables are the ideal bearing solution for clean room or safe transportation applications of the food, medical and textile industries[45].

- For precision and ultraprecision machine tools: Aerostatic bearings are able to provide extremely precise speed control, zero friction and low vibration, thus resulting in increased machining accuracy. By using aerostatic bearing spindles, rotary tables and slideways, machining errors in precision and ultraprecision engineering can reach sub-micron or even nano levels[46].

- For Coordinate Measuring Machines (CMM): In 1965, aerostatic bearing technology with finely polished granite slideway was firstly applied in CMMs. The related study proved that porous carbon aerostatic bearing slideway can provide straighter and frictionless motion, smoother error correction and greater repeatability than conventional rolling element bearing slideways[47].

- For turbomachinery: By eliminating the need for an external or internal oil supply system, aerostatic bearing supported turbomachinery can significantly reduce overall weight, simplify structure and enhance the ability to tolerate high temperatures and speeds, thus be able to meet the increasing the demand of turbomachinery for more economical and cleaner lubrication technology[48].

However, aerostatic bearing products normally have higher requirement for machining tolerances, which increases manufacturing costs as well. In addition, the load capacity

of air bearings is relatively lower, which also limits their application.

Regarding the industrial applications, the study on aerostatic bearing products various a long time period as well. In 1989, Rowe conducted a study and systematically classified the practical implementation of various aerostatic bearing structures into three distinct scenarios, namely the spindle, rotary table, and slideway[49]. The family-tree diagram in Figure 2.4 depicts the structural illustration of entire fluid film bearing family systems, which is categorized by the lubrication material and the configuration.
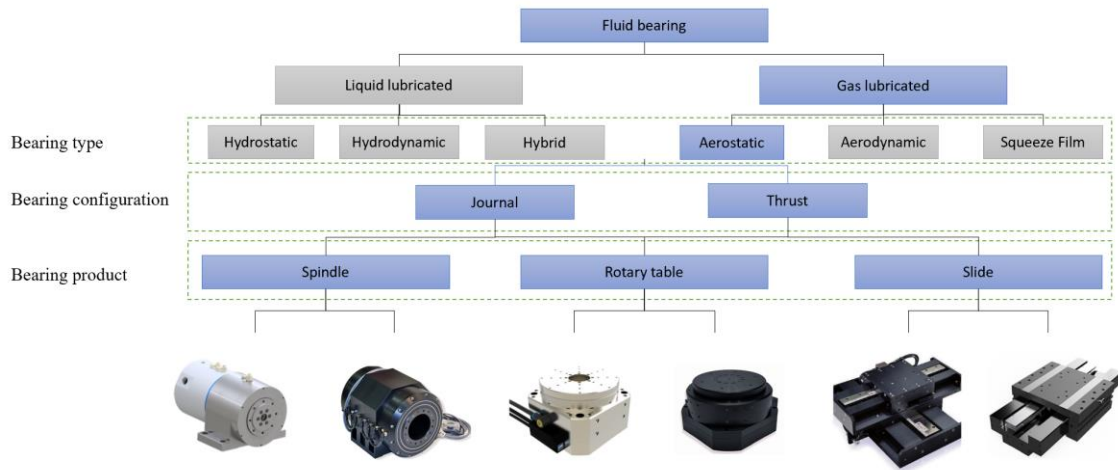
Figure 2.4. Family-tree of fluid bearing products.

The table 2.1 lists some selected manufacturers on aerostatic bearing products in precision engineering and related fields. An analysis of their founding dates offers valuable insights into the evolutionary trajectory of UPM equipment in different regions.

Table 2.1. Examples of aerostatic bearing manufacturers.

Region	Company	Found
America	Professional Instruments	1946
	Dover Motion	1963
	OAV air bearings	1964
	Newport Corporation	1969
	Aerotech	1970
	AMETEK Precitech	1992
	New Way Air Bearings	1994
sEurope	Westwind Ltd	1950
	Physik Instrumente	1970
	Loadpoint Bearings	1980's
	Kugler	1983
	MAGER Air bearing	1989
	Air Bearings Ltd (ABL)	1993
	Aerolas	1997
	LAB Motion Systems	2005
	Loxham Precision	2011
Asia	Canon	1917
	DISCO Corporation	1937
	SOONHAN Engineering	1993
	U-Precision	2012
	Aus-Precision	2018
	JITRI UPTech	2019

It can be seen from Table 2.1 that most of the manufacturers of bearing products on the market currently come from the United States, followed by European countries such as the United Kingdom, the Netherlands, Germany, Italy and Belgium, and Asian countries such as Japan, South Korean and China, which have more increasing needs and capabilities for aerostatic bearing products particularly in high-tech related industries.

2.4.2 Mathematic fundamentals of aerostatic bearing products

With the purpose to develop high performance aerostatic bearing products, it is imperative to accurately predict their parameters and operating conditions based on mathematical, physical, and technical fundamentals at the design stage. In this regard, the very first theoretical calculations applied in the performance of gas lubrication can be dated back to 19th century from the works of Petrov[50], Sommerfeld[51], and Chaplygin[52]. Since then, numerous researchers have contributed their theories on the design and analysis of aerostatic bearing products from various perspectives, for instance, Cunningham et al.[53] theoretically and experimentally analysed the critical speed of an air bearing spindle rotor with different radial clearances and supply pressures based on rigid-body theory; Majumdar[54] theoretically analysed the load capacity of an aerostatic journal bearing with multiple orifices for different design parameters such as radial clearance, L/D ratios. based on Reynolds equation, with the considering of a laminar, viscous, compressible, isothermal air film; Lo et al.[55] theoretically investigated the static and dynamic performance of a high-speed aerostatic bearing spindle based on Navier-Stoke equation, nonlinear dimensionless Reynolds equation and Newton method, and further studied the influence of air film thickness, eccentricity ratio, air supply pressure and orifice diameter at the different rotational speeds; Mo et al.[56] improved the mathematical model of air-bearing platform with single-row restrictors based on the implementation of modern finite element calculator. It can be seen that although these researches were focused on different perspective, but the kernel of the problem is based on fluid dynamic.

As a classic algorithm that describes the pressure distribution of compressible viscous fluid, the Navier Stokes equation is widely used in aerostatic bearing design, it is normally described as:

Conservation of momentum:

$$\rho \frac{du}{dt} = \rho f_x - \frac{\partial P}{\partial x} + \frac{\partial}{\partial x}\left\{\mu\left[2\frac{\partial u}{\partial x} - \frac{2}{3}\left(\frac{\partial u}{\partial x} + \frac{\partial v}{\partial y} + \frac{\partial w}{\partial z}\right)\right]\right\} + \frac{\partial}{\partial y}\left[\mu\left(\frac{\partial u}{\partial y} + \frac{\partial v}{\partial x}\right)\right] + \frac{\partial}{\partial z}\left[\mu\left(\frac{\partial u}{\partial z} + \frac{\partial w}{\partial x}\right)\right]$$

$$\rho \frac{dv}{dt} = \rho f_y - \frac{\partial P}{\partial y} + \frac{\partial}{\partial y}\left\{\mu\left[2\frac{\partial u}{\partial y} - \frac{2}{3}\left(\frac{\partial u}{\partial x} + \frac{\partial v}{\partial y} + \frac{\partial w}{\partial z}\right)\right]\right\} + \frac{\partial}{\partial z}\left[\mu\left(\frac{\partial v}{\partial z} + \frac{\partial w}{\partial y}\right)\right] + \frac{\partial}{\partial x}\left[\mu\left(\frac{\partial u}{\partial y} + \frac{\partial v}{\partial x}\right)\right] \quad (2\text{-}1)$$

$$\rho \frac{dw}{dt} = \rho f_z - \frac{\partial P}{\partial z} + \frac{\partial}{\partial z}\left\{\mu\left[2\frac{\partial u}{\partial z} - \frac{2}{3}\left(\frac{\partial u}{\partial x} + \frac{\partial v}{\partial y} + \frac{\partial w}{\partial z}\right)\right]\right\} + \frac{\partial}{\partial x}\left[\mu\left(\frac{\partial u}{\partial z} + \frac{\partial w}{\partial x}\right)\right] + \frac{\partial}{\partial y}\left[\mu\left(\frac{\partial v}{\partial z} + \frac{\partial w}{\partial y}\right)\right]$$

Conservation of mass:

$$\frac{\partial \rho}{\partial t} + \frac{\partial(\rho \cdot u)}{\partial x} + \frac{\partial(\rho \cdot v)}{\partial y} + \frac{\partial(\rho \cdot w)}{\partial z} = 0 \quad\quad\quad (2\text{-}2)$$

where:

ρ—Air density;

u, v, w—Velocity of air in x, y, z directions;

f_x, f_y, f_z—External body force;

μ—Dynamic viscosity.

Unlike liquid-lubricated bearings, gas lubricants must be considered compressible, so the nonlinear differential equations are extremely hard to solve. Therefore, the Reynolds equation which is derived from the NS equation is generally used to explain and calculate the distribution of external pressurized air in the clearance, the general Reynolds equation is:

$$\frac{\partial}{\partial x}\left(\frac{\rho h^3}{12\mu}\frac{\partial p}{\partial x}\right) + \frac{\partial}{\partial y}\left(\frac{\rho h^3}{12\mu}\frac{\partial p}{\partial y}\right) = \frac{\partial}{\partial x}\left(\frac{\rho h(u_a+u_b)}{2}\right) + \frac{\partial}{\partial y}\left(\frac{\rho h(v_a+v_b)}{2}\right) + \rho(w_a - w_b) - \rho u_a \frac{\partial h}{\partial x} - \rho v_a \frac{\partial h}{\partial y} + h \frac{\partial \rho}{\partial t}$$

(2-3)

Where:

p — fluid film pressure;

x and y — the bearing width and length coordinates;

z — fluid film thickness coordinate;

h — fluid film thickness;

u — fluid viscosity;

ρ — fluid density;

u, v, w —   the bounding body velocities in x, y, z respectively.

a, b — subscripts denoting the top and bottom bounding bodies respectively.

Based on the above-mentioned mathematical models, after decades of development, the properties of aerostatic bearing products have become increasingly mature, many academic studies have proposed solutions to optimize the aerostatic air bearing products from different perspectives, for instance:

- Air film: air film thickness, air supply pressure, air consumption.

- Restrictions: form, hole size and shape, orifice amount, chamber, pattern.
- Surface structure: manufacturing accuracy, flatness, surface shape & microstructure.
- Drive & control system: PID-feedback time, overshoot, positioning chatter.

2.4.3 Focuses and challenges for aerostatic bearings design and analysis

As previously discussed, the capabilities of aerostatic bearing products are evident, but their limitations are in a plain sight as well. For instance, the lower static performance (load capacity and stiffness) caused by the physical properties of lubrication material and the limited supply pressure (normally less than 7 bar in industrial environment), higher rate of gas consumption, and the well-known "pneumatic hammer" instability phenomenon, which has been systematically studied for several decades by Stout and his team[57]. Thus, how to maximize the advanced characteristics and overcome the limitations is the long-standing theme in the design of aerostatic bearing products.

When acting as the key enabling technology and products for precision engineering, according to the description of the objectives for precision engineering provided by Nakazawa and McKeown[34] and the development of aerostatic bearings technology in last few decades, the trend of design and analysis for aerostatic bearing products can be broadly summarized as follows:

- Create highly accurate linear and rotary motion.
- Reduce initial costs.
- Reduce operating costs.
- Extend service life.
- Enable the design safety factor to be lowered.
- Improve reconfigurability of components so that they are able to be replaced by corresponding components made by other manufacturers or companies.
- Make further advances in technology and science.

The rotary accuracy of aerostatic bearing spindles and rotary tables and the linear accuracy of aerostatic bearing slideways have a direct impact on their implementation scenario. Regarding this, Khim and Park[58] studied the aerostatic bearing rotary stage with porous restrictors by considering the air leakage, inlet pressure and velocity based on theoretically analysis, simulation and also experimentally test trail, the result

showed a rotational accuracy of 0.23 μm in the radial direction; Ekinci et al.[59] in their study theoretically and experimentally investigated the motion accuracy of an aerostatic bearing slideway, the results showed that the geometric error played a critical role for product performance failure.

In conclusion, the technical challenges for the design of aerostatic bearing components to meet the different requirements of use can be summarised as higher precision, interdisciplinary and complexity, economic benefit, environment friendly. The scientific challenges arising from these technical challenges are related to engineering science, design methodology, advanced modelling and analysis, which tightly meet the objectives for precision engineering as mentioned above.

In the following sections, the evolution of the design and analysis method of aerostatic bearing products since the 19th century will be reviewed separately, the development trends and future design possibilities with new theory and technologies and their applications and services in the context of industry 4.0 and beyond will also be discussed.

2.5 Design and analysis methods for aerostatic bearings and the associated products

2.5.1 Experimental-based method

The experimental-based method or empirical method was the mainstay for early mechanical design and analysis and was widely used in scientific research as well as in industry before the maturity of computer simulation technology, its results are normally intuitive, costly, with high authority, and difficult to describe detailed physical phenomenon.

After 1960s, aerostatic bearings technology began to be widely employed in industrial fields, thus more and more researchers and companies began to carry out experiments to analyse and optimize the design of aerostatic bearing products. One classic industrial case as Rasnick's publication in 1972[60], through the replacement of the original roller bearing slides by aerostatic bearing slides of a precision X-Y turning machine, although the load capacity of the slideway was reduced, the lower friction, almost-zero wear and the elimination of short-wavelength error caused by rollers resulted in a more satisfactory machining performance. After several revisions

and optimization of design, the Rasnick team finally designed the aerostatic bearing slideway with more performance advantages and applied the results directly in the machining environment. But the whole design process is costive, meanwhile the observation of the performance also only remained in the load capacity, stability of movement and other relatively apparent phenomena, without much discussion of the mathematical and physical principles.

Following on from several decades of research, many cases from research perspectives are also representative: In order to accurately describe the pressure distribution, load carrying capacity, stiffness and airflow consumption in the air film, many researchers have studied the flow coefficients of small orifices in aerostatic bearing products by experimental methods, of which, Belforte et al.[61] conducted a systematic study of the flow coefficients of simple and annular orifice types by carried out experimental methods. Renn et al. [62] studied the critical pressure ratio and flow coefficient of small-hole restrictors using the combination of numerical and experimental methods. The results showed that the flow coefficient ranged from 0.8 to 0.85, and the critical pressure ratio should be taken between 0.35 and 0.4 to replace the value of 0.528 obtained from the classical model, which makes the calculation more accurate.

Experimental study methods are generally based on engineering algorithms as the theoretical fundament, as such algorithms are relatively simple to be built up and compute. In the early aerostatic bearing related research, many researchers simplified the two-dimensional air flow in air film to one dimension, thus to get a simple analytical solution of the Reynolds equation. For instance, Liu et al.[63] studied the engineering algorithms for aerostatic radial bearings and planar thrust bearing, calculated the design curves for the engineering algorithms for aerostatic bearings and experimentally studied its performance. The engineering algorithm is easy to operate, and the existing design curves greatly simplify the calculation design process, but for small clearance in aerostatic bearings, it will produce large errors due to the large deviation between the linear air flow assumption and the actual air flow in the air film. In addition, the engineering algorithm can only be used to calculate bearings at standstill and is no longer valid when the actual operating speed of the bearing is considered.

2.5.2 Differential equations as the design aid

As elaborated and discussed in previous section, the Reynolds equation is the dominant and fundamental mathematical model used to describe the status of a liquid or gas film in a fluid lubricated bearing, this differential equation which govern the pressure distribution in a fluid film bearing was presented by Reynolds in his classical paper in 1886[64], and then after the extension and derivation of Cope[65], Wannier[66], Halton[67], Zienkiewiez[68], Dowson[69], resulted in valid forms of the reduced Reynolds equation. After a long period of development, the finite difference method (FDM), finite volume method (FVM) and finite element method (FEM) has become the mainstream methods for solving Reynolds equation in air lubricated bearing technology[70] and are widely used in the related simulation studies.

FDM: As far back as 1986 Gero[71] has in his study systematically discussed and demonstrated the advantages of using the FDM to solve Reynolds equation in terms of accuracy, computational efficiency and programming complexities. Although compared to FEM, the FDM as a direct numerical solution method has clear disadvantages in accuracy and convergence, but its utter simplicity and lower programming complexities made this method widely used before the rapid development of computer technology, especially around 1980s[72][73][74]. Till today, FDM is still one of the mainstream methods used to solve Reynolds equations for aerostatic bearing product design. For example, Dal[75] in 2017 solved the Reynolds equations from a theoretical and simulation perspective by using the DTM (differential transform method) and FDM hybrid numerical solution method and discussed the effects of angular misalignment on the performance of rotor system supported by aerostatic bearing spindle.

FVM: The advantage of FVM over other methods is its superior numerical convergence, together with the multi-grid solving technology, FVM normally shows higher calculation speed but lower simulation accuracy at the same time in compared with FEM[76]. Till now the industry has dedicated significant efforts and resources towards the development of these methods. Consequently, a diverse range of techniques has been incorporated to enable efficient and precise computation and integration of fluxes for both structured (e.g., hexahedrons) and unstructured (e.g., tetrahedrons) meshes. FVM is widely applicated as the core algorithm of modern simulation software and also been used to support the design and simulation of aerostatic bearing products. The studies with the purpose of improve the calculation

time and simulation accuracy for FVM is mainly from the mesh generation perspective. As an example of related researches in aerostatic bearing slideway simulation, Wu and Bogy[77] extended Lu[78]'s research by replacing the structured rectangular mesh with unstructured triangular mesh, which increase the suitability of boundaries of meshes. The study proved that the unstructured triangular mesh is much more efficient than the structured rectangular mesh in the step of mesh generation due to less nodes and flexible grid division, which can effectively reduce the simulation time and improve the calculation accuracy as well.

FEM: The first analytical study of variational calculus which directly related to the FEM can be traced back to 18th century by Schellbach[79], due to its requirement for a large number of calculations, the quantum leap of the development for FEM was only discovered after the development of high-power computers. Compared with other methods, FEM was invented to the division of the element mesh and the selection of boundary conditions in the calculation. By application in aerostatic bearing design and analysis, by using FEM the influence of bearing speed is normally ignored[80]. For example, Li et al.[81] used a functional extremum method to discretize the second order partial differential equation (PDE), and then used FEM to solve the load capacity and stiffness of the aerostatic bearing. Meanwhile, Neves et al. [82]used triangular finite elements and solved the Reynolds equation for an aerostatic radial bearing and calculated the bearing load capacity and air consumption rate. As advantages, FEM has high calculation accuracy and can adapt to complex bearing structures. However, the complexity of element meshing, calculation process, and algorithms also limited its application before 20th century.

The difference between the above-mentioned numerical methods are shown in Figure 2.5:

Differential equation of flow problem

FVM	FDM	FEM

$$\frac{\partial U}{\partial x} \qquad \frac{\partial U}{\partial x} \qquad \frac{\partial U}{\partial x}$$

Integral form | Difference Equations | Using basis function

$$\int_{CV} \frac{\partial U}{\partial x} dV \qquad \qquad U = U_G \cdot \phi_G + U_I \cdot \phi_I$$

$$U_{i+1} = U_i + \Delta x \cdot \frac{\partial U}{\partial x}$$

$$U_{i-1} = U_i - \Delta x \cdot \frac{\partial U}{\partial x}$$

Divergence theorem | Taylor series

$$\int_A n \cdot U \, dA \qquad \frac{U_{i+1} - U_{i-1}}{2\Delta x} \qquad \frac{\partial U}{\partial x} = U_G \cdot \frac{\partial \phi_G}{\partial x} + U_I \cdot \frac{\partial \phi_I}{\partial x}$$
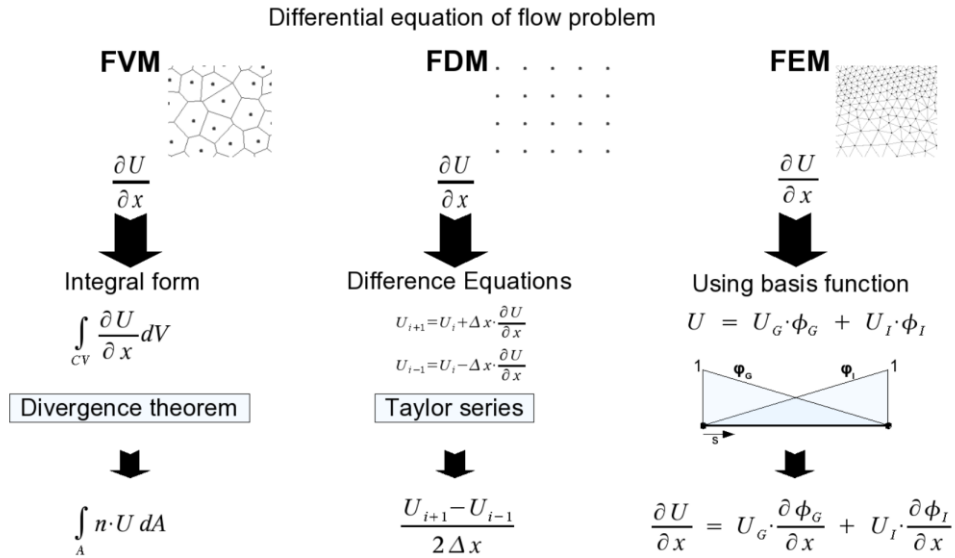
Figure 2.5. Essential differences between FVM, FDM and FEM[83]

As illustrated in Figure 2.5, Milbradt and Abed summarized the differences between FVM, FDM and FEM from a mathematical perspective[83].

2.5.3 FEA method

As a specific numerical technique which aims to solve the continuous problem stated in the form of a partial differential equation (PDE), FEA is widely applied as a computerized method of simulation software, which are used to predict the behaviour of a part or assembly under given physical conditions so that it can be assessed using the FEM[84]. In 2004, Hutton[85] proposed a systematic review of the fundamentals for FEM from both scientifical and application perspectives. To date, FEA software is widely used by engineers to support simulation of physical phenomena and thereby reduce the need for physical prototypes, while allowing for the optimisation of components as part of the design process within a project[86]. So far, the FEA software has been extended from the field of solid mechanics to other fields that require the solution of differential equations, such as fluid mechanics, heat transfer, electromagnetism, and acoustics.
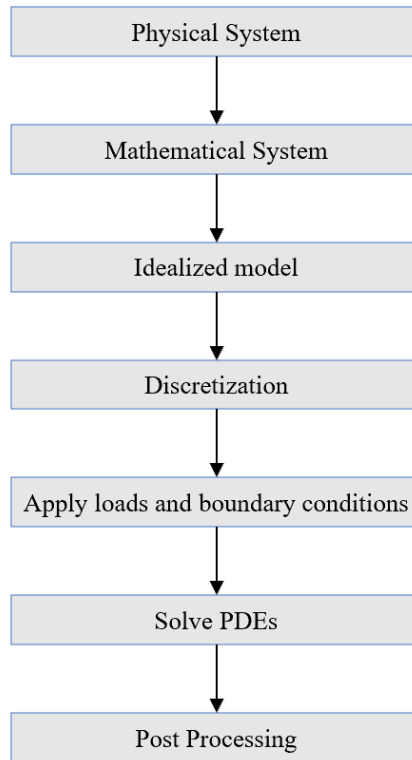
Figure 2.6. Flow chart of FEA process.

Figure 2.6 depicts the schematic representation of the FEA simulation flowchart. Diverse adaptations derived from physical structures serve as the foundation for formulating pertinent mathematical models. Subsequently, boundary conditions are imposed to align with the simulated environmental settings. The following process involves the utilization of PDE-based computational algorithms and post-processing methodologies, ultimately yielding simulation outcomes presented in an anticipated data format.

The main applications of FEA in precision engineering are structure analysis or dynamics modelling and simulating, some of the representative studies are: Zaeh and Siedl[87] combined FEA with multibody simulation to simulate dynamic machine tools; Zhang et al. [88] and Yao et al. [89]used dynamic simulation software ADAMS[TM] [90]and FEA software ANSYS[TM] [91]and ABAQUS[TM] [92]to analyse the static and dynamic vibration characteristics of a machine tool system, which successfully identified the weak components of the system. In the past decades FEA is also widely used in the design of aerostatic bearings to simulate and analyse the performance. For example, Allan et al.[93] used ANSYS[TM] to assist the X-Ray for beamline I19 at diamond light source design, aiming to maximise the air bearing stiffness while not

adding excessive weight for the slideway; Yang et al.[94] carried out a dynamic FEA of the aerostatic spindle in ANSYS Workbench after modelling the surface morphology and obtained that the dynamic characteristics of the aerostatic spindle were the main factor in the scratching of the surface. With the maturity of FEA technology, many commercial software for FEA simulation have emerged on the market, bringing great convenience to the design and analysis of aerostatic bearing products.

2.5.4 CFD and FEA combined approach

Computational Fluid Dynamics (CFD) is a combination of modern fluid mechanics, numerical mathematics and computer science, it starts with mathematical models which supported by the computing ability of computers to obtain approximate solutions of fluid equations. With the rapid development of computer hardware and software, CFD is now widely used in engineering, especially in manufacturing to study and optimise the performance of fluid systems. The early commercial CFD software packages have conventionally relied on FVM, but modern CFD solution algorithms are not only FDM, FVM, FEM, but also Smoothed Particle Hydrodynamics (SPH), Lattice Boltzmann Method (LBM).

CFD and FEA do not focus on same physical phenomena, but in order to describe problems such as fluid-solid interaction more accurately, more and more studies use both method as a combination to simulate and analyse engineering problems. Some scholars, such as Qiao[95], used FLUENT^{TM} [91] software to model an aerostatic bearing in a pendulum angle milling head, investigated the effects of the thickness of the air film and the eccentricity of the bearing on the static stiffness, load capacity and air consumption, and analysed the effect of the dynamic pressure effect on the bearing performance. By this study, FLUENT^{TM} showed its powerful ability in simulation, calculation, and post-processing; Neves et al. theoretically investigated the effect of flow coefficient on the performance of aerostatic radial bearings and solved the Reynolds equation for gas lubrication using the finite element method and obtained the relationship between the flow coefficient and pressure ratio with the aid of ANSYS^{TM}-CFX simulations; Gao et al.[13] presented an integrated Multiphysics modelling using the CFD and FEA integrated approach for design and analysis of the high-speed aerostatic spindle, including thermal, electromagnetic, mechanical, and

fluidic analysis models. The structural deformation induced by pressurized air film is also discussed based on their simulation model.
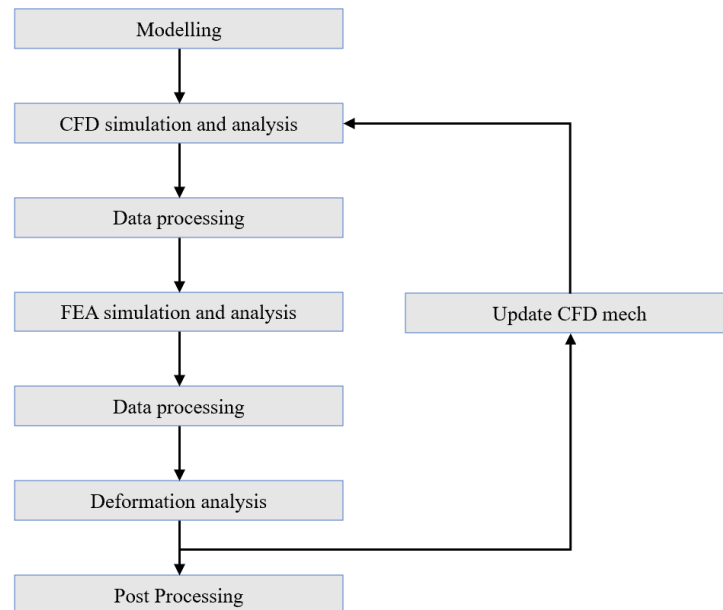
Figure 2.7. Flow chart of CFD and FEA combination process.

The process of combining CFD and FEA for aerostatic bearings design and analysis is illustrated in a flow chart as shown in Figure 2.7, with the continuous upgrading of simulation technology, their results are getting even closer to the real physical phenomena. Many engineering software began to focus on the approach of CFD + FAE as their kernel algorithms. In recent years, this type of software have been extended with multi-physics coupling modules based on their own CFD or FEA algorithms. However, with the continuous expansion of the functions, the problem of the opacity of the algorithms within the software has slowly emerged, many simulation software processes are black boxes, which make it difficult for users to identify the accuracy of simulation results, and the errors are also hard to be traced.

2.5.4　Multiscale multiphysics based design and analysis

Whether solving differential equations using the finite method or assisting the model simulation with FEA and CFD software, the purpose of design and analysis methods is to support industrial design, predict mechanical properties, optimise performance, and prevent errors. Meanwhile, the influence factors of product performance or instabilities are generally not in a single spatial scale or one physical field, so the

approach of multiscale and multiphysics coupling method to design analysis is thus essential.

- Multiscale-based analysis and design simulations: According to Weinan's theory[96], the factors and features from the machine itself, the component metalogical surface or tolerance, and the machine assembly clearance in multiple scales will have effects collectively on the performance of the entire machine. Among the numerous studies of aerostatic bearing products, researchers were focused on single scale. As instance, the most discussed influence factors are air film, restrictor shape and parameter, and microstructures.

- Multiphysics-based analysis and design simulations: In the latest decade, increasing number of researchers has begun to focus on the coupling of influences from multiple physical fields on aerostatic bearing performance, such as heat transfer[97], electro-magnetism[98], acoustics[99], vibration[100], and fluid-structural interaction[101]. It is proved that the multiphysics simulation approach is more powerful and more accurate in studying complex phenomena in aerostatic bearings, such as gas turbulence effects and oscillatory instabilities. However, although many multiphysics models for specific conditions have been developed by researchers, the flexible and adaptability of such models are still urgent issues needs to be solved.

It can be observed that as future oriented method, multiscale and multiphysics method has showed their potential as a next generation of simulation tool for aerostatic bearing design and analysis. Although some commercial software such as COMSOL™ MULTIPHYSICS has already developed a platform to simulate multiphysical complex phenomes in large range of length scale and researchers like Gao[13], also carried out their research from this perspective, but the simulation accuracy, modelling difficulty, model versatility still needs more investigation in future work.

2.5.5 Aerostatic bearing products design and digital twin technology

Under the increasing demands from high-tech applications and intelligent manufacturing system, there has been a trend of extending modelling and simulation beyond the products design phase to their lifecycle, which is fundamentally important for continuously improving the design and development of high value engineering products. For instance, aerostatic bearings, as high value precision engineering products with substantial engineering complexity and added application and service

values, are naturally applicable in design with digital twin technology particularly in the context of precision engineering industry 4.0.

The design and analysis methods described in the previous sections predominately attempt to support the air-bearing design modelling and analysis from the engineering science point of view, which makes it be crucial to develop a unified multidisciplinary design model for aerostatic bearing products. Furthermore, the function of these pre-established models is limited in dealing with the 'in-service' or 'in-process' dynamic phenomena/issues for aerostatic bearing products such as motion errors[102], dynamic imbalance[103], micro vibrations or dynamics[104], interference caused by electromagnetic effect[105], thermal effects[106] or external forces[107] during the working (in-service) process. For addressing and coping with these influences and effects occurring and vanishing in a dynamic status, it is necessary and essential to develop a computational design method and system for not only computational simulations of the product, but also continuously sensing, monitoring and improving the performance of the product in the process. With the aim to extend the functions and applications of the precision engineering product, the digital twin (DT) can fulfil the high level digital design goals for the product as discussed above, and be particularly applicable to aerostatic bearing products design and be utilized to combine with the air-bearing design for the air-bearing products optimization and continuous improvement during the product services[108][109][110].

The most accepted definition of DT is the collection of all digital artifacts that accumulate during the product development, integrating all data generated during the product design and usage[111][112]. In 2021, Wu et al [113] provided a comprehensive review of the application of digital twins in UPM from the perspectives of voxel modelling, process planning, process monitoring, vibration control, and quality control, which is highly valuable for research in this field.

With the advances of modern sensing technologies, the encoders, optical surface measurement equipment, and force, displacement and temperature sensors are all able to play the role as 'in-process' sensing and data collectors for DT. With their further cooperation with the analytic algorithms for in-process modelling, computations and simulation in a close loop and dynamic manner[114][115][116] , the design and analysis method for aerostatic bearing products with digital twin can likely reach to a higher intelligent level for their advanced precision engineering applications and services in particular.

2.6 Future research and development trends for aerostatic bearings design

Although numerous theoretical and experimental works have been conducted in the field of aerostatic bearings design and analysis, the design methodology and application perspectives for UPM machine platform are still facing challenges and not fully understood scientifically in particular against the increasingly stringent requirements in more and more high-tech industrial applications. In spite of the current achievements, the future research and development on aerostatic bearing based UPM machine platform components design are proposed and summarized below.

1) Substantial researches have been conducted on the orifice-type aerostatic bearings, and massive available design information and guidelines are developed for design of orifice-type air bearings. However, orifice-type restrictors have the limitation to meet the demands for higher loading capacity, stiffness and high-speed stability for aerostatic bearings. Air bearings with slot-entry restrictors, grooved restrictors, or porous restrictors will lead to much improved loading capacity, stability, and stiffness, but the manufacturing methods for such restrictors are still limited[16]. Therefore, more efforts should be made to develop the design and analysis methods for aerostatic bearings with slot-entry, grooved and porous restrictors particularly by combining with the integrated design and manufacturing of these aerostatic bearing products with the aid of new manufacturing and embedded sensing techniques[117].

2) At present, the causes of 'pneumatic hammer' vibrations are still not elucidated clearly, particularly for aerostatic bearings with slot-entry, grooved and porous restrictors as these new restrictors imposing new engineering complexity. Various causes, such as the gas compressibility, the negative damping of the system, the interference force, the phase difference of motion, and manufacturing and assembly errors for the bearing systems, are regarded to induce 'pneumatic hammer' vibrations. Some critical issues, e.g. the negative effect of the microscopic turbulent airflow inside the bearing and porous structures, the influence of fluid-solid interactions at the bearing and porous structures, remain unclear. The generation mechanism of 'pneumatic hammer' vibrations needs further research and exploration particularly through 'active' precision engineering control. The multiscale multiphysics based design and analysis approach

combining with in-process monitoring and advanced algorithms may lead to a powerful engineering design and analysis method to address the complex precision engineering phenomena in-process simultaneously, which is surely suitable for future research and development.

3) The turbulent flow inside the air film is generally recognized as the reason of nanometric order vibrations and uncertainty. However, the negative impact of air-induced vibration on positioning accuracy of the slideway and/or rotary table driven by direct drive systems on the machine working towards nanometric level accuracy is still not clearly described. Furthermore, the air-bearing supported motion driven by direct drive and control system/algorithms often requires both high-speed stability and positioning accuracy, design and analysis method for such a high performance aerostatic bearings system particularly working in a multi-axis manner needs further investigation[118], particularly against the stringent requirement of nanometric level accuracy in a complex multiscale multiphysics context[119][120].

4) Applying AI 2.0 techniques such as machine learning combined with in-process condition monitoring and advanced algorithms for aerostatic bearings design and development will likely help go beyond the limitation in working towards higher precision (such as industrial nanometric scale and even towards Pico precision) and higher robust performance (such as higher stiffness and loading capacity, adaptiveness of the bearings in various precision engineering applications and scenarios)[121], which is worthwhile for further research and development, and explorations.

2.7 Summary

This chapter intends to present a critical review on the state of the art in the research and development of the design and analysis method for aerostatic bearings based UPM machine platform components, particularly in the context of the bearings design methodology applicable to advanced precision engineering applications. The review also attempts to discuss the likely knowledge gaps, future research development and trends in the field. The conclusions can thus be drawn up as follows:

● Status: Over the last 5-6 decades, the research and development on design and analysis methods for aerostatic bearings have gone through the stages of

experimental-based, using differential equations, using FEA and CFD or FEA/CFD combined, and multiscale multiphysics modelling and simulations, in light of precision engineering needs and applications. Scientifically, there are matured analytical solutions developed based on physical and mathematical modelling and analysis towards precision requirement to some extent. Technologically, there is a number of engineering tools available in R&D for further supporting the bearings design and analysis, but it requires specialist expertise. There are still practical gaps and limitations for industrial scale application of the methods for design and development of aerostatic bearings and their associated products.

- Challenges: Because of the ever-increasing demands on motion and positioning accuracy and the complexity of the application scenarios particularly in high precision manufacturing and instrumentation, aerostatic bearing products design and analysis often require more complex and stringent precision engineering processes combining the collective efforts of mechanical design, direct electric drive, in-process condition monitoring and sensing, and advanced control and algorithms. The industrial feasible design and analysis methods for aerostatic bearings and the associated products are essentially important and desperately needed in precision engineering field. Furthermore, most aerostatic bearing products are ordered by mass customization with small quantities, which further imposes practical industrial challenges on productivity, quality and delivery times. In the meantime, as a complex product system including mechanical design, electric drive system, and advanced control and algorithms often working in multi-axis, existing design and analysis methods are difficult in addressing the multiscale multiphysics couplings among these three system aspects and/or combined, which further imposes the challenges on design and development of aerostatic bearing products working towards the nanometric level of precision engineering applications and beyond.

- Future Trends: In order to address the existing issues and challenges discussed above, future research and development on the design and analysis methods for aerostatic bearings are essentially needed particularly in the context of their industrial feasibility and precision engineering solutions to applications at truly industrial scales. The future R&D trends will be focused on design and developing the air-bearings products with much improved loading capacity, stability, and stiffness; developing the multiscale multiphysics based design and analysis

approach for air-bearings working with higher accuracy and high-speed stability; applying AI 2.0 techniques such as machine learning combined with in-process condition monitoring and advanced algorithms for future aerostatic bearings design and development.

Chapter 3　Development of the multiscale multiphysics based method for design, modelling and analysis of a precision machine platform

3.1　Introduction

Engineering modelling and simulation have been widely applied over the past three decades or so. For instance, macroscopic models are used to reveal the relationship between geometrical structure and kinematic, dynamic or mechanical performance in machine design. While the influences of surface features of machine components are often discussed through mesoscopic modelling, meanwhile, much R&D attention has been paid to the crystal morphology of the component materials in microscopic modelling or the molecular dynamics[122][123].

There has been a considerable amount of research efforts on multiscale modelling applied to various engineering fields over the last two decades or earlier. Weinan[96] summarized several classic multiscale modelling methods and the related principles from applied mathematics aspects, and Tadmor, et al. developed the classic nonlocal quasi-continuum method (QC) for simulating isolated defects including dislocations and cracks in single crystals[124]. Over the years in parallel, the multiscale modelling and analysis and the associated simulations development have been widely attempted in applications for material science[125], Biomedical Engineering[126], and Mechanics[127].

On the other side, FEA-based multiphysics simulation tools and modelling applications represented by ANSYS, ABAQUS, COMSOL^{TM} MULTIPHYSICS have made substantial progress in recent years and are maturing in terms of accuracy, stability, reliability, efficiency and scalability. These multiphysics simulation tools offer opportunities and convenience for long-term industrial research, although considerable challenges still remain in terms of interface coupling, physics domain integration and complex problem solving. By applying and simulating the interplay of various static/dynamic performance and physical fields, such analytical simulation methods are able to provide outstanding engineering design solutions for end users. However, lot of research and development which related to multiscale multiphysics

modelling and simulation often comes down to the individual application case driven, i.e., focused on one specific case. According to the statistics from Clarivate Analytics [128], there are only few research published including the keywords of 'multiscale multiphysics modelling' and 'air bearing' or 'aerostatic slideway'.

In precision engineering, aerostatic bearings have emerged as a key enabling technology particularly for high-precision machines and facilities[15][129]. However, as precision products, the aerostatic bearing slideways, rotary tables or spindles are becoming technologically more complex because of the high-precision mechanical components, electrical direct drive, feedback devices, and advanced control algorithms involved. This further imposes challenges on the design and development of these products particularly towards even higher precision and application performance requirements. The multiscale multiphysics modelling and analysis, the associated advanced simulations and digital twin approach, have substantial potentials and impacts on aerostatic bearing components design and development by likely helping in-process or remote tuning, tracking error prediction, higher precision enhancement, and continuous improvement of the product[130].

This chapter begins with an introduction to the overall UPM machine platform design. Followed with the investigation of multiscale multiphysics based approach for design, modelling and analysis of the multi-axis machine platform against its stringent UPM requirements and the corresponding system design specifications, with a particular focus on the core principles. Modelling methods for UPM machine platform are presented separately for different scales and physical fields. Application examples are then presented to illustrate how different scales (macroscopic, mesoscopic, microscopic) and physical fields (mechanical, electrical, control signal) can be combined and integrated into the simulations. Due to the complexity and interdisciplinarity involved, the interplay between multiple scales and physical fields is of great importance for industrial research and development. Finally, the potential and future development of the method to integrate with digital twin technology is further discussed.

3.2 Modelling and analysis method for UPM machine platform design

In recent years, the manufacturing industry has seen a rise in the demand for

miniaturized and micromachined components, particularly in biomedical, electronics, opto-mechatronics, and automotive applications. To achieve the needed tolerances, a new generation of ultraprecision machines and measuring equipment have emerged. With this purpose, UPM machine platforms are designed for providing precise motion solution for digital lithography, Computer Numerical Control (CNC) precision machining, biotechnology, micro and nano processing, micro and nano surface topography measurement and other fields by providing a carrier platform to achieve ultraprecise positioning and movement. The structural form of the UPM machine platform can be roughly divided into H-shaped, T-shaped and box-shaped (as shown in Figure 3.1). In general, when the air bearing is installed and configured, the symmetrical structure is used to reduce the influence of normal-direction electromagnetic force on the system.

(a)   (b)

(c)
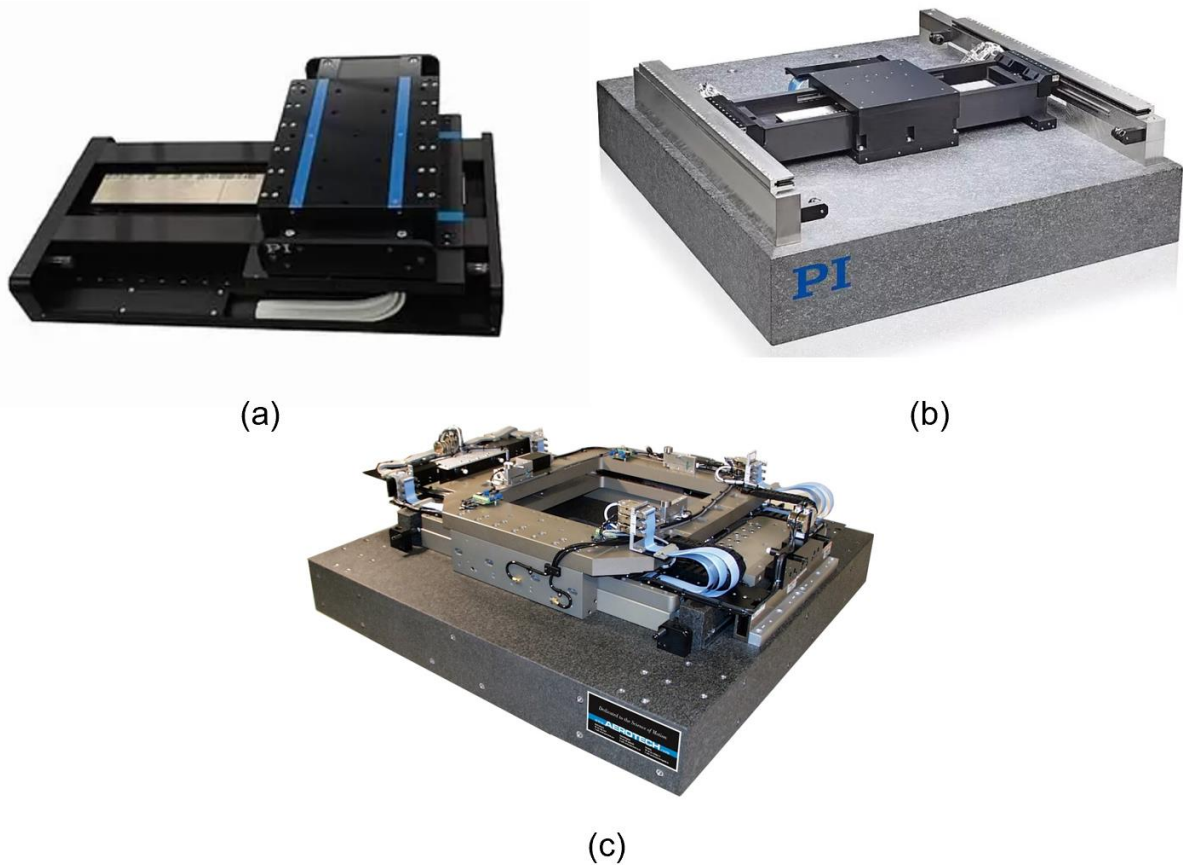
Figure 3.1 Common structures for ultraprecision machine platform

(a) T-shaped; (b) H-shaped; (c) Box-shaped

The industrial demand of different UPM machine platform varies significantly in terms of load, operating conditions, stroke range, motion accuracy, structural layout, stability, control strategies. Furthermore, activities in the detailed solution design process, as

well as the modelling, analysis and optimization methods used therein, are not the same. It is therefore difficult to describe a generic design process for different UPM machine platforms with a detailed and universal process model. However, the overall steps in different design processes are roughly similar, which including mechanical structure design, control system design, characterization and equivalent modelling of key components, dynamics analysis, electromechanical simulation. From the relevant literature on examples of ultraprecision machine platforms, as well as engineering experience in product design and development, the design process can be summarized as in the Figure 3.2:
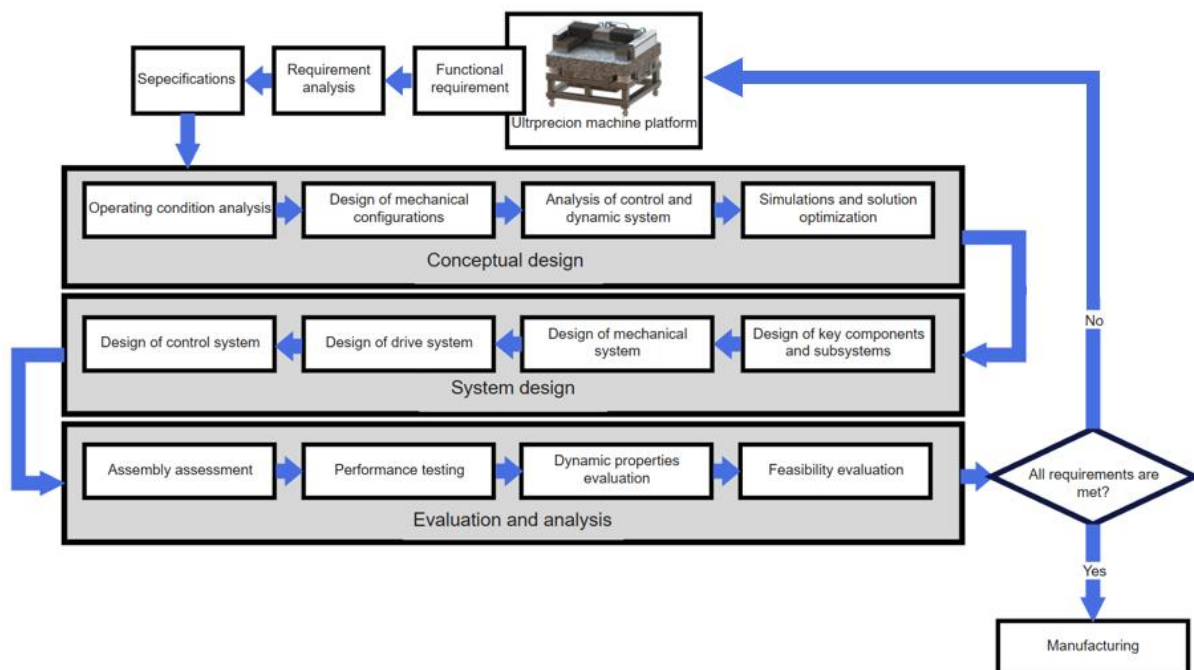
Figure 3.2 Design process for ultraprecision machine platform

During the conceptual design phase, several crucial aspects must be considered, including the structural layout, topological relationships, and motion control strategies. Equally important is the identification and specification of the key components and sub-systems, along with their corresponding structural and performance requirements.

● At the outset, a thorough analysis of design specifications and constraints is undertaken to determine the requisite operational parameters for the ultra-precision machine platform. This encompasses a range of factors, such as vibration, static load and its variation, motion trajectories. These parameters are typically indicative of the common operating conditions for the machine platform, or may correspond to the extreme operating conditions that would result in sub-

optimal platform performance. Subsequently, simulation tests are devised on the basis of these representative operating conditions to gauge the efficacy of the proposed design solution.

● Secondly, under typical operating conditions, the performance of various components, such as motors, slideways, rotary tables, sensors, and dampers, are evaluated by using design indicators and constraints to make preliminary selections. The spatial layout of the platform structure and the topological connection relationships between key components are then determined to form the configuration scheme of the mechanical system. During the modelling process, the primary flexible connections for slideways, rotary tables, and related support elements in the kinematic chain are modelled as spring-damped connections. Meanwhile, the primary structural elements are simplified to several rigid bodies with spring-damped combinations. Based on the parametric configuration scheme model of the mechanical system, a preliminary solution for the motion control system can be developed. This allows for the construction of an electromechanical model that considers the coupling between the mechanical and electrical systems.

● Based on the kinetic model and the electromechanical model of the conceptual solution, simulations are developed to analyse the structural dynamics, kinematic accuracy, and sensitivity of these properties to structural design factors. This sensitivity analysis helps to identify critical parameters and variables that have the most significant impact on the system's performance. By optimizing these critical parameters and variables, the proposed solution can be improved to meet the desired performance specifications. Thus, to ensure the final structural design variables and control parameters such as mass, stiffness, and joint position are obtained in a more reasonable manner. These variables and parameters are used to determine the design specifications for each key component and subsystem in following phases.

The next step is system design, which involves the characterization or product selection of key components and subsystems according to the design specifications set in the conceptual design phase.

● The behavioural characteristics of the key components and subsystems of the ultraprecision machine platform are studied to obtain a comprehensive understanding of the system's dynamic behaviour. These dynamic characteristics under ideal or rated operating conditions, such as the stiffness of

the air bearing under rated load and the equivalent servo stiffness of the drive motor under ideal performance conditions, are obtained through dynamic characterization using appropriate engineering software or experiments. The results can be used to optimize the design of the ultraprecision machine platform by identifying critical parameters and analysing the system's dynamic behaviour.

- When designing mechanical systems, finite element models of the main structural components are usually created first, and the necessary equivalents are made based on the dynamics. The structural deformations and displacements of the key elements of the overall mechanical system are analysed under the equilibrium condition of the rated load. Based on these, the results of the static and dynamic analysis of the main structural components and the system as a whole can be realized.

- During the design of motion control system, the crucial enabling tasks involve developing solutions for the drive, feedback subsystem, and controller. The structural factors that influence the drive and feedback subsystems comprised of inherent machining and mounting errors. Additionally, it is essential to consider the structural displacements, vibrations, and deformations that may occur during the operation. These factors play a significant role in the overall design and must be given due attention during the design phase.

- During the system design phase, it is essential to develop a comprehensive machine platform model that includes a variety of dynamic simulations. These simulations are designed to assess the solution's performance characteristics and design feasibility across different performance indicators. The use of dynamic simulations enables a rigorous evaluation of the solution's functionality, performance, and operability, thereby facilitating the identification of potential issues and the development of effective mitigation strategies.

- Compared to simulations conducted during the conceptual design phase, the design and simulation process of the detailed scheme is considerably more rigorous, and the results analysis is more comprehensive and detailed. The system solution design phase entails several iterations to refine and enhance the design of each essential component and subsystem continually. Any modification, improvement, or refinement made to the key components and subsystems necessitates timely updates to the entire system model, followed by simulations and analyses to evaluate the dynamic performance and feasibility. This iterative

process ultimately yields an ultraprecision machine platform design solution that meets the performance requirements and is reasonably feasible. The design characteristics of the components and subsystems in the solution must be detailed enough to provide the necessary design objectives and constraints for the subsequent detailed design of the manufacturing and processing-oriented subsystems and key components.

Finally, in accordance with the "evolution" of the UPM machine platform design process, a multiscale multiphysics integrated design approach incorporating design thinking should be implemented to address potential developments such as novel processes, system configurations, components, control strategies, analysis and equivalence methods, and system performance evaluation and diagnostic procedures that may emerge at any given time. The entire process should be effectively integrated and swiftly incorporated into subsequent design work. In order to achieve this, the system model should possess the capacity to integrate new entities and be adaptable to novel configurations and design processes.

3.3 Multiscale modelling and simulation for UPM machine platform

The system performance of UPM machine platform is sensitively influenced by parameters across multiple spatial scales, thus, developing design guidelines based on multiscale analysis and establishing a method system is a critical issue to address. UPM machine platforms possess unique structural characteristics that distinguish them from conventional machines. The thin fluid film bonding surface, which is formed by the fluid media between the structures, exhibits a certain stiffness and load capacity, which significantly influences the performance of the components, therefore, even small changes in the position, morphology, and bonding surface of the platform elements during operation can have a decisive impact on the overall machine performance. Despite this, there is currently no systematic approach to describe the relationship between the performance of the entire system, the key components, and the parameters of the interfaces. Moreover, there is a lack of analysis regarding the formation mechanism of the system-level performance, which hinders the establishment of system design methods based on the analysis of performance influencing factors. Consequently, the current design work of ultraprecision machine platforms is inadequate to meet the industrial challenges and demands on nanometric

movement and positioning.

3.3.1 Geometric modelling

The model presented below is an industrial case study of the JITRI UPTECH Co, Ltd., three-axis platform, which serves as a classic example of an UPM machine platform. It can be observed that such platforms typically comprise a frame structure, a granite base, multi-axis air bearing slideways and/or rotary tables, a direct drive system, a control system with encoders, and other components.

The frame structure provides rigidity and stability to the machine, while the granite base enhances its vibration damping properties. The multi-axis air bearing slideways and/or rotary tables facilitate smooth and precise movement of the machine components, and the direct drive system enables efficient and accurate power transmission. The control system with encoders ensures that the machine operates in a closed-loop system, allowing for accurate positioning and feedback control.
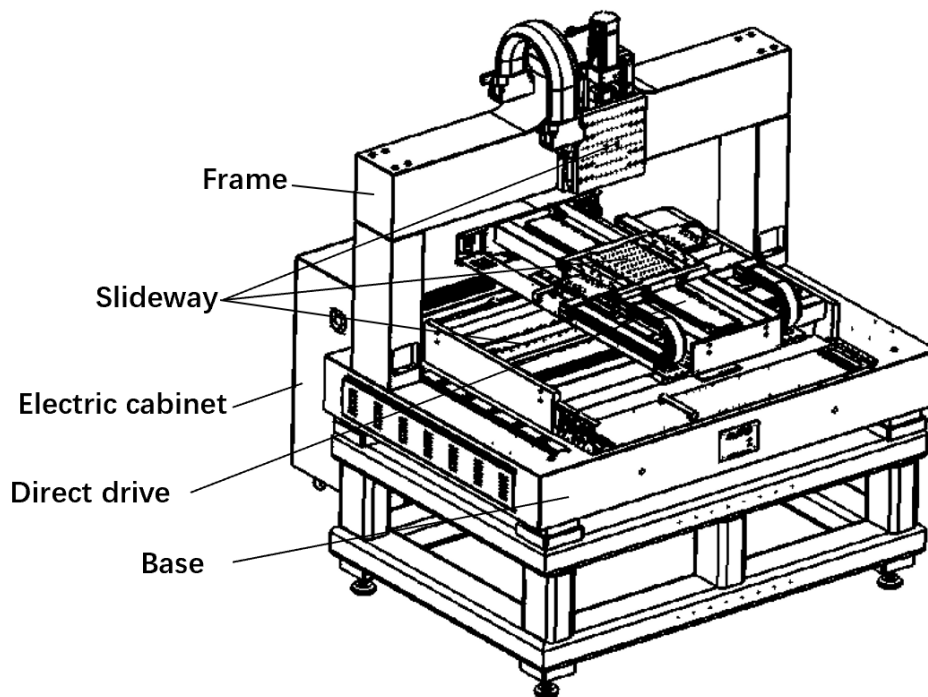
Figure 3.3 Example of 3 axis UPM machine platform

During the research and development (R&D) process, it is essential to evaluate the functional parameters of the machine and its components to ensure their performance meets the desired specifications. The functional parameters commonly evaluated include positioning accuracy, repeatability, straightness, and the Pitch/Yaw/Roll of

slideways. Additionally, the modal analysis, maximum load capacity, power transmission, and feedback resolution are also critical factors to assess. Of which the accurate and repeatable positioning, consistent straightness, and minimal deviation from the ideal motion trajectory are crucial for achieving high-precision machining, modal analysis and maximum load capacity determine the machine's ability to operate under various loads and conditions, power transmission efficiency and feedback resolution are vital parameters that influence the machine's overall performance, providing insight into the machine's power consumption, speed, and accuracy. Therefore, the assessment of these parameters is important in ensuring the quality and reliability of the machine and its components during the R&D process.

3.3.2 Multiscale modelling and simulation, and design work

One possible way to delineate spatial scale, as per prevailing mainstream perspectives, is shown in Figure 3.4:
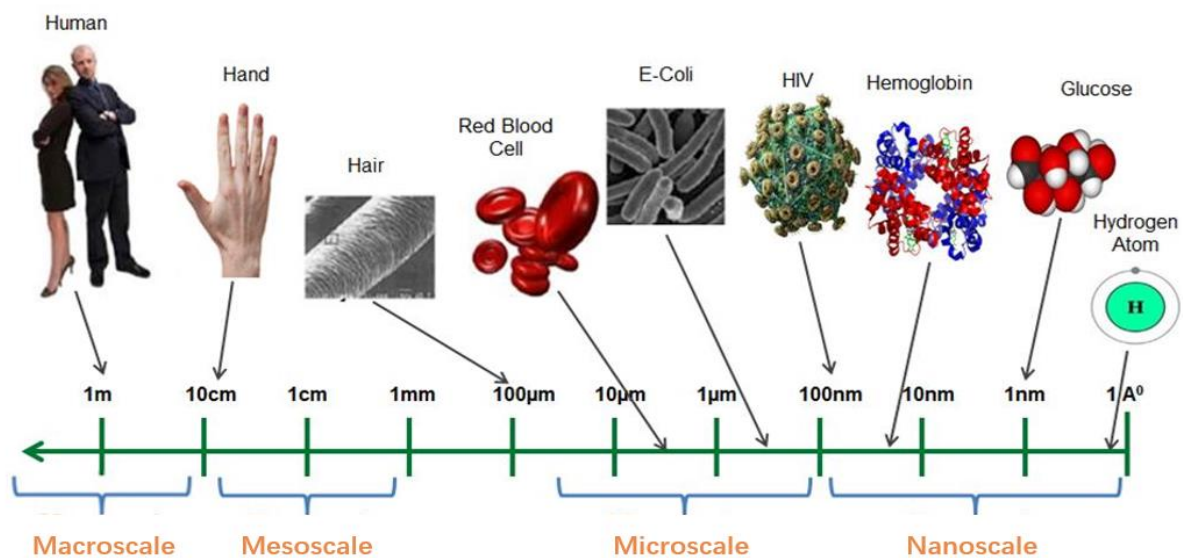
Figure 3.4 Examples of spatial scale

Figure 3.4 shows that the scaling of the components during the design of ultraprecision machine platform can be divided as follows.

- Macroscale: Based on the generic characteristics of UPM machine platform, the macroscale context is defined as the overall performance exhibited, including accuracy, stiffness, overall modals and other indicators of the complete machine, the defining of largest objectives can facilitate further scale refinement. On this

basis, the correlation analysis between these characteristics and the design variables is completed and thus obtain an optimised solution for overall performance.

- Mesoscale: According to the key characteristics, the main components of the machine platform are categorized into mesoscopic scales, which include the dimensional parameters of the stable/motion part, the shape and structure parameters of the base, column and frame, the parameters of joint elements, the speed, position and flatness accuracy of the motion mechanism, and the resolution of the monitoring and feedback devices.

- Micro/nano-scale: Compared to traditional motion systems, which rely on mechanical transmission components such as ball screws, ultraprecision machine platforms utilize fluid bearings to provide lubrication and establish a connection between stationary and moving parts. Due to the benefits outlined in the preceding chapter, the research of this thesis is centred on the investigation of aerostatic bearings. Therefore, the primary focus of this thesis is the micro/nano-scale objects, encompassing the factors that affect air film properties (including air film geometry, orifice parameters, and surface micromorphology), as well as the precision of manufacturing and assembly for each component.

3.4 Multiphysics integration for mechanical, electrical and control system

As shown in Figure 3.5, in addition to the multiscale design consideration, UPM machine platforms suffer the influence from multiple physical fields as well. The overall performance is contingent upon influential factors derived from various physical fields. Addressing distinct parameters within these physical fields necessitates the utilization of different tools for constructing specific design and analytical models. Thus the design process varies from different modelling method and physical calculation.
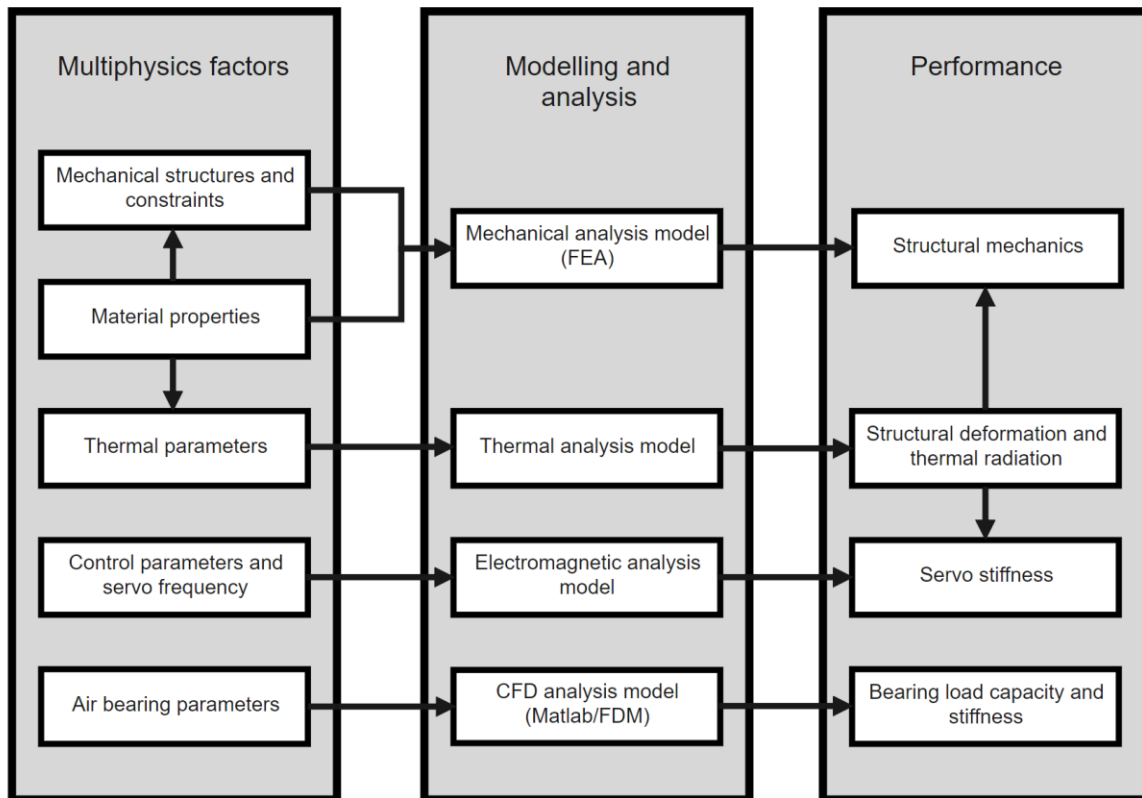
Figure 3.5 Multiphysics modelling and analysis approach of ultraprecision machine platform design

The related individual physics fields are:

● Basic mechanics including statics, dynamics and kinematics.

● Mechanics of solid body including mechanics of material, structure, elastic, plate and shell, plastic, fracture, vibration, and acoustics mechanics.

● Mechanics of fluid media including fluid dynamics, viscoelasticity.

● Electromagnetism.

● Thermodynamics.

● Signal processing and control algorithm.

Based on the above-mentioned individual physics, the multiphysics consideration including the coupling, interaction and integration between multiple physical fields involving fluid-structure interaction (FSI), magneto-mechanical coupling, and the integration of control system, signal input and encoder feedback. These factors generate effects in their respective scales/fields and simultaneously influence the overall platform performance as a synthesized complex system.

3.5 Multiscale multiphysics modelling and analysis method for UPM machine platform system

The UPM machine platform with aerostatic bearing motion components is a highly intricate and integrated system comprising physical structure components such as slideways and rotary tables, direct drive systems such as linear motors and encoders, and a control system consisting of industrial PCs and control algorithms. Its primary objective is to achieve positioning and movement functions with sub-micron level accuracy within a specified displacement range. The multiscale features of the UPM machine platform are evident in the platform's composition, accuracy, stiffness, and overall performance. Additionally, its multiphysics characteristics encompass mechanical structure, statics and dynamics, drive systems, structural mechanics, control logic, power transmission, and signal processing.

The overall performance of an UPM machine platform is functionally related to almost every factor mentioned above. As the position and state of the moving parts change, the characteristics lead the precision domain and the stiffness domain change as well. Thus, the structural configuration, material properties, topological connections and other structural factors, as well as the process parameters of key components such as air bearing and linear motors, will influence the multiscale and multiphysics characteristics of the overall performance of the machine platform.

Drawing on an analysis of the intricate interplay between diverse spatial and temporal scales and their respective impacts on function and performance, coupled with the establishment of effective stiffness and accuracy principles and the formulation of judicious design solutions, it is possible to achieve the design of UPM machine platforms possessing heightened accuracy, thereby better fulfilling the exacting demands of the manufacturing industry.

To this end, the design modelling framework for the UPM machine platform can be illustrated by Figure 3.6. The analysis of overall performance stems from modelling the influencing factors of various physical and scale fields. These factors based corresponding foundational concepts of physics and mathematics, employing pertinent analytical methodologies to systematically formulate a multiscale, multiphysics modelling and analysis framework. For instance, the bearing performance of a product is derived from fluid mechanics-based modelling and analysis of air bearings, while the dynamic performance of a product results from

employing multi-body dynamics modelling and analysis methodology.
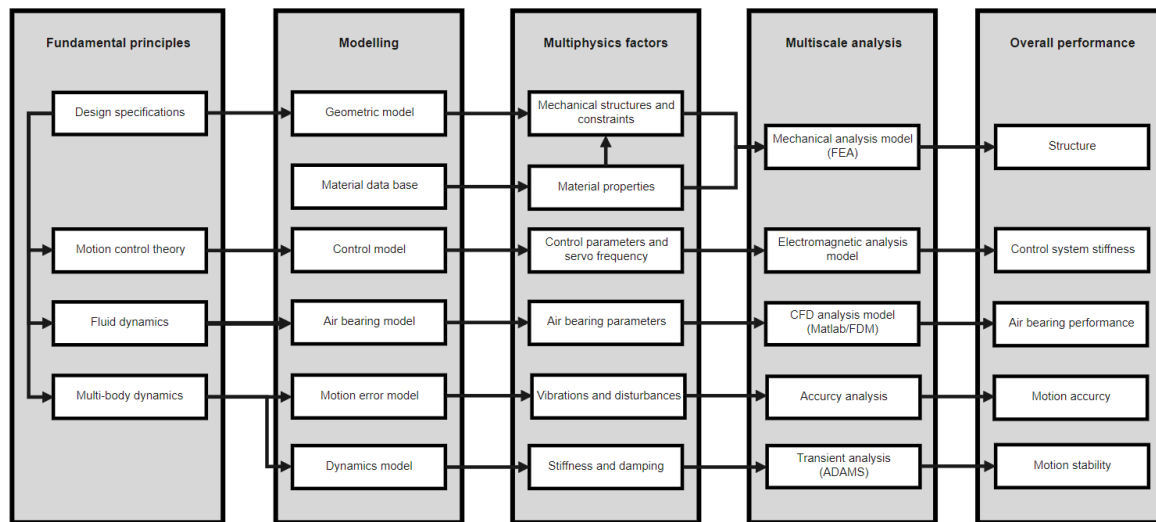
Figure 3.6 multiscale multiphysics modelling and design methodology for UPM machine platform

With the purpose of establishing a multiscale multiphysics design methodology for UPM machine platform, the modelling objectives can be classified into the following typologies:

- Geometric model: the geometric model, which constitutes a vital aspect of UPM machine platform design in both industrial and academic contexts, may take on various file formats. However, it necessitates parametric modelling to ensure that the geometric features can be extracted and utilized in subsequent analyses. Engineering software can be employed to generate the geometric model. The geometric parameters of the ultraprecision machines platform can be distinctly defined for all types of industrial or academic design.

- CFD model: the air film thickness of ultraprecision machine platforms typically ranges from 1 to 40 micrometres. This parameter can be leveraged to derive the air support force and flow field effect through the use of continuous fluid mechanics equations. Consequently, this approach can facilitate the analysis and calculation of time- and space-varying parameters, including but not limited to the load carrying capacity and related coefficient, static stiffness, flow rate, and air consumption. Fluid dynamic models, such as those for aerostatic bearing slideways, rotary tables, spindles, or air load pads, can be simulated using various engineering software packages (e.g., COMSOL[TM] MULTIPHYSICS, Abaqus[TM][92],

AnsysTM[91]) or mathematical programming tools.

● Control and drive models: Mathematical models for UPM machine platform can be constructed through various approaches such as transfer functions and state space methods. Alternatively, advanced computer software tools such as MATLAB Simulink can offer accurate visualization and simulation capabilities with configurable modules. Moreover, the interaction between the control system and mechanical system can be explicitly encoded using multi-body dynamics software such as ADAMS. Theoretically, ultraprecision machines exhibit diverse control logic and algorithms, necessitating the development of specific control models for each platform. However, given that the mechanism fundamentally entails the transmission of command signals such as position, velocity, and acceleration, the interface data can be regarded as universal.

● Kinematic error models: the designed UPM machine platform can be defined as a multi-body kinematic system. Thus, kinematic error can be simulated by programmable implementations, engineering software or using approximate model.

● Dynamic model: based on rigid-flexible coupled multi-body dynamics, the dynamical model can be simulated using software such as Dynamic Analysis and Design System (DADS) or ADAMS.

3.6 Multiscale multiphysics approach combining with digital twin

As discussed in the previous chapters, the DT is utilized as a comprehensive life-cycle monitoring process that integrates data from physical models, sensors, and cloud databases, among others, in order to facilitate multi-disciplinary, multi-physical, and multiscale simulations. In essence, it is a digital system that encompasses one or more critical and interdependent subsystems.

The development of a DT for an UPM machine platform involves several key stages, including concept definition, structure formation, and fine-tuning to ensure optimal performance. The concept phase typically involves rapid multidisciplinary simulations to quickly validate solutions, while the formation stage focuses on determining the key technical parameters of the DT via physical simulations. Since the real machine platform remains an indeterminate design at this stage, these simulations are crucial

in defining the final design. The fine-tuning process involves optimizing the DT during the early stages of usage, leveraging its reconfigurability and flexibility to achieve optimal results. The integration of DT into the design and analysis of ultraprecision machine platforms offers significant benefits, including optimization of physical commissioning costs and operational performance. The designed DT can be used for optimal control, diagnosis, and prediction in subsequent life cycle activities, providing a valuable tool for enhancing efficiency and reducing downtime.

To achieve an effective DT modelling approach for ultraprecision machine platforms, a geometry, logic, and data-based approach should be employed, encompassing mechanical, control, and electrical systems, as depicted in Figure 3.7:
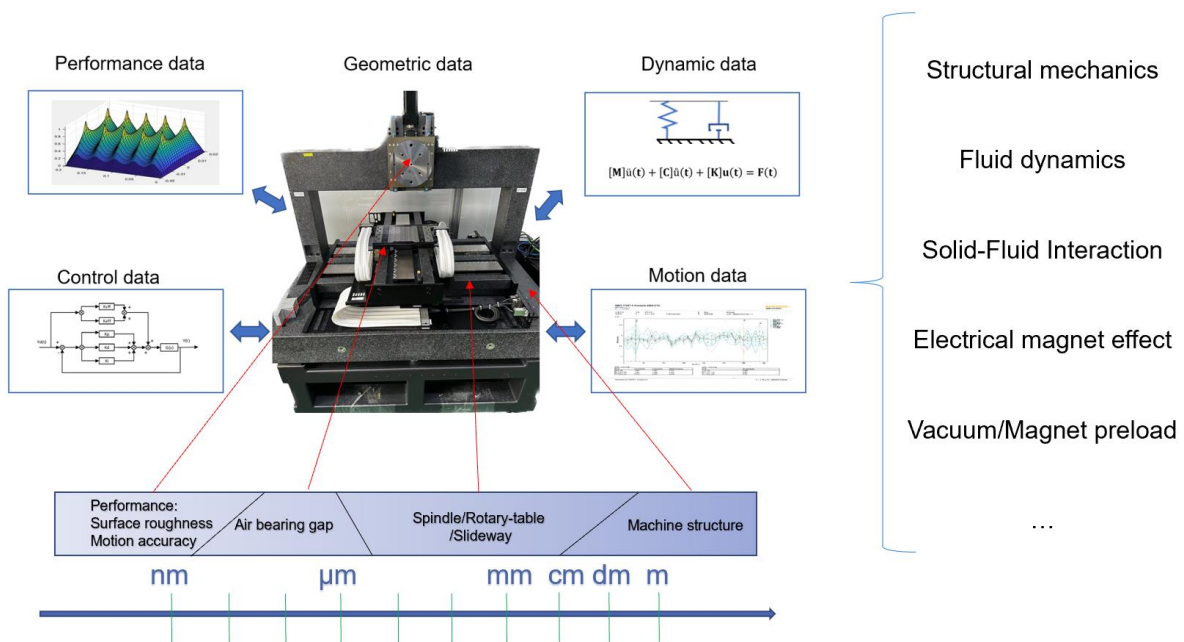
Figure 3.7 Multiscale multiphysics approach combining with DT modelling for UPM machine platform

As expounded above, subsequent to the construction of the multiscale multiphysics virtual model as described in the preceding section, all pertinent data including geometric properties, performance data, and control parameters will be amalgamated and integrated into the virtual realm and imparted to an exact 1:1 replica (twin) of the physical entity. The DT model is used in mirroring the physical machine platform with regards to its geometry, material properties, control logic, and further evinces the

assembly relationships, static properties, and crucial performance indicators of the physical platform.

The specifics of the construction and application of DT technology shall be explicated in subsequent chapters.

3.7 Summary

This chapter presents a systematic methodology for the modelling, design, and analysis of UPM machine platforms using a multiscale multiphysics approach. Firstly, a hierarchical classification of spatial scales is defined, and the physical fields and their associated influence factors involved in the design process are specified. Then, the design objectives of the UPM machine platform are defined, and guidelines for modelling and simulation are established to enable multiscale modelling and physical field coupling. In summary, a multiscale multiphysics integrated design method is presented, highlighting the role of DT technology plays in the design and analysis process of UPM machine platforms. The objective of this methodology is to provide theoretical and methodological support, as well as an analysis environment, for the subsequent chapters.

In addition to the motion accuracy, load capacity, and stiffness properties detailed in this chapter, the performance of an UPM machine platform necessitates further examination of the impacts of thermal, vibration, and noise phenomena in order to establish a comprehensive multiscale multiphysics integrated system. To accomplish this, modal analysis results can be imported into acoustic analysis software to enable noise analysis and optimization. By supplementing the predictive analysis of vibration and noise performance, the design methods for UPM machine platforms can be further refined, resulting in a more thorough guide for the designer and a richer practical data. In order to validate the efficacy of this methodology, the experimental trials in this thesis will involve conducting tests to accurately evaluate the platform's motion accuracy and stability. This analysis will provide valuable insights into the true capabilities of the platform.

Chapter 4   Multiscale multiphysics modelling and analysis method in design and development of aerostatic bearing slideway and its digital twin

4.1 Introduction

As the key component of UPM machine platform, aerostatic bearing slideways have been increasingly applied in the precision engineering industry and other high-tech sectors over the last decades, due to their considerable advantages over conventional slideways in terms of high motion accuracy, high speeds, low friction, and environment-friendly operations. However, new challenges in aerostatic bearings design and analysis have been occurring and often imposed along the journeys. An industrial-feasible approach for the design and development of aerostatic bearing slideways as standard engineering products is essential and much needed particularly for addressing their rapid demands in diverse precision engineering sectors, and better applications and services in a continuous sustainable manner.

For precision and ultraprecision machines, however, the factors and features from the machine itself, the component metalogical surface or tolerance, and the machine assembly clearance in multiple scales will have effects not only on themselves, but also collectively on the performance of the entire machine. Therefore, as the machine performance and precision are ever increasing, it is essentially important to develop a multiscale modelling and analysis-based approach for design and development of high precision machines, particularly for overcoming the limitations in design and building of the machine systems for generating nanometric surfaces on an industrial scale. Furthermore, such an approach combining with digital twin will likely lead to continuous improvement of the performance of the machine system in operations and services, as well as their design and development in a predictable, producible, and highly productive manner in the competitive engineering marketplace. The multiscale multiphysics modelling and analysis and the associated simulation development can be the kernel of the digital twin, which cover the mechanical design, direct drive and control, dynamics tuning of the slideway, and their entire mechatronic system integration. With the approach and implementation of DT, the performance of an aerostatic bearing slideway can be predicted and assessed in the process.

This chapter presents the multiscale multiphysics modelling and analysis-based approach for design and development of the aerostatic bearing slideways and its digital twin. The development of multiscale modelling and simulation for the aerostatic bearing slideway is presented firstly while focused on the key influence factors working at different scales in particular, e.g., the effect of air film thickness in the microscale, orifices' parameters, pattern and distribution in mesoscale, the slideway structure in macroscale, and the slideway's application performance as a whole. Then simulation development with COMSOL™ MULTIPHYSICS is described to analyse the static performance of the slideway. Furthermore, through the simulations on a linear motor control system for the aerostatic bearing slideway with MATLAB™/SIMULINK integrated with COMSOL™, the dynamic performance of the slideway designed is explored and further analysed. These simulations are used as the kernel for further developing the digital twin system of the slideway. Finally, this chapter is concluded with further discussion on implementation perspectives of the digital twin system, and their application potentials. Overall, the implementation perspectives for the sideway digital twin are presented and discussed in steps. The digital simulations and digital twin system can be fundamentally important for continuously improving the design and development of aerostatic bearing slideways, and their applications and services in the context of industry 4.0 and beyond.

4.2 Design of the aerostatic bearing slideway and its digital twin

Aerostatic bearing slideways are an important industrial application of fluid lubricated bearing technology, which rely on a high-pressure external air source to generate appropriate lubrication and load support. The principle of aerostatic bearing slideways is based on the generation of an air film between the moving part, which is driven by a linear motor, and the stationary part. This thin air film acts as a lubricant during relative motion, and is created by numerous orifices in every direction on the slide surface, as shown in Figure 4.1.

Compared to other lubrication materials like oil, compressed air lubrication offers the main advantage of very low friction, which is almost zero at low speeds. Although the stiffness of air film is lower than fluid or solid, it however generates less heat and surface adhesion, thus providing the slideway with an extremely long service life and

low damping ratio. As a result, air bearing slideways can compete favourably with other slideway types in ultraprecision machining applications, where high dimensional precision and surface quality are essential.
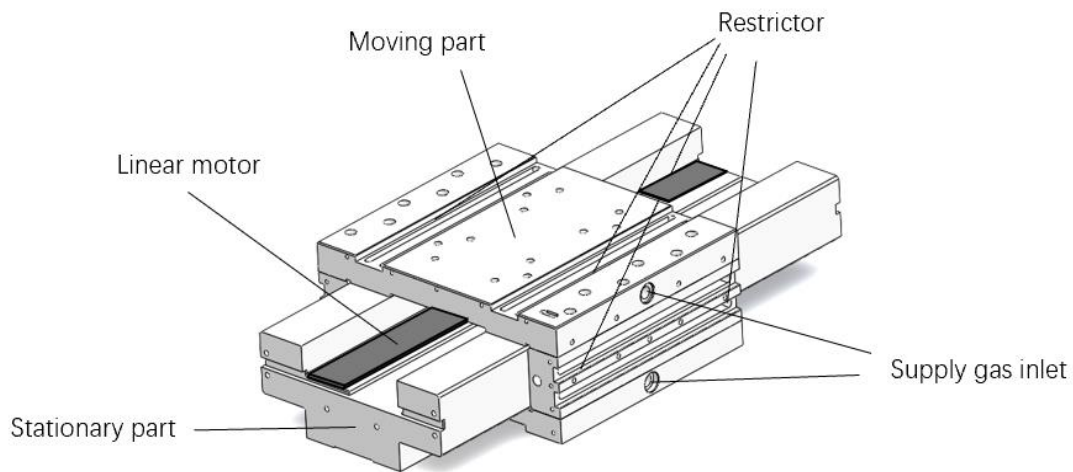
(a)
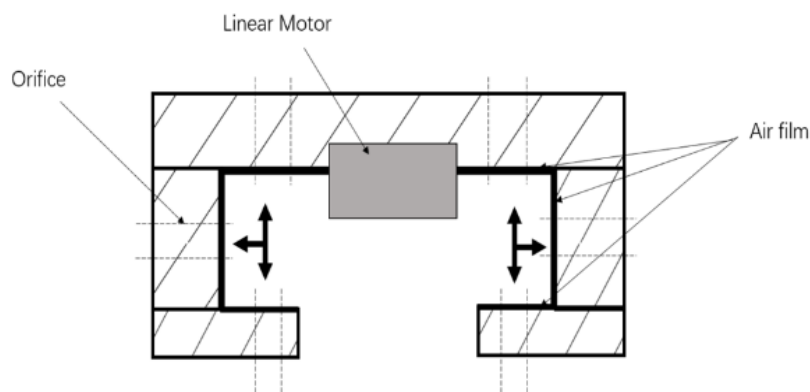
(b)

Figure 4.1 The aerostatic bearing slideway designed: (a) key components; (b) Schematic illustration.

In application scenarios, the static performance of aerostatic bearing slideway is critically important. As the density of air is very low, the lubricating air film thickness or internal clearance within an aerostatic bearing slideway must be kept in micron level, so that a reasonable working pressure can be maintained within the slideway, and the air consumption can be kept down to an acceptable level due to economic consideration. The recognized reasonable air film thicknesses are in the 5–40 µm range[35], with such small clearances, every small deviation or change in parameter will have great influence on the performance of the slideway.

Figure 4.1 also illustrates the aerostatic bearing slideway designed and developed by the author's team in cooperate with industrial partner. The parameter of each part, the layout, amount, diameter and pattern of the orifices, the supply pressure of air and the thickness of the air film will affect the static stiffness and load capacity of the slideway on various scales; details of these influence factors will be discussed in subsequent sections.

In order to achieve and maintain extremely high accuracy and stability in different working environments, the control system of aerostatic bearing slideway products often needs to be tuned before and after work, thus, in order to provide an appropriate solution, this study aims to discuss the integrated approach combining multiscale modelling-based simulation and digital twin technology in the development and design of an aerostatic bearing slideway. As an important part of the German "Industry 4.0" national strategic initiative, digital twin technology uses a physical model, sensor update, operation history, and other data to integrate a multi-disciplinary, multi-physical, multiscale simulation process to complete the "twin" in virtual space, so as to reflect the status of corresponding "physical twin" in real time. Currently, it is widely used in product design, medical analysis, engineering construction, and other fields.

In this study, the optical encoder is used as an in-process monitor to realize the data transmission between digital and physical slideway, it transports feedback signals of the dynamic characteristics such as the position and velocity of the moving part in real time, so as to realize the remote monitoring, adjustment, and even error prevention of the aerostatic bearing slideway.

In the very first development stage, the digital twin consists only of an exact CAD representation of the aerostatic bearing slideway. The air film is regarded as rigid with solid size. Next stages include the combination of finite element method and transfer function in order to accurately simulate the entire aerostatic bearing slideway's static and dynamic performance, and the function of remote monitoring and tuning are realized with the help of an in-process monitor and related algorithms. In following sections, details of the simulation work, which are developed in the collaboration with Solidworks, CFD, FDM and SIMULINK module of COMSOL^{TM} MULTIPHYSICS and MATLAB^{TM} will be discussed separately.

4.3 Multiscale modelling applied to the aerostatic bearing design and analysis

In order to build the appropriate multiscale modelling, it is necessary to discuss the influence factors in different scales. For modelling challenges across various scales, the computational demands vary significantly. As the precision aerostatic bearing slideway serves as a core component of the UPM machine platform, ensuring adequate accuracy across all scales within its modelling is imperative. Modelling features at the micron scale, such as air films or orifices, exhibit computational requirements orders of magnitude in 10^4 level, but still thousand times less than the modelling for overall slideway. Thus, establishing a scientific approach for multiscale modelling is profoundly crucial.

The equations and theories have been divided into different length scales against the computational magnitude (degree of freedom) as illustrated in Figure 4.2. Those fundamental theories and the associated implementation approaches are used to solve both scientific and industrial problems. The following description attempts to discuss the influence factor to the slideway's performance of each scale.
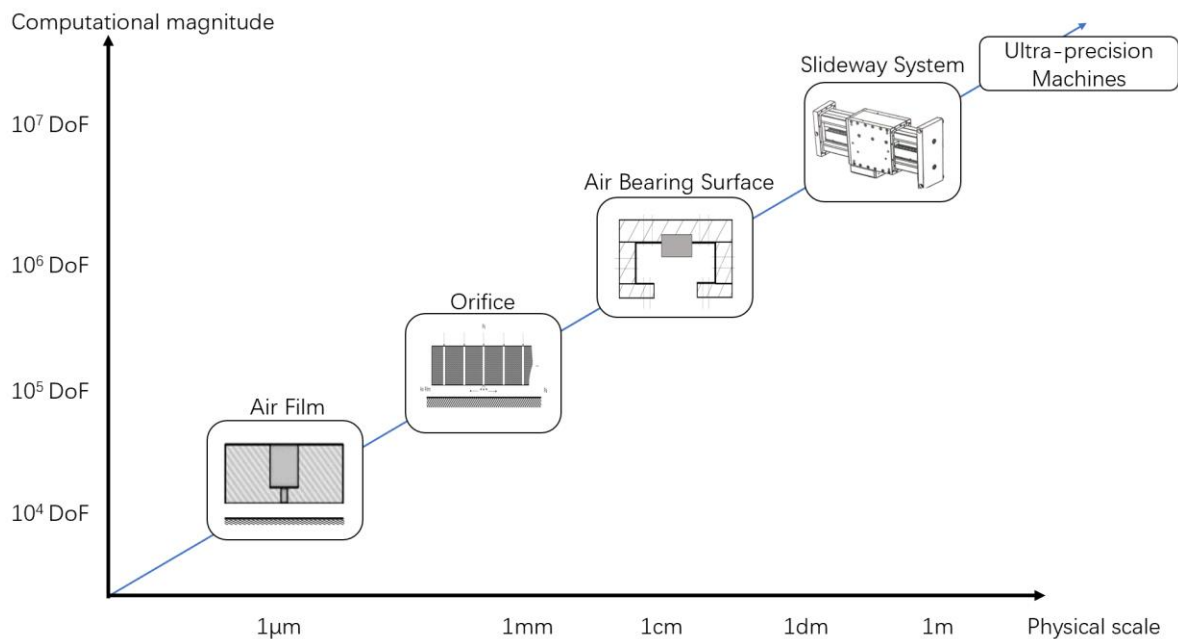
Figure 4.2 Different scales against the computational magnitude

The performance of aerostatic bearing slideway can be roughly divided into two types: static performance and dynamic performance. The static performance refers to the mechanical characteristics of the slideway in working environment, including air bearing load capacity, stiffness, and the volume of gas flow. The dynamic performance

refers to the non-steady state of the slideway, including motion accuracy, stability, response speed. Since these two kinds of performance are reflected in different physical systems, they will be discussed separately.

4.3.1 Modelling at Macroscale

The design and simulation in macroscale focus on the overall performance of the aerostatic bearing slideway. In this study, gas is defined as incompressible fluid, so it follows the law of conservation of mass, conservation of momentum, liquid continuity, and continuum mechanics. The load capacity of a slideway can be obtained by integrating the pressure of the entire air film surface. The related calculation formula is:

$$W_0 = \int_A (p - p_a)dA \qquad (4\text{-}1)$$

where:

W_0- the load capacity of a gas film surface;

A- the surface area of air film;

p- the pressure distribution; and

p_a- the atmospheric pressure.

The static stiffness of a slideway illustrates the extent of change in the load capacity when the air film thickness changes under an applied load, which can be calculated by：

$$K_0 = \frac{W_1 - W_2}{\Delta h} \qquad (4\text{-}2)$$

where:

K_0- the static stiffness of aerostatic bearing slideway;

W_1, W_2- the load capacity with different air film thickness;

Δh- the change of film thickness.

Meanwhile, the air flow volume can be calculated by:

$$Q = \int_A \rho v dA \qquad (4\text{-}3)$$

where:

Q- the air flow volume;

ρ- the density of air;
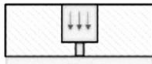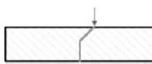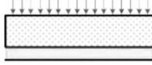
v- the velocity of air; and

A- the area of export border.

4.3.2 Modelling at Mesoscale

Several studies have discussed the influence of restrictor on the load capacity and stiffness of an aerostatic bearing slideway in mesoscale; for example, Gao et al. showed the relationship between the type of restrictor and the air film performance under a certain supply pressure[16], as shown in Table 4.1. In this study, due to the consideration of technical, economical and practical consideration, the annular orifice is studied as the initial choice due to its low manufacture difficulty and low risk for 'pneumatic hammer'. The influence factors like diameter, pattern structure, and amount of the selected orifice type are discussed separately in the following sections.

Table 4.1 Characteristics of different types of restrictor type[16]

Restrictor Type	Load Capacity	Stiffness	Stability	Gas Consumption	Manufacture
Annular orifice	Low	Low	Fair	Small	Easy
Simple orifice	High	High	Poor	Small	Easy
Slot	Medium	Medium	Good	Large	Medium
Groove	High	High	Good	Medium	Hard
Porous	High	High	Excellent	Large	Hard

4.3.3 Modelling at Microscale

In micrometer – millimeter scale, the static performance of aerostatic bearing slideway is mainly influenced by the parameters of air film. The operating principle of orifice aerostatic bearing slideway is shown in Figure 4.3, the air film thickness h0 is normally about eight times smaller compared with the dimension of human

hair, nevertheless, it still plays an important role in improving the load capacity and motion stability of the entire machine tool.
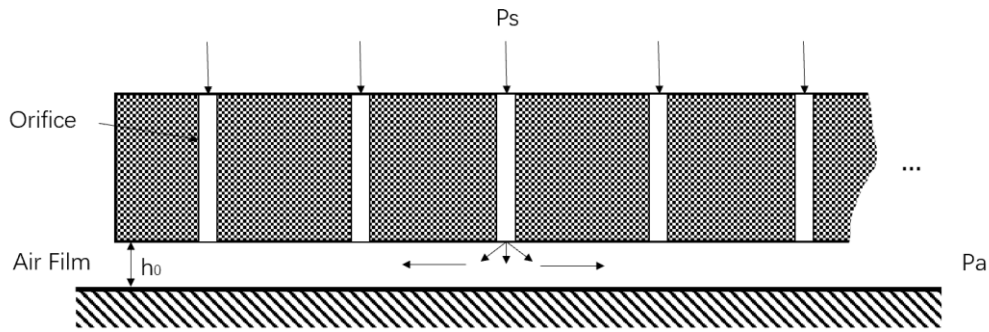
Figure 4.3 Operating principle of annular orifice aerostatic bearing slideway

As a classic equation that describes the pressure distribution of compressible viscous fluid, the Navier–Stokes equation is here introduced:

$$\rho \frac{du}{dt} = \rho f_x - \frac{\partial P}{\partial x} + \frac{\partial}{\partial x}\left\{\mu\left[2\frac{\partial u}{\partial x} - \frac{2}{3}\left(\frac{\partial u}{\partial x} + \frac{\partial v}{\partial y} + \frac{\partial w}{\partial z}\right)\right]\right\} + \frac{\partial}{\partial y}\left[\mu\left(\frac{\partial u}{\partial y} + \frac{\partial v}{\partial x}\right)\right] + \frac{\partial}{\partial z}\left[\mu\left(\frac{\partial u}{\partial z} + \frac{\partial w}{\partial x}\right)\right]$$

$$\rho \frac{dv}{dt} = \rho f_y - \frac{\partial P}{\partial y} + \frac{\partial}{\partial y}\left\{\mu\left[2\frac{\partial u}{\partial y} - \frac{2}{3}\left(\frac{\partial u}{\partial x} + \frac{\partial v}{\partial y} + \frac{\partial w}{\partial z}\right)\right]\right\} + \frac{\partial}{\partial z}\left[\mu\left(\frac{\partial v}{\partial z} + \frac{\partial w}{\partial y}\right)\right] + \frac{\partial}{\partial x}\left[\mu\left(\frac{\partial u}{\partial y} + \frac{\partial v}{\partial x}\right)\right] \quad (4\text{-}4)$$

$$\rho \frac{dw}{dt} = \rho f_z - \frac{\partial P}{\partial z} + \frac{\partial}{\partial z}\left\{\mu\left[2\frac{\partial u}{\partial z} - \frac{2}{3}\left(\frac{\partial u}{\partial x} + \frac{\partial v}{\partial y} + \frac{\partial w}{\partial z}\right)\right]\right\} + \frac{\partial}{\partial x}\left[\mu\left(\frac{\partial u}{\partial z} + \frac{\partial w}{\partial x}\right)\right] + \frac{\partial}{\partial y}\left[\mu\left(\frac{\partial v}{\partial z} + \frac{\partial w}{\partial y}\right)\right]$$

where:

ρ- Air density;

u, v, w- Velocity of air in x, y, z directions;

f_x, f_y, f_z- External body force;

μ- Dynamic viscosity.

Sun, Chen and Cheng presented Equation (4-5) to calculate the pressure distribution between two parallel plates in 2005[131]; it is based on the Navier–Stokes equation, continuity equation and ideal gas law. Since these mathematical models are not able to be solved accurately in most cases, researchers have developed many approximate methods of which one-dimensional analytic method is usually used. Figure 4.4 illustrates the simplified model of one-dimensional air flow in an aerostatic bearing slideway.
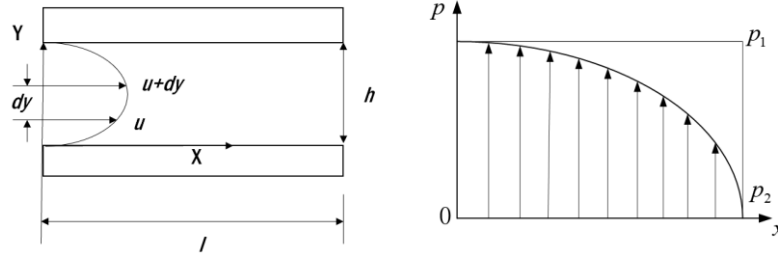
Figure 4.4 One-dimensional model of the parallel plates

According to the study of Sun et al.[131], based on the one-dimensional assumption, Reynolds equation can be simplified as:

$$\frac{\partial p}{\partial x} = \mu \frac{\partial^2 u}{\partial y^2}$$

$$\frac{\partial p}{\partial y} = 0 \qquad\qquad (4\text{-}5)$$

$$\frac{\partial p}{\partial z} = 0$$

Supposing the clearance between two parallel plates is h, and then the boundary conditions are:

$$y = 0, \ u = 0;$$

$$y = h, \ u = 0. \qquad\qquad (4\text{-}6)$$

Insert the ideal gas law equation:

$$\rho = \frac{p}{RT} \qquad\qquad (4\text{-}7)$$

where:

T- the temperature;

R- the gas constant;

Omit the mathematical deviation process, the final formula of the pressure distribution is:

$$p_x^2 = p_1^2 - (p_1^2 - p_2^2)\frac{x}{l} \qquad\qquad (4\text{-}8)$$

As a short conclusion of this section, mathematical and geometrical models have been established at three different scales, which aim to discuss the influence parameters and factors of the designed aerostatic bearing slideway on the static performance at every single scale. The establishment of multiscale models can clearly show the design concerns of aerostatic bearing slideway product at various scales and provide a theoretical foundation for subsequent simulations.

4.4 Simulations development: results, analysis and discussion

4.4.1 Simulation on static performance with MATLAB based algorithm

As outlined in Chapter 2, the FDM is a widely used mathematical approach CFD due to its simplicity, flexibility, and versatility. It can be easily implemented on a computer, making it one of the common and mainstream tools for solving CFD problems. MATLAB as a powerful numerical computing tool with matrices as the fundamental unit, offers a highly integrated and versatile system. Leveraging MATLAB to program FDM algorithms for solving the Reynolds equations in aerostatic bearing slideways enables rapid simulation of the static performance of air bearings and streamlines the modeling process. Moreover, the implementation of a customized interface, generated by coding the corresponding Graphical User Interface (GUI), facilitates fast and model-free calculations by entering key parameters. Parts of the GUI are presented in Figure 4.5, and the complete MATLAB algorithm code is appended to this thesis.
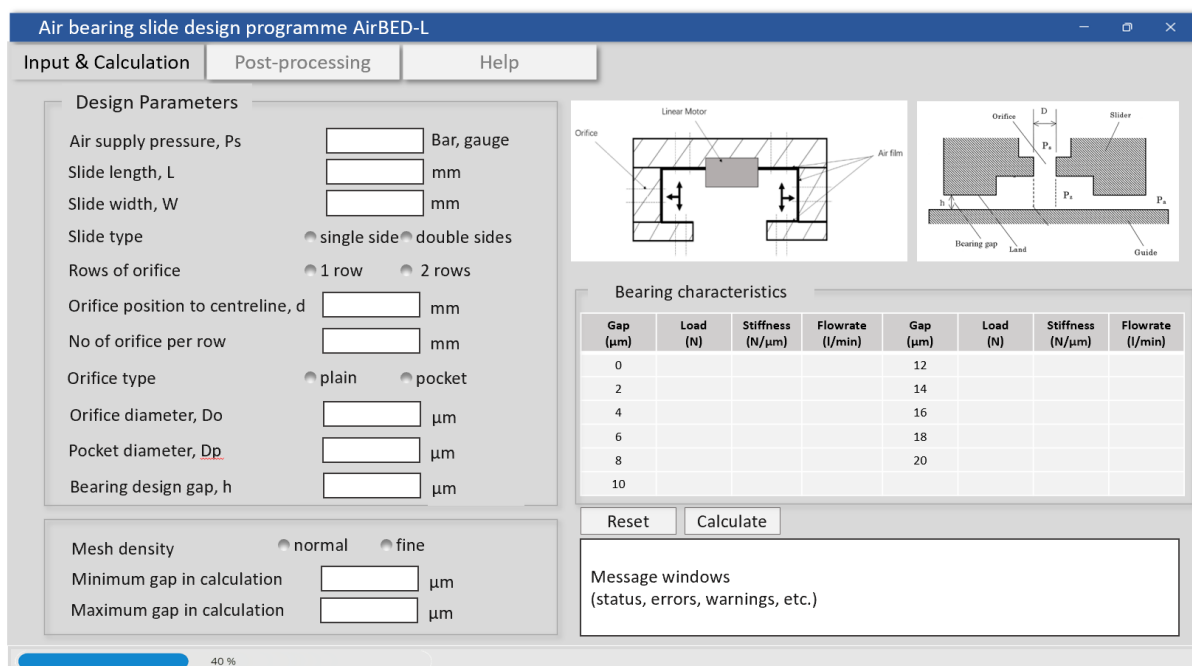
Figure 4.5 GUI of the MATLAB FDM algorithm for aerostatic bearing slideway design

Since the algorithm is written in MATLAB programming environment, every function listed in Figure 4.5 is realised by code and command, furthermore, the GUI developed provides an intuitive Human-Machine Interface (HMI), other users can thus run the simulation without any programming ability.

Start	→	Input bearing design data	→	Define mesh size and adjust orifice positions to fit mesh

Solve Reynolds' equation and obtain pressure distribution for the air film	←	Initialization of pressure field across the air film

Postprocessing	←	Balance air flows and calculate total load/mass flow	→	Plot results	→	End
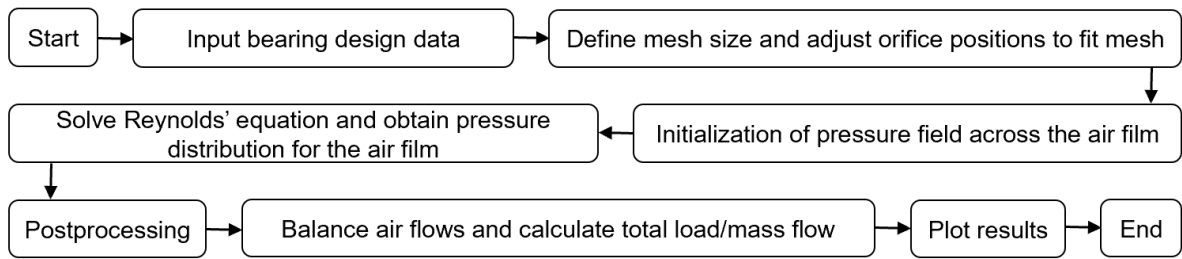
Figure 4.6 Flow chart of FDM calculation of MATLAB algorithm

As illustrated in the process flow chart in Figure 4.6, in this MATLAB algorithm the pressure distribution of fluid media along the workpiece surface is calculated first by solving Reynolds' equation. Then based on this, the load capacity and static stiffness for air bearing are calculated and displayed in plots. The calculation result is shown in Figure 4.7.

(a)

(b)　　　　　　　　　(c)
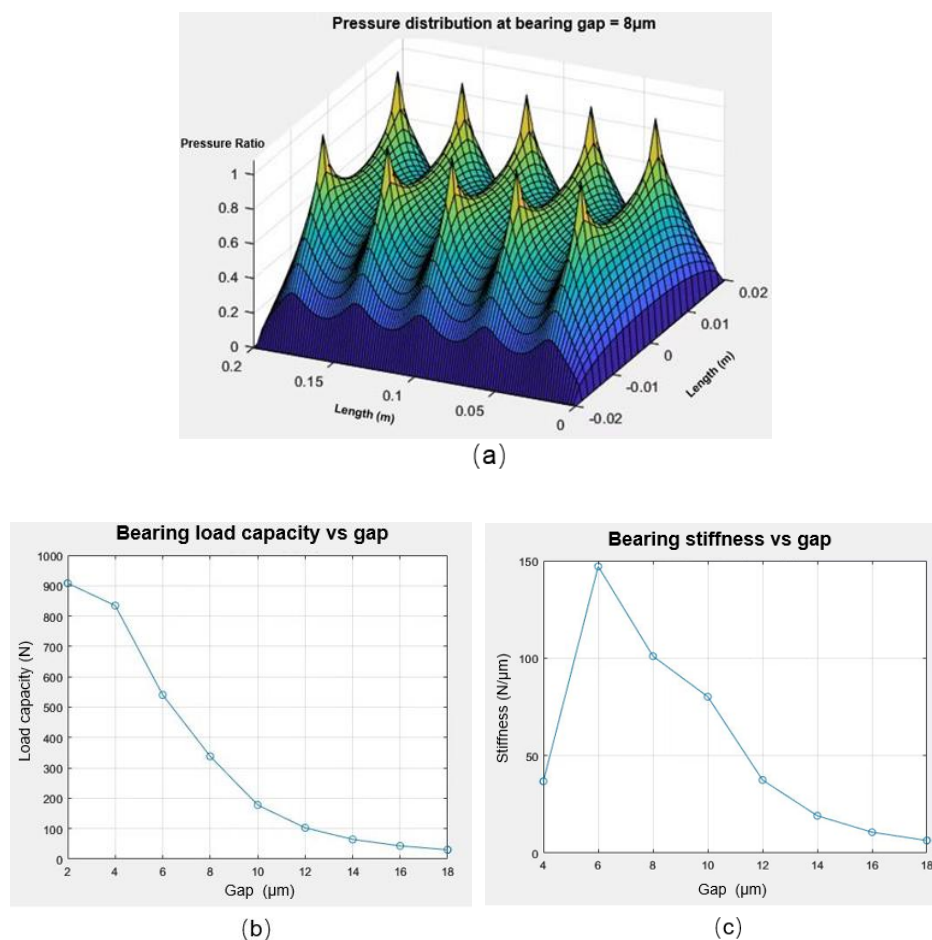
Figure 4.7 Example of calculation results

(a) Pressure distribution at bearing gap 8μm;

(b) Bearing load capacity; (c) Bearing stiffness

The input parameters are:

Inlet pressure Ps: 0.5 Mpa

Bearing length BLEN: 200mm

Bearing width BWID: 40mm

Rows of orifice NROW: 2

Distance of orifice row from bearing center DJET: 10

Number of orifices in every row NJET: 5

Orifice diameter D0: 0.06mm

It can be seen from Figure 4.7 that the pressure distribution and performance curve fit the characterization of laminar phenomenon well. The values are as well in a reasonable range which can be validated by equation 4-8.

The limitations of the developed MATLAB algorithm, such as workload, mesh density, and imprecise experience coefficient, constrain its function and accuracy. Nonetheless, its significance lies in providing comparative data for the simulation outcomes of commercial engineering CAE software, where the underlying algorithm and calculation logic are proprietary and inaccessible to the public.

4.4.2 Simulation on static performance with COMSOL™ MULTIPHYSICS

As a powerful and readily available cross-platform finite element analysis solver, and multiphysics simulation software, COMSOL™ is able to simulate, calculate, and analyse the flow of media in an arbitrary geometry. In this study, the CFD module of COMSOL is used to simulate the pressure distribution and load capacity of the air film surface. With the appropriate setup of simulation, the static performance of aerostatic bearing slideway is predictable in advance. The calculation of the CFD module of COMSOL™ is based on equations 4-9, 4-10 ,4-11, and Figure 4.8 shows the calculation process with a flow chart:

$$\rho(\mathbf{u} \cdot \nabla)\mathbf{u} = \nabla \cdot [-p\mathbf{l} + \mathbf{K}] + \overbrace{\mathbf{F}}^{\text{External Force}}$$

$$\underbrace{\phantom{\nabla \cdot [-p\mathbf{l} + \mathbf{K}]}}_{\text{Internal and External pressure}}$$

(4-9)

$$\rho\nabla \cdot \mathbf{u} = 0 \tag{4-10}$$

$$\mathbf{K} = \mu\big(\nabla\mathbf{u} + (\nabla\mathbf{u})^T\big) \tag{4-11}$$

Where:

ρ: fluid density;

$\mathbf{u}$: velocity vector;

∇: gradient;

p: pressure;

$\mathbf{l}$: identity matrix;

$\mathbf{K}$: viscous stress tensor;

$\mathbf{F}$: volume force vector;

μ: dynamic viscosity of fluid media;

T: absolute temperature;
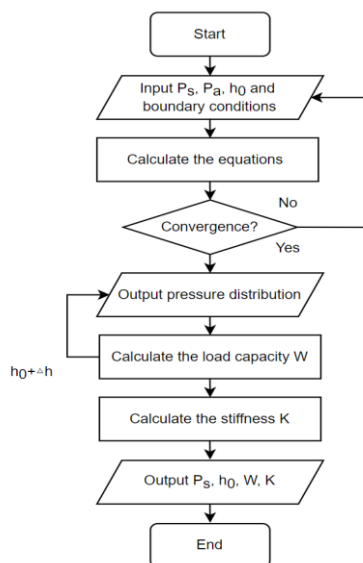
Figure 4.8 Calculation process of COMSOL™ CFD model

The implementation of COMSOL™ in the static performance simulation for aerostatic bearing slideway can be summarized in Figure 4.8. In compared with the self-developed MATLAB™ algorithm, COMSOL™ is a commercial engineering software with high maturity, thus makes the underlying algorithms not visible to end-user. So considering the COMSOL™ as a "black box" with input and output interface, the simulation process can be roughly shown in Figure 4.9:
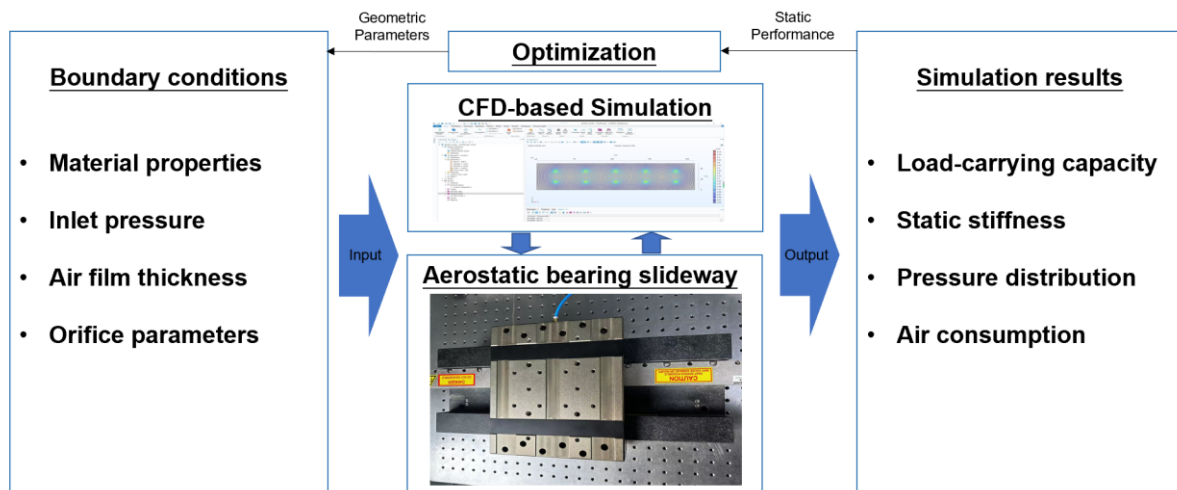
Figure 4.9 Methodology illustration of aerostatic bearing performance simulation

4.4.2.1 Software setup

Figure 4.10 is a screenshot of the COMSOL™ modelling and simulation interface after modelling.
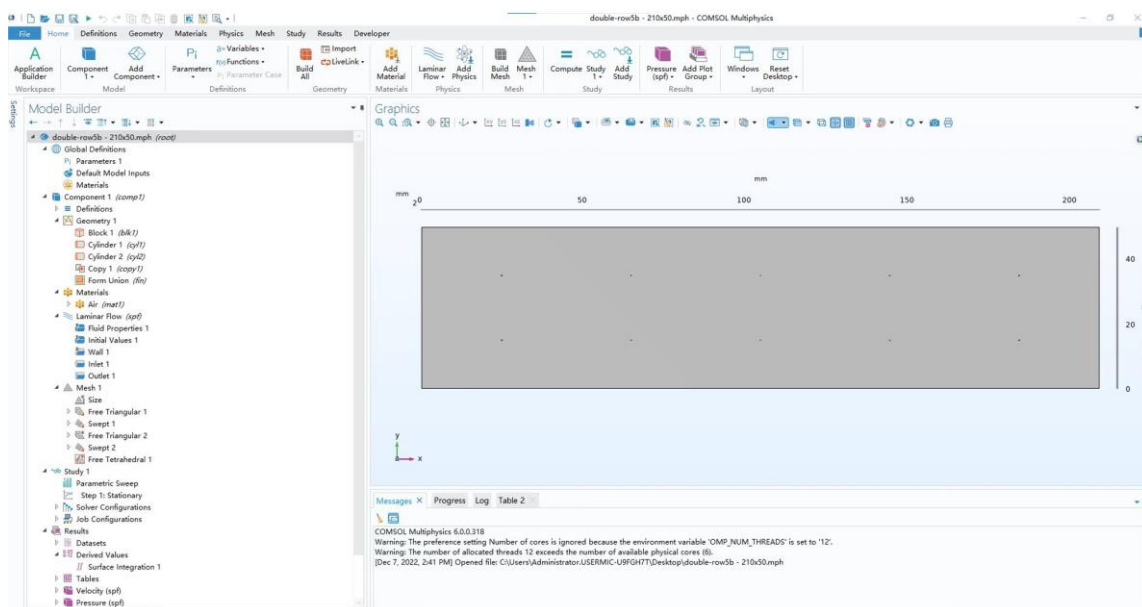
Figure 4.10 COMSOL™ modelling and simulation interface

The model setup proceeds in accordance with the left panel from top to bottom. Initially, the geometry of the aerostatic bearing is approximated as a rectangular film with cylindrical orifices. Subsequently, the physical field of fluid dynamics is incorporated, whereby the airflow within the aerostatic bearing is deemed to exhibit laminar flow characteristics. To specify the boundary conditions, the following list of selections is provided, each of which is appropriately labelled:

- Fluid properties: The fluid is defined as normal air and the related density, viscosity, thermal capacity can be read directly from the material data base.

- Walls: Select the fluid domain in which the simulation will run.

- Inlet and outlet: Define the property of pressurized air and the air flow path.

- Mesh: The model span from serval micrometres to hundreds of millimetres, so mesh must be created with different method in different domains. Orifice meshing is realized by "sweep" the upper surface 10 times and the mesh in air film thickness domain are also swept at least 5 times, thus to ensure the calculation accuracy. The remaining meshing is handled by COMSOL™'s automated algorithm with an overall mesh density.

After defining the geometric parameters, such as air film length, width, and orifice patterns, a numerus repetitive body of simulation work must be done for the observation of the static performance of the generated air film under different conditions. To streamline the modelling process and enhance the user interface, a novel simulation program was developed using COMSOL™'s internal application builder. The GUI facilitates rapid adaptation to new simulation needs and minimizes repetitive tasks, as demonstrated in Figure 4.11.
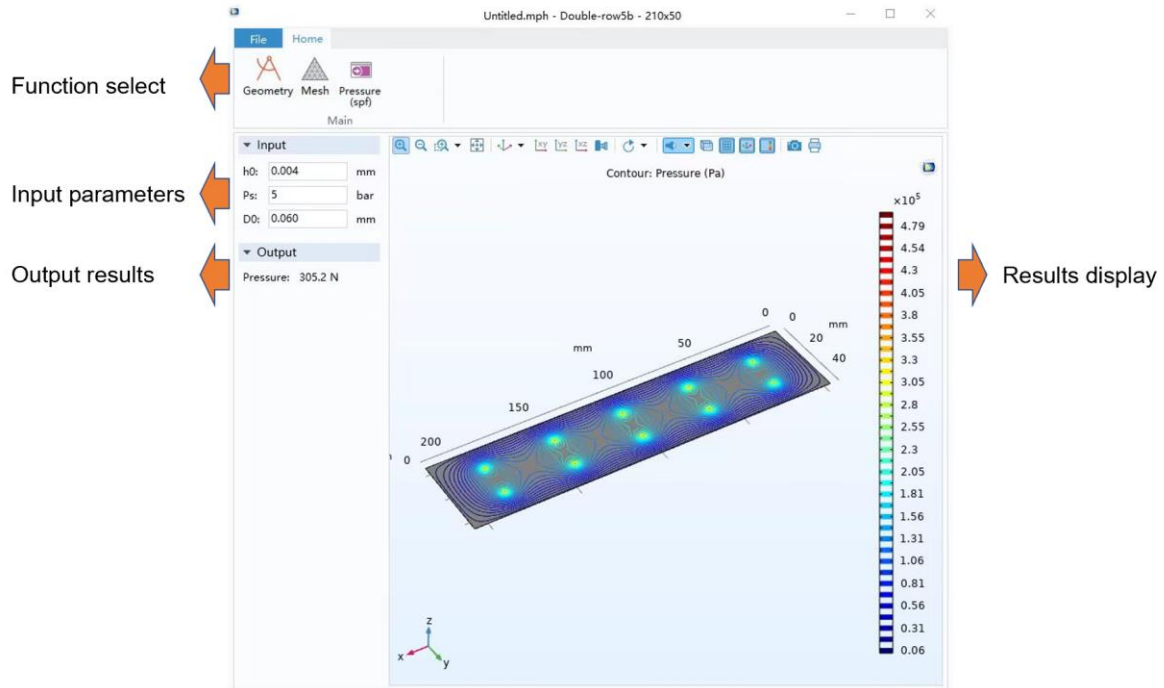
Figure 4.11 GUI of developed COMSOL™ application and its description

The left panel contains settings and input parameters required for model building, the graphics window on the right serves to display the geometry, mesh and pressure distribution of interest by selecting different buttons on top panel. This mini application can be used independently on various type of smart devices such as computers, tablets and mobile phones.

The simplified GUI has only few key parameters as input, where:

h0: Air film thickness in mm;

Ps: Inlet pressure (gauge pressure) in Bar;

D0: Orifice diameter in mm.

The bottom side pressure of the air film, which is considered as the load capacity of the air bearing, will be calculated automatically and shown in the "Output" tab.

4.4.2.2 Simulation results and analysis

After establishing the model and simulation system, the result of a trial run is shown in Figure 4.12, details of system input are:

Air bearing surface: 40 mm × 200 mm

Inlet pressure: 0.5 MPa

Air film thickness: 0.008 mm

Orifice diameter: 0.06 mm

Load-carrying capacity: 491.21 N

Stiffness: 47.95 N/µm
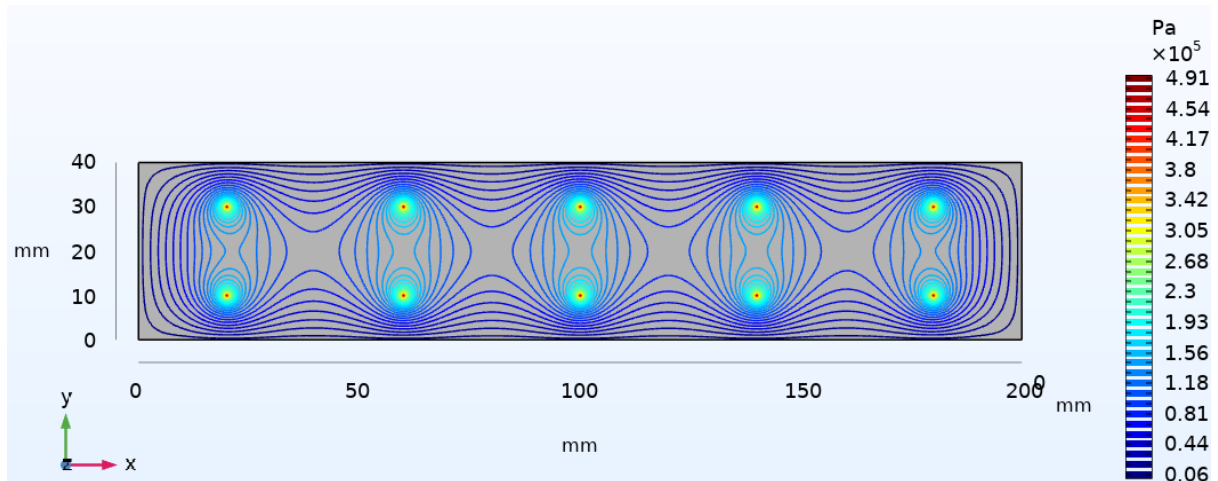
Figure 4.12 Pressure distribution of trial run

It can be seen that the pressure distribution diagram and related values can meet the characteristic of laminar flow.

Then running the simulations with different input parameters 11 times, the results are obtained and shown in Figure 4.13- 4.15:
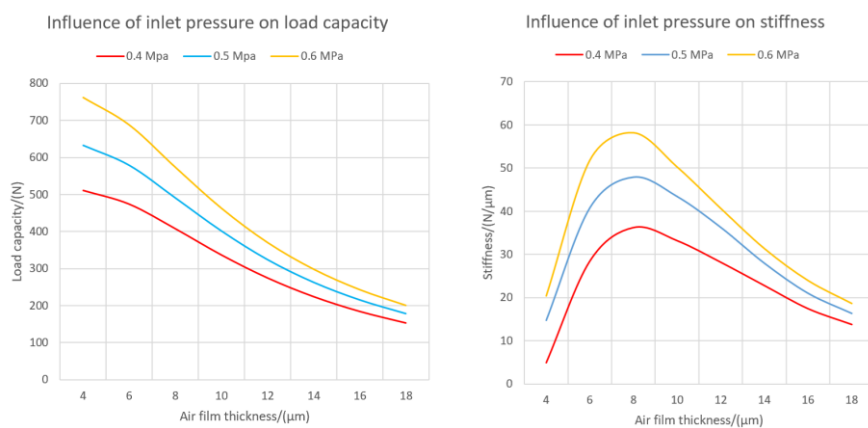
Figure 4.13 Load capacity and stiffness under different supply pressures
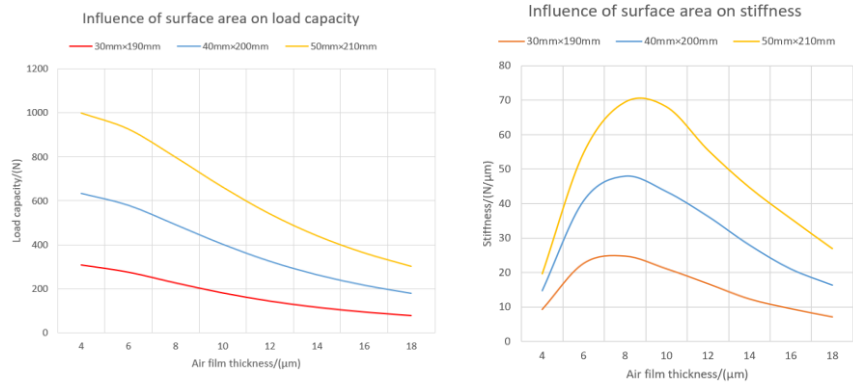
Figure 4.14 Load capacity and stiffness under different air film sizes
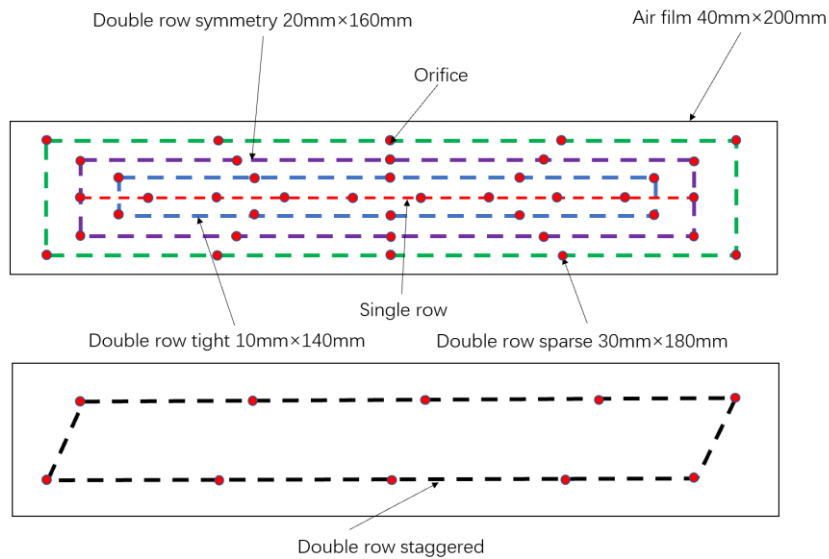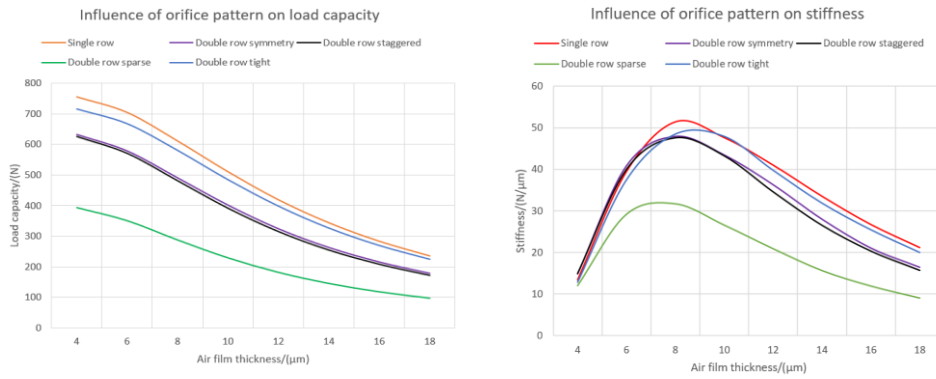
Figure 4.15 Load capacity and stiffness under different orifice patterns

From these results presented in Figures 4.13 – 4.15, it can be found that:

● From the load capacity and stiffness point of view, the bigger air film surface area and higher inlet pressure can bring the slideway better static performance.

● Figures 4.13 and 4.14 illustrate that the influence of air film thickness on the slideway's static performance is not linear. No matter what the inlet pressure and surface area were, with the increase of air film thickness, the air film load capacity kept decreasing. However, their stiffness curve can be seen behaving as a parabolic form and reaching the maximum value for the optimum air film thickness of 7–9 μm while depending on the bearing surfaces and orifice diameter.

● Under a certain inlet air pressure and same orifice amount, the double row orifice structure showed no benefit on the static performance of the slideway in comparison with single row orifice, but the increasing of orifice amount has positive affect on both load capacity and stiffness of air bearing. Furthermore, according to Tao's research study[132], the presence of a high pressure zone between orifices can be strengthened by a tighter orifice layout, which improves the stability of the slideway during working operations.

● Different orifice patterns can affect the pressure distribution and further influence the performance of air film. The certainty of this phenomena needs more experimental data.

4.4.3 Simulation on Dynamic Performance

After the static performance simulation, the basic design of the aerostatic bearing slideway including structure, parameters, and specifications have been completed and integrated into the virtual model, which plays the role as one of the fundaments for DT. In order to obtain the real time dynamic performance of the slideway during working, the control system as shown in Figure 4.16 was constructed. As illustrated, the orders from IPC is sent to the control and drive system and further fed back, thus to build a close loop for position and current.
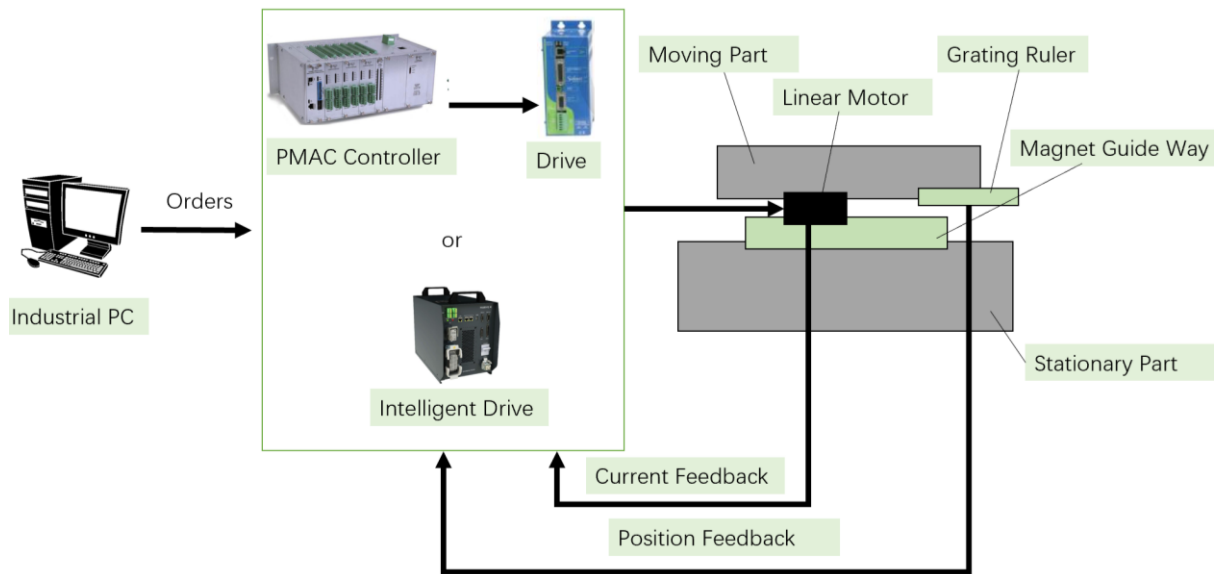
Figure 4.16 Structure of aerostatic bearing slideway control system

Simulink is a MATLAB-based graphical programming environment for modelling, simulating, and analysing multidomain dynamical systems, which is widely used in automatic control and digital signal processing for multidomain simulation and model-based design. In this study, the simulation of the dynamic performance e.g., motion accuracy and stability of the aerostatic bearing slideway, is based on the modelling in SIMULINK environment.

The details of established control system for aerostatic bearing slideway are shown in Figure 4.17. The input signal undergoes acceleration feedforward (Kaff), velocity feedforward (Kvff), and PID tuning before being applied to the linear motor (plant). The signal is the converted by the amplifier and motor coefficients, constituting the motor output force. Subsequently, this output force undergoes two-time integrations based on the values of motion parts' mass and payload, generating a position feedback signal that returns to the input terminal. The disparity between this position signal and the input signal constitutes the tracking error that necessitates compensation.

Figure 4.17 SIMULINK system model and subsystem details

In the aim of obtaining precise control, an open system with a PC and a PMAC controller is chosen, an optical encoder can be integrated here as external position feedback device so as to close the system loop. Due to the study presented in[133], this kind of control system has high scalability and is convenient for integrating subsequent control systems of other machine tool components. The performance in the aerostatic bearing slideway control system is mainly manifested as motion accuracy and stability, which means the response time, overshoot, and oscillation need to be kept at a low magnitude. In order to perform suitable control of the linear motor, a PID controller is implemented. After tuning the system with appropriate PID gains, the corresponding response curve can be obtained from the oscilloscope, as shown in Figure 4.18: The response time of the system to the step signal after tuning is 0.03 - 0.04 s; the system is relatively stable and has no obvious overshoot, which can meet the demand for precision motion of the aerostatic bearing slideway; and it has also good stability under the simulated external interference force (50 N, 50 Hz), as shown in Figure 4.19. Meanwhile, except for the interference force like cutting force or air resistance, aerostatic bearing slideway often bears additional load during practical working. The study on steady state response of the control system under variable loads can help the digital twin system to predict the influence of different load states on the stability and dynamic performance of the slideway system.

Figure 4.18 System response time to the step signal
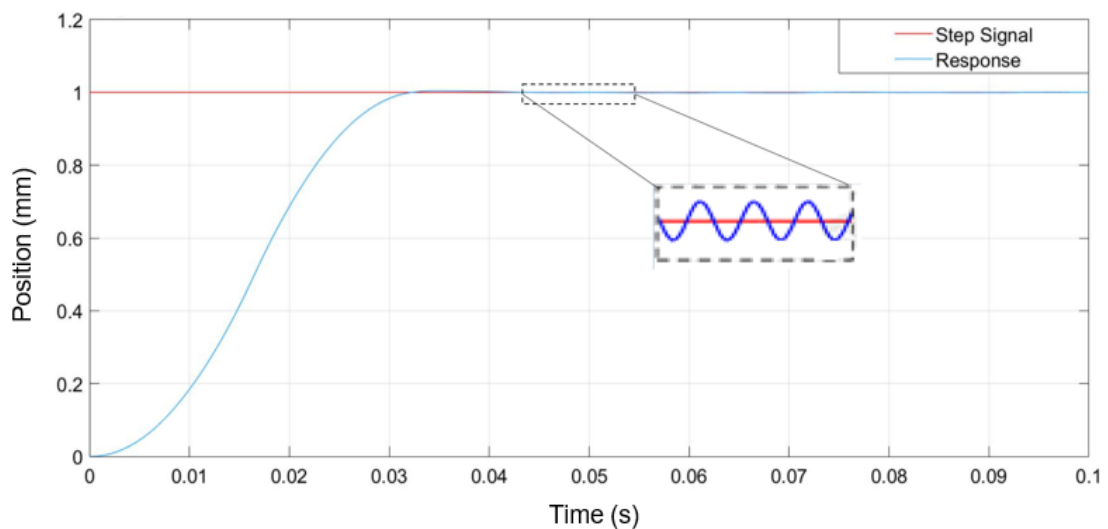
Figure 4.19 System response under external interference

Figure 4.20 shows the response time and steady state of the aerostatic bearing slideway control system under 0 kg, 5 kg, 10 kg, and 15 kg payloads. It can be found that with the increase of load mass, the overshoot and response time of the step signal get increased as well. If the load mass is over range, it will cause notable instability of the system and seriously affect the processing quality during manufacturing. Therefore, it is necessary to tune the PID parameters according to different working environments. Since not all end-users have competent control

engineering skills and the preset automatic tuning algorithm is not applicable to provide the ideal solution against all application scenarios, the remote tuning of the slideway system is thus of significance for both the end-users and the slideway product provider.
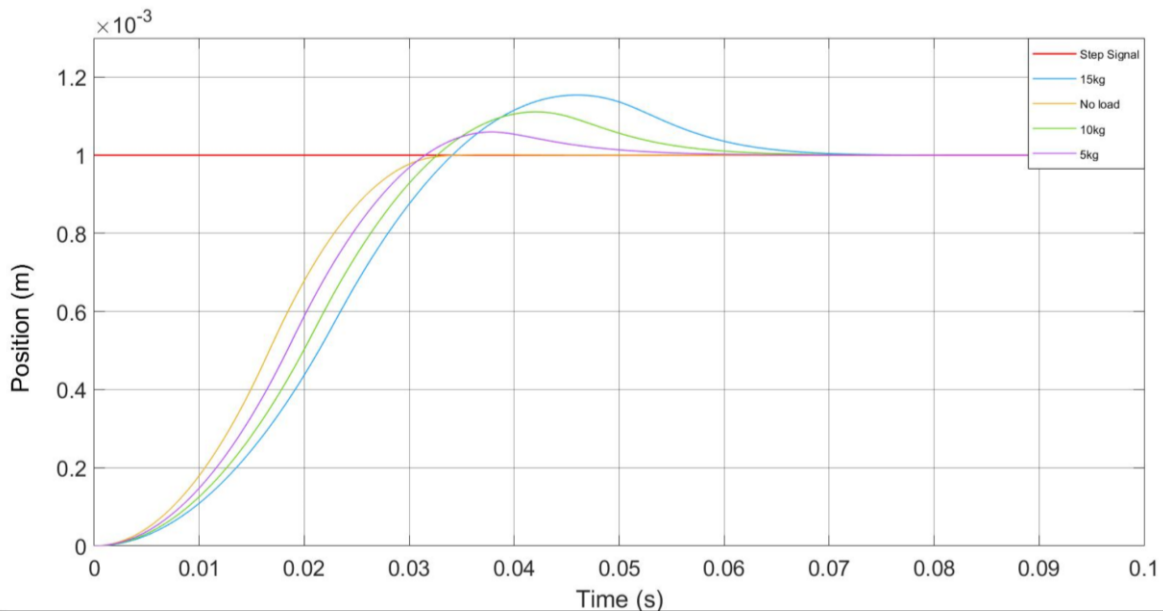
Figure 4.20 The system response time under different loads

After finishing the design and simulation process of the dynamic performance, the function of remote monitoring and tuning for the DT can be further progress. By analysing the real time data which is fed back, collected and stored in-situ, as shown in Table 4.2, the dynamic characteristics in every instantaneous aerostatic bearing slideway can be obtained.

When the system is disturbed by external force or load, the R&D or electrical engineer can remotely adjust the corresponding parameters of the system, thus to improve the system stability and dynamic performance of aerostatic bearing slideway, and reduce or solve the performance loss as well.

Table 4.2 Data output from the MATLAB programs.

Time (s)	Velocity (m/s)		Time (s)	Position (m)
0	0		0	0
0.0025	0.0092		0.0026	1.2201×10^{-5}
0.0053	0.0189		0.0054	5.1920×10^{-5}
0.008	0.0287		0.0081	1.1921×10^{-4}
0.0107	0.0385		0.0109	2.1460×10^{-4}
0.0134	0.0482		0.0137	3.3646×10^{-4}
0.0161	0.0579		0.0164	4.8626×10^{-4}
0.0188	0.0521		0.0192	6.3931×10^{-4}
0.0215	0.0423		0.022	7.6572×10^{-4}
0.0242	0.0325		0.0247	8.6457×10^{-4}
0.0269	0.0228		0.0275	9.3587×10^{-4}
0.0297	0.013		0.0303	9.7960×10^{-4}
0.0324	0.0039		0.033	9.9681×10^{-4}
0.0351	7.6856×10^{-4}		0.0358	0.001
0.0378	6.1492×10^{-5}		0.0386	0.001

More detailed studies regarding the aerostatic slideway and ultraprecision machine platform control and drive system will be further discussed in Chapter 5.

4.5   Aerostatic bearing slideway digital twin and its implementation

The most accepted definition of DT is the collection of all digital artifacts that accumulate during product development, integrating all data that is generated during product design and use[134][135].

Figure 4.21 illustrates the steps and functions of aerostatic bearing slideway digital twin, which can be roughly divided into four steps:

● Step 1: design stage.

In the design stage of aerostatic bearing slideway, the implementation of DT can improve the accuracy of the design and verify the performance of the product in the real environment. The DT at this stage only includes the use of CAD tools to develop virtual prototypes of products that meet technical specifications, which accurately record the physical parameters of the product.

- Step 2: simulation stage.

Through the simulation experiments with repeatable and variable parameters, the static and dynamic performance of aerostatic bearing slideway under different operating environments and the adaptability are verified.

- Step 3: manufacturing stage.

In the manufacturing stage, the use of DT can speed up product introduction time, improve product design quality, and reduce expense and time costs.

- Step 4: service stage.

With the maturity of the Internet of Things (IOT) technology and the decline in sensor costs, increasing number of industrial products results in the use of sensors to collect the environment data and working status during operation. Based on this, the seamless data transmission realised by sensors can help DT realise remote monitoring and predictive maintenance. In this study, these functions are realized by feeding back, collecting, and storing real time data from the encoder installed on the moving part of aerostatic bearing slideway, which can help end users avoid malfunctions caused by product misuse, and improve the accuracy of product parameter configuration.
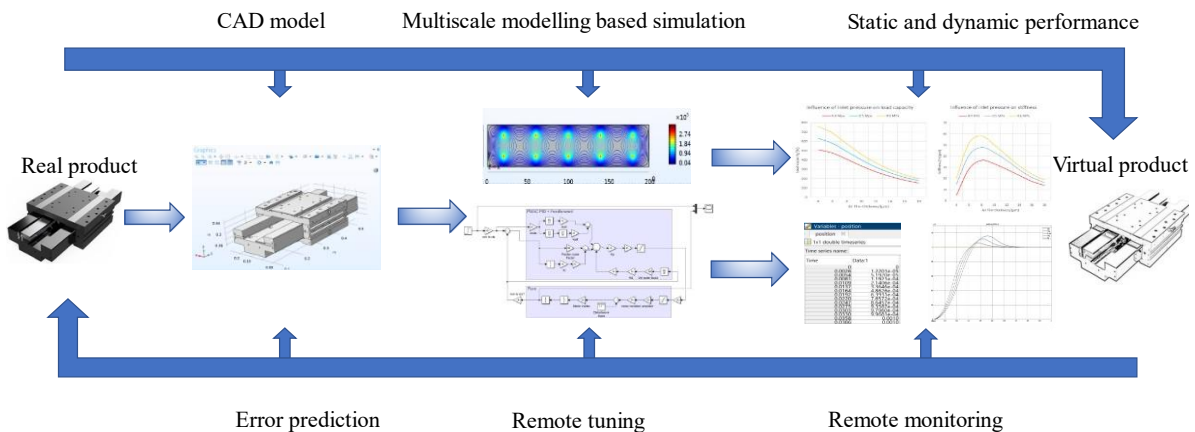
Figure 4.21 Schematic of the aerostatic bearing slideway digital twin

The application of DT technology can provide many practical solutions for aerostatic bearing slideway from implementation perspectives like improving the processing quality of ultraprecision machine and optimising end-user experience. For instance, the algorithm preset in DT system can solve the problem of the decline in machining accuracy caused by the acceleration change of the slideway at the end of the running

track; by recording and feeding back the usage data and slideway operating parameters, overload and excessive vibration can be interpreted as early warnings; thus, engineers are able to make corresponding optimization through remote tuning or adjustment of control parameters; the recording data of the full life cycle of aerostatic bearing slideway can help R&D engineers to carry out product iteration and design optimization[136][137].

4.6 Conclusion

The development and results presented in this paper reveal that multiscale modelling and analysis can be used as an enabling methodology for design and development of high-precision engineering products such as aerostatic bearing slideways. Through this approach, it is likely to reveal the intrinsic complex relationships among key design factors working in macro-meso-micro-nano scales and their collective effects on the performance of the slideway system, and to develop a forward-looking design and analysis method for future air bearing slideway and spindle systems.

The chapter also presents the development of the multiscale modelling and analysis approach by using the multiphysics programming environment combined with MATALB simulations. Explorations into the implementation perspectives of this approach have been further discussed, and as an enabling kernel for its extension into DT development for the slideway system. For future research work, the approach, development, and underlying fundamentals are expected to be tailorable organically to two-axis and three-axis slideway systems, although this should be thoroughly investigated and expected to report separately in the future.

Chapter 5 Modelling and analysis of the electric drive and control system for a precision machine platform

5.1 Introduction

As the kernel of a motion system, the design, simulation and tuning of drive and control systems for UPM machine platform have received increasing R&D attention, as they directly affect the overall accuracy and dynamic performance of the machine platform. However, for most precision machines, their motion/positioning systems are often composed of multi-axis slideways as a platform, while individual single-axis slideway being tuned and commissioned during operation separately, which often produces unexpected errors when work together simultaneously in the complex multi-axis CNC working environment. Therefore, with the increasing demands for higher motion and positioning precision of complex machine platform, the development of a multi-axis integrated control method and the corresponding advanced control algorithms is essentially needed to realize integrated tuning of the multi-axis motion system, especially for rapid modular reconfiguration of slideways/stages at a high precision machine. Thus, the cross-coupling control method is applied in this study to help compensate for contouring errors based on the feedback of actual tracking errors and thus further improving the motion and positioning accuracy particularly in machining complex freeform surfaces.

In this chapter, the drive and control methods for aerostatic bearing slideway are firstly discussed and analysed. Based on this, a control system for single-axis aerostatic slideway is built, tuned and tested in MATLAB SIMULINK environment. Then, an integrated modelling and analysis approach is presented for the multi-axis ultraprecision machine platform system. The approach is focused on addressing two folds of challenges, i.e. the integrated analysis of mechanical design, electric drive actuation through the advanced cross-coupling-controller with variable gains for a direct drive aerostatic bearing linear stages as a complete high precision mechatronic system, and the simultaneous tuning and further analysis of the multi-axis platform through PID control algorithms. It thus aims to achieve the higher positioning accuracy, response time and stability of the stage motions, especially during the high-speed multi-axis synchronized actuations in a precision engineering application. The

modelling and analysis are implemented in MATLAB/Simulink environment and further supported by advanced control functions particularly for coupling, tuning and dynamic performance analysis. This chapter is also concluded with a further discussion on the potential and application of the approach for high precision multi-axis platform.

5.2   Modelling and simulation of linear motor drives

5.2.1   Principle of direct drive linear motors

Direct drive linear motor is an evolution of the traditional rotary motor, the original linear motor can be seen as a rotary motor after simply radially splitting and circumferentially expanding. During working, the iron cylinder is normally affixed onto a metallic or granite guide, where the coil, affected by magnetic forces, enables relative floating and serves as the rotor so as to realize the motion within air bearing slideway assembly. The structure for direct drive linear motor is as shown in Figure 5.1:
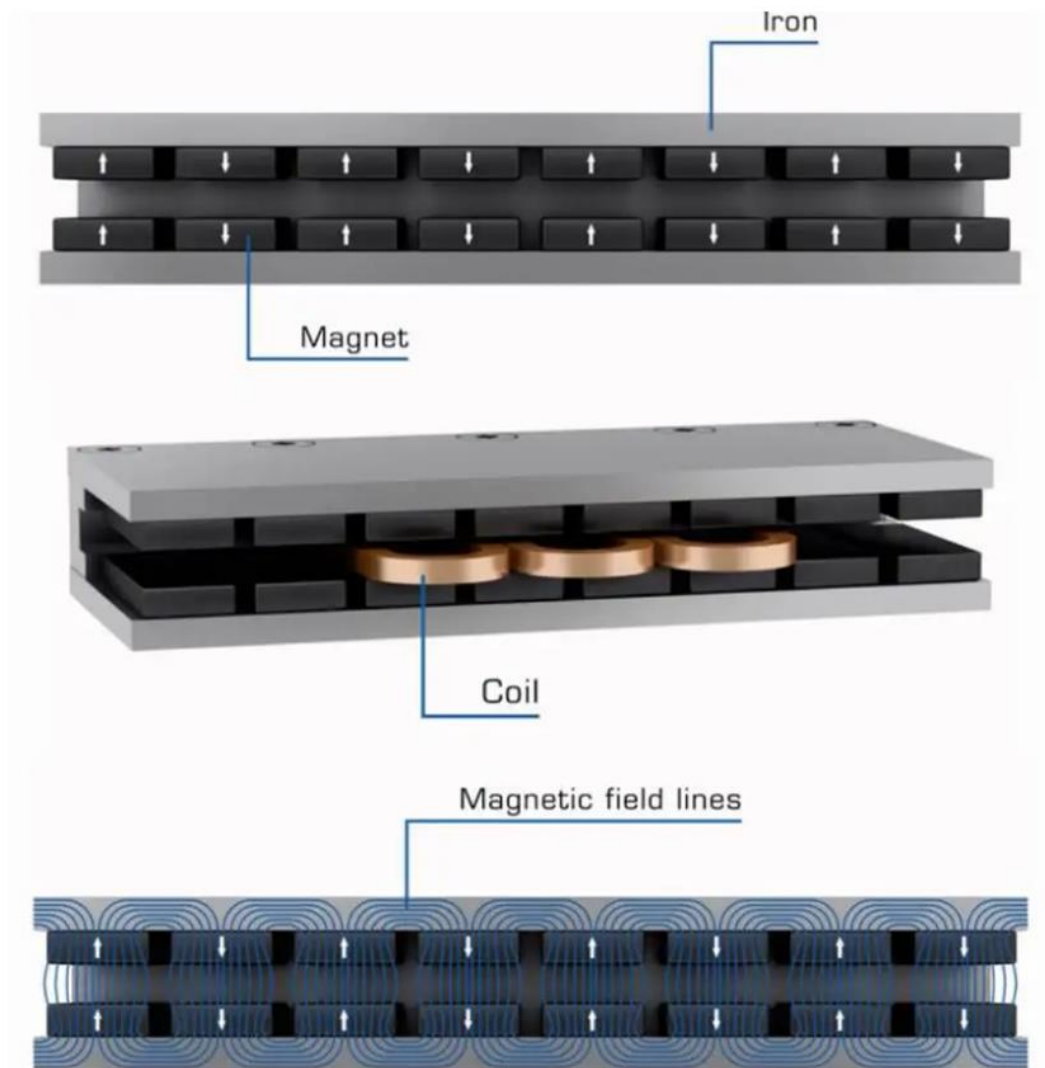
Figure 5.1 Structure of direct drive linear motor[138]

In industrial scenarios, direct drive mechanisms are commonly employed in order to minimize static and dynamic errors in displacement, as documented in several studies[140]. These errors typically arise in mechanical slideway-based long travel linear motor stages due to a variety of imperfections, including backlash, imprecise component assembly, payload, eigenfrequencies of parts, measurement system errors, and unfavourable ambient conditions. Given the stringent accuracy requirements of ultraprecision machine platforms, these factors are deemed unacceptable. Linear motors represent a type of direct drive system that obviates the need for gears, such as ball screws, belt drives, or rack and pinions, to transform rotational motion into linear motion. Rather, they rely on the generation of linear force by means of a Lorentz force that is induced proportionally, thus enabling direct thrust

without any conversion of rotational energy into translational energy.

5.2.2 Modelling of linear motor drive system

Without considering the effect of magnetic field saturation, the rotor equivalent excitation current is assumed to be constant in the rotor coordinate system, hysteresis or eddy current losses are assumed as zero, and the rotor is considered to be an undamped winding, based on the above assumptions, the linear motor thrust equation can be obtained as:

$$F_m = K_f i_q \tag{5-1}$$

Where:

F_m: Magnetic thrust force;

K_f: Magnetic thrust coefficient;

i_q: Electric current.

In the ultraprecision machine platform, the aerostatic bearing slideway is driven by the magnetic thrust force generated by linear motor, which is subject to disturbing forces, viscous resistance. The equations of this motion system are established as follows:

$$m\frac{d^2x}{dt^2} + c\frac{dx}{dt} + Kx + F_f = K_f i_q \tag{5-2}$$

Where:

m: Motion part mass;

c: Viscous friction coefficient;

K: Motion part elasticity coefficient;

F_f: Disturbance forces in the direction of motion.

The transfer function can thus be obtained by performing Rasch transform:

$$G(s) = \frac{X(s)}{I(s)} = \frac{K_f}{ms^2 + cs + K} = \frac{K_1\omega_n^2}{s^2 + 2c_1\omega_n s + \omega_n^2} \tag{5-3}$$

Where:

c_1: Damping ratio;

ω_n: Free oscillation frequency.

During modelling the elastic and viscous friction coefficients of the aerostatic bearing slideway are small enough to be neglected and the above equation can be simplified

as:

$$G(s) = \frac{X(s)}{I(s)} = \frac{K_f}{ms^2 + cs} \tag{5-4}$$

Combining the transfer functions of motion part and linear motor:

$$\begin{cases} L\frac{di_q}{dt} + Ri_q = u_q - K_e v \\ K_f i_q = m\frac{d^2 x}{dt^2} + c\frac{dx}{dt} + F_f \end{cases} \tag{5-5}$$

Where:

K_e: Motor potential coefficient;

u_q: Input voltage;

v: Velocity;

L: Inductance;

R: Armature resistance.

Perform the Rasch transform:

$$\begin{cases} (Ls + R)i_q(s) = U_q(s) - K_e v(s) \\ K_f i_q(s) = (ms + c)v(s) + F_f(s) \end{cases} \tag{5-6}$$

Thus the model of linear motor drive motion system can be built:
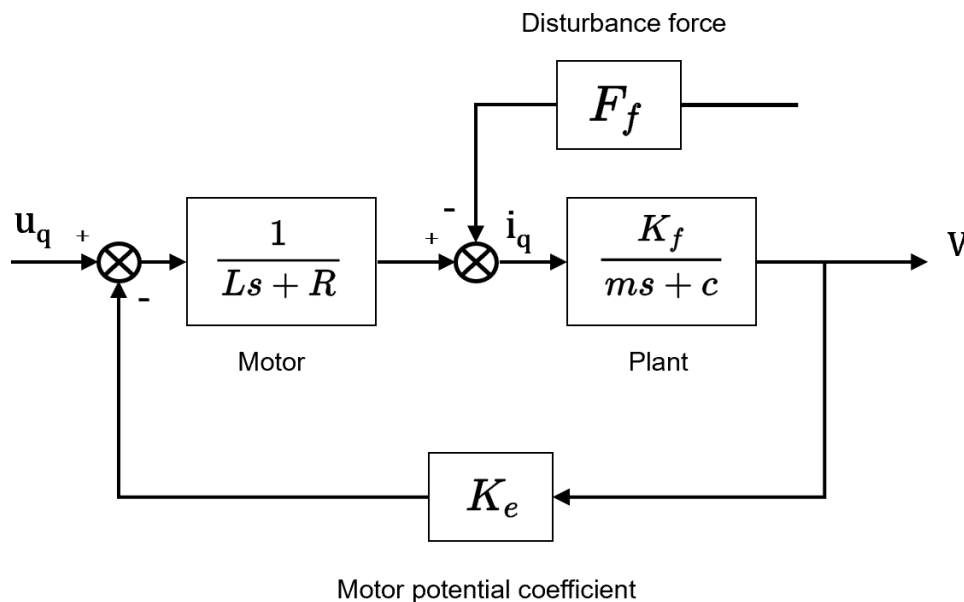
Figure 5.2 Block model of direct drive linear motor

In ultraprecision machine platforms, direct drive linear motors often form a drive control

system together with an Industrial Personal Computer (IPC), power supply, signal feedback & processing devices and control algorithms.

5.2.3 Modelling of single axis aerostatic bearing slideway control system

For the control system of single axis aerostatic bearing slideway, the feedforwards, motor amplifier, controlled plant, and encoder feedback should also be considered based on the above established drive model, together forming a classic close-loop control system with current loop, velocity loop and position loop, as shown in Figure 5.3:
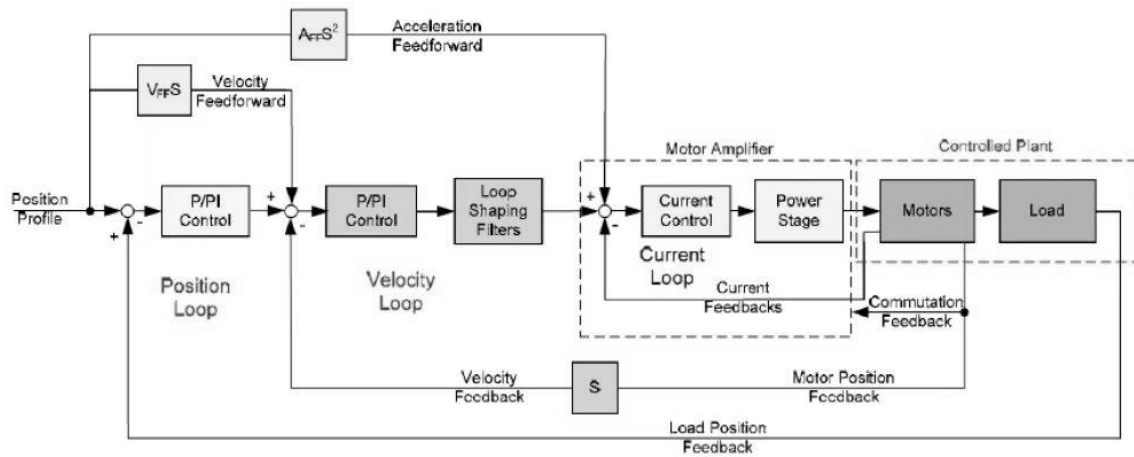
Figure 5.3 Schematic of single axis aerostatic bearing slideway control system[139]

Based on the above classical single axis control system and the control logic of the controller, the control model shown in Figure 5.4 was developed in MATLAB SIMULINK as also shown in chapter 4:
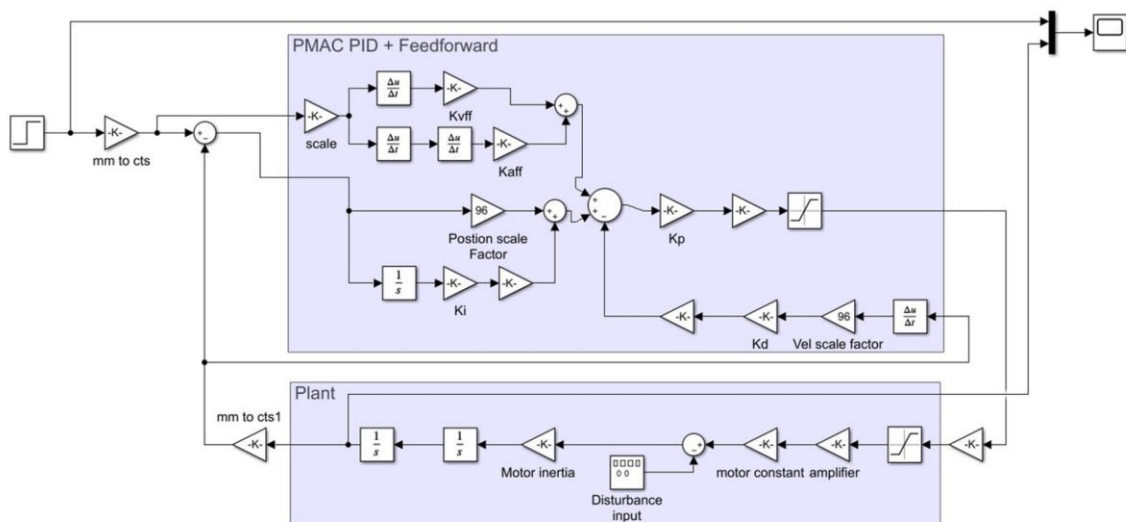
Figure 5.4 control system of single axis aerostatic bearing slideway

The specific parameters, tuning results and dynamic performance are listed in Table 5.1, which shows the ability of the established control system for providing a practical and feasible control and drive for singe axis aerostatic bearing slideway.

Table 5.1 Parameters of established control system

K-mm to cts	6400*32
K-scale	1/128
Kvff	15000
Kaff	2000
Ki	50000
Kp	180700
Kd	10.8
K-amplifier	0.5
K-motor constant	16.7

5.3 Multi-axis aerostatic bearing platform system for high precision motion

The motion system of UPM machine platform can be roughly divided into three parts: the mechanical actuation system, the motion control system, and the related algorithms.

5.3.1 Biaxial coupled control system

For the UPM machine platform, the motion/positioning systems are often consisting of multi-axis slideways, so only focusing on the controlling and tuning for individual single axis slideway often produces unexpected trajectory errors. Hence, the development of a multi-axis cross-coupling control and the corresponding advanced control algorithms is essentially needed to realize integrated tuning of the multi-axis motion system.

Accurate trajectory control is a fundamental requirement for modern precision manufacturing systems. In a biaxial system, two drive systems are usually linked by a sliding table or other mechanical structure. During the working process, contour error usually occurs because of the unbalanced load, mechanical assembly error and uncertain disturbances. This synchronous error will reduce the working life of products

or even damage the equipment[141]. Hence, the research of high-performance biaxial control strategies has practical significance and necessity.

Koren firstly introduced the biaxial control strategy in 1980s and further developed the cross-coupling-control (CCC) method in early 1990s[143]. However, most of the early research and development related work for CCC was applied to the control of conventional CNC machines with servo motor driven, ball screw lead linear motion system. The stiffness of the motion system is often dependent on and limited by the ball screw-lead mechanical structure, and the advantage of using CCC for machining high precision complex surfaces would not be well demonstrated. In late 1990s, however, multi-axis platform using linear motor direct driver was started as almost the 'standard' design configuration for ultraprecision machines and other precision engineering applications. Typically, the aerostatic bearing slideways on these machines have become more technically complex. The high precision mechanical components, electrical direct drivers, encoders as positioning feedback and advanced control algorithms involved, are highly dependent on the mechatronic system control, which further challenge the design and development of such products[142].

Depending on the control method, biaxial coordinated motion control systems can be classified as uncoupled or coupled. Uncoupled control focus on the corresponding motor for each single axis, through the improvement of single-axis performance, for example, the design and development of large gain controllers or feedforward controllers. In order to reduce the contour error of whole system. However, when another motion axis is involved, the synchronization or coordination problem cannot be effectively solved if another axis is not able to receive the real-time dynamic information (e.g., the change of load, or speed) about the changing axes and adjusts accordingly. In addition, the dynamic performance of each axis in the actual system is affected by many factors such as load or noise disturbances, so uncoupled control has certain limitations in the complex coordination control of high speed and high accuracy motion system.

Coupled control is an overall control strategy for multi-axis systems. It is based on the tracking error of each axis to directly reflect the contour error, and the position compensation value of each axis is obtained by computing through the cross-coupled controller, then the value of each axis is added to each axis as a gain, thus ensuring that one axis can adjust to the dynamic characteristic changes of another, and ultimately eliminating dynamic effects between axes so that to improving coordinated

control performance. To realize the coupling of biaxial system, researchers have proposed various control methods such as dynamic characteristic matching[144], and predictive control[145]. To address these issues, this study selects the cross-coupled controller (CCC) as the control method for biaxial coupling, based on the single-axis control system in the previous section, with the aim of further optimizing the control system and reducing contour errors. The block diagram of CCC based control system is shown in Figure 5.5:
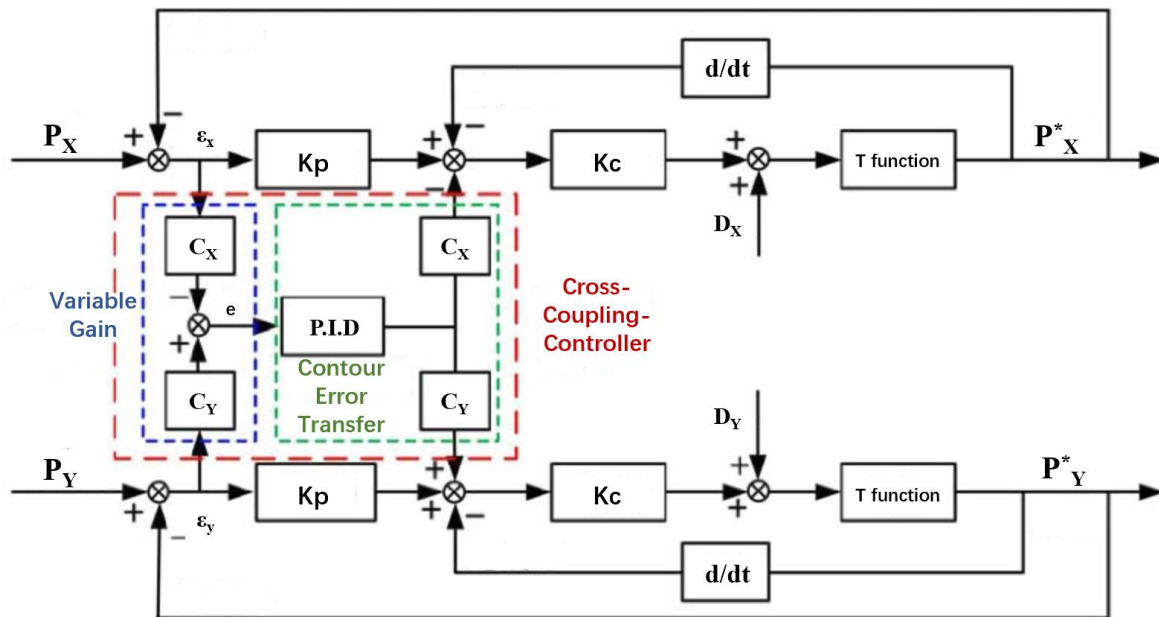
Figure 5.5 Block diagram of CCC based control system

As illustrated by Figure 5.5, control systems of each axis are coupled through CCC. The difference between input signal and feedback signal from one axis is calculated as tracking error, which is converted into the contour error through the equations before input to the CCC, which is internally controlled by the PID and then returned to each axis though the variable gain C_X and C_Y. The principle of contour error e is shown in Figure 5.6:
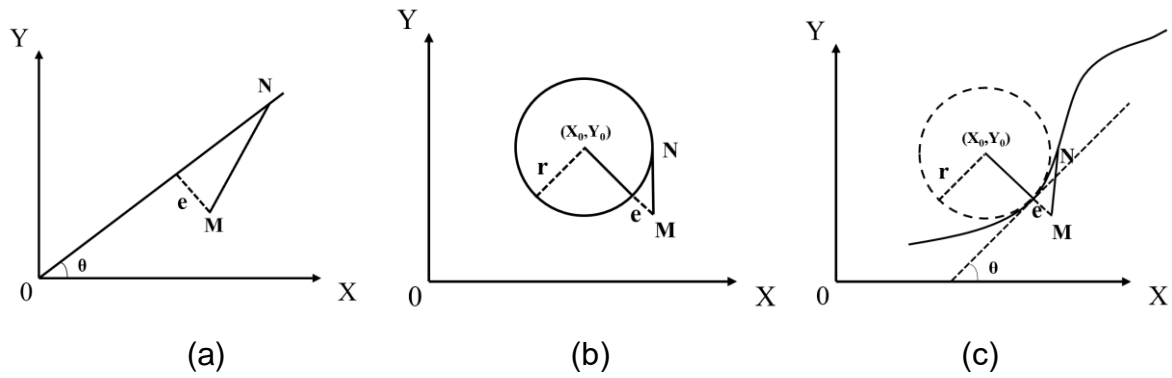
Figure 5.6 Principle of contour error

Figures 5.6 (a), (b), (c) are three types of contour errors, i.e. (a): linear; (b): circular (radius r, center coordinate X_0, Y_0); and (c): generic (dashed circle is the inscribed circle of the corresponding curve at the point N). Where: The curve in the diagram is ideal trajectory, at a given moment the desired position of stage is N while the actual position is M, so line MN is the tracking error ε of stage, divided by each axis into ε_x and ε_y. According to the definition, contour error is the shortest distance from point M to the trajectory and is represented by the dash line, with e as its length.

According to the control theory and analysis, the contour error is calculated as follows:

Type (a): $e = MN = \varepsilon_y \cos \theta - \varepsilon_x \sin \theta$ $\qquad$ (5-7)

Type (b): $e = \sqrt{(X_0 - x)^2 + (Y_0 - y)^2} - r$ $\qquad$ (5-8)

Type (c): $e \approx \left(\sin \theta + \frac{\varepsilon_x}{2r} \right) \varepsilon_x - \left(\cos \theta - \frac{\varepsilon_y}{2r} \right) \varepsilon_y$ $\qquad$ (5-9)

When the value of is relatively big, type (c) can be simplified as:

Type (c)*: $e \approx \varepsilon_x \sin \theta - \varepsilon_y \cos \theta$ $\qquad$ (5-10)

Where:

θ is the angle between the tangent line through the point and the axis, with:

$$\theta = \tan^{-1} \frac{dy}{dx}$$ $\qquad$ (5-11)

The contour error is defined as the shortest normal distance from the actual position point to the commanded trajectory curve[146]. It is normally caused by the uncoordinated movement of displacement velocity of single axis motion and is an important component in assessing the accuracy of motion control. The aim of CCC is to establish a real-time contour error model and making the corresponding

compensation for each coordinate axis, thus to reduce or ideally eliminate it. The following simulation will use circular trajectory as an example.

5.3.2 Simulation results

Based on the theoretical principles of the previous chapters, the model was created in the MATLAB Simulink environment. The trajectory is set as a circle with radius 1mm, input signal frequency 2*PI*2 for each axis. After initial tuning of the single axis control system, CCC is implemented for coupling the whole system, in order to simulate the actual working environment, the disturbance of 2N/50Hz for X axis and 1N/44Hz for Z axis are added. The results are shown in Figure 5.7:
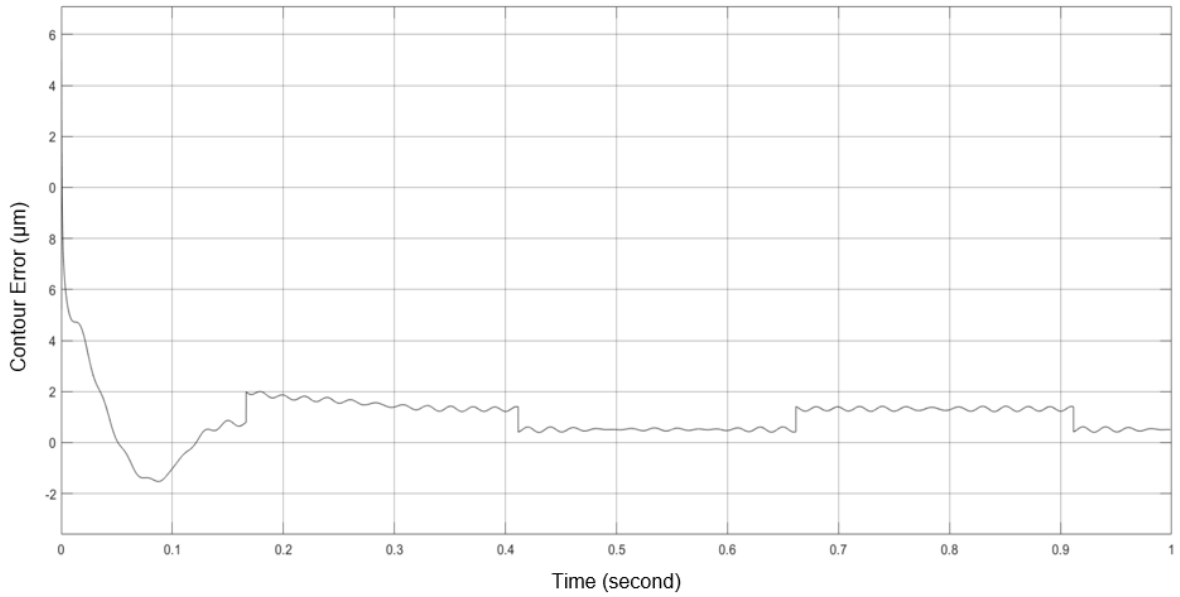
(a) Contour error without applying CCC
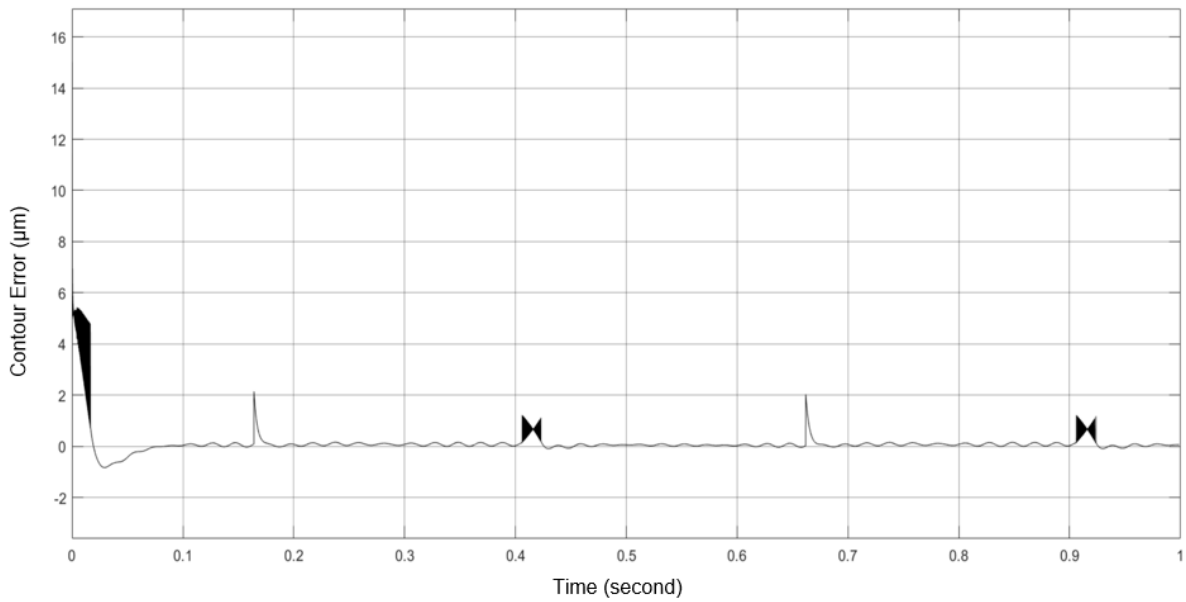
(b) Contour error with applying CCC

Figure 5.7 Simulation results of the system contour error

As illustrated by the Figure 5.7, the average contour error after 0.2 sec is reduced from1.78μm to 1.16μm and the oscillation time is reduced from 0.178 sec to 0.085 sec as well.

5.4　Conclusion

Based on the simulation results obtained from the programming environment of MATLAB Simulink, it can be inferred that the use of a variable gain cross-coupling controller in a biaxial motion control system can effectively mitigate contour errors and improve system accuracy. These findings suggest that the cross-coupling control method has great potential as a methodology for enhancing the precision of aerostatic bearing machine platform products. Additionally, the proposed approach may also shed light on the collective impact of contour error compensation on system dynamics and facilitate the development of advanced design strategies for future aerostatic bearing stage control systems.

Explorations on implementation perspectives of this approach are worth further discussion. For a future-oriented precision machine platform, the reconfigurability and the ability to be combined with digital twin system is necessary. According to the above discussed CCC technology, this kind of integrated tuning and compensation method can assist single slideway products directly integrated as a multi-axis stage, it is more in line with the future trend of manufacturing smarter and more flexible ultra-precision machine platform products and realize the function of "plug and produce" function for digital twin system.

Chapter 6　Development of the digital twin for the ultraprecision diamond turning system

6.1　Introduction

With the latest development in power electronics, direct drives, sensors, and control technologies, the UPM machines and machining systems aim to continually achieve the higher machining accuracy in an industrial competitive manner. However, the constraints and bottlenecks for the further development of the UPM machines and systems are also becoming obvious. It is essential and much needed to develop an innovative approach to overcoming the nanometric level hurdle in the context of industrial scale ultraprecision manufacturing. The approach has to address the multiple factors in multiscale multiphysics, such as cutting mechanics and fundamentals, workpiece materials, machines and tooling design, fixtures, in-process monitoring, measurement and error compensations, in-process and/or real-time diagnosis of the machining conditions (e.g., machining temperature, vibrations, cutting forces, and cleanness). Furthermore, this often comes at the expense of machining efficiency and increased the technological complexity and costs. At the same time, real-time data monitoring and processing has always been challenging while addressing the need for nanometric-level motion accuracy and higher control resolution at the ultra-precision machining system.

Conventionally, the hardware and software of the UPM machine systems are integrated through encoders as the feedback devices in the systems, while the encoders are feeding back the positioning data of the slideways and/or spindles but not the direct data of the tool and workpiece engaged, which may impose the limitations in acquisition of in-process real time machining data and information. These kinds of information asymmetry phenomenon existing in the mechanical and electrical systems of UPM machines, may render the inconsistency between the designed performance and operation performance. Furthermore, they may reflected in static/dynamic stiffness, thermal stability, and motion accuracy of the UPM system as well, which may also impose the fundamental limitation in achieving higher accuracy beyond the nanometric level. Currently, the next paradigm shift in manufacturing is emerging, i.e. continuously improving product quality and precision through DT

technology for modern UPM technology.

Digital twin is widely regarded as the future for advanced engineering manufacture, addresses the critical challenge for continuous improvement and optimization of manufacturing systems through real-time machining process monitoring, in-process diagnosis and dynamic process optimization, and digital and physical data fusion for higher manufacturing precision. Therefore, developing a DT for the UPM system is inevitably essential for future generation UPM systems and machines. In this thesis, an investigation on digital twin of the ultraprecision machining system and its implementation perspectives are presented particularly against the ever-increasing demand for higher precision machining accuracy, e.g. the increasingly more stringent requirement in manufacturing freeform surfaced components and devices. The investigation is focused on the kinematics and dynamics modelling of the machining system (as the foundation of the DT development), the DT implementation, and the application case study, which reflects the innovative attempt on seamless integration of ultraprecision machining fundamentals, innovative development of applied DT technology, and high value ultraprecision applications. Design, manufacturing and control, combined with computationally efficient DT design and optimization algorithms will lead to the higher form/dimensional accuracy and finer surface roughness of the ultraprecision components/parts, in a competitive and promising industrial manner.

Single point diamond turning (SPDT) is one of the most representative industrial application scenarios for ultraprecision machine platforms, thus it is of great academic and practical importance for this PhD research to study and discuss the application possibilities and implementation methods of DT technology.

This chapter presents the feasibility and innovative application of using a DT for an ultraprecision SPDT machine system. The study and application described in the thesis will demonstrate the significance of developing and applying DT technology to UPM of optical components, and in particular those with freeform surfaces. The effect of how contact forces affecting the toolpath will be investigated as well, whilst it also shows the limitation of using automated dynamic analysis of mechanical systems (ADAMS) only for this application. This chapter will also be concluded with a further discussion on the potential and application of a DT-integrated UPM machine system, and how in-process data and information being acquired in real time both virtually and physically, and used to continuously optimize the machine system against the stringent ultraprecision machining requirements.

6.2 Ultraprecision diamond turning system

6.2.1 Background of ultraprecision diamond turning

Diamond turning is defined as a process of ultraprecision mechanical turning of precision elements using natural or synthetic diamond-tipped tools. When turning, the workpiece is rotated and diamond tool is traversed along X, Z, and/or C axes of motion to produce precise diameters and depths, as shown in Figure 6.1. It is widely used for machining high-quality aspheric optical components from crystals, non-ferrous metals, acrylics and other materials, as well as moulds for plastic optical components. With the assistance of CNC technology, precise control of the machine parts and the processing environment can be achieved, and thus, workpieces can be turned directly with complicated structure and surface quality.
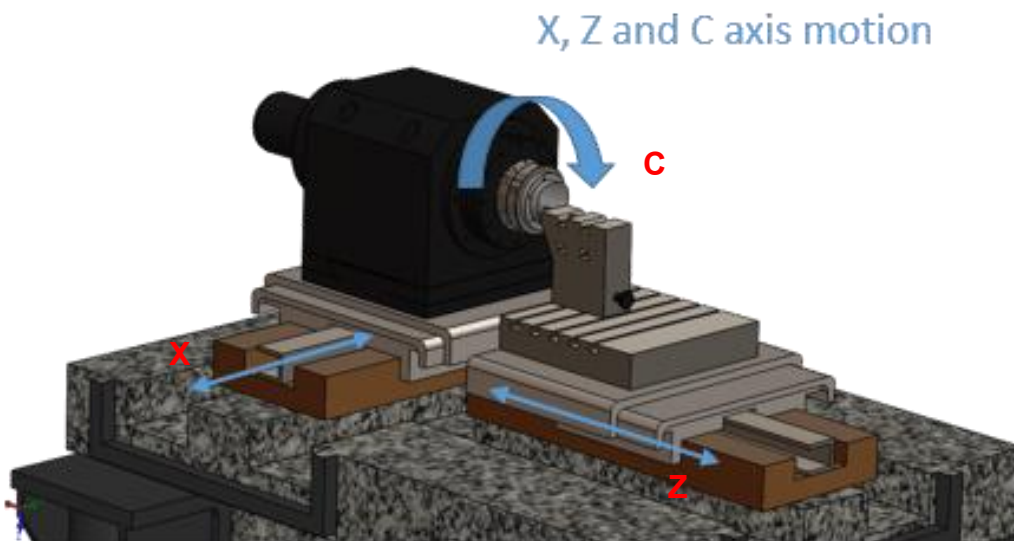
Figure 6.1 Motion system of diamond turning machine

Conventional turning process is limited in creating accurate contours and surface, thus been impossible to meet the demand for high precision complex contoured parts, especially those with freeform surfaces. The advantages of diamond turning machines over conventional turning machines are thus obvious: nanoscale smooth freeform surfaces can be obtained under a single, reproducible turning process.

Diamond turning technology is to date relatively mature and has a wide range of applications, for example, the manufacturing of ultra-high precision aspherical optical

components under the combination with ion beam polishing technology, or production of inexpensive precision aspheric mirrors and lenses under the combination of hard carbon plating and epoxy replication.

6.2.2 Design and development of the ultraprecision diamond turning system

As shown in Figure 6.2, the key components of an ultraprecision diamond turning system are normally including a high-quality granite base, high-accurate motion system with aero/hydro-static bearing slideways, linear motor and encoder, air bearing spindle system with electric motor and air chuck, and Fast Tool Servo (FTS) or Slow Tool Servo (STS) system depends on the cutting process.

Analysis of machine components

Motor | Air bearing spindle | Tool | Tool holder

B1

B7

Air bearings for accuracy

B2

B3

B6

B5

Encoder (linear motor)

B4

B= body
7 bodies
B1= rotatory motion
B2= movement in the X plane
B3= fix to granite
B4= stationery
B5=Encoder for linear motor
B6 = Movement in X and possible Y direction
B7= Movement in the Z direction

Granite
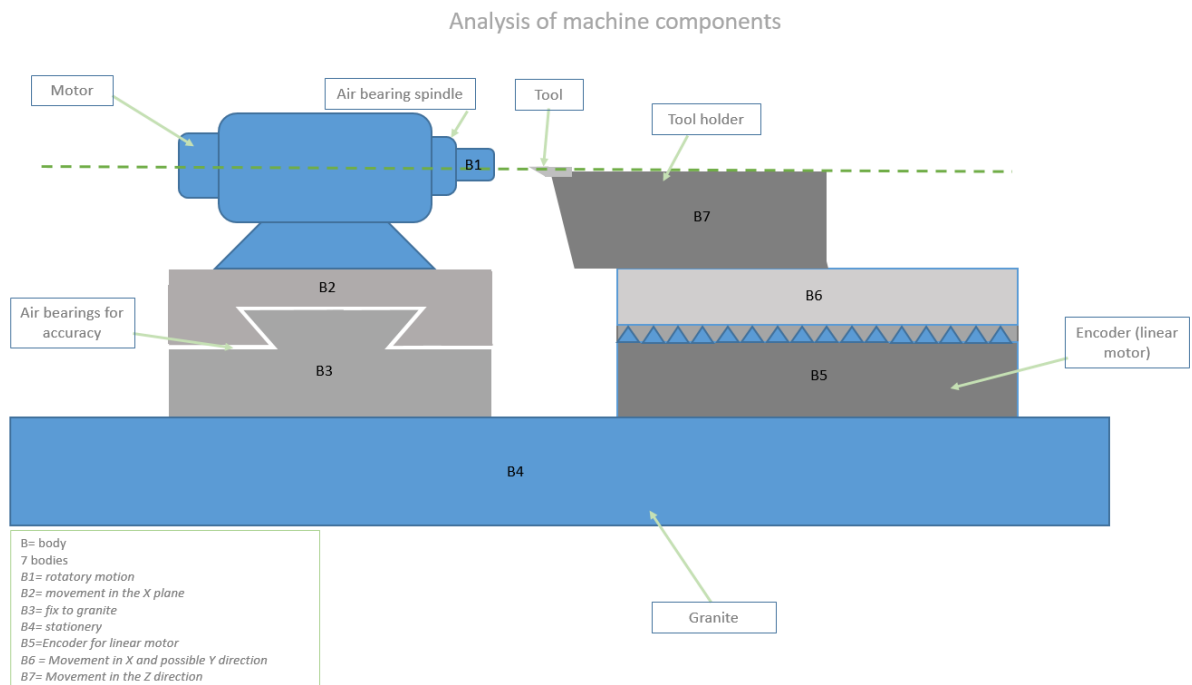
Figure 6.2 Schematic of the ultraprecision diamond turning machine system

After decades of development, existing design and analysis methods for ultraprecision diamond turning system have matured in terms of computing and simulation capabilities. Technically, there is already a wide range of convenient and powerful commercial CAD/FEM software available on the market to support engineering design and analysis, which has directly led to the diversification and economisation of existing devices. Nevertheless, existing design and analysis methods are normally not able to take into account machining errors from multiscale and multiphysics sources, as shown in Figure 6.3, it refers to the transformation of the relative movement of the cutting tool and the workpiece in progress caused by the imbalance of the heat

distribution and machining environment of the UPM equipment in the machining state, specifically reflected in the position error, shape error and surface roughness of the workpiece. It generally includes the geometric error, control error, thermal error, force. In order to achieve ultraprecision patterns (2D) and shapes (3D), it is essential that the causes of apparent random errors in processing machines be analysed, upgraded, refined or replaced, i.e., virtually eliminated and that the systematic errors be minimized. It is thus inevitably needing DT technology, very relevant and meaningful, which enables real-time monitoring and in-process processing and optimizing the complex data from multiple sources and aspects. Therefore, the objective of developing DT for ultraprecision diamond turning system can be summarized as follows:

● Real-time monitoring of the machining process, and in-process data transfer and the process optimization;

● Prevention for possible failures and machining errors;

● Prediction of the machined freeform surface and the in-process decision makings.
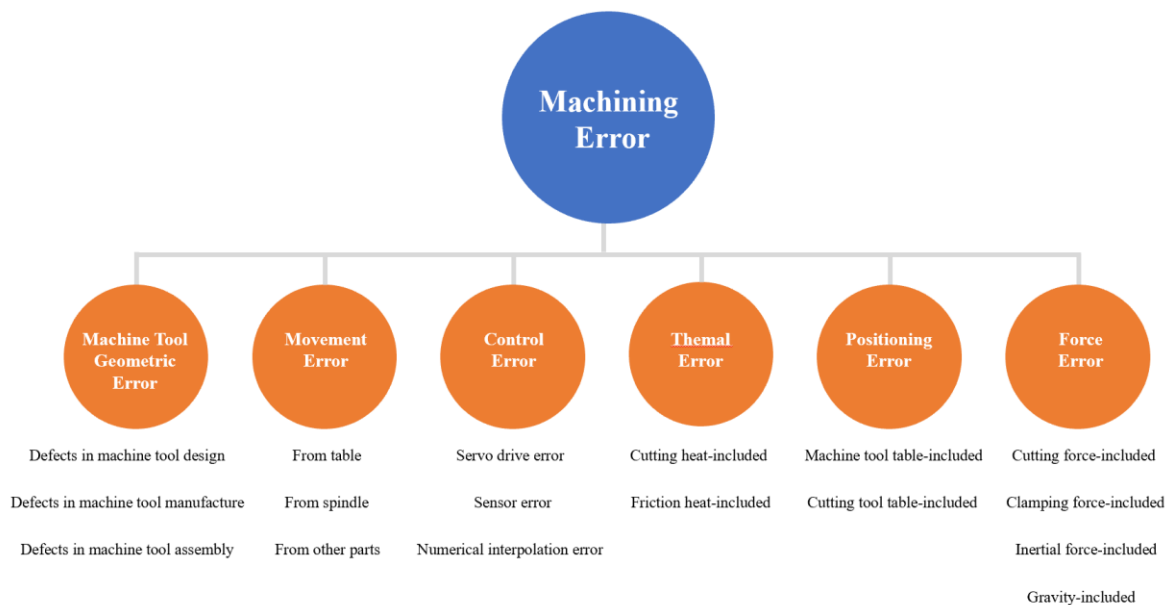
Figure 6.3 UPM machining error sources[113].

The implementation of DT in design and analysis for UPM is still limited, but many researchers are already engaged in active exploratory studies, for instance:

● Regarding motion system development, Gou et al. [12]in his article proposed the application of COMSOL^{TM} MULTIPHYSICS based DT in aerostatic bearing slideway design and analysis, as shown in Figure 6.4, aiming to achieve real-time

data observation and static/dynamic performance analysis, visual simulation and error prevention for precision motion mechanisms of SPDT devices.

- In terms of spindle system design, Liu et al.[147] presented a semi-physical simulation-based model for the design of electric spindle drive systems by their research. By designing a digital twin model of the spindle drive system, cost/scrap calculations can be realized in digital world, instead of destructive testing. The designed control system can be easily deployed on a digital signal processing chip to verify its performance in a time- and cost-efficient manner. Thus the cost/scrap prediction and fault diagnosis of the physical entity are realizable.

Based on the high demands of building accurate multiscale and multiphysics models and breaking through the existing technical bottlenecks, incorporating reconfigurable product structure theory and incorporating with Industry 4.0 concepts especially E-manufacturing, DT and Cyber-Physical System (CPS) is thus the future research trend and development focus.

6.2.3 Industrial needs and enhancement through digital twin in the context of Industry 4.0

Since the beginning of 21st century, ultraprecision technology has been increasingly used as an enabler for design and manufacturing of high precision freeform surfaced optics, devices and components particularly driven by the demands and development in precision engineering related high-tech industries. As ultra-precision machining technology continues to advance, future ultra-precision machining systems are increasingly focused on the machining of micro structured surface features, non-rotationally symmetrical, complex freeform optical parts/devices, and are further becoming a vital technology for the machining of high value-added optoelectronic products and optical communication products. Typical industrial applications of UPM include freeform surfaced Head Up Display (HUD), vari-focal lenses, medical endoscopy devices and surgeon invasive micro tools, and even the space optics for next generation communications (e.g. SpaceX) and space activities. The multiscale modelling and analysis, and the associated advanced simulations and digital twin integration, have substantial potentials and impacts for extension of simulation from the product design stage to following-up lifecycle stages by in-process or remote tuning, error prediction, higher precision enhancement, and continuous improvement

of the product[10].

Nowadays the DT technology is used in a wide range of industrial scenarios, for example, in large production plants and factories to optimize working space layouts and improving safety, effectiveness, and ergonomics[148], for production optimization of the petrochemical industry[149],or to improve the vertical and horizontal integration of automotive manufacturing systems[150]. However, there are few for DT applications in UPM, as which represents the most advanced machining technology and material processing capability.

6.3 Design and development of the digital ultraprecision diamond turning system

6.3.1 Digital twin infrastructure for the diamond turning machine

As illustrated in Figure 6.4, the DT infrastructure for diamond turning machine adapted from Deloitte Insights[151], expresses five components for facilitating a DT, those being from the physical world taking the sensors and actuators, and then the integration brought with data, analytics and continuous development.
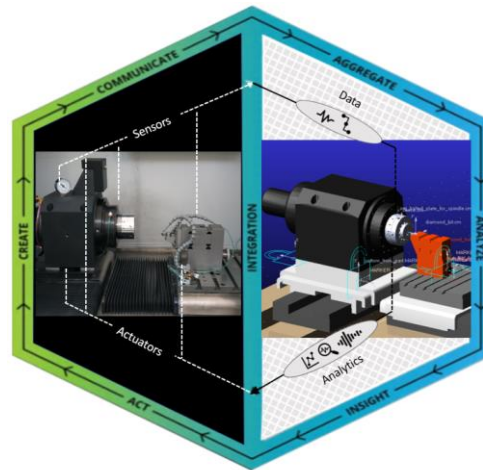
Figure 6.4 Overview of DT concept in SPDT based on the framework from Deloitte Insights

The overall objective of DT is to identify conditions which are not yet optimal, through looking into every dimension which constitutes the model. This can have significant effects on the physical world in dimensions such as speed and cost. The creation of a DT involves a physical model that can be fitted with an array of sensors, allowing information to be sent on critical points within the physical parts and its surroundings.

There are two main types of sensors, which can be categorised as operational and environmental, with the capability of monitoring factors that significantly affect the accuracy performance and lifetime of the diamond turning equipment. All sensory information is aimed to provide data that can be communicated with different systems within the manufacturing process, as shown in Figure 6.5:
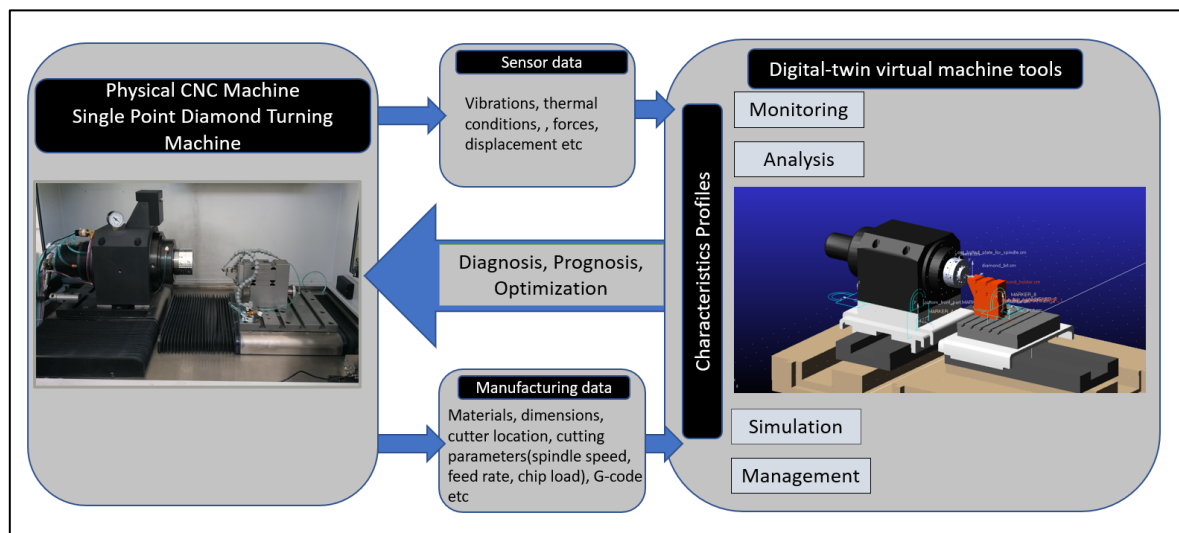

Figure 6.5 Digital-Twin using sensory data and information integration

6.3.2 Automatic dynamics Analysis by using the Newton Method

It was proved that the algorithm based on Newton-Raphson method is an efficient tool to generate toolpath for diamond turning process by producing freeform surfaces due to the capability of solving non-linear functions[152]. Using this approach, it can precisely generate the coordinate position of the tool at each given step time, as seen in Figure 6.6.
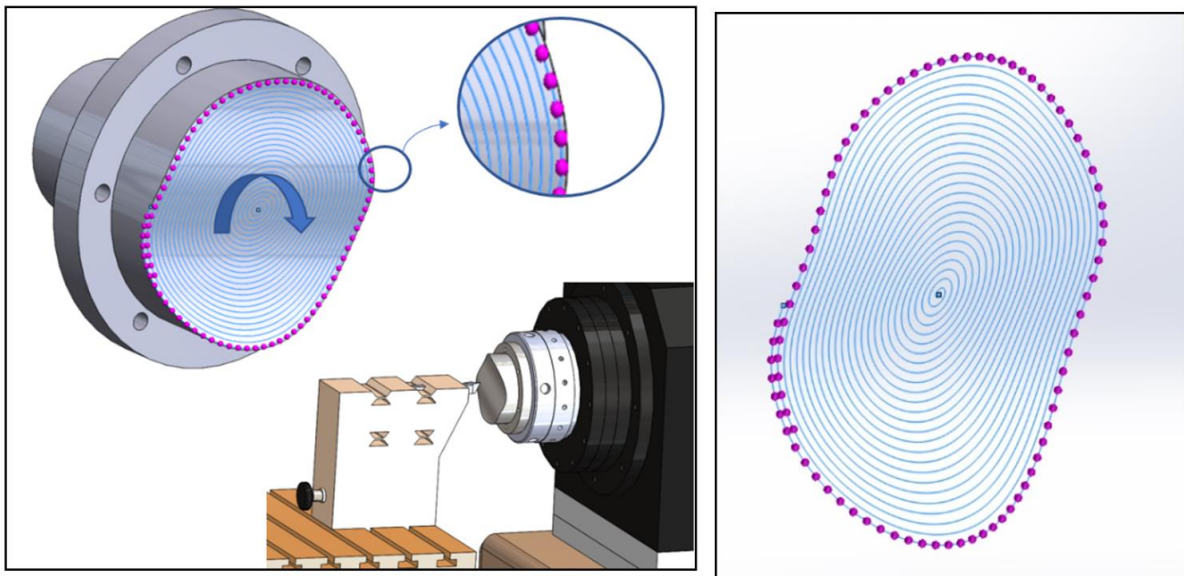
Figure 6.6 DT using sensory data and information integration

Considering the system as a simple single degree of freedom mass-spring, which is represented by equation (6-1). Whereby (m) is the mass, which is affected by force which was applied (F) by the direction which is represented by (u). Through which displacement for the mass is only permitted within the direction of (u). As a result of this, Newton's second law is considered within the system, as force within the system is equal to mass times acceleration, at (t) being step time.

Whereby:

$M\ddot{u}$ = the mass acceleration at time (t), which is the second derivative of (u), with a specific step time.

K = the stiffness constant

C = the constant for damping induced through any loss in energy friction that is between contacts.

$$M\ddot{u}(t) + C\dot{u}(t) + Ku(t) = F(t) \qquad (6\text{-}1)$$

With regards to the damping phenomenon, due to the complexity of it, it can be pre-noted that, where viscous damping is the damping force, is normally proportional to the velocity.
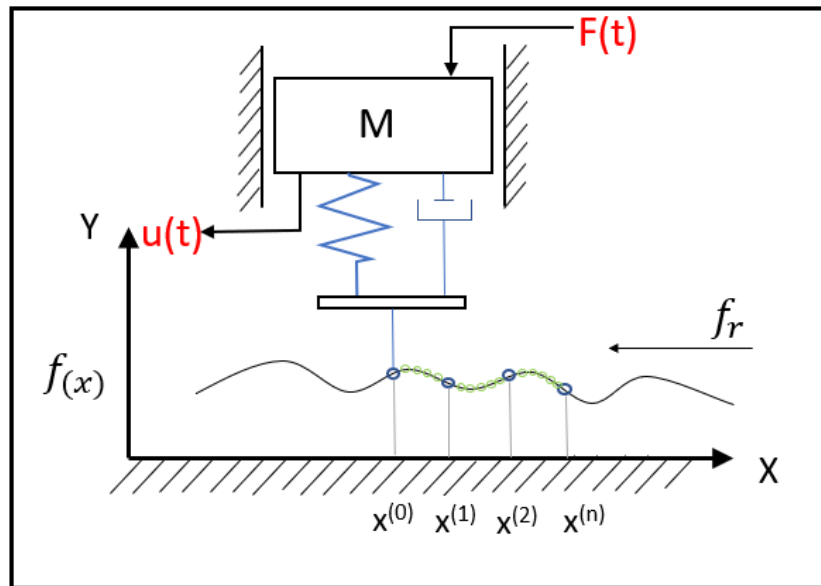
Figure 6.7 Simplified motion system of surface turning

Instead of a single value for the mass, damping and stiffness constant matrices will need to be considered as well. Due to the system of SPDT being multibody whilst also having multi-degrees of freedom as seen above, the equation (6-2) proposed below, with [M] mass, [K] stiffness & [C] damping becoming matrices.

$$[M]\ddot{u}(t) + [C]\dot{u}(t) + [K]u(t) = F(t) \qquad (6\text{-}2)$$

Then whereby:

u(t) = represents the vector for displacement at (t) time;

$\dot{u}$(t) = represents the vector for velocity at (t) time;

ü(t) = represents the vector for acceleration at (t) time;

F(t) represents the force vector variation at each given time step.

Differential and algebraic equations as a group are used to define the equation of motion. The integration of the differential equations can produce solutions numerically which can satisfy the algebraic constraints equation that takes place at each step size of the motion. With resolving the stiff system, a method which is extremely effective in computation is the stiff integration method, other processes for solving the differential equation have often been seen to perform badly and fall behind in a timewise manner. In the realms of multibody dynamic systems, the bodies' orientation and positions can be found by the absolute coordinates. Within the context of ADAMS solver, it uses the three Cartesian coordinates X, Y and Z for the position of rigid bodies. As seen in equation (6-3).

$$p=\begin{bmatrix}x\\y\\z\end{bmatrix} \tag{6-3}$$

The rigid bodies orientation within ADAMS solver uses a set of three Euler angles, which in turn correspond to the 3– 1– 3 sequence rotation: α, β, and γ which are in turn kept in an array.

$$\varepsilon=\begin{bmatrix}\alpha\\\beta\\\gamma\end{bmatrix} \tag{6-4}$$

Then, in turn, the generalised coordinate which is associated to the rigid body i within Adams is denoted as follows:

$$q_i = \begin{bmatrix}p_i\\\varepsilon_i\end{bmatrix} \tag{6-5}$$

Then by following the logic, the multibody requires an additional equation to allow the motion of the system. Which is demonstrated below by equation (6-6) that shows the generalised coordinate vector for the application at hand:

$$q_n \text{ x } 1 = [q_1 q_2 \dots q_n]^T = [q_1^T q_2^T t \dots q_N^T]^T \tag{6-6}$$

Which contains the following:

$$q_i = [x_i y_i z_i \alpha_i, \beta_i, \gamma_i]^T \qquad \text{(6-7)}$$

n: at any point in time the orientation and position of the given body in the system.

N: the number of bodies in the system

Then, as seen above, x, y and z describe coordinates of the body i – n in translation to the origin global reference coordinates.

With the system being represented by α_i, β_i, and γ_i as the Euler angles, as previously mentioned, then we can take the motion equation which was previously examined and adapt it as follows:

$$M\ddot{q} + \Phi_q \, T_\lambda = Q \qquad \text{(6-8)}$$

Whereby:

Q : the generalised vectors of the forces

M: the inertia matrix

$\Phi_q \, T_\lambda$:   the generalised vector of the reactions,

Φ_q: the Jacobian matrix constraint equations

λ : the Lagrange multiplier vector

Furthermore, position level at each step is needed to be achieved by generalised coordinates in order fulfil the constraint equations.

$$\Phi_m x \, 1 = \Phi(q, t) = 0 \qquad \text{(6-9)}$$

Which represent the following:

t: the time

m: the constraint numbers.

Then the equation can be conveyed by differentiation of equation which is above with regards to the time at the given velocity level.

$$\dot{\Phi} = \Phi_q \dot{q} + \Phi_t = 0 \tag{6-10}$$

Then the following equation for Jacobian matrix can be written as:

$$\Phi_{q(mxn)} = \begin{bmatrix} \frac{\partial \Phi_1}{\partial q_1} & \frac{\partial \Phi_1}{\partial q_2} & \cdots & \frac{\partial \Phi_1}{\partial q_n} \\ \frac{\partial \phi_2}{\partial q_1} & \frac{\partial \Phi_2}{\partial q_2} & \cdots & \frac{\partial \Phi_2}{\partial q_n} \\ \vdots & & & \\ \frac{\partial \Phi_m}{\partial q_1} & \frac{\partial \Phi_m}{\partial q_2} & \cdots & \frac{\partial \Phi_m}{\partial q_n} \end{bmatrix}_{m \times n} \tag{6-11}$$

The Jacobian matrix can be used for understanding and representing the force, position, acceleration and any reaction forces. In turning process, this can be used for the tool path generation for the unknowns at every iteration along the curve.

6.3.3 Kinematics analysis and integration of position level

The initial point of the system is known at (t0) time. However, at (t1), which is the second time step, is unknown. As shown in preceding equations the systems nature is of non-linear constraint, and the Newton-Raphson iterative method is used within ADAMS to calculate q_1 at time t_1. Therefore, the Taylor-expansion-based linearization with regards to non-linear constraint equation can be achieved by using the following:

$$\Phi(q_1, t_1) = \Phi(q_0, t_1) + \Phi(q_0, t_1)(q_1 - q_0) \tag{6-12}$$

By utilising this method at any given time, unknown constraints can be found easily. Then, by following this logic, the unknown acceleration and Lagrange Multiplier can be found at any given step from within the integration process of the equation. The most frequent solver within ADAMS is the direct index 3 differential algebraic equation (DAE). Which was demonstrated within the kinematic constraint.

The modelling of ultraprecision diamond turning system is carried out by using multi-body dynamics analysis method and tool (ADAMS), while considering the mechanical structure of the system as multibody mass-spring-damping. Newton's second law is thus considered on the system, the modelling process for the ultraprecision diamond turning system is illustrated in Figure 6.8:
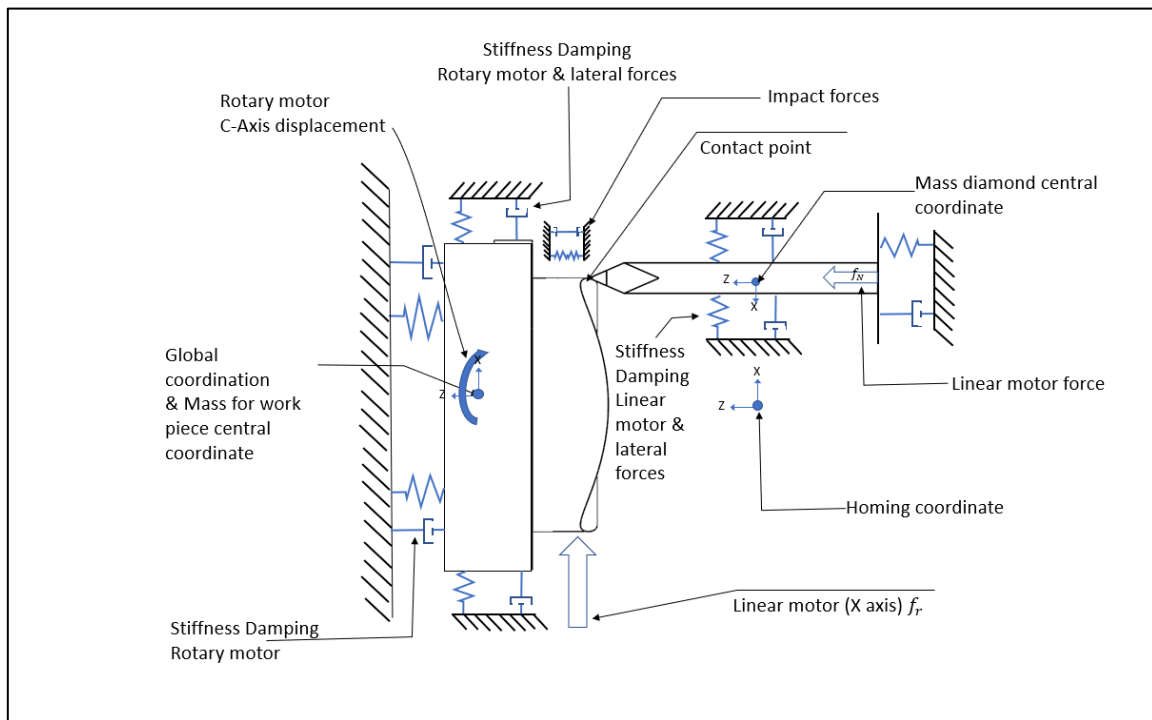

Figure 6.8 Motion system model build by ADAMS

As demonstrated in Figure 6.9, the approach of ADAMS allows data to be taken in real time from the virtual system which in turn can be cross examined with that coming from the physical system. The multi-body dynamics-based approach and the associated modelling and simulation (implemented with ADAMS) allow simulated data to be taken in real time from the virtual system.
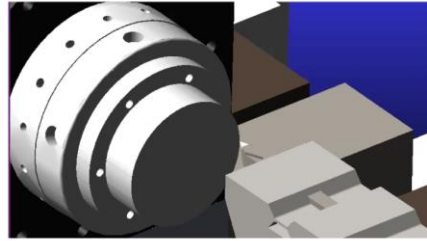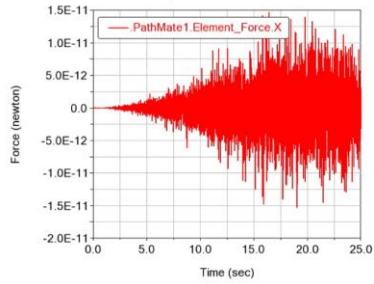
(a)
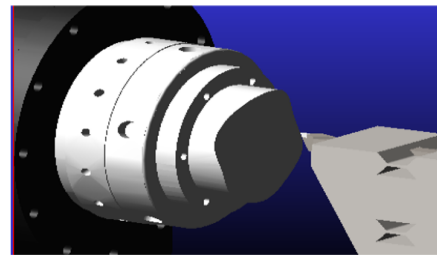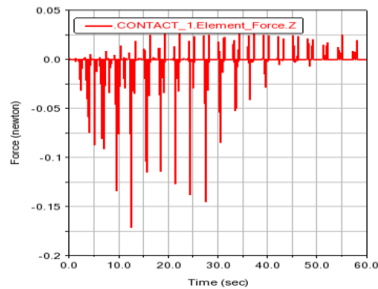
(b)

Figure 6.9 Cutting forces prediction by using ADAMS based simulations, (a): Flat surface machining; (b): Freeform surface machining.

As shown in Figure 6.9, Through developing a multibody dynamics-based system (in ADAMS), cutting forces and machining error prediction can be realized by the created virtual digital simulation system, thus to provide measurement and insights during the entirety of the cutting process. The main parameters that have a profound effect on the surface finish, are the cutting forces and tool wear. For cutting forces, this is down to the interfacial actions between the diamond tool and workpiece surface. In this scale, there are numerous influence factors being involved, those being feed rate and depth of cut. By understanding the cutting forces in a digital twin manner, it can provide better understanding of its behaviour and the consequent effect on the machining system dynamics and consequently the machining errors of the system. Therefore, it is able to further in process monitor these cutting forces in the physical system and optimize the machining process dynamically and the surface finishing, which is particularly beneficial for ultraprecision diamond turning of freeform surfaces.
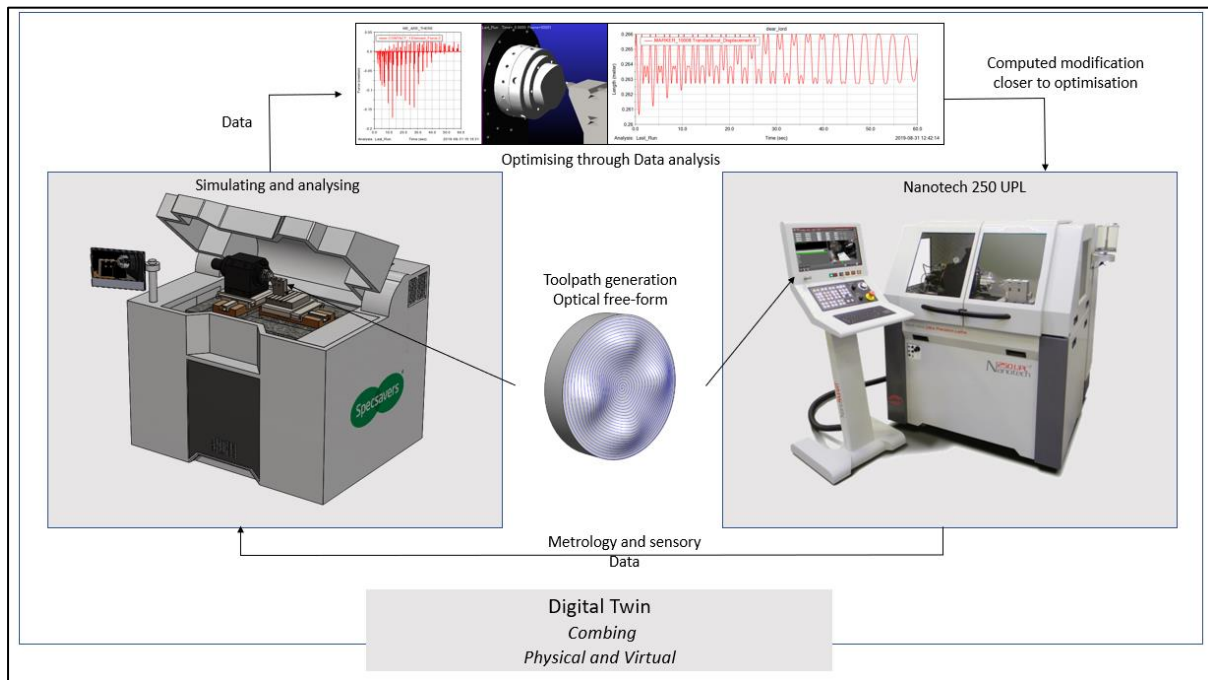
Figure 6.10 Retrieving Data from The Physical System using Metrology Systems

Data retrieval will be done through the metrology systems which are already in use and have had vast amounts of research undertaken into them. Those being such systems as scanning probing method, optical detection method and microsensors. These sensors in real-time feedback the totality of what is happening in the physical system to the digital system as seen in Figure 6.10. The feasible methods for data transmission and collecting of DT system will be discussed in following sections separately.

So far, the construction and dynamic, kinematic simulation for the digital part of a diamond turning DT system are completed. The next step is the implementation of data transfer and communication between the physical and digital twins.

6.4 'In-process' data retrieval from the machining system

It is proved by the previous sections that the collection of critical data from the cutting process is essential for realizing the communication between physical and digital world, from this aspect, the industrial-scale applications with the aid of advanced in-process

monitoring and prediction models, algorithms, and digital-enabling technologies for diamond turning system are thus required.

The degradation of surface quality during UPM processes is often attributed to dynamic instabilities. However, the existing methods for predicting instabilities in UPM processes are still in their infancy. In order to applicate the DT from this aspect, the relationship between different parameters and surface characteristics should be investigated using a combination of analytical modelling and real-time monitoring means. Therefore, by combining suitable virtual models and sensing data, it is possible to help select suitable and "stable" process conditions, observe variations in surface roughness while obtaining it at the nanoscale, and predict machining errors that are barely visible, thus reducing post-processing difficulties.

6.4.1 Using the encoder outputs (position, velocity, acceleration) within the machine system

Optical encoders are high-precision positioning sensors based on the interference patterns produced by the relative movement between two gratings, the nanometric resolution and MHz-level data response led it to be an ideal real-time monitor for DT. According to the operating principle, the displacement, velocity and even acceleration for the motion parts of UPM system can be directly obtained during machining in real time based on the approach of encoders. These data provide a very visual representation of the relative movement between cutting tool and workpiece, which directly influences the machining quality. By integrating the collected data into the virtual model of DT, it is possible to observe the state of the motion system in real time throughout the machining process, thus to detect and predict machining defects in advance and to reduce repetitive post-processing works. As shown in Figure 6.11. Its high accuracy and resolution, combined with its relatively low price, has led to a wide range of applications for position and speed measurement in position or motion control, particularly in UPM equipment.
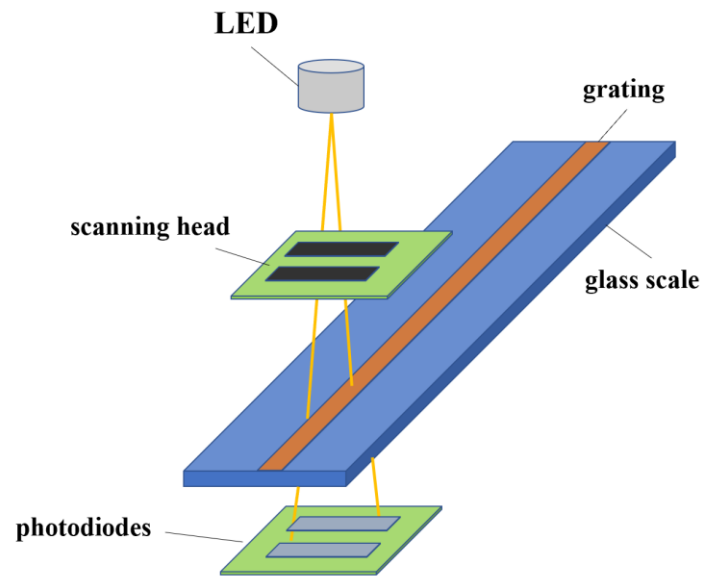
Figure 6.11 Main components of an optical linear encode[153]

According to the operating principle above, the displacement, velocity and even acceleration for the motion parts of UPM system can be directly obtained during machining in real time based on the approach of encoders. These data provide a very visual representation of the relative movement between cutting tool and workpiece, which directly influences the machining quality. By integrating the collected data into the virtual model of DT, it is possible to observe the state of the motion system in real time throughout the machining process, thus to detect and predict machining defects in advance and to reduce repetitive post-processing works.

6.4.2 Using cutting forces data from the machining process

Cutting force calculation, modelling and analysis has been always an important process indicator in UPM, which can collectively reflect the various cutting process phenomena and dynamics such as size effect, chip formation, energy consumption and cutting heat partition, in addition to the machining instability and chatter. It can also be correlated with the tool cutting performance particularly with the tool wear and tool life. Therefore, cutting force is seen as a key factor to optimize the cutting process variables and tool geometries in micro-cutting processes, and thus make it meaningful

to use cutting forces data as an in-process monitoring aspect for the DT. The use of cutting forces as a data resource of DT enables in-process detection of the variation such as energy input, environmental disturbances during machining and prediction of tool wear. From another aspect, with the integration of pre-established cutting force models in DT enables the observation of unexpected changes of cutting force and thus the prediction of possible defects before post-processing and surface inspection work. In ultraprecision and micro-cutting processes, cutting forces are in the range of 0.1-1N[10], whereas in conventional machining they are typically hundreds or thousands of times higher. Thus, accurately measuring and analysing their values can be challenging, especially during machining process. Regarding this, the dynamometer with small temperature error, high sensitivity and natural fraction, is nowadays widely used as the dominant cutting force detection device in UPM, which can measure three perpendicular cutting force components simultaneously during machining and the measured numerical values can be stored in computer though the data acquisition system. For instance, by the study of Niu et al[154], as seen in Figure 6.12, the Kistler dynamometer 9256C2 was used for measuring small force less than 0.002 N during micro milling process.
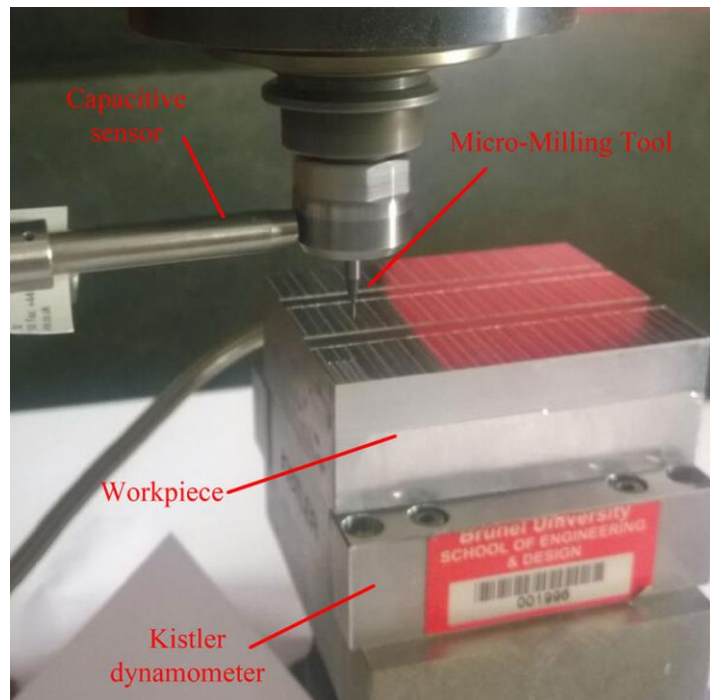
Figure 6.12 Experiment set-up for evaluating and validating the cutting force modelling[154]

6.4.3 Using the surface 'signature' data from the component machined

Direct inspection of the 3D surface texturing and characteristics of the machined workpiece surface during processing is a relatively more intuitive method. The real-time monitoring and control of surface morphology variations in their incipient stages are vital for assuring nanometric range finish in SPDT process. To date, the method for surface monitoring of UPM are various, for instance, by the analytical approach of non-parametric Bayesian to capture the inherently complex, non-Gaussian, and non-stationary sensor signal patterns observed in process[155], or use acoustic emission (AE) to collect the signals of the transient elastic waves generated from the rapid release of energy from one or more sources within the material[156]. With these data, DT can thus directly intervene the cutting process and compensate surface errors based on the pre-implemented algorithms.

These kinds of in-process monitoring methods are proved to be very beneficial to the UPM DT from application standpoints, for example, during the wafer dicing, which is

a typical application scenario of UPM, wafer yield losses will be mitigated to a great extent, if the onset of UPM process drifts can be detected timely and accurately.

6.5　Application case studies for DT on ultraprecision manufacturing of freeform surfaced devices/components

Freeform surfaces, also known as Non-Rotationally Symmetric (NRS), can be defined as surfaces with no axis of rotational invariance (within or beyond the optical part)[157]. The difference between freeform surface with other kinds of surfaces is shown in Figure 6.13.
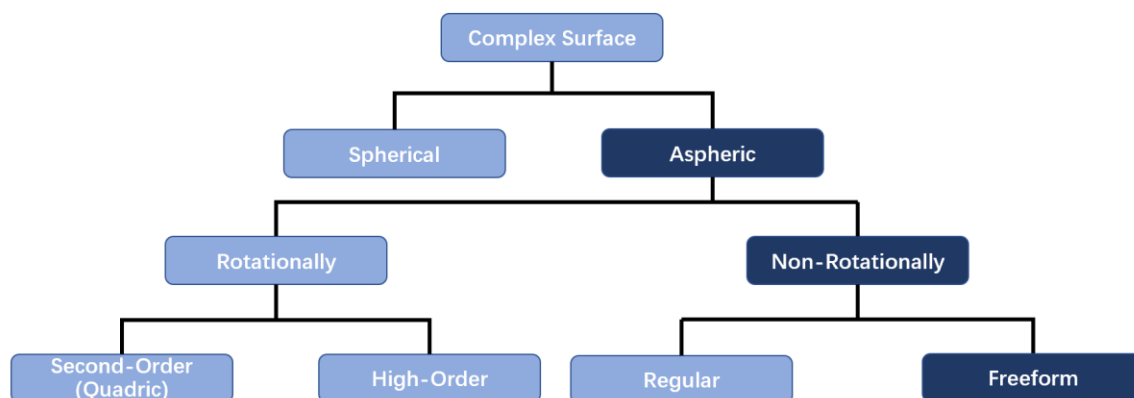
Figure 6.13 Difference between optical surface types

Freeform surfaces generally denote complex and unconventional continuous surfaces without rotational symmetric axes. Their mathematical representation is highly intricate, demanding advanced design capabilities. Due to the combination of asymmetric, irregular, and complex surface configurations, they can broadly encompass surfaces of any shape. Consequently, the mathematical representation complexity and challenges associated with describing freeform surfaces far exceed those of spheres, rotationally symmetric non-spherical surfaces, off-axis cones, and toroidal surfaces.

In optics elements, freeform surfaces not only enable functionalities challenging for traditional spherical or non-spherical surfaces but also require fewer elements for the entire system. This results in a more simplified, lightweight, and highly efficient optical system, meeting the demands of high-performance, lightweight, and miniaturized modern optical systems. As a result, freeform optical components find extensive applications across various domains, primarily within imaging, illumination, and display fields[157][158].

Ultraprecision machining of freeform surfaced component requires more degrees of freedom than conventional methods, which brings in numerous challenges. The experimental setup and partial results are shown in Figure 6.14, based on an ultraprecision diamond turning machine (Moore Nanotech UPL 250), computer aided manufacturing (CAM) + non-uniform rational B-splines (NURBS) generated tool paths, and synchronized multi-axis actuation in a digital twin manner. Although the in-process data collection facility is limited, the cross-validation with the created digital twin is still realizable.

(a)   (b)   (c)
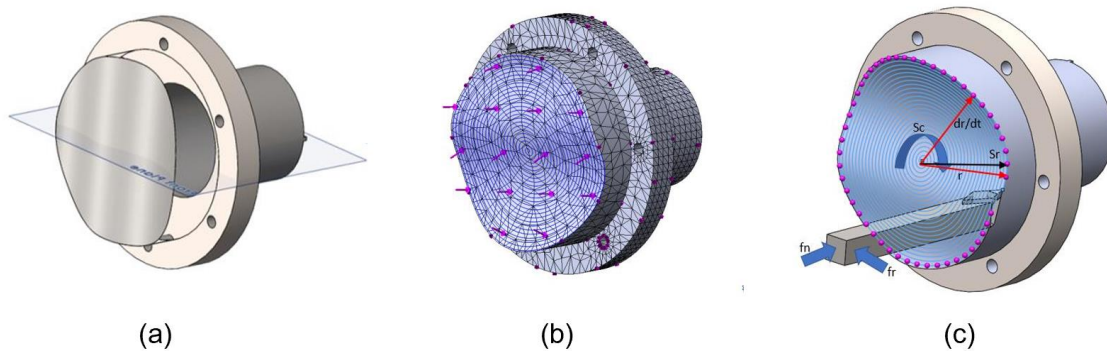
Figure 6.14 Freeform surface DT model generation
(a): 3D freeform surface structure; (b): Generated mesh for finite elements; (c): Tool path and cutting force calculation

The generation of freeform surface and the related calculation are shown in Figure 6.14. With the help of NURBS, freeform surface can be obtained in 3D model, then

detailed surface contour is differentiated into finite elements and calculated by the pre-set mathematic models regarding cutting force and tool path in ADAMS.
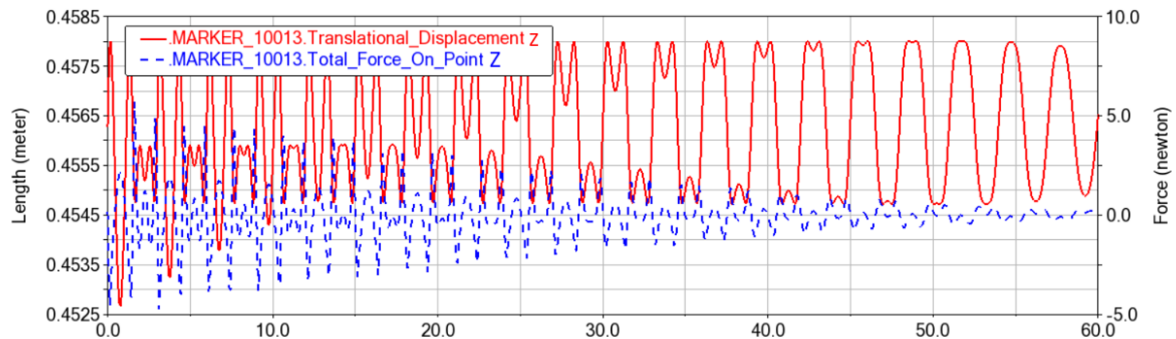

Figure 6.15 Displacement and cutting force data generated by DT

Figure 6.15 illustrates the Z-axis displacement data and cutting force data calculated based on the pre-established mathematic model in DT, both with a processing time of 60 seconds.

The cutting force and tool path simulated by DT can be used to predict the machining process in advance, and by comparing with the in-process data fed back from the encoder and the dynamometer, it is possible to realize the prediction and prevention of machining defects during the turning process directly. If the corresponding CAM algorithms is integrated, it is possible to achieve the remote monitoring of the machining process and online defects compensation through the operating of G-Codes.

Figure 6.16 Freeform surfaced components ultraprecision machined at the diamond turning machine with further support of digital twin approach.

The scientific understanding of the corresponding micro cutting mechanics in freeform surface machining is thus essentially important, while constantly achieving the nanometric level optical surface finishing, multiscale modelling and analysis is likely a useful technique on this combined with advanced algorithms spanned out from NURBS. Ultraprecision diamond turning of freeform surfaced components and devices are increasingly demanded in particular in industrial scale ultraprecision manufacturing of head-up display (HUD) and light detection and ranging (LiDAR) devices, ophthalmic lenses, off-axis laser mirrors, and space optics. The experimental and application case studies above have indicated the potential and applications of the ultraprecision diamond turning system working with its DT.

6.6   Ultraprecision manufacturing of freeform vari-focal lenses

Over the past two decade or so, a dramatic application change of freeform surfaces was occurred in design and manufacturing of vari-focal lenses also known as Progressive Addition Lenses (PAL)[159]. The demands for freeform optics also drive the development of ultraprecision machining technology. Due to the complexity of

freeform surface, the design of vari-focal lens is much more challenging and requiring specific expertise compared with that of traditional ophthalmic lens. For lens manufacturers, the machining accuracy, productivity, and unit cost in vari-focal lens manufacturing are key challenges. While eye features are unique for and individual customer, it means the prescription of vari-focal lenses for an individual customer is different and personalized. Therefore, mass customization for personalized lens manufacturing is required, and the quality assurance, delivery time, costs, tracking and tracing of the lens product, and its personalized experience are essential for customers.
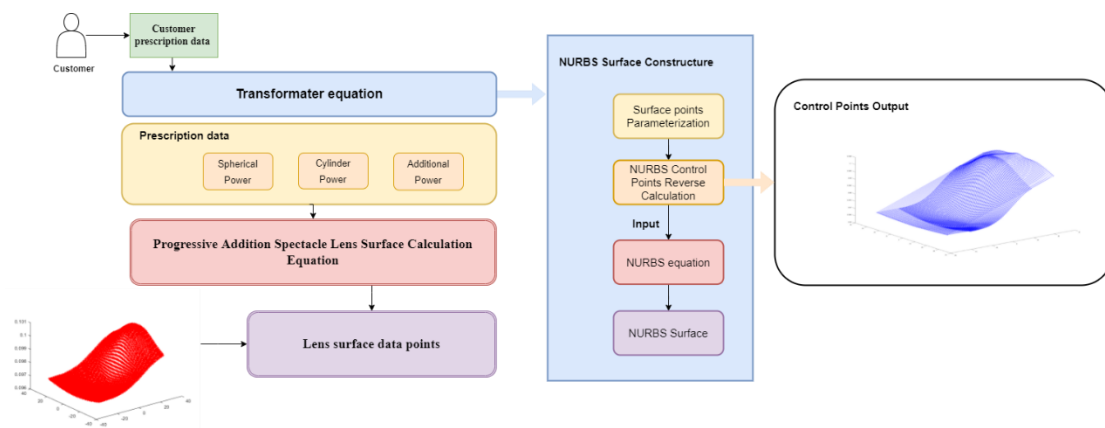

Figure 6.17 Vari-focal lenses surface construct process

Figure 6.17 describes the method to generate vari-focal lenses surface based on NURBS. NURBS serves as a powerful tool in the design of freeform surfaces, it utilizes polynomials for curve and surface representation, which enables the creation of three-dimensional models that capable of achieving exceptionally precise depictions of freeform surfaces. Moreover, this methodology significantly streamlines the adaptation of lens surfaces to meet diverse customer requirements.

After the construct process, tool path can be easily generated during algorithms or Computer Aided Manufacturing (CAM) software, and the surface will be further generated by ultraprecision machines with FTS. The application of FTS in freeform surface machining device is shown in Figure 6.18
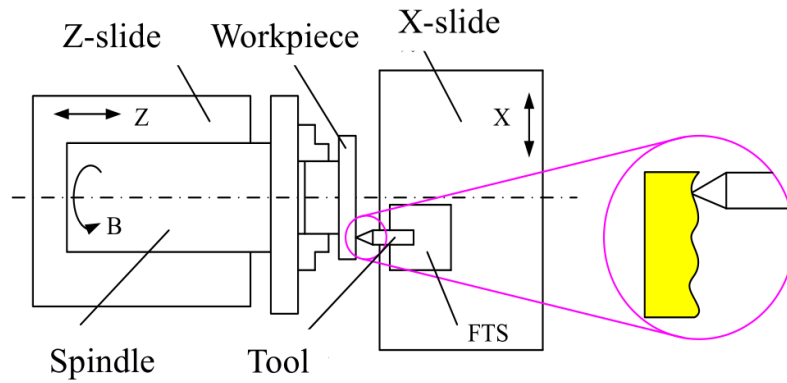
Figure 6.18 Vari-focal lenses surface machining process with FTS

The whole manufacturing system can be integrated as follows:
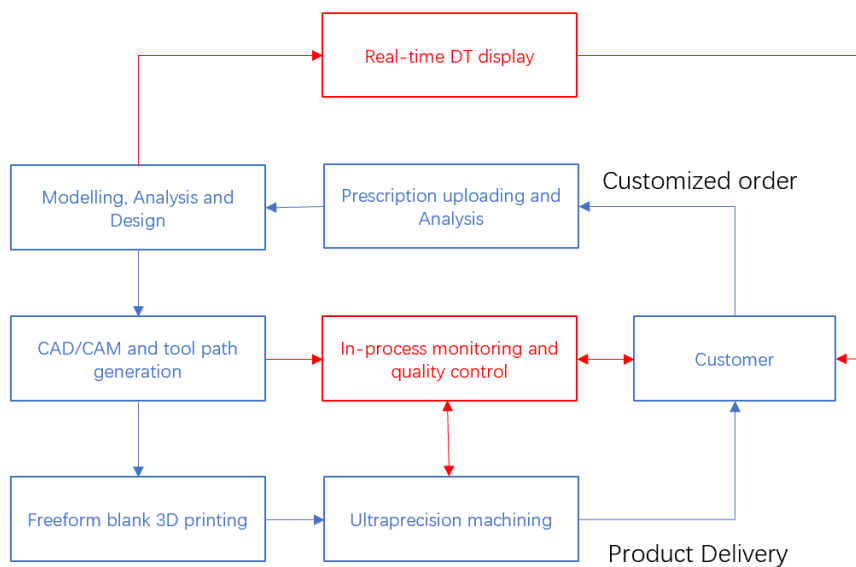
Figure 6.19 Vari-focal lenses manufacturing system information processing activities

Figure 6.19 illustrates the manufacturing system for vari-focal lenses and the role DT plays in it. The information and material flows of the traditional manufacturing system are marked in the blue, where customer demands are divided into design requirements and processing requirements and integrated into the UPM process to be realised. In this whole progress, information transfer is in a linear/non-crossover system, as there is no reverse feedback between the customer and the "modelling, analysis and design" module, and no real-time data output from the machining process as well, which

making after-sales service and demand adjustment from end-user much more difficult. Based on this situation, the intervention of DT, which is marked in red, makes significant sense. The customer can observe and intervene in the design process through the virtual "twin", which presents the design data in real time, and through the in-process monitoring method mentioned in above chapter, e.g., real-time surface observation, to obtain real-time information on the machining progress and quality, thus reducing the production cycle time of the vari-focal lenses, simplifying the quality control work, increasing productivity, and improving customer satisfaction.

6.7 Ultraprecision manufacturing of HUD devices

Head-up display (HUD) is transparent display that present data and are designed to enable end-users to read the information they need without taking their eyes off their usual point of view. As shown in Figure 6.20:
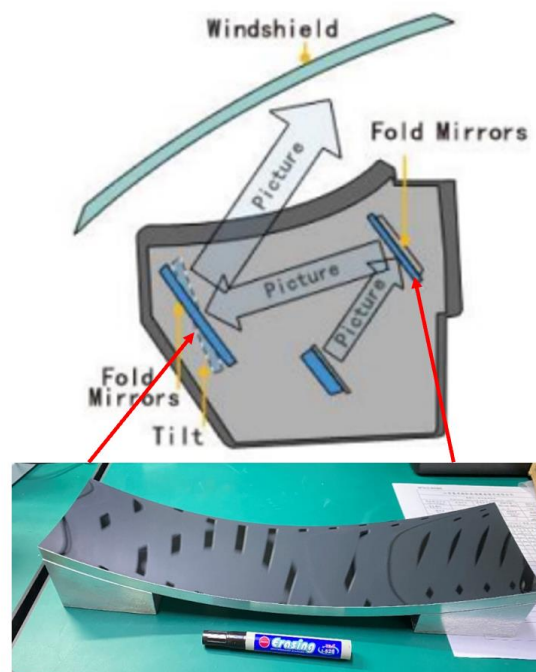

Figure 6.20 Free-form shape for HUD

The HUD was limited in military and civil aviation applications in the early stage after invention due to the high processing costs. Recently it is widely used in motor vehicles based of the maturity soft injection moulding technology[160]. As the optical image of a vehicle HUD is formed by reflections on the windshield, and each type of vehicle has its own unique form, it is thus necessary to adapt the image-forming optics uniquely for each variable type, which requires an effective approach in optical design and surface generation.

As another typical freeform industrial component, the manufacturing system of HUD is similar to that of vari-focu lens, the design and generation phase of surface can be described by NURBS without any lack of performance. This kind of description can then easily be transfered to CAD systems by standardized formats like IGES or STEP without any error-prone conversion, and furthur tranlate into G-code for machining process.

As illustrated in Figure 6.21, the study of Park et.al[161] purposed a manufacturing process of SPDT machining with diamond turning machine (DTM).
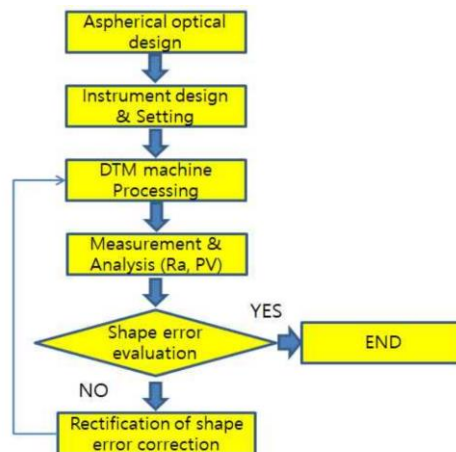

Figure 6.21 Flow chart for manufacturing process of HUD

It is obvious that the HUD manufacturing process has the similar limitations like vari-focal lens, although the demand of flexibility in customization is not as much, the capability and effectivity of mass production are also limited by the rapid design word, data lagging and post-processing. Since the DT has been proved to have great

potential in data transparency, in-process machining monitoring and post processing optimization, the approach of DT would definitely be the trend of academical research and industrial development for HUD.

6.8 Conclusion

This chapter presents an innovative approach to developing DT- for the ultraprecision diamond turning system and its implementation and application perspectives. It will likely provide new insights into the development of next generation ultraprecision machining systems in the era of Industry 4.0. The advanced modelling, design and analysis methods are used in the development, including multi-body dynamics modelling and analysis, machining system dynamics, in-process cutting forces monitoring, and DT integration. The ultraprecision machining system DT has shown the capability map organically and can coordinate the functional, structural, behavioural, control, intelligence and performance of a machine system represented both virtually and physically. However, there is still the systematic gap in building multi-dimensional and high-fidelity DT in particular effectively integrated with ultraprecision manufacturing. This should be the future research and development direction for applying DT in ultraprecision diamond turning systems, albeit the work presented here has made the attempt and efforts along the line.

Chapter 7   Experimental and industrial case studies

7.1   Introduction

In the previous chapters, theoretical studies were performed on UPM machine platform development by the proposed multiscale multiphysics modelling, simulation and analysis approach. The design of aerostatic bearing components was also introduced in Chapter 4 and Chapter 5.

In this chapter, the details of design related industrial experiments for UPM machine platform and its key components are described with the following purposes:

● Evaluation and validation of the multiscale multiphysics modelling and simulation approach on the design of aerostatic bearing rotary table and machine platform.

● In-depth study on the effects of design parameters on aerostatic bearing product performance.

● Optimization of the multiscale multiphysics modelling and analysis methodology on UPM machine platform and its aerostatic bearing components in real industrial scenario to make the design work better and more efficient.

7.2   Industrial case study on aerostatic bearing rotary table design

7.2.1 Overview

In addition to the previously discussed aerostatic linear slideway, the aerostatic rotary table represents another notable air bearing product utilized in UPM applications. The precision aerostatic bearing rotary table is a sophisticated mechatronic device employed primarily for achieving highly precise rotational positioning of objects. It boasts several advantages, including exceptional precision, extended service life, and minimal pollution. Consequently, this technology finds widespread usage in precision machining, precision inspection, and inertial simulation. The objective of this experiment is to undertake a comprehensive "design-simulation-production-assembly-

commissioning-optimization" process from an industrial design and application perspective, thereby validating the multiscale and multiphysics modeling and analysis methodology and design theory mentioned previously.

7.2.2 Experimental set up

A series of experiments were conducted under the auspices of an "UPTech Co. Ltd." industrial project, with the objective of identifying the key factors that have a significant impact on the performance characteristics (such as load capacity, static stiffness, and motion accuracy) of the product. The resulting data is intended to inform the development of general models that can be applied to standard products. The experimental design was developed in consultation with industrial partners, taking into consideration the specific requirements of the project.

7.2.2.1 Mechanical system design

The development of aerostatic bearing rotary tables necessitates consideration of various aspects such as design, manufacturing, assembly, drive and control, quality testing, and optimization to ensure compliance with the relevant accuracy requirements. Leveraging the fundamental design methodology for aerostatic bearing components outlined in previous chapters, a prototype of an aerostatic bearing rotary table was designed with the following specifications as shown in Table 7.1:

Table 7.1 Specifications of aerostatic bearing rotary table

Supply pressure	0.4-0.6 MPa
Positioning accuracy	±2 arcsec
Repeatability	±1.5 arcsec
Max. Rated speed	300 rpm
Axial stiffness	96 N/µm
Axial load	200 N
Axial run-out	1 µm
Air consumption	<20 L/min

The designed aerostatic bearing rotary table comprises various components such as the air bearing system, torque motor, circular grating, thrust collar, rotor shaft, grating shaft, housing, and turntable. The turntable, thrust shaft ring, and rotor shaft are secured to the motor rotor and rotor shaft through bolts. The motor stator is interference-fitted to the turntable housing, while the angle grating is bolted to the grating shaft. The installation of the angle grating and shaft employs a tapered fit, which enables the optical encoder to obtain high concentricity, even in the presence of eccentricity in the shaft. This results in an improvement in the sensing accuracy of the rotary table. Furthermore, by adjusting the mounting bolt preload to the appropriate level, the system exhibits strong resistance to thermal or shock disturbances. The 3D model of the aforementioned system is depicted Figure 7.1:
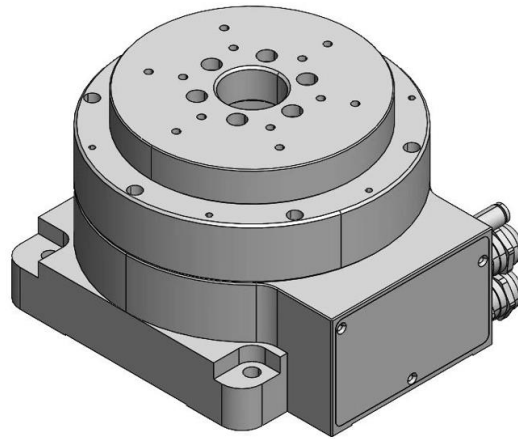
Figure 7.1 3D model of UPTech ARST 100 aerostatic bearing rotary table product

The structure details of the rotary table design are illustrated in Figure 7.2. The aerostatic bearing is supplied with pressurized air via a compressor. Upon filtration and pressure regulation, the compressed air is channelled into the bearing through an annular tunnel. This, in turn, generates an annular air film between the sleeve and the shaft, providing suitable load support and lubrication.
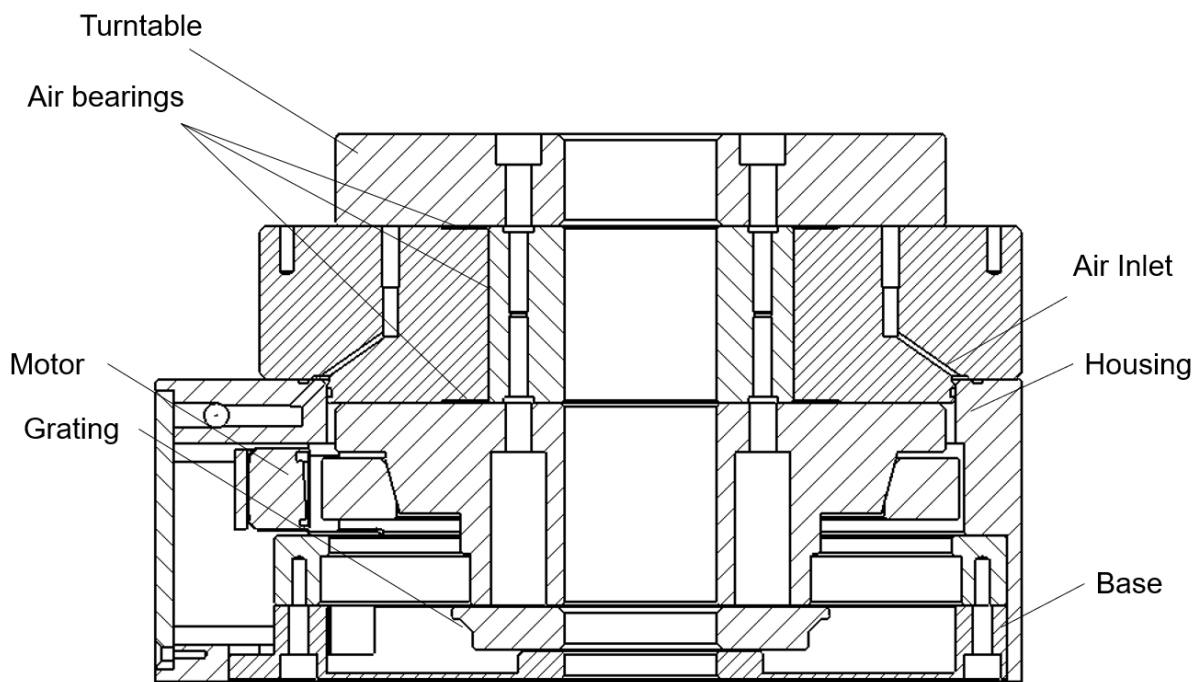

Figure 7.2 2D structure of the aerostatic bearing rotary table

The entire mechanical assembly comprises components constructed from 7075 aluminum alloy, treated with anodic hardening on the surface to enhance material properties, such as resistance to oxidation, corrosion, abrasion, among others. To ensure precision movement of the rotary table, the rotary shaft, sleeve, and air bearing are subjected to grinding processes to improve the accuracy of their inter-fitting.

7.2.2.2 Air flow system design

The design of air flow system should be based on the following requirements:

- Ensure that the compressed air can reach every orifice smoothly.
- Avoid the loss of pressure during the process of air transmission.
- Ensure that the air is emitted smoothly and quickly to the atmosphere.

When designing an aerostatic bearing, it is important to consider not only its performance, but also the air flow path, with the aim of minimizing pressure loss and gas consumption while maintaining simplicity and reliability. The supply air is first filtered and regulated through a valve before entering the orifice hole of the bearing from the outer frame of the turntable, thereby creating a thick film of air between the turntable and the bearing that supports lubrication. The designed air flow path is depicted below:
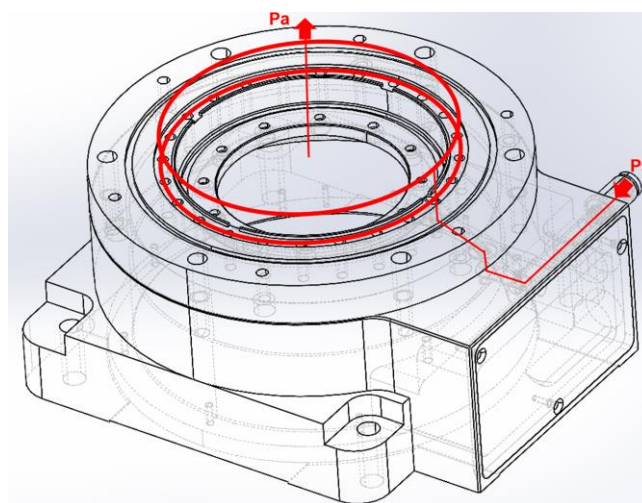

Figure 7.3 Air flow system of precision rotary table

7.2.2.3 Air bearing design

The precision rotary table employs three air bearings, comprising of two opposite annular thrust bearings and a radial thrust bearing with a multitude of small orifices. Specifically, the small orifice thrust bearing consists of a bearing surface integrated with orifices and a thrust disc. The thrust surface contains a single row of ring-shaped distribution of orifices, with 24 in axial direction and 12 in radial direction in the current experimental prototype. The opposite layout of the air bearings is responsible for preloading, which ensures that the spindle remains free from axial runout and provides the necessary static stiffness. The air bearings are preloaded at a thickness of 10μm, as it corresponds to the stiffness peak. Given the operational environment of the aerostatic bearing rotary table, the focus of the design and calculation work lies in the thrust bearings. Accordingly, the following section outlines the design and calculation of the bearing structure:

(1) Thrust bearing parameters.

The bearing diameter D_1 is the same as the diameter of turntable shaft at 100 mm and the inner diameter D_2 is 65mm.

(2) Orifice parameters.

Orifices located in the middle between the bearing inner and outer boundary, uniformly distributed according to the circumference, the Pitch Circle Diameter (PCD) D_p is:

$$D_P = \frac{D_1 + D_2}{2} = 82.5mm$$

The orifice is round holes with diameter $D_0 = 0.06mm$, drilled directly into the thrust plate by a laser perforation process.

(3) Supply air parameters.

To provide the best support and lubrication performance and avoid pneumatic hammer effect, supply air is compressed to gauge pressure P_S of 0.55MPa, with an ambient atmospheric pressure of 0.1MPa.
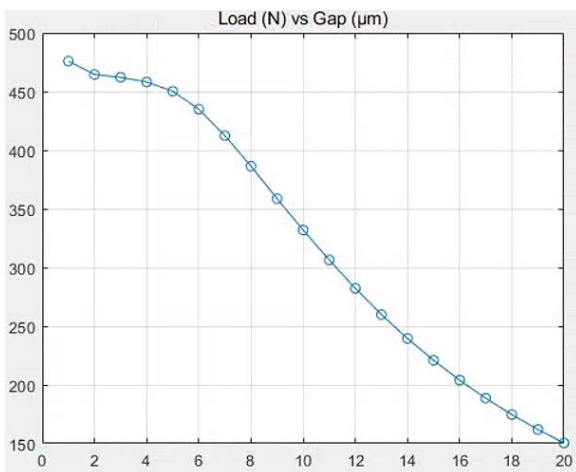
7.2.2.4 Static performance modelling and simulation

Based on the designed air bearing parameters above, the simulation results regarding static performance are shown in Figure 7.4:
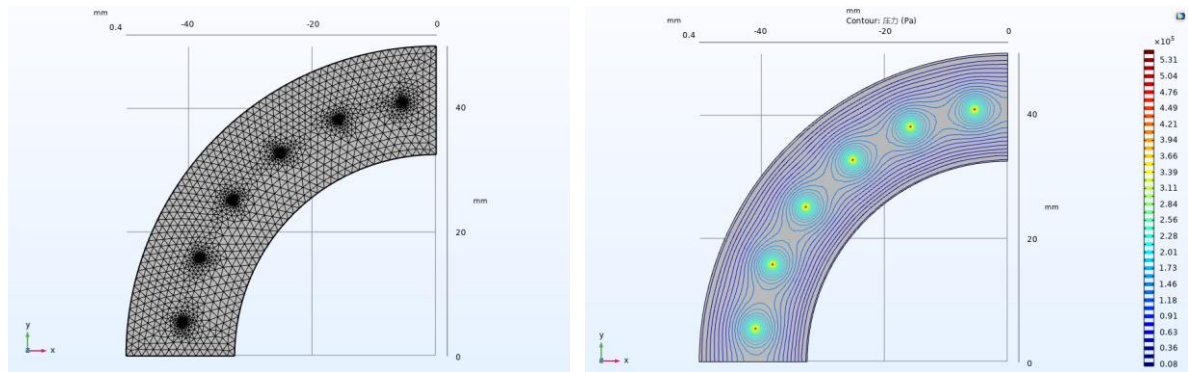
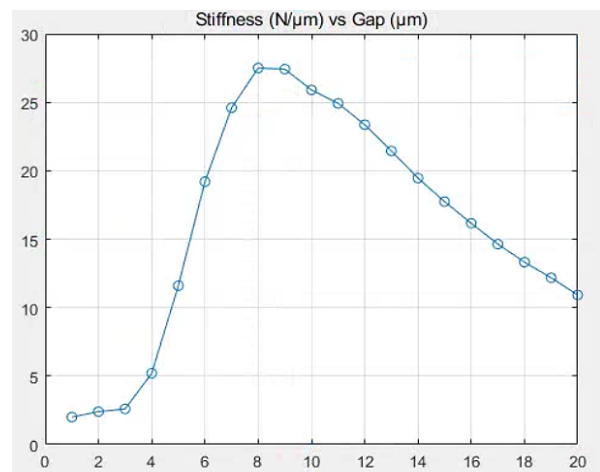(a)   (b)

(c)   (d)

Figure 7.4 CFD simulation result of air bearing static performance:

(a) Generated mesh; (b) Pressure distribution; (c) Load capacity; (d) Stiffness

The data from Figure 7.4 shows that the overall trend of the load capacity and stiffness curves aligns with the analysis presented in Chapter 4. The stiffness peak is observed within the 8-10 μm range of the air film thickness. Hence, in designing the opposite preloaded air film, it is recommended to maintain it at a thickness of 10 μm. At this point, the air bearing's load capacity reaches approximately 340N.

The aforementioned theoretical calculations and simulation data serve as empirical

evidence that the static performance of the designed air bearing is in complete adherence with the designated specifications and requirements. In order to attain more precise performance metrics, it is necessary to undertake the design of the control and drive system for the aerostatic bearing rotary table, and subsequently conduct corresponding experimental tests on the actual machined product.

7.2.3 Control and drive system design

7.2.3.1 Torque motor selection

The torque output of a torque motor can be calculated by using the formula:

$$\tau = \frac{R^2 4\mu_0 k_S L M_0 \omega}{Gap+L} \tag{7-1}$$

Where:

τ: torque output;

R: rotor radius;

μ_0: the conversion factor between magnetic flux and magnetic field strength;

k_s: the coil surface current coefficient;

L: the thickness of the permanent magnet section;

M_0: the first term of the Fourier expansion of the magnet magnetization in the radial direction;

ω: the length in the axial direction;

Gap: the length of the gap between the permanent magnet and the coil.

Based on the specification, the QTR series of TECNOTION torque motor is initially chosen.

7.2.3.2 Control system design

The control system for the aerostatic bearing rotary table is comprised of the ACS motion controller as the central control unit and an IPC for human-machine interaction via monitor, keyboard, and mouse. The SERVOTRONIX CDHD2 product was selected as the servo drive, it can also independently control and drive the single motion axis

with reduced function.

The motor stator is affixed to the outer frame, while the rotor is interference-fitted to the rotating shaft, so that the rotor of the rotary table is directly driven by the motor after power is applied. The IPC, serving as the host computer, communicates with the ACS motion controller through Ethernet. Subsequently, the controller processes commands and transmits signals to the actuator, which amplifies the signals and regulates the torque motor. The control system of the aerostatic bearing rotary table employs internal current loops in the drive and incorporates circular grating feedback signals into the speed and position loops to ensure a high degree of accuracy. Figure 7.5 illustrates the signal transmission of the control system:

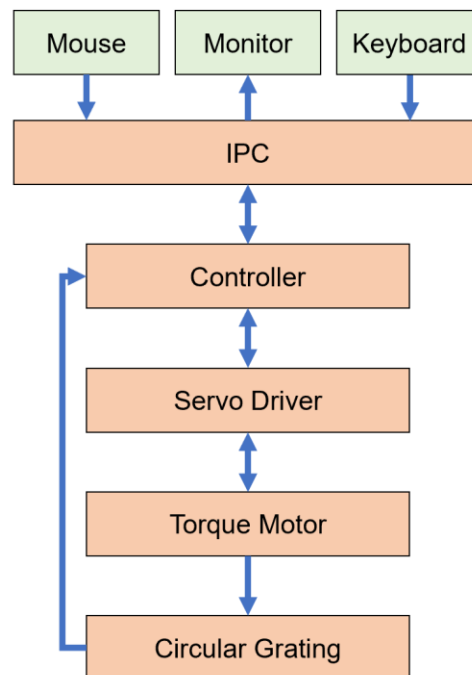Figure 7.5 Schematic of signal transmission between aerostatic bearing rotary table control system hardware

The embedded control system resides within the controller, limiting end-users to a restricted set of permissions for operational tasks, namely the tuning of the PID parameters and the adjustment of environmental parameters. However, the modification of the control logic is precluded. The position, velocity, and current loops

are depicted in Figure 7.6. As illustrated, the HMI of commercial control software offers a limited set of adjustable parameters, lacking a comprehensive display of the specific system architecture and logic. Figures 7.6 (a) and (b) represent the position and velocity loops respectively. These loops allow signal tuning by adjusting the gain and corresponding PID parameters. Subsequent enhancements in vibration proof and filter further augment the stability of the output signal. The control of the current loop as shown in Figure 7.6 (c) involves adjustments through the motor's anti-potential constant and PID parameters. All values within the figure represent the optimized parameters obtained through iterative testing and tuning via trial and error methods.

(a)

(b)
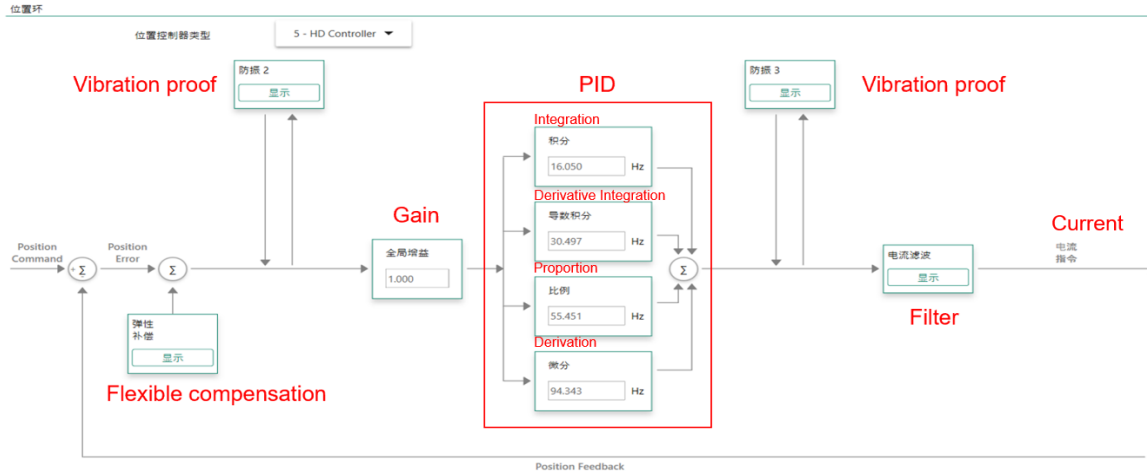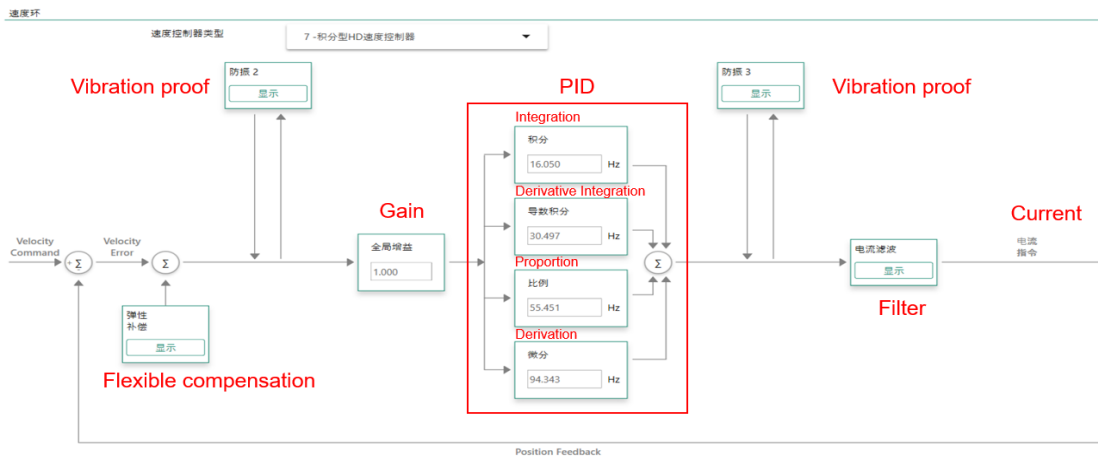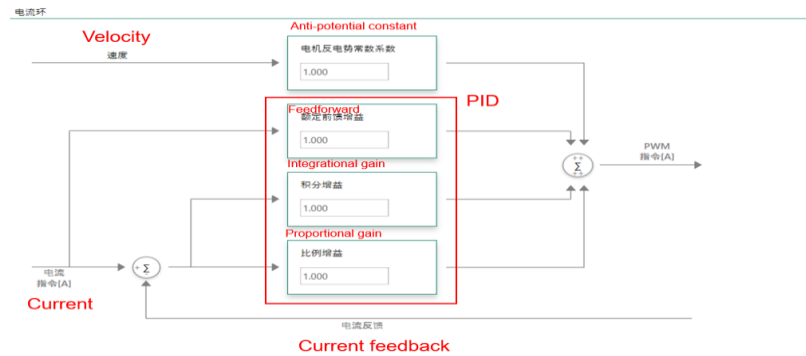
(c)

Figure 7.6 Control system of the aerostatic bearing rotary system:

(a) Position loop; (b) Velocity loop; (c) Current loop

It can be found from Figure 7.7, the system has remarkable respond curve and acceptable tracking error (0.005° of 90° rotation) after tuning, which fits the design specification well.
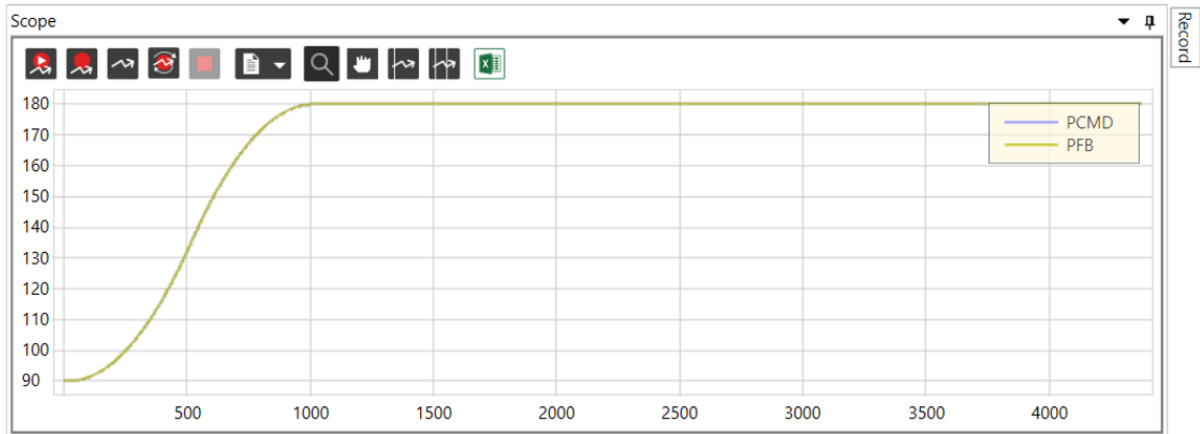
(a)
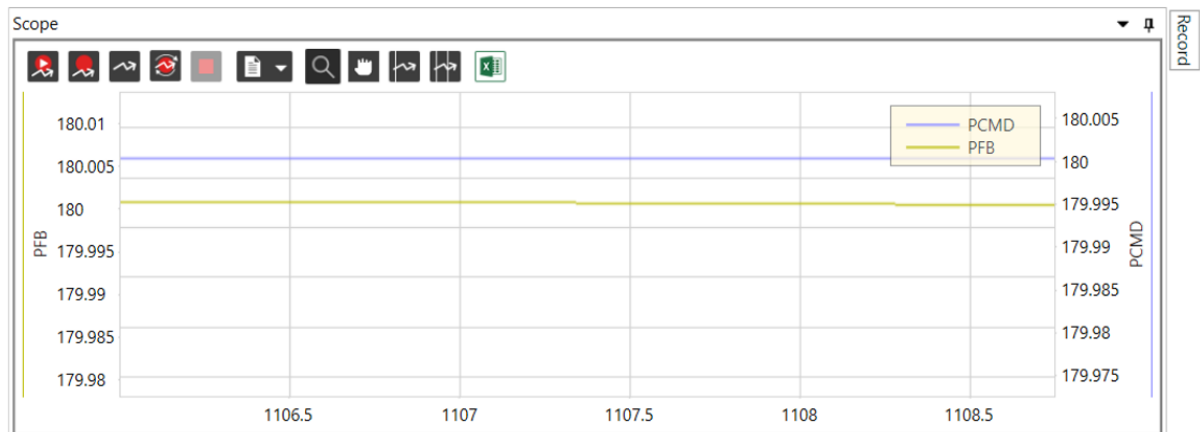
(b)

Figure 7.7 Results of system tuning:

(a) Respond curve; (b) Tracking error

7.2.3.3 Drive system design

The transmission of rotary tables can be achieved through various methods, namely gear transmission, turbo-screw transmission, timing belt, friction transmission, and direct drive. Each method has distinct characteristics and is suitable for different application scenarios:

- Gear and screw drive rotary tables possess the ability to attain large transmission ratios and transmit higher torques at lower energy costs. However, the presence of transmission clearance (slot) between gears results in poor transmission accuracy and large errors, rendering them unsuitable for ultraprecise scenarios.

- Friction-drive rotary tables exhibit high transmission accuracy, making them suitable for small displacement movements with high precision. However, due to their frictional contact method, they are subject to significant wear and tear losses, which can cause accuracy degradation after prolonged usage.

- Direct-drive rotary tables are suitable for high precision applications due to their high accuracy and rapid response without slot effects. Direct drive is a well-established transmission method and is widely used for precision rotary table production.

In consideration of the high accuracy requirements of the aerostatic bearing rotary table system, a direct drive motor has been selected as the power source for this prototype from a practical standpoint. Direct drive motors offer significant advantages over traditional motor systems, including improved accuracy and reduced mechanical complexity.

In terms of direct drive motor, common options are AC motors and DC motors:

- AC motors regulate speed by adjusting the frequency of the AC current. However, varying the frequency can result in changes in inductive resistance and load characteristics, leading to instability and difficulties in achieving fine speed control.

- In contrast, DC motors operate under constant voltage and constant DC power supply, generating a rotating magnetic field by changing the sequence of motor coils, thereby driving the rotor. DC motors offer excellent speed regulation characteristics and high output torque, making them well-suited for high-precision applications such as the aerostatic bearing rotary table system.

Based on the analysis presented, it can be concluded that the DC torque motor is the suitable drive solution for aerostatic bearing rotary table prototype. After a comprehensive comparison of various products, the TECNOTION QTR-A-105-17N

132

frameless torque motor has been selected as the most suitable option. The structural design of the motor is depicted in Figure 7.8:
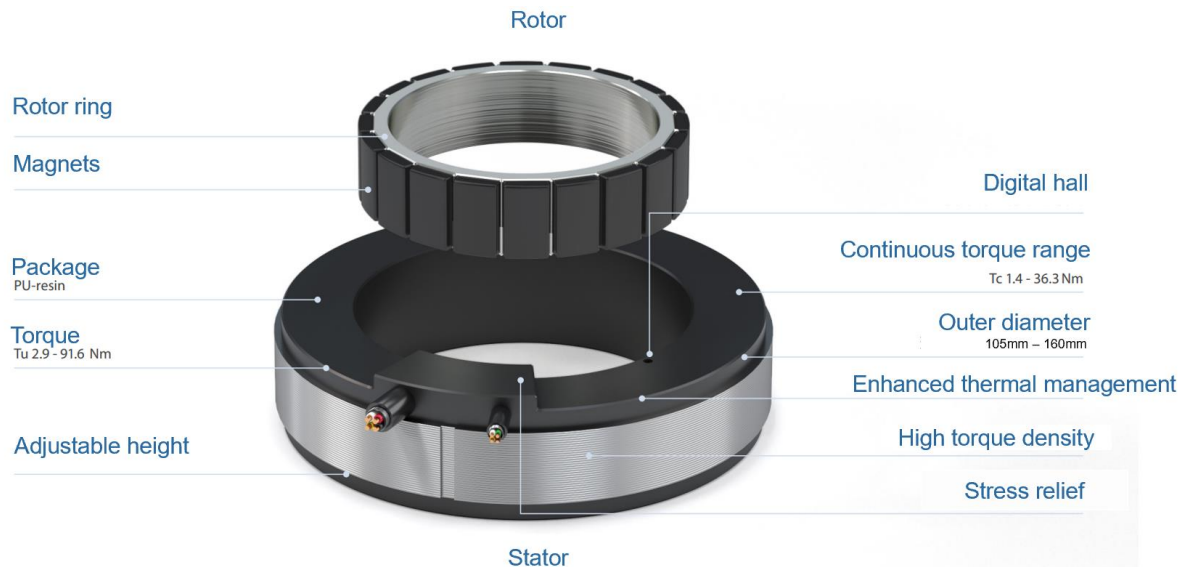

Figure 7.8 Schematic of QTR-A-105-17N frameless torque motor[162]

The QTR series, specifically the QTR-A-105-17N model, has been widely adopted in a range of industries such as semiconductor, medical, machine tools, printing machines, rotary tables, factory automation, and robotics. It is a direct drive brushless torque motor that eliminates the need for mechanical drive components, thereby reducing transmission losses and avoiding maintenance requirements for transmission components. This proven technology has demonstrated its reliability and efficiency in various applications. Detailed information on the specifications of the QTR-A-105-17N model is shown in Appendix II.

7.2.3.4 Feedback system design

Due to the high demand for positioning accuracy in the aerostatic bearing rotary table, full closed-loop control is adopted. It is demonstrated by the theory in Chapter 5 that the accuracy of the feedback components in the system directly impacts the positioning accuracy and repeatability of the overall system. As a result, the angular position sensor is one of the most crucial devices in the feedback system.

Various methods exist to achieve accurate angle measurement, including the resolver,

optical encoder, and circular grating. Among these methods, the circular grating stands out for its ability to provide accurate displacement signal feedback, high immunity to interference, and high resolution. As a result, it can significantly enhance the accuracy of the control and drive system for the aerostatic bearing rotary table.

The selected feedback device is RENISHAW incremental circular grating, which consists of a RESM20 rotary ring with a diameter of 20mm and a T2011-05A read head. As the ring rotates with the rotary table, light interferes with the grating in the vertical direction. In the perpendicular direction of the grating line, Moiré stripes of light and dark appear due to the phenomenon of light interference. The reading head detects changes in the light signal and performs photoelectric conversion to transmit changes in position via an electrical signal. The RESM20 rotary ring's specifications are detailed in Appendix III.

7.2.4 Prototype testing

The photograph of designed aerostatic bearing rotary table is shown in Figure 7.9:
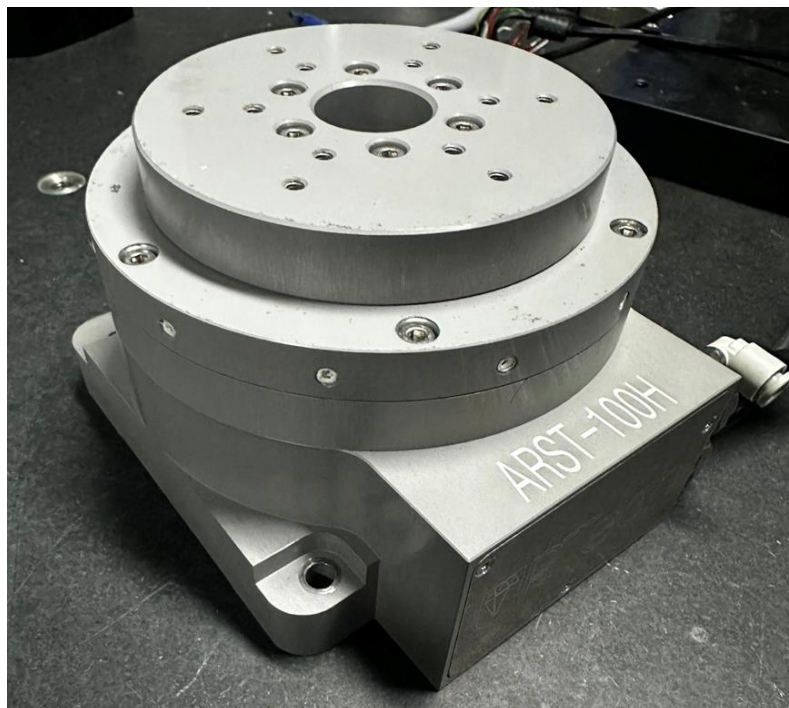

Figure 7.9 Photograph of the designed ARST-100H aerostatic bearing rotary table

Prototype

Following the design of the primary systems for the aerostatic bearing rotary table, it is essential to conduct a prototype evaluation under authentic operating conditions. The objective of this evaluation is to obtain critical performance indicators such as stability, motion accuracy, and static jitter, and to assess the overall efficiency of the design. In this section, the results of testing the key performance metrics of the precision aerostatic bearing rotary table design are presented using a bespoke static load test bench and a set of laser interferometers.

7.2.4.1 Static performance test

Figure 7.10 depicts a load test rig, which are situated on a vibration isolation platform that rests on a granite base. This setup ensures that the system remains impervious to most of disturbances caused by external environmental factors. The load is applied to the rotary table's aerostatic thrust bearings through pressurized air that is regulated by a valve. The resultant force is measured with a TEDEA 620 load cell, which has a digital resolution of 0.02% at Full Scale Output (FSO), ensuring high accuracy. Furthermore, the displacement of the air film is measured using a KEYENCE LK-H008 displacement sensor, which is capable of detecting changes in nanometer-level. The displacement sensor is positioned at the upper edge of the aerostatic rotary table, providing precise measurements of the air film's thickness.
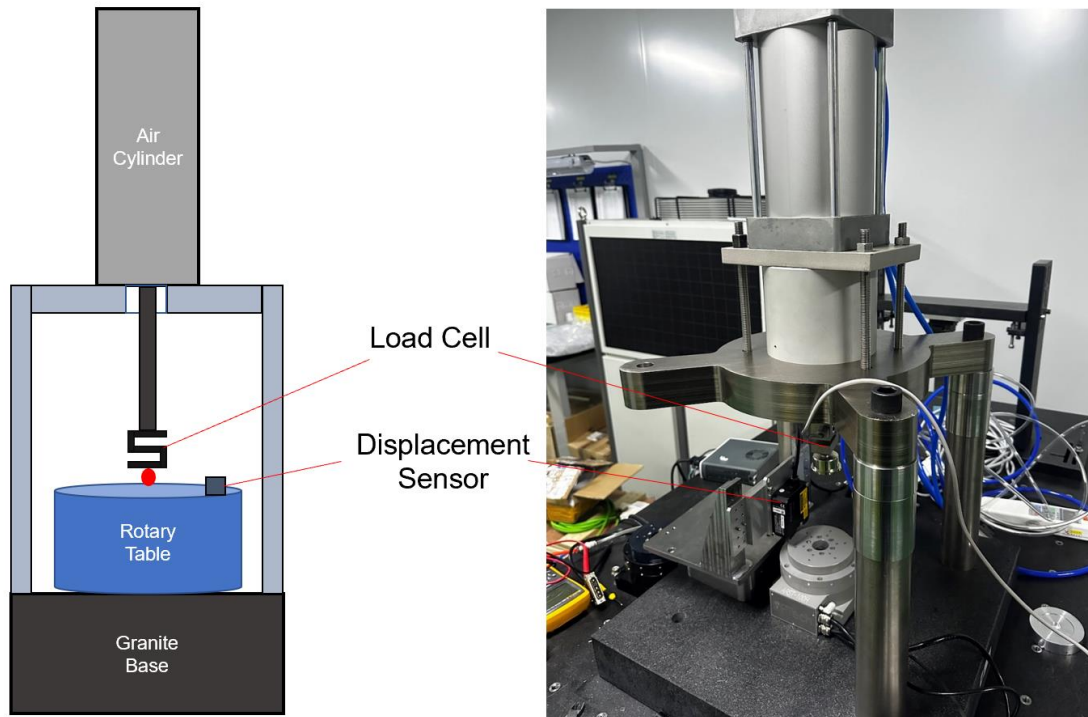
Figure 7.10 Static load test bench

By utilizing the test bench presented in Figure 7.10, the tested load capacity of the designed aerostatic bearing rotary table is shown in Figure 7.11:
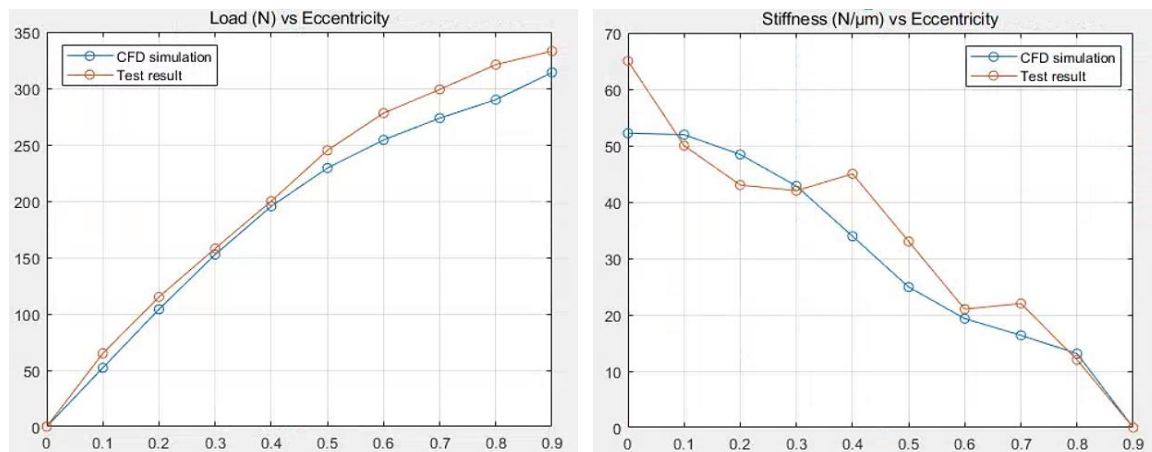

Figure 7.11 Test and simulation results of aerostatic bearing rotary table static performance

As illustrated in the figure, the orange curve represents the average of four sets of test data obtained from two reciprocating strokes of the cylinder. The load capacity curve

demonstrates a reasonable consistency with simulated values, exhibiting fluctuations within an 8% margin. However, there is noticeable variability in stiffness values, speculated to arise from internal deformation of the test part, internal deformation within the cylinder, environmental vibrations, or machining precision of the air bearing surface. Overall, the test outcomes generally align with the simulated results, indicating a commendable level of reference and accuracy in the simulation model.

Due to the inherent motion characteristics of the air cylinder and the limited resolution of the displacement sensor, achieving an accurate 2 µm step during testing poses a significant challenge. As a result, the measured air film thickness values are subject to an error margin of ±1 µm. Moreover, direct conversion of pressure from the load cell to an electrical signal introduces transmission errors, which are difficult to estimate, while other sources of error are not accounted for in this test.

The static performance of the designed rotary table is found to meet design requirements with high fidelity, and the test results serve to validate the accuracy of the CFD simulation method based on the multiscale modelling methodology presented in Chapter 3. This modelling, design, and analysis approach enables subsequent products to be optimized for static performance in accordance with specific application requirements. Such optimization can be achieved through the modification of air bearing surface size, orifice parameters, supply air pressure, or other relevant parameters. The resulting product family or series can be iterated in a highly effective and efficient manner.

7.2.4.2 Dynamic performance test

The evaluation of motion accuracy for a rotary table is primarily based on two key parameters: positioning accuracy and repeatability. While the standard-bar and ball-bar methods have been traditionally used to measure motion accuracy for machine tool spindles and rotary tables, the former is limited to low-precision machine tool testing, and the latter suffers from issues related to environmental interference and poor test repeatability.

This experimental study employs a laser interferometer to assess the dynamic rotation error of the aerostatic bearing rotary table. Laser interferometry is a widely accepted instrument in international standards for evaluating the positioning accuracy and repeatability of CNC machine tools. According to the machine tool standard BS3800 Part 2 (1991), the rotary axis' rotation error should be measured at the main position and a minimum of nine random target positions within the range of 0° to 360°. The conventional approach that utilizes automatic collimators fails to meet these requirements due to a fixed number of polyhedral faces, limiting the number of targets and equal angular separation between them.

To satisfy these requirements, the Renishaw laser interferometer XL 80 is selected as the measurement tool, the layout for the whole test system and necessary devices are shown in Figure 7.12:
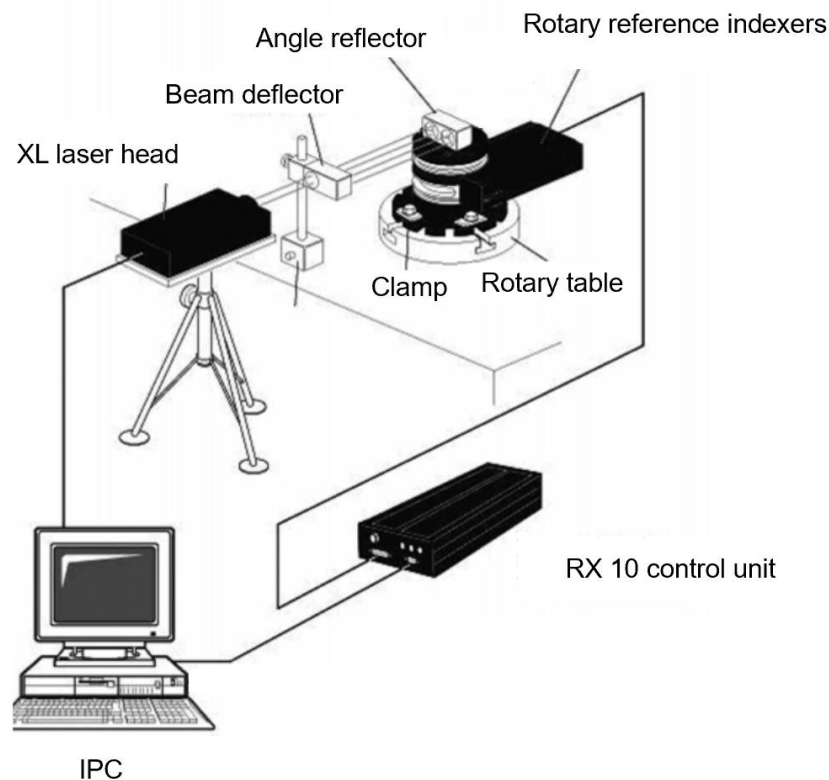

Figure 7.12 Installation of Renishaw laser interferometer

The underlying principle of laser interferometer measurement, as illustrated in Figure 7.13, involves the use of a Renishaw XL 80 laser system equipped with a double

longitudinal mode He-Ne laser. This laser emits a double-frequency laser beam which is subsequently transformed from circularly polarized light to linearly polarized light through the use of a λ/4 waveplate. By removing a frequency from the polarization beam splitter located in the lower section of the angle reflector, a single-frequency laser output is obtained. One of the beams directly passes through the polarization beam splitting prism, travels to the lower section of the angle reflector, and is reflected back to the laser through the angle interferometer, thus forming the reference beam A1. The other beam is directed at a 90° angle by the beam deflector located in the upper section of the angle reflector and is subsequently reflected by the upper prism back to the laser to create the measurement beam A2. After the reference and measurement beams are combined, they converge while maintaining their individual polarization states. Once this is achieved, they are transformed into rotating polarized light by passing through the λ/4 waveplate before being received by the photoelectric receivers via the horizontal, vertical, and 45° directional deflectors. Each time there is a change in the optical range difference, an intensification and extinction signal are generated between the two poles. As a result, the interference fringe of the laser shifts relative to a fixed point. When the measurement angle exceeds ±1°, the number of bright stripes passing through that point is recorded by a grating counter to determine the change in optical range difference. The nominal spacing between the two reflectors in the angle reflector remains constant, allowing for the detection of the rotary axis' angle of rotation.
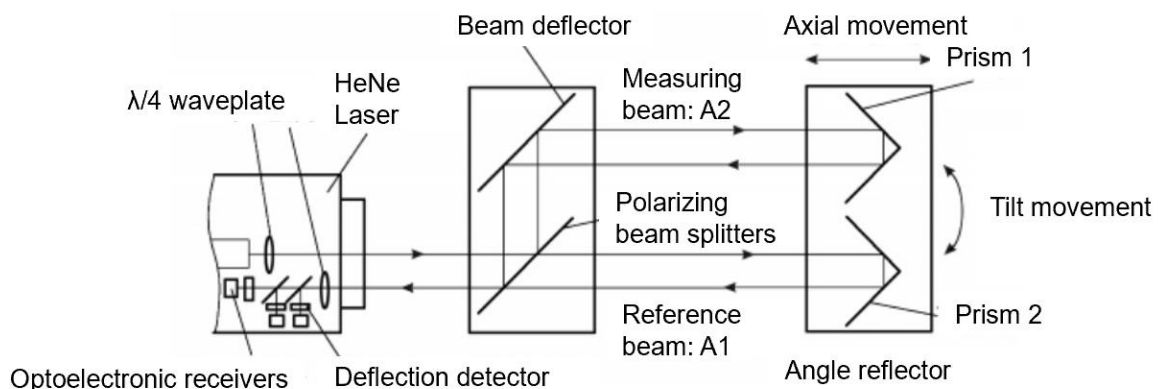
Figure 7.13 Schematic of laser interferometer measurement process

The experimental set up is shown in Figure 7.14:
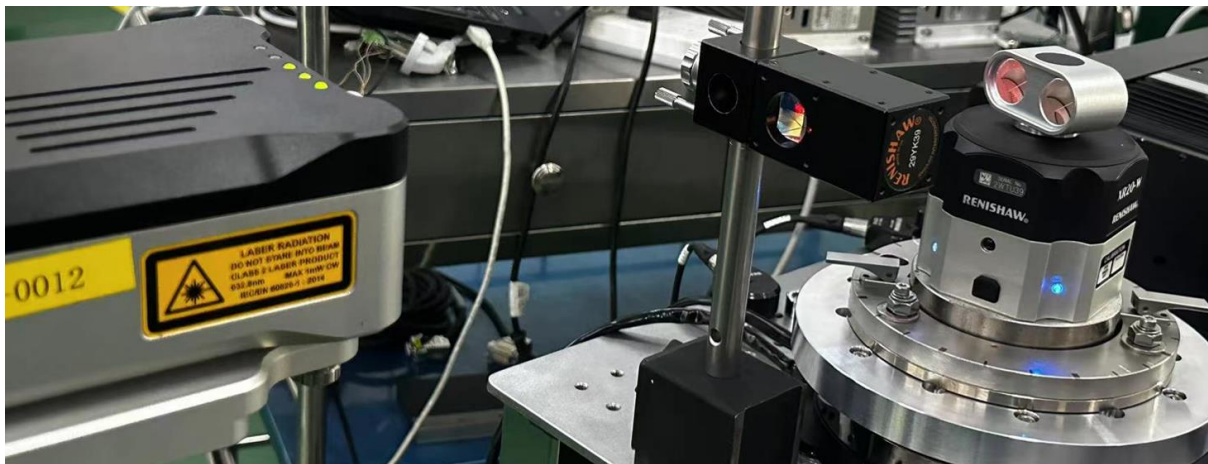
Figure 7.14 Set up of laser interferometer measurement devices

In the afore mentioned procedure, a two-way measurement is utilized to determine the mean value of each target. Subsequently, the positioning accuracy and repeatability can be computed, and the corresponding outcomes are presented in Figure 7.15:
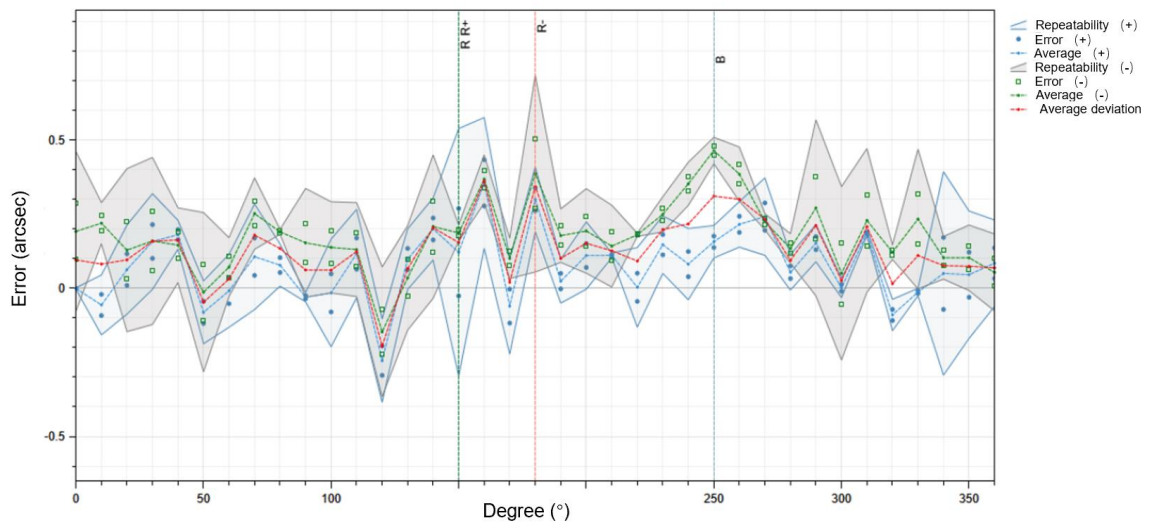
Figure 7.15 Test results of aerostatic bearing rotary table motion accuracy

The curves in Figure 7.15 represent the repetitive error and positioning error of the aerostatic bearing rotary table at different positions within a 360-degree travel. The points and lines of different colours denote positive error, negative error, and average

error. When testing the product's performance, the peak-to-peak value is seen as the main evaluation criterion.

According to the test results, the positioning accuracy of tested aerostatic bearing rotary table from 0° to 360° is 1.103 arcsec, repeatability is 0.834 arcsec, which can fit the design specifications well.

7.2.4.3 Conclusions

In this section, the design and experimental study of the precision aerostatic rotary table were described, including the overall structural design, the description encompassed the overall structural design, performance modeling and analysis of the air bearing, and the measurement and testing of static and dynamic performance. Results reached are as follows:

1) During the product design phase, simulations were conducted based on the modelling and analysis methods outlined in the previous sections to evaluate the load capacity and stiffness of the aerostatic bearing rotary table. To validate the simulation results, a test rig was constructed appropriately, and the results from four subsequent tests consistently aligned well with the simulated expectations.

2) The structural design of the aerostatic rotary table was carried out. In the design of rotation scheme, a torque motor direct drive was used, which eliminated the influence of intermediate transmission errors; in the support and lubrication scheme, opposite aerostatic thrust bearing preload was used to increase the axial stiffness.

3) The detailed design and performance calculation of the rotary table were carried out, the influence of key parameters on the bearing performance was analyzed and optimized. The calculation results indicated that the bearing can satisfy the design requirements of the aerostatic bearing rotary table adequately.

4) The tested positioning accuracy and repeatability is 1.103 arcsec and 0.834 arcsec, which showed that the designed aerostatic bearing rotary table is academically and practically feasible.

7.3   Industrial case study on UPM machine platform and its digital twin

7.3.1   Overview

Based on the theoretical research presented in the preceding chapters and the experimental investigations of single-axis precision components detailed in the previous sections, this section endeavours to develop an integrated methodology for modelling, simulating, and analysing the structure and performance of multi-axis UPM machine platforms and their digital twins. Unlike the design of single-axis machine components, the design of multi-axis platforms is significantly more complex and challenging. Furthermore, a second experimental trial was carried out as part of the 'UPTech Co, Ltd.' industrial project, which aims to provide a precision motion platform for industrial wafer inspection. The design considerations are depicted in Figure 7.16.
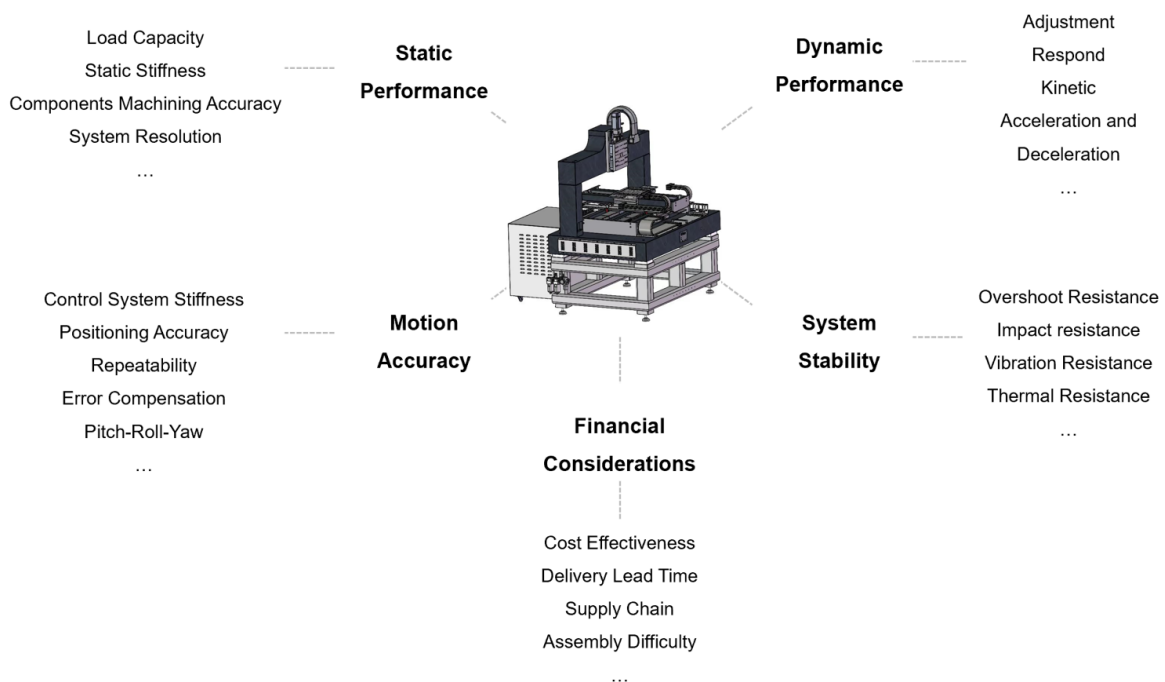

Figure 7.16 Academical and industrial considerations for the UPM machine platform design

As illustrated by the above figure, the design emphases were put on five major issues:

- Static performance.
- Dynamic performance.

- Motion accuracy.

- System stability.

- Financial consideration.

In order to achieve micron- or even nano-level positioning and motion capability, the integrated modelling, simulation and analysis from multiscale and multiphysics aspect are thus necessary.

7.3.2 Mechanical system and static performance design

As a real industrial project case, the design specification is based on the functional requirements from the technical agreements with customer, as shown in Table 7.2:

Table 7.2 Specifications of UPM machine platform

	X-Axis	Y-Axis
Stroke (mm)	550	450
Positioning Accuracy (µm)	±0.5	±0.5
Resolution	1Vpp Sin/Cos (*16384≈1.2nm)	
Repeatability (µm)	±0.35	±0.35
Straightness (µm)	±0.4	±0.4
Flatness (µm)	±0.5	±0.5
Pitch (arc sec)	±4	±4
Yaw (arc sec)	±2	±2
Max.Velocity (mm/s)	1500	1500
Rated acceleration (G)	0.6	0.6
Rated thrust (N)	360	135
Max. Payload (Kg)	Y+10	10

Considering the stress deflection, slideway stroke, motor size and overall assembling, an extra aerostatic bearing is applied in the middle of the X-axis to prevent the deformation of aluminium parts due to the slideway width. The mechanical structure is therefore designed as follows:
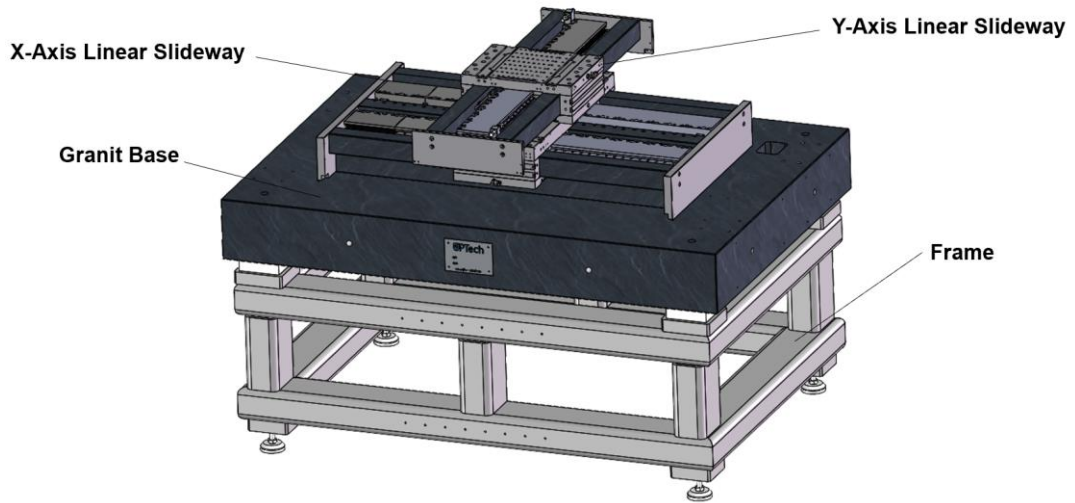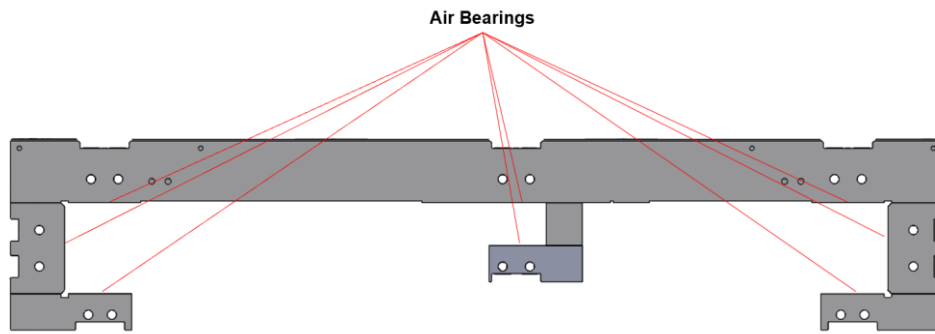
Figure 7.17 Mechanical structure of designed UPM machine platform

(a) overall structure; (b) X-Axis motion part; (c) Y-Axis motion part

As presented in Figure 7.17(a), the motion system is mounted on a 1240mm*860mm*150mm natural granite base, supported by steel frame at four corners, to ensure the motion accuracy, the flatness of granite base surface is ground to less than 2µm.

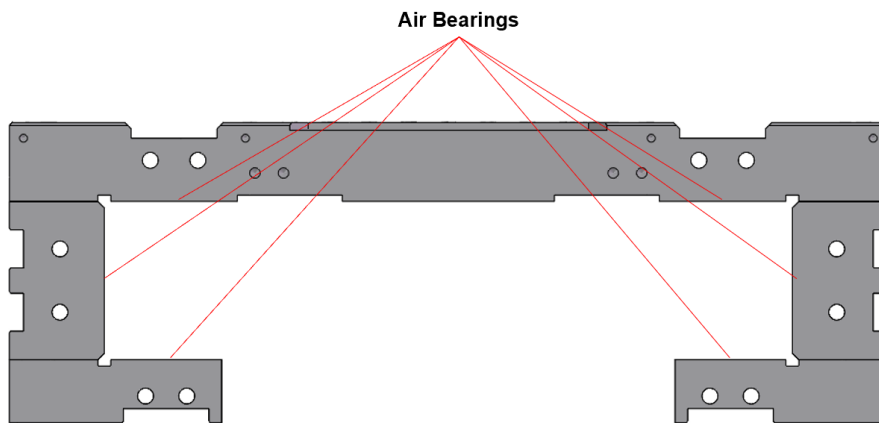To ensure that the static performance of each air bearings can cover the extreme operating conditions, CFD simulations are then introduced to predict the load and stiffness of the individual air bearings, and thus to adjust the mechanical structure dimensional parameters accordingly.

After the adjustment of inlet pressure, orifice amount, bearing size, the final parameters for each air bearings are shown in Figure 7.3:

Table 7.3 Parameters of designed air bearings of UPM machine platform linear slideways

	X- and Y-Axis		Extra bearing in X-Axis	
	top and bottom	side	top and bottom	side
Bearing Size(mm)	200*40	200*45	200*30	200*20
Inlet Pressure(Bar)	5.5	5.5	5.5	5.5
Orifice Diameter(µm)	60	60	60	60
Orifice Amount	10	10	10	10

Simulation results are shown in following diagrams:

	X-Axis and Y-Axis	
	Load Capacity	Stiffness
Top and Bottom		
Side		
	Extra Bearing in X-Axis	
	Load Capacity	Stiffness
Top and Bottom		

Figure 7.18 CFD simulation results for air bearings of UPM machine platform linear slideways

As shown in Figure 7.18, the stiffness peak for each air film appears in 6-8 μm, so the opposite preload for every axis side are settled in 8 μm, thus to ensure the air bearings in their best working condition. Furthermore, the load capacity for each axis with 8 μm air film is in an acceptable range as well.

The present work utilizes a modelling and simulation approach to investigate the impact of multiscale parameters on the static performance of a slideway, as detailed in the preceding chapters. By considering real machine platform applications and industrial design specifications, the goal is to design a mechanical structure that exhibits superior performance and high producibility. Specifically, the digital CAD and CFD models are integrated into the UPM machine platform DT, enabling the prediction and evaluation of static performance changes that may arise due to payload or acceleration/deceleration motion during operation.

7.3.3 Control, drive system and dynamic performance design

Based on engineering experience, the machine platform has been designed to utilize a distributed open CNC system based on Ethernet. In this system, the controller receives instructions from the IPC for arithmetic processing, which are then transmitted to the amplifier for signal conversion and amplification. The motor is subsequently driven and mechanical movement is achieved, allowing the execution parts to execute commands such as feed and rapid movement. Encoders are utilized

to provide position feedback to the servo amplifier, facilitating servo control operation. This system centralizes processing in the controller, as illustrated in Figure 7.19:
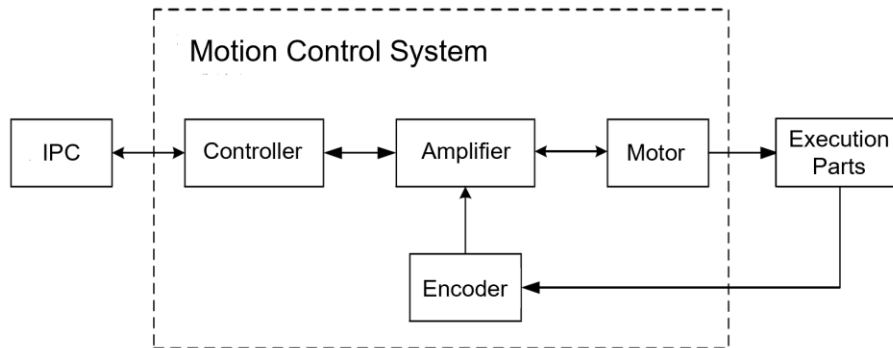
Figure 7.19 Motion control system for single-axis slideway

Compared to the single-axis control logic utilized in precision aerostatic bearing rotary tables, the control system of UPM machine platforms requires simultaneous precision motion control of multiple axes during operation. While Chapter 5 has demonstrated that cross-coupling control is an effective multi-axis integrated control and tuning method, the underlying logic of most commercial controllers is not accessible to customers. Therefore, the ACS SPiiplusCMhp-ba series motion controller has been selected. This controller is a well-established product specifically designed for multi-axis motion control. Its multi-processor architecture is capable of supporting up to 32 axes of motion profile generation and servo control algorithms, thereby maximizing motion system performance. Comprehensive specifications and data sheets of the ACS SPiiplusCMhp-ba series motion controller are presented in Appendix IV for reference.

After tuning, the dynamic performance can be directly read from the ACS software based on the feedback signal from Renishaw T1001-30A TONIC incremental no-contact encoders placed on each axis, as shown in Figure 7.20:
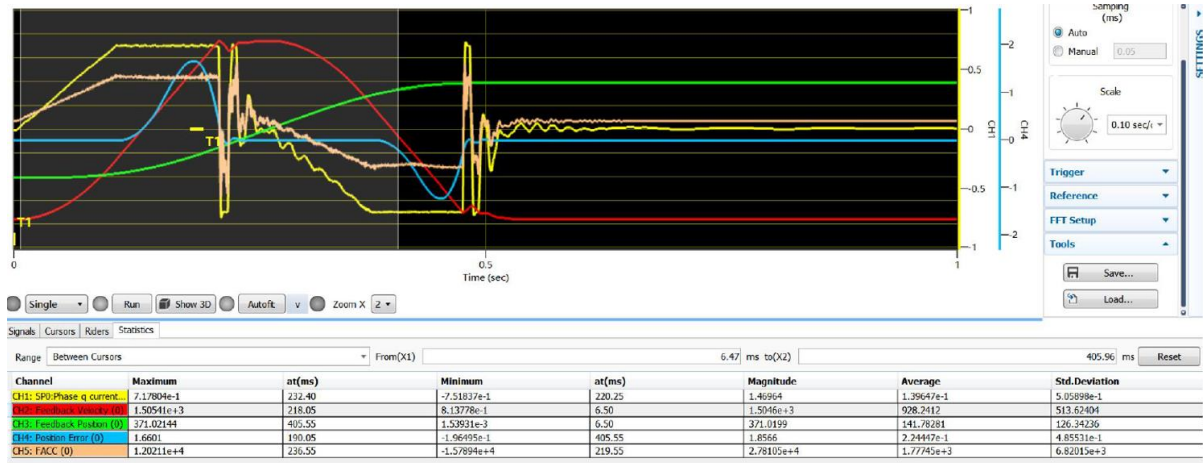
(a)
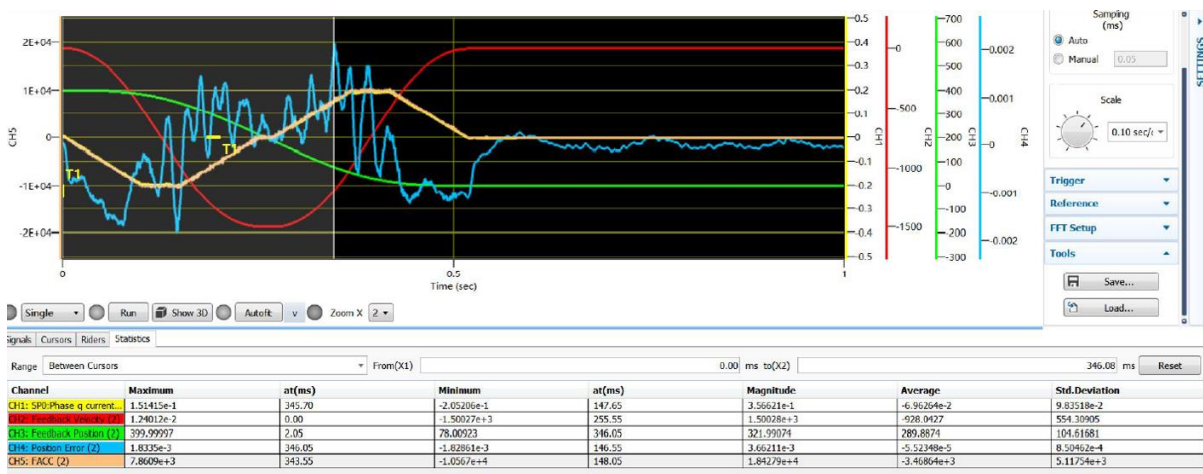
(b)

Figure 7.20 Dynamic performance of machine platform slideways

(a) X-Axis; (b) Y-Axis

As shown in Figure 7.20, the distinct loads and air bearing structures of the two axes result in significant disparities in their positioning errors (X-position error 0.22µm and Y-position error 55.23 nm, as shown in blue lines from each picture, and also in the table unit 'position error - average') and acceleration profiles due to the combined effect of inertial forces and gravity. Nevertheless, the overall performance like velocity stability or feedback overshoot remains at a high level and falls within acceptable limits. The modelling and simulation work is based on the study of the influence of multiphysics parameters on the final dynamic performance of the slideway, aims to

ensure the control and drive system with superior performance. The digital control system and CFD model are further integrated into the UPM machine platform DT, in order to obtain and predict the change of dynamic performance caused by the working environment or acceleration/deceleration motion.

7.3.4 Performance test of the designed precision machine platform

After the simulation, calculation and theoretical verification of the design process, the machine platform was manufactured and assembled by the production department, with an additional Z-axis gantry and mechanical servo system according to the customer's requirements, as shown in Figure 7.21:
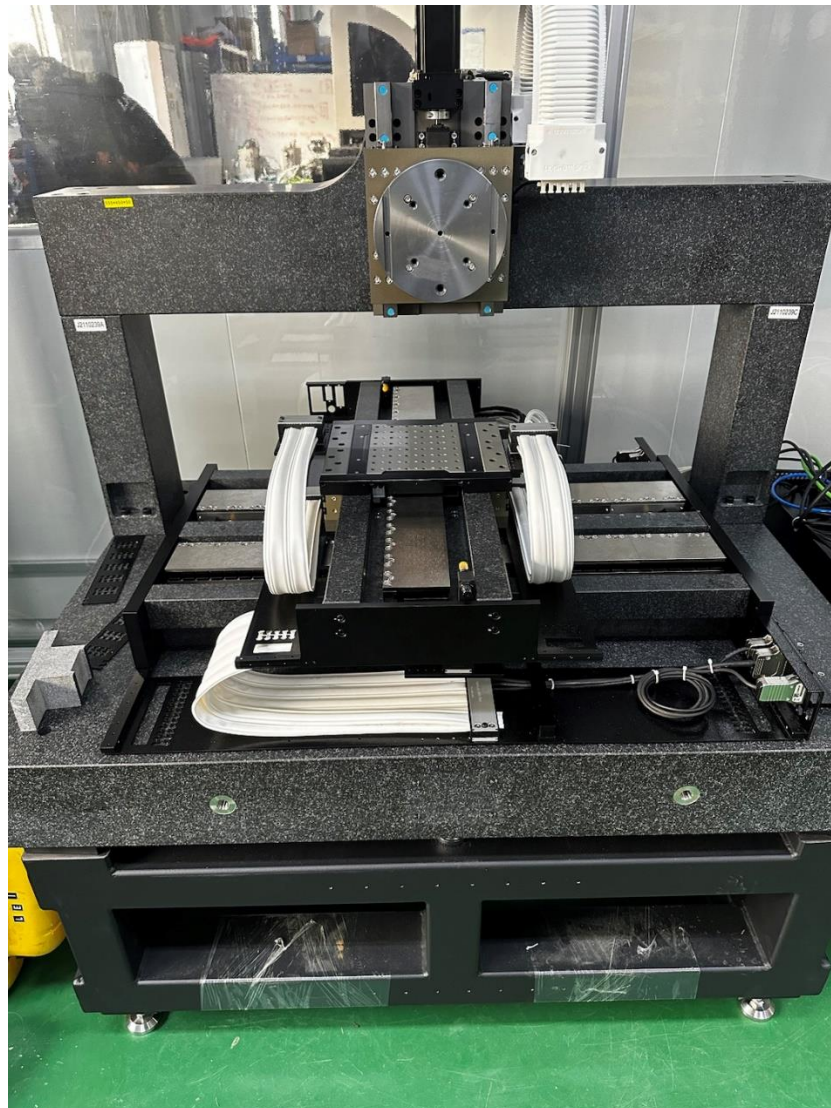
Figure 7.21 Assembled UPM machine platform with extra Z-axis

After the assembly and commissioning of the machine platform, the compressed air with 5.5 Bar pressure was introduced, the condition of each axis was basically good under naked eye observation, there was no obvious resistance to sliding within the full stroke, no pneumatic hammer phenomenon occurred, no machining defects and motion failure in the macroscopic scale, the feedback signal of the drive and control system was normal, and no faulty signal was generated, which could initially verify the feasibility of the design work.
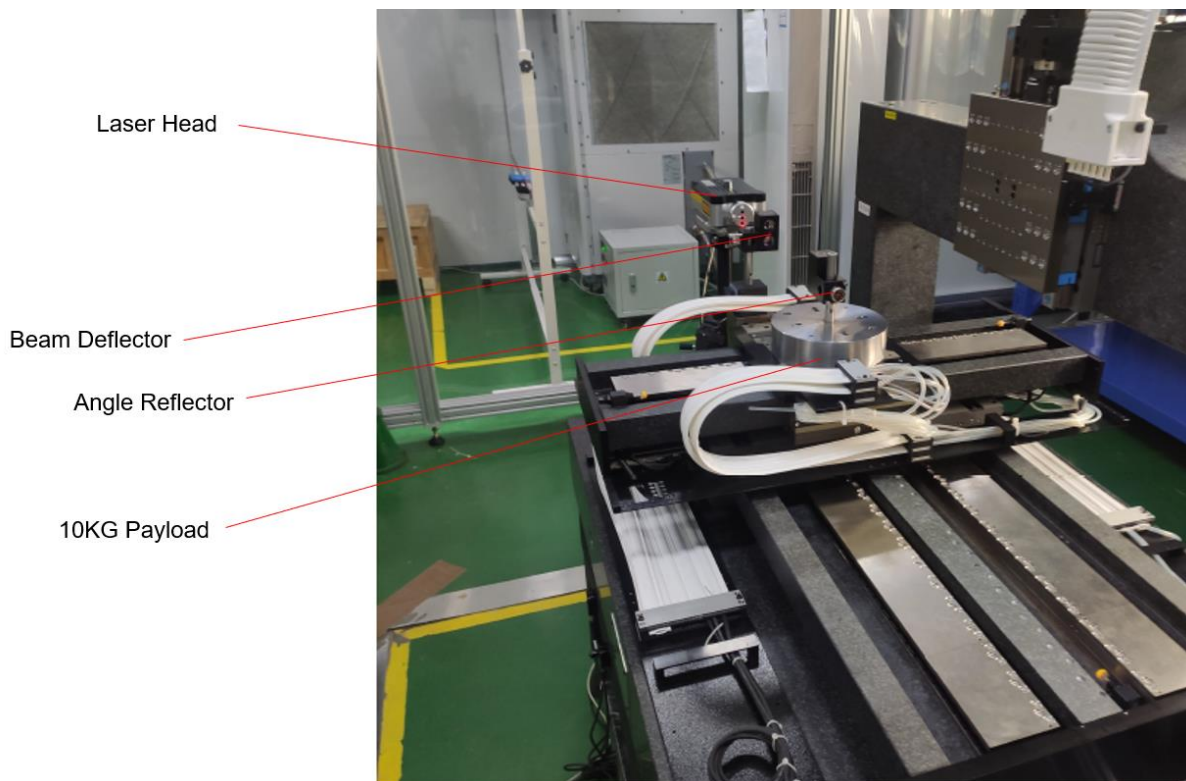
Figure 7.22 Set up of laser interferometer measurement devices on UPM machine platform

As shown in Figure 7.22, the specific performance indicators of the machine platform need to be evaluated by measuring instruments, RENISHAW's XL series laser interferometer is used again to test and evaluate the motion accuracy of the machine platform, the technical and functional details for this device have been described in the previous section, the test results are presented in Figure 7.23-25:
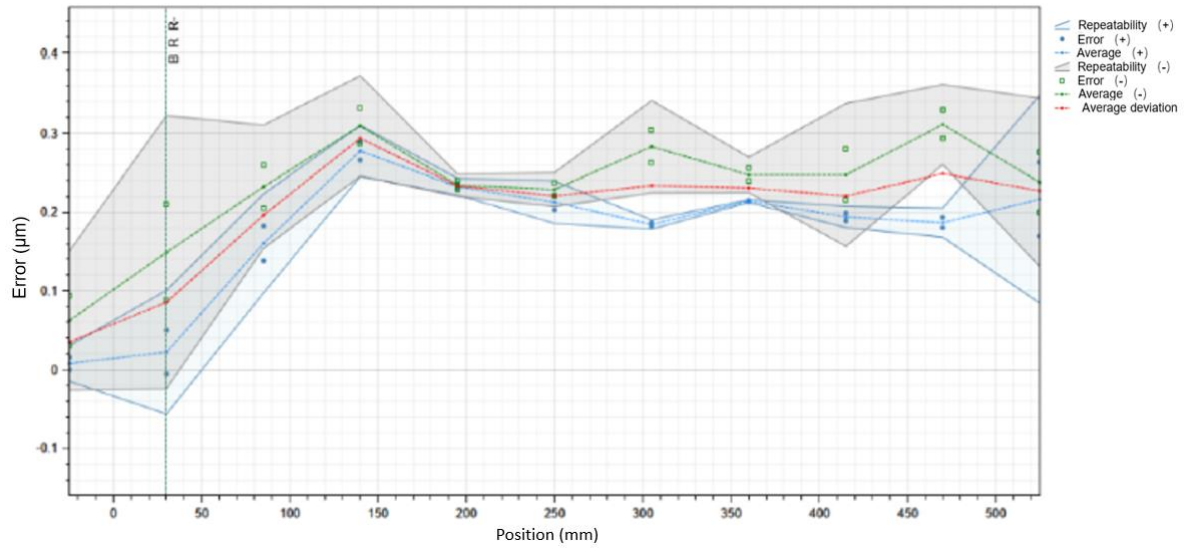
(a)
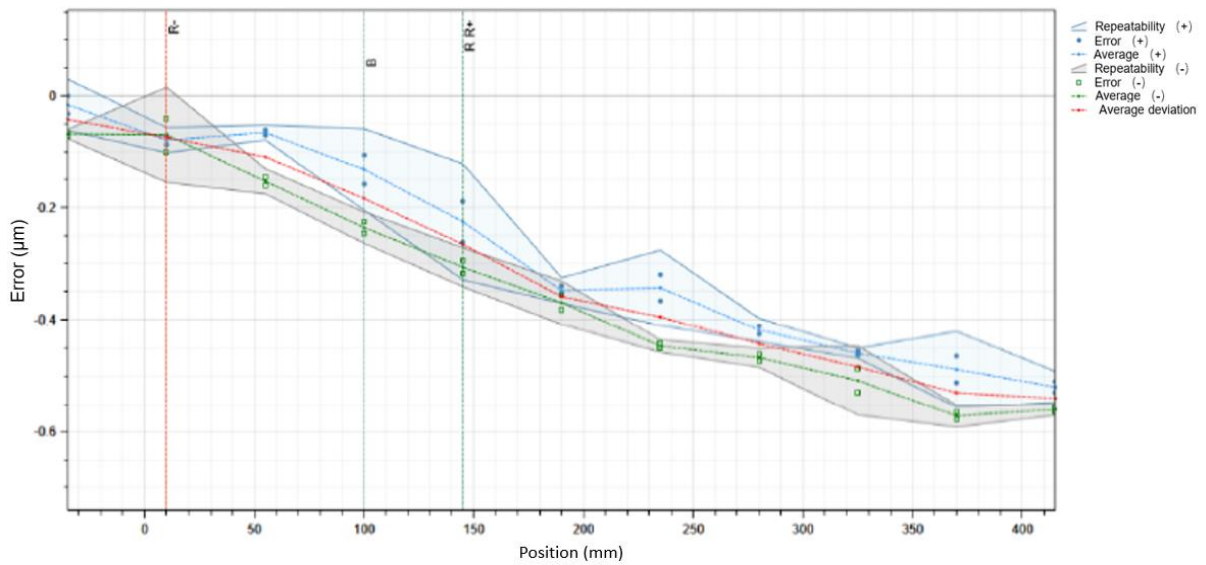
(b)

Figure 7.23 Positioning accuracy and repeatability of test slideways

(a) X-Axis; (b) Y-Axis

(a)

(b)

(c)

153
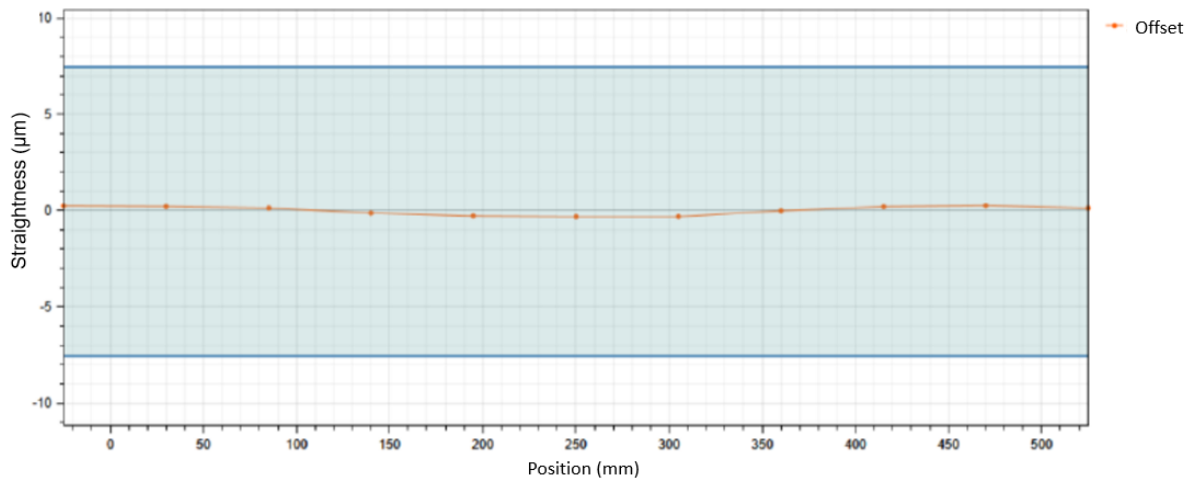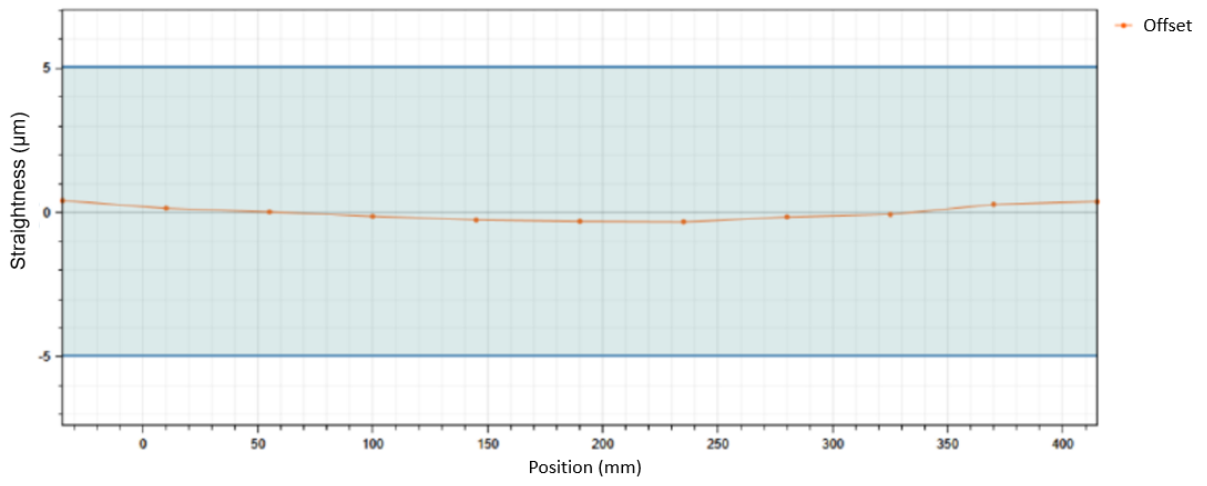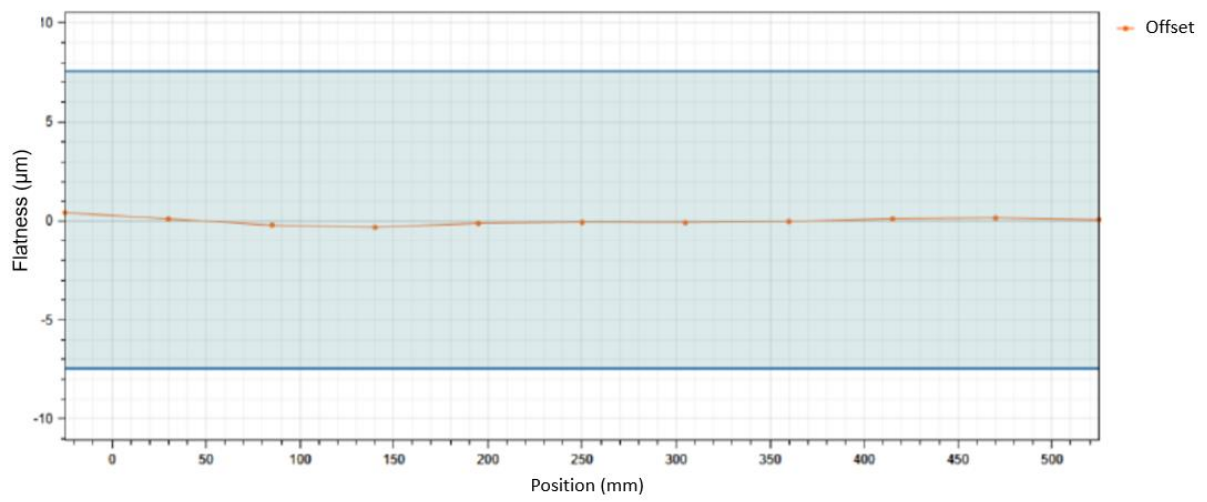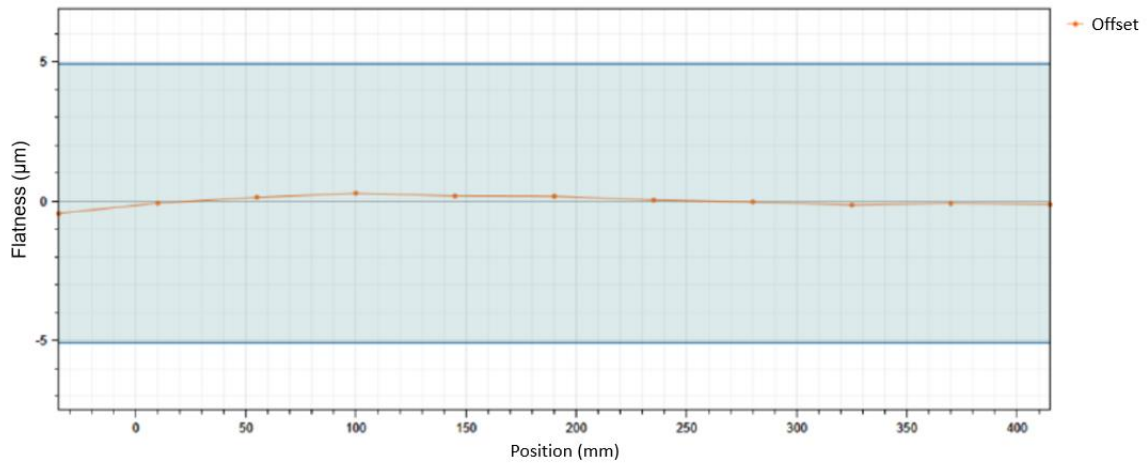
(d)

Figure 7.24 Straightness and flatness of test slideways

(a)X-Axis Straightness; (b) Y-Axis Straightness

(c)X-Axis flatness; (d) Y-Axis flatness

(a)

(b)

(c)

155
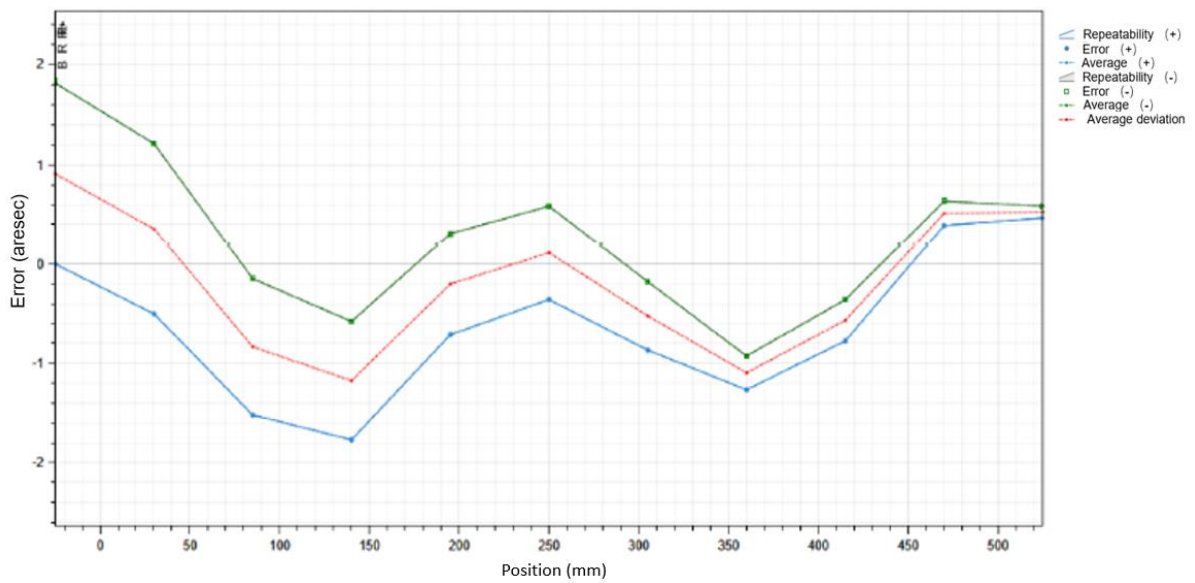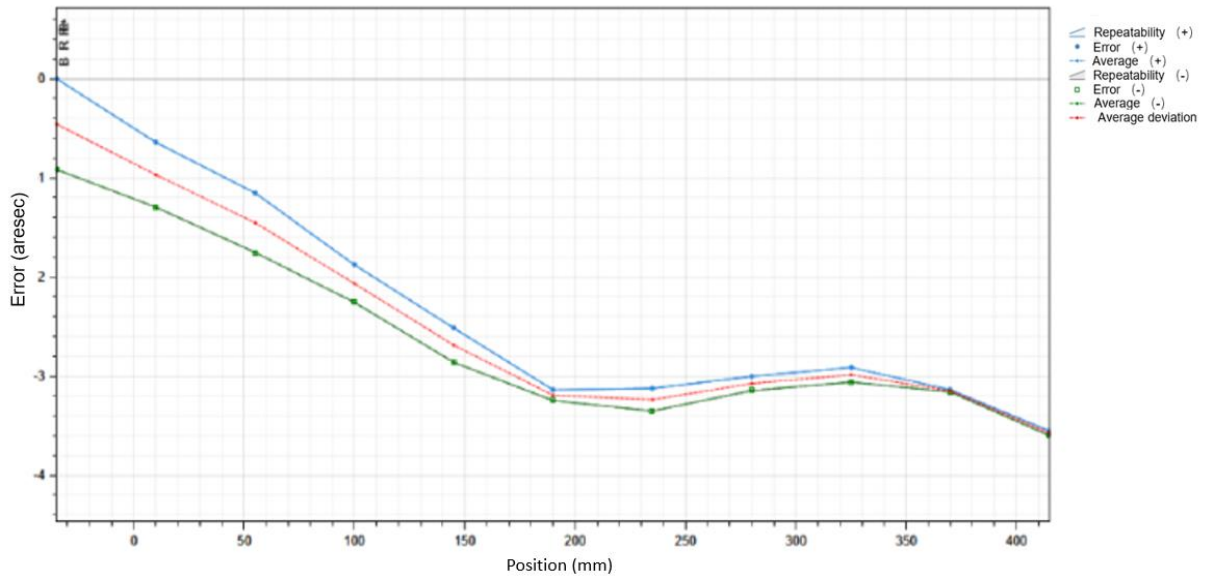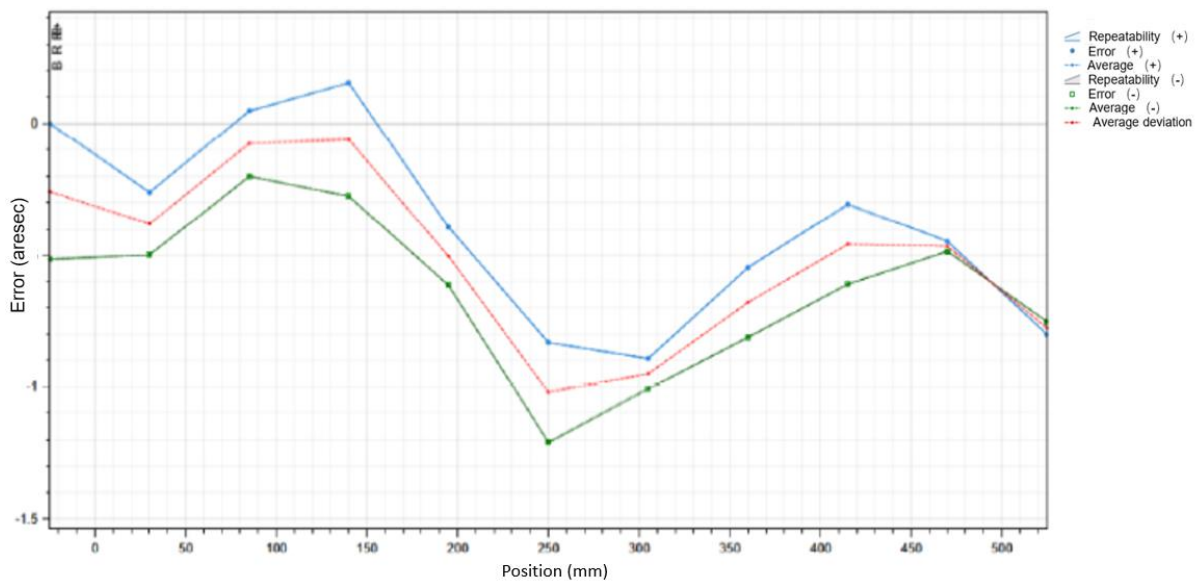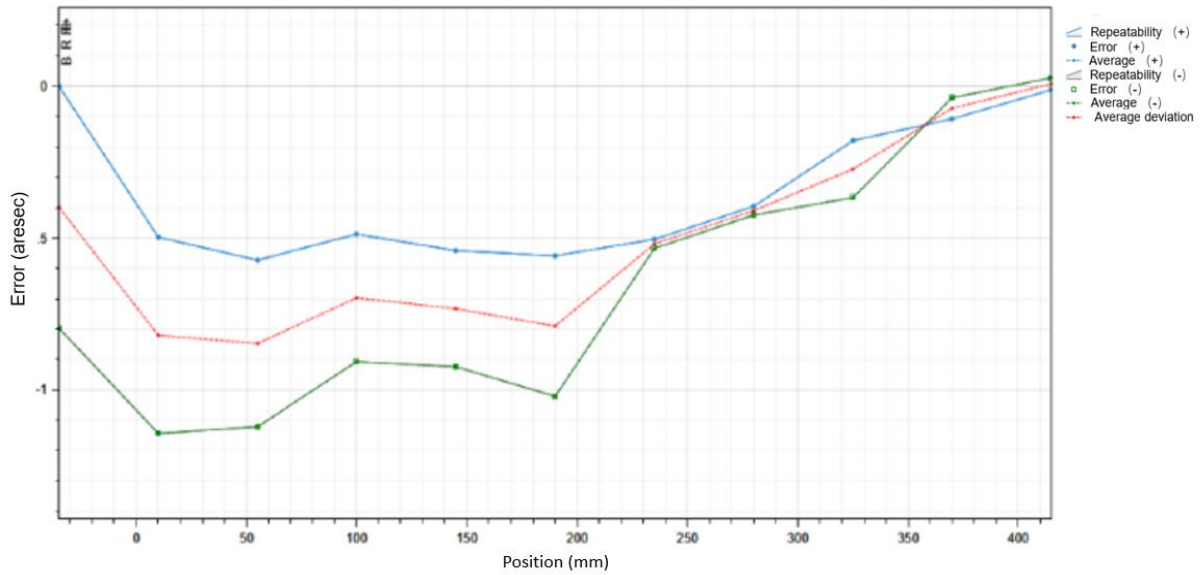
(d)

Figure 7.25 Pitch and Yaw of test slideways

(a)X-Axis Pitch; (b) Y-Axis Pitch

(c)X-Axis Yaw; (d) Y-Axis Yaw

As presented in Figure 7.23-25, the test results of machine platform are summarized in Table 7.4:

Table 7.4 Test results of UPM machine platform

	X-Axis	Y-Axis
Positioning Accuracy(µm)	±0.2145	±0.3105
Repeatability(µm)	±0.189	±0.1095
Straightness(µm)	±0.29	±0.3685
Flatness(µm)	±0.3665	±0.359
Pitch(arcsec)	±1.797	±1.8
Yaw(arcsec)	±0.681	±0.5855

It can be seen from the specifications listed in Table 7.2 and the test results presented above, the performance of designed UPM machine platform meets the design specification well, as conclusion, the superiority of the design and analysis

methodology in this industrial experiment can be summarized as:

- From a design perspective, precise prediction and design of multiscale air bearing parameters with a safe tolerance for air film thickness variation due to machining errors are essential to ensure sufficient load-bearing capacity and stiffness for each motion axis. This results in highly stable working conditions for each motion axis. The integration of multiphysics in the design process, including mechanical structure, electrical drive, and control system, further enhances the performance of the platform system.

- From the components selection aspect, the utilization of natural granite as a base offers the advantage of effectively attenuating environmental vibrations, while simultaneously achieving exceptional surface processing accuracy at the micron level. Furthermore, the implementation of a direct motor drive circumvents the potential influence of intermediary transmission errors, whereas the adoption of a grating ruler with high feedback precision affords seamless speed control. Finally, the air film generated by aerostatic bearings serves to homogenize errors, thereby enhancing the motion accuracy of the machine platform.

7.3.5 Application approach of UPM machine platform digital twin

Until now, the development of UPM machine platforms has entailed the separate creation of physical objects and their corresponding DT. The DT, which comprise virtual 1:1 3D models, static and dynamic performance simulation models, control logic, and parameters, are generated during the design phase. Conversely, the physical objects represent the actual manufactured and commissioned machine platforms that meet all performance requirements with long service life.

In order to enable real-time sensing and feedback, in-process data transmission between the physical objects and DT is facilitated by encoders positioned on each motion axis. Consequently, the DT of UPM machine platforms are capable of collecting and storing full lifecycle data, monitoring real-time performance, predicting and alarming potential errors, and other such functions. With the application of suitable

algorithms, DT can be endowed with self-organizing and self-adaptive capabilities, which enable them to automatically optimize motion accuracy, compensate for various types of errors, and perform other related functions, shown as a concept diagram in Figure 7.26, which provides a visual representation of the aforementioned system:
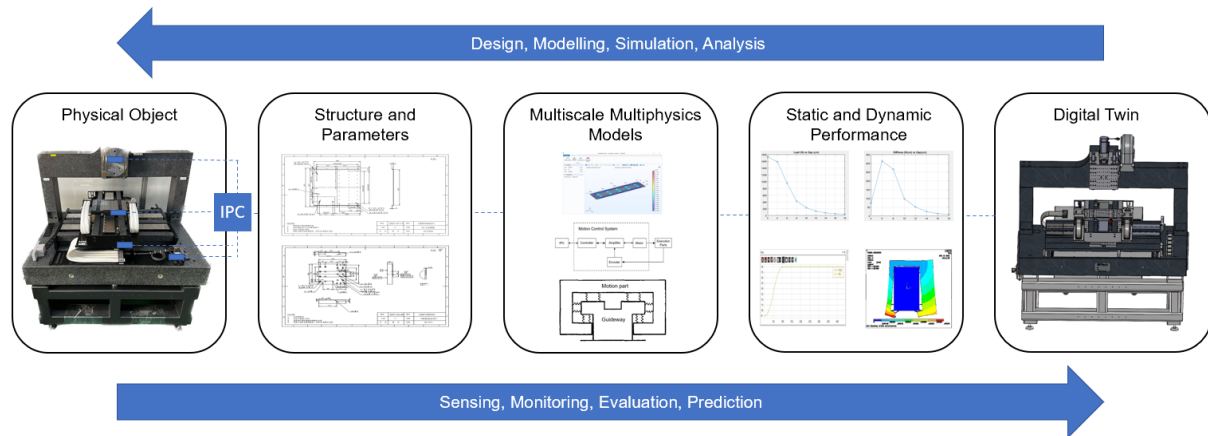
Figure 7.26 Schematic of UPM machine platform digital twin

Due to the limitations of simulation technology and the development of the corresponding algorithms, a functionally sound UPM machine platform DT was not actually completed in this study, but the possibility of its realization was proved throughout the theoretical research and industrial experiments.

7.3.6   Conclusion

The objective of this chapter is to validate the modelling and analysis approach, as well as the simulation method, utilized for the design of an UPM machine platform. In order to achieve this aim, a comparative analysis was carried out between the results obtained from performance simulations and actual test results. Based on this analysis, the following conclusions can be drawn:

1)   The CFD simulation results agree quite well with the test results. The modelling and simulation proposed in the previous chapters can accurately predict the static performance of aerostatic bearings to some extent.

2)   Air bearing plays one of the most significant roles on the UPM machine platform performance. The increase of the air bearing stiffness will greatly benefit the

motion accuracy of the aerostatic bearing slideways with high capacity anti pitch/roll/yaw. Inlet pressure and bearing size of air bearing could be important parameters for increase the static performance of air film, but high inlet pressure will also increase the chance of occurrence of pneumatic hammer.

3) The tested performance fit the product specification very well, which proved that the designed UPM machine platform is academically and practically feasible.

7.4   Conclusion

The industrial case studies in this chapter are designed to validate the multiscale multiphysics modelling and analysis approach and the CFD simulation accuracy on air bearing performance in previous chapters. Industrial project-based trials on precision rotary table and machine platform development have been carried out to achieve this aim. The industrial data from JITRI UPTECH company is also used to validate the results of simulation and design. The following conclusions can be drawn:

- The CFD simulation results agree quite well with the industrial trials results based on aerostatic bearings with different parameters. The modelling and simulation proposed in the previous chapters can accurately predict the aerostatic bearing static performance to some extent. The aerostatic bearing components (rotary table and linear slideway) were optimized significantly and help a lot with the development and manufacturing process of JITRI UPTECH company.

- The integrated design of mechanical, electrical and control system is proved as a practical approach in UPM machine platform development, which validated the multiscale multiphysics modelling, analysis and design methodology presented in previous chapters.

- The application approach of DT is further discussed, although the ideal functions are not fully realized due to the limitation of hardware and software, it still provides a feasibility for the implementation of DT technology in UPM scenario.

- The self-designed CFD and FDM simulation application based on COMSOL^{TM} and

MATLAB environment with simplified GUI has been handled to the R&D department of UPTech Co. Ltd. and be used to predict and optimize the product performance of other aerostatic bearing products under mass production and to be developed. It is recognized as a convenient engineering tool for all unexperienced and senior practitioners.

From these conclusions, the multiscale multiphysics based modelling and analysis method for UPM machine platform design and development and its DT application approach has achieved the aims and objectives of this project.

Chapter 8   Conclusions and recommendations for future work

8.1 Conclusions

By and large, the aim of this PhD research is to investigate the design, modelling and analysis of UPM machine platform from different spatial scales and physical fields, including the integration of its mechanical system, drive system and control system, and to investigate the application of digital twin technology. The modelling and simulation of single-axis motion components is carried out via MATLAB^{TM} and COMSOL^{TM} MULTIPHYSICS. The developed modelling and simulation method is proved valuable for the design work of relevant industrial products with effective simulation of complex fluid dynamic factors and precision control, and is validated on real industrial products. The main results that meet the objectives of this research lie in:

1) The multiscale multiphysics modelling and analysis methodology is a critical and future-oriented methodology in both academical study and engineering design. It can dramatically improve the feasibility and accuracy comparing to the methods which focus on only one individual scale and/or physical field.

2) The developed CFD application in COMSOL^{TM} MULTIPHYSICS environment and MATLAB^{TM} algorithm can be used to realize the multiscale multiphysics modelling and simulation in aerostatic bearing components with significant advantages in terms of efficiency, convenience and accuracy.

3) An improved single axis control system with PID tuning parameters is introduced to provide high robustness and motion stiffness. The further development of CCC with variable gains for biaxial slideway system presents a possibility of an integrated control and tuning method for the multi-axis UPM machine platform.

4) The measurement of properties of air bearing in aerostatic slideway and rotary tables is described with both simulation prediction method and case study from the industrial partner. The details of properties are essential in the validation of modelling and simulation results.

5) The simulation results show a quite well agree with the UPM machine platform trials results with different design parameter and product type. The modelling and simulation proposed in the previous chapters can accurately predict the load capacity and static stiffness of aerostatic bearing slideway and rotary table to some extent.

6) The simulation results on control system with different tuning parameter fits well with the industrial data of tracking and contour accuracy.

7) The implementation of DT in freeform surface SPDT process provide a future-oriented guide for the subsequent study regarding the approach of DT in precision and ultraprecision machines and machine platforms.

8) The modelling and analysis based method for ultraprecision machine platform design has been handled to UPTech Co. Ltd. and be used to optimize the air bearing components manufacturing for customers. It is proved to be economically valuable for the company during engineering product R&D.

8.2   Contributions to knowledge

This doctoral research aims to develop an integrated scientific approach for design modelling and analysis of a multi-axis precision machine platform for ultraprecision manufacturing, utilizing multiscale multiphysics modelling and digital twin. This approach is evaluated in the context of precision engineering and industry 4.0. To fulfil this aim, a thorough investigation of the approach and its implementation perspectives has been conducted against design and development of aerostatic bearing products and the precision machine platform. Well-designed experimental trials and industrial case studies have been carried out to further evaluate and validate the design modelling and simulation, the products design and development. The conclusion

sections at each respective chapter provide summative highlights of the modelling and simulation process, the results, the underlying philosophy, and the implementation and application perspectives of the approach.

Therefore, the novelty and contributions to knowledge from this research can be further highlighted as follows:

1) The development of design and analysis method for single-axis aerostatic bearing slideway and its DT implementation approach.

2) The development of an integrated approach for the design of multi-axis precision machine platform.

3) Multiscale multiphysics modelling and analysis method for the aerostatic bearing products design.

4) The development of DT for aerostatic bearing products and its application to UPM machines.

5) Development of the prototype virtual machine DT with the validation from SPDT machining process experiments and industrial manufacturing data on freeform surface components. The DT can be used to further optimise the diamond turning process for precision and ultraprecision manufacturing.

6) The method and basic experimental design to determine the load capacity and static stiffness of single axis aerostatic bearing slideway using load cells and displacement sensors, which provide the possibility to build the data base of aerostatic bearing slideway product design.

7) The well-designed industrial case studies provide solutions for both academical and industrial design demands. The seamless integration of academical calculation, simulation data and industrial requirements on load capacity, straightness and stiffness shows a possibility of a practical application of this research theme.

8.3 Recommendations for future work

As recommendations for future work, the following is suggested:

1) There are still numerous physical fields not considered from the working environment of UPM machine platform, such as thermal fields, acoustic fields. These physical fields can affect or harm the performance of the machine platform to a certain extent. It is worthy for future studies to consider more physical influence factors in the simulation work.

2) The PID tuning method has a high degree of stability and accuracy, but lacks in intelligence. The value of using more flexible method like sliding mode control, fuzzy control and other method has been proven in many studies. Subsequent research on multi-axis CCC integrated control methods could introduce adaptive control methods to improve the flexibility of the control system.

3) Currently the UPTech Co. Ltd. is facing the increasingly challenge in design of reconfigurable UPM machine platform and aerostatic bearing slideway/rotary table/spindle products as required by the industries, this can be seen as a trend for the design of future UPM machines due to its high economical value. It is thus meaningful and worthy for further research.

4) The methods for in-process monitoring during UPM process are still limited or hard to be realized. It is possible to discuss and involve more kinds of sensor and monitor hardware and intelligence algorithm like AI 2.0 besides the 3 types of monitoring method mentioned in Chapter 6.

References

[1] Taniguchi N. Integrated Processing Systems for Ultra-precision and Ultra-fine products. Nanotechnology.

[2] Denkena B, Bergmann B, Klemme H. Cooling of motor spindles—a review. The International Journal of Advanced Manufacturing Technology. 2020 Oct;110:3273-94.

[3] Zhang S, Zhou Y, Zhang H, Xiong Z, To S. Advances in ultra-precision machining of micro-structured functional surfaces and their typical applications. International Journal of Machine Tools and Manufacture. 2019 Jul 1;142:16-41.

[4] Yuan J, Lyu B, Hang W, Deng Q. Review on the progress of ultra-precision machining technologies. Frontiers of mechanical engineering. 2017 Jun;12:158-80.

[5] Altintas Y, Brecher C, Weck M, Witt S. Virtual machine tool. CIRP annals. 2005 Jan 1;54(2):115-38.

[6] Cheng K, Shore P. Special issue on design of ultraprecision and micro machine tools and their key enabling technologies. International Journal of Machine Tools and Manufacture. 2010;4(50):309.

[7] Shinno H, Yoshioka H, Taniguchi K. A newly developed linear motor-driven aerostatic XY planar motion table system for nano-machining. CIRP annals. 2007 Jan 1;56(1):369-72.

[8] Khan AW, Chen W. A methodology for systematic geometric error compensation in five-axis machine tools. The International Journal of Advanced Manufacturing Technology. 2011 Mar;53:615-28.

[9] Fesperman R, Ozturk O, Hocken R, Ruben S, Tsao TC, Phipps J, Lemmons T, Brien J, Caskey G. Multi-scale alignment and positioning system–MAPS. Precision Engineering. 2012 Oct 1;36(4):517-37.

[10] Al-Bender F. Air bearings: theory, design and applications. John Wiley & Sons; 2021 Jan 11.

[11] Rowe WB. Hydrostatic, aerostatic and hybrid bearing design. Elsevier; 2012 Mar 28.

[12] Gou N, Cheng K, Huo D. Multiscale modelling and analysis for design and development of a high-precision aerostatic bearing slideway and its digital twin. Machines. 2021 Apr 25;9(5):85.

[13] Gao Q, Lu L, Chen W, Wang G. Optimal design of an annular thrust air bearing using parametric computational fluid dynamics model and genetic algorithms. Proceedings of the Institution of Mechanical Engineers, Part J: Journal of Engineering Tribology. 2018 Oct;232(10):1203-14.

[14] Bao X, Mao J. Dynamic modeling method for air bearings in ultra-precision positioning stages. Advances in Mechanical Engineering. 2016 Aug;8(8):1687814016664290.

[15] Wardle F. Ultra-precision bearings. Elsevier; 2015 Feb 10.

[16] Gao Q, Chen W, Lu L, Huo D, Cheng K. Aerostatic bearings design and analysis with the application to precision engineering: State-of-the-art and future perspectives. Tribology International. 2019 Jul 1;135:1-7.

[17] Willis R. On the pressure produced on a flat plate when opposed to a stream of air issuing from an orifice in a plan surface. J. Smith; 1828.

[18] Kingsbury A. EXPERIMENTS WITH AN AIR‐LUBRICATED JOURNAL. Journal of the American Society for Naval Engineers. 1897 May;9(2):267-92.

[19] Lu S. Numerical simulation of slider air bearings. University of California, Berkeley; 1997.

[20] Sugimori S, Kawaguti M, Yamamoto SS. Characteristics of Air Bearings with Small Inlet Holes for a Precision Coordinate Measuring Device. Japanese Journal of Applied Physics. 1975 Feb 1;14(2):280.

[21] Balandin FI, FOREIGN TECHNOLOGY DIV WRIGHT-PATTERSON AFB OHIO. Study of an Annular Air Bearing with External Pressurization. US Air Force, Systems Command, Foreign Technology Division; 1972 Apr 11.

[22] https://www.comsol.com. Accessed date: 12 August 2021.

[23] Al-Bender F. On the modelling of the dynamic characteristics of aerostatic bearing films: From stability analysis to active compensation. Precision Engineering. 2009 Apr 1;33(2):117-26.

[24] Yu HC, Ma WQ, Wang ZW, Xu LF. CFD research on aerostatic bearing with tangential supply holes. Advanced Materials Research. 2010 Mar 26;97:2021-6.

[25] Yu H, Ma W. Study on two different calculation methods for thrust aerostatic bearings with single supply hole at large gas film clearance. In2010 IEEE International Conference on Mechatronics and Automation 2010 Aug 4 (pp. 53-58). IEEE.

[26] Gao Q, Qi L, Gao S, Lu L, Song L, Zhang F. A FEM based modeling method for analyzing the static performance of aerostatic thrust bearings considering the fluid-structure interaction. Tribology International. 2021 Apr 1;156:106849.

[27] Miyatake M, Yoshimoto S. Numerical investigation of static and dynamic characteristics of aerostatic thrust bearings with small feed holes. Tribology International. 2010 Aug 1;43(8):1353-9.

[28] Belforte G, Raparelli T, Trivella A, Viktorov V, Visconte C. CFD analysis of a simple orifice-type feeding system for aerostatic bearings. Tribology Letters. 2015 May;58:1-8.

[29] Shu PC, Xiao SH, Wu H. Finite Element Analysis and Calculation of Load Capacity on Aerostatic Thrust Bearing. Advanced Materials Research. 2011 Apr 6;188:566-71.

[30] Luo X, Han B, Chen X, Li X, Jiang W. Multi-physics modeling of tunable aerostatic bearing with air gap shape compensation. Tribology International. 2021 Jan 1;153:106587.

[31] Yuan ZJ, Wang XK. Precision and ultraprecision manufacturing. China Machine Press; 1999.

[32] Taniguchi N. Current status in, and future trends of, ultraprecision machining and ultrafine materials processing. CIRP annals. 1983 Jan 1;32(2):573-82.

[33] Lee WB. Prediction of microcutting force variation in ultra-precision machining. Precision engineering. 1990 Jan 1;12(1):25-8.

[34] McKeown PA, Carlisle K, Shore P, Read RF. Ultraprecision, high stiffness CNC grinding machines for ductile mode grinding of brittle materials. InInfrared Technology and Applications 1990 Oct 1 (Vol. 1320, pp. 301-313). SPIE.

[35] Huo D, Cheng K, Wardle F. A holistic integrated dynamic design and modelling approach applied to the development of ultraprecision micro-milling machines. International Journal of Machine Tools and Manufacture. 2010 Apr 1;50(4):335-43.

[36] An CH, Zhang Y, Xu Q, Zhang FH, Zhang JF, Zhang LJ, Wang JH. Modeling of dynamic characteristic of the aerostatic bearing spindle in an ultra-precision fly cutting machine. International Journal of Machine Tools and Manufacture. 2010 Apr 1;50(4):374-85.

[37] Harrison WJ. The hydrodynamical theory of lubrication with special reference to air as a lubricant. University Press; 1913.

[38] Ro SK, Kim S, Kwak Y, Park CH. A linear air bearing stage with active magnetic preloads for ultraprecise straight motion. Precision engineering. 2010 Jan 1;34(1):186-94.

[39] Stanev PT, Wardle F, Corbett J. Investigation of grooved hybrid air bearing performance. Proceedings of the Institution of Mechanical Engineers, Part K: Journal of Multi-body Dynamics. 2004 Jun 1;218(2):95-106.

[40] Yoshimoto S, Yamamoto M, Toda K. Numerical calculations of pressure distribution in the bearing clearance of circular aerostatic thrust bearings with a single air supply inlet.

[41] Ford GW, Harris DM, Pantall D. Principles and applications of hydrodynamic–type gas lubricated bearings. Industrial Lubrication and Tribology. 1956;8(11):32-6.

[42] Majumdar BC. Introduction to tribology of bearings. S. Chand Publishing; 2008.

[43] Powell JW. A review of progress in gas lubrication. Review of Physics in Technology. 1970 Jun 1;1(2):96.

[44] Morosi S, Santos IF. Experimental investigations of active air bearings. InTurbo Expo: Power for Land, Sea, and Air 2012 Jun 11 (Vol. 44731, pp. 901-910). American Society of Mechanical Engineers.

[45] Tabilo-Munizaga G, Barbosa-Cánovas GV. Rheology for the food industry. Journal of food engineering. 2005 Mar 1;67(1-2):147-56.

[46] Gao S, Cheng K, Ding H, Fu H. Multiphysics-based design and analysis of the high-speed aerostatic spindle with application to micro-milling. Proceedings of the Institution of Mechanical Engineers, Part J: Journal of Engineering Tribology. 2016 Jul;230(7):852-71.

[47] Küng A, Meli F, Thalmann R. Ultraprecision micro-CMM using a low force 3D touch probe. Measurement Science and Technology. 2007 Jan 12;18(2):319.

[48] Dykas B, Howard SA. Journal design considerations for turbomachine shafts supported on foil air bearings. Tribology Transactions. 2004 Oct 1;47(4):508-16.

[49] Rowe WB. Advances in hydrostatic and hybrid bearing technology. Proceedings of the Institution of Mechanical Engineers, Part C: Mechanical Engineering

Science. 1989 Jul;203(4):225-42.

[50] Petrov NP. Friction in machines and the effect of the lubricant. Inzh. Zh., St-Peterb.. 1883.

[51] Sommerfeld A. Partial differential equations in physics. Academic press; 1949.

[52] Chaplygin SA. Gas jets. National Advisory Committee for Aeronautics; 1944.

[53] Cunningham RE, Gunter Jr EJ. Critical speeds of a rotor in rigidly mounted, externally pressurized, air-lubricated bearings. 1971 May 1.

[54] Majumdar BC. Analysis of externally pressurized gas bearings with journal rotation. Wear. 1973 Apr 1;24(1):15-22.

[55] Lo CY, Wang CC, Lee YH. Performance analysis of high-speed spindle aerostatic bearings. Tribology International. 2005 Jan 1;38(1):5-14.

[56] Mo DY, Ma P, Lian HS, Gong MF. Improvement and Verification of Mathematical Model of Bearing Capacity of Single-row Restrictors Air-bearing Platform. Lubrication Engineering, 2019, 44(6): 88-94.

[57] Stout KJ, Sweeney F. Design of aerostatic flat pad bearings using pocketed orifice restrictors. Tribology international. 1984 Aug 1;17(4):191-8.

[58] Khim G, Park CH. A rotary stage in a vacuum using an air bearing. Vacuum. 2014 Jul 1;105:39-45.

[59] Ekinci TO, Mayer JR, Cloutier GM. Investigation of accuracy of aerostatic guideways. International Journal of Machine Tools and Manufacture. 2009 May 1;49(6):478-87.

[60] Rasnick WH. AIR-BEARING SLIDES FOR PRECISION XY TURNING MACHINES. Union Carbide Corp., Oak Ridge, Tenn. Y-12 Plant; 1972 Jan 1.

[61] Belforte G, Raparelli T, Viktorov V, Trivella A. Discharge coefficients of orifice-type restrictor for aerostatic bearings. Tribology International. 2007 Mar 1;40(3):512-21.

[62] Renn JC, Hsiao CH. Experimental and CFD study on the mass flow-rate characteristic of gas through orifice-type restrictor in aerostatic bearings. Tribology International. 2004 Apr 1;37(4):309-15.

[63] Liu T. Aerostatic gas lubrication. Harbin Institute of Technology Press; 1990.

[64] Reynolds O. IV. On the theory of lubrication and its application to Mr. Beauchamp tower's experiments, including an experimental determination of the viscosity of olive oil. Philosophical transactions of the Royal Society of London. 1886 Dec 31(177):157-234.

[65] Cope WF. The hydrodynamical theory of film lubrication. Proceedings of the Royal Society of London. Series A. Mathematical and Physical Sciences. 1949 Jun 7;197(1049):201-17..

[66] Wannier GH. A contribution to the hydrodynamics of lubrication. Quarterly of Applied Mathematics. 1950 Apr 1;8(1):1-32.

[67] Halton JH. Lubrication of Plain Bearings, Applicability of Reynolds's Hydrodynamic Theory. Engineering. 1958;186:59.

[68] Zienkiewicz OC. Temperature distribution within lubricating films between parallel bearing surfaces and its effect on the pressures developed. InProc. Conference on Lubrication and Wear 1957 (Vol. 135).

[69] Dowson D. A generalized Reynolds equation for fluid-film lubrication. International Journal of Mechanical Sciences. 1962 Mar 1;4(2):159-70.

[70] Castelli V, Pirvics J. Review of numerical methods in gas bearing film analysis. ASME 1968.

[71] Gero LR, McC. Ettles CM. An evaluation of finite difference and finite element methods for the solution of the Reynolds equation. ASLE transactions. 1986 Jan 1;29(2):166-72.

[72] Oh KP, Rohde SM. A theoretical analysis of a compliant shell air bearing. 1977.

[73]ONO K, KOGURE K, MITSUYA Y. Dynamic Characteristics of Air-Lubricated Slider Bearings under Submicron Spacing Conditions. Bulletin of JSME. 1979;22(173):1672-7.

[74]KOGURE K, KANEKO R, OHTANI K. A study on characteristics of surface-restriction compensated gas bearing with T-shaped grooves. Bulletin of JSME. 1982;25(210):2039-45.

[75]Dal A, Karaçay T. Effects of angular misalignment on the performance of rotor-bearing systems supported by externally pressurized air bearing. Tribology International. 2017 Jul 1;111:276-88.

[76]Hua W, Yu S, Zhou W, Sett Myo K. A fast implicit algorithm for time-dependent dynamic simulations of air bearing sliders. 2012.

[77]Wu L, Bogy DB. Unstructured adaptive triangular mesh generation techniques and finite volume schemes for the air bearing problem in hard disk drives. J. Trib.. 2000 Oct 1;122(4):761-70.

[78]Lu S. Numerical simulation of slider air bearings. University of California, Berkeley; 1997.

[79]Hensel K. Journal für die reine und angewandte Mathematik. W. de Gruyter.; 1854.

[80]MITSUYA Y. Molecular Mean Free Path Effects in Gas Lubricated Slider Bearings: An Application or the Finite Element Solution. Bulletin of JSME. 1979;22(168):863-70.

[81]Li S, Liu T. Analysis of the dynamics of a aerostatic bearing spindle system in a precision centrifuge. Journal of Mechanical Engineering, 2005, 41(2): 28-32.

[82]Neves MT, Schwarz VA, Menon GJ. Discharge coefficient influence on the performance of aerostatic journal bearings. Tribology International. 2010 Apr 1;43(4):746-51.

[83]Milbradt P, Abed WA. Generalized stabilization techniques in computational fluid

dynamics. ICHE 2008. Proceedings of the 8th International Conference on Hydro-Science and Engineering, Nagoya, Japan. 2008.

[84]Bhavikatti SS. Finite element analysis. New Age International; 2005.

[85]Hutton DV. Fundamentals of finite element analysis. The McGraw Hill Companies; 2004.

[86]Autodesk Inc. What is finite element analysis software? https://www.autodesk.com/solutions/finite-element-analysis. Accessed date: 12 August 2021.

[87]Zaeh M, Siedl D. A new method for simulation of machining performance by integrating finite element and multi-body simulation for machine tools. CIRP annals. 2007 Jan 1;56(1):383-6.

[88]Zhang M, Liu Q, Yuan S. Machine tool spindle unit analysis system based on second development of ANSYS. Machine Tool & Hydraulics. 2008;36(2):11-6.

[89]Yao YF, Liu Q, Wu WJ. Dynamic simulation of a linear motor feed drive system based on rigid-flexible & electrical-mechanical coupling. Journal of Vibration and Shock, 2011, 30(1): 191-196.

[90]https://hexagon.com/products/product-groups/computer-aided-engineering-software/adams. Accessed date: 12 August 2021.

[91]https://www.ansys.com. Accessed date: 12 August 2021.

[92]https://www.3ds.com/products/simulia/abaqus. Accessed date: 12 August 2021.

[93]Allan DR, Nowell H, Barnett SA, Warren MR, Wilcox A, Christensen J, Saunders LK, Peach A, Hooper MT, Zaja L, Patel S. A novel dual air-bearing fixed-χ diffractometer for small-molecule single-crystal X-ray diffraction on beamline I19 at diamond light source. Crystals. 2017 Nov 2;7(11):336.

[94]Yang X, An C, Wang Z, Wang Q, Peng Y, Wang J. Research on surface topography in ultra-precision flycutting based on the dynamic performance of

machine tool spindle. The International Journal of Advanced Manufacturing Technology. 2016 Nov;87:1957-65.

[95] Qiao J. Study of gas bearings for precision pendulum milling head based on numerical simulation. Harbin Institute of Technology; 2006.

[96] Weinan E. Principles of multiscale modeling. Cambridge University Press; 2011 Jul 7.

[97] Zhang S, Bogy DB. A heat transfer model for thermal fluctuations in a thin slider/disk air bearing. International journal of heat and mass transfer. 1999 May 1;42(10):1791-800.

[98] Ro SK, Kim S, Kwak Y, Park CH. A linear air bearing stage with active magnetic preloads for ultraprecise straight motion. Precision engineering. 2010 Jan 1;34(1):186-94.

[99] Korzhyk O, Kozak A, Didkovskyi V, Naida S. Construction the Device of Acoustic Noise Air Bearing. IEEE 40th International Conference on Electronics and Nanotechnology (ELNANO) 2020 Apr 22 (pp. 683-687). IEEE.

[100]   Cao H, Dörgeloh T, Riemer O, Brinksmeier E. Adaptive separation of unbalance vibration in air bearing spindles. Procedia CIRP. 2017 Jan 1;62:357-62.

[101]   Gao Q, Qi L, Gao S, Lu L, Song L, Zhang F. A FEM based modeling method for analyzing the static performance of aerostatic thrust bearings considering the fluid-structure interaction. Tribology International. 2021 Apr 1;156:106849.

[102]   Gao W, Arai Y, Shibuya A, Kiyono S, Park CH. Measurement of multi-degree-of-freedom error motions of a precision linear air-bearing stage. Precision engineering. 2006 Jan 1;30(1):96-103.

[103]   Cao H, Riemer O, Brinksmeier E. Dynamic modelling and vibration simulation of air bearing spindle systems due to unbalance. International Journal of Mechatronics and Manufacturing Systems. 2017;10(3):260-76.

[104]   Aoyama T, Kakinuma Y, Kobayashi Y. Numerical and experimental analysis for the small vibration of aerostatic guideways. CIRP annals. 2006 Jan 1;55(1):419-22.

[105]   Sun Y, Wu Q, Chen W, Luo X, Chen G. Influence of unbalanced electromagnetic force and air supply pressure fluctuation in air bearing spindles on machining surface topography. International Journal of Precision Engineering and Manufacturing. 2021 Jan;22:1-2.

[106]   Ju YS. Thermal conduction and viscous heating in microscale Couette flows. J. Heat Transfer. 2000 Nov 1;122(4):817-8.

[107]   Lee KW, Noh YJ, Gao W, Arai Y, Shimizu Y, Tanaka K, Fukuta M, Kai Y. Experimental investigation of an air-bearing displacement sensor for on-machine surface form measurement of micro-structures. International Journal of Precision Engineering and Manufacturing. 2011 Aug;12:671-8.

[108]   Tao F, Xiao B, Qi Q, Cheng J, Ji P. Digital twin modeling. Journal of Manufacturing Systems. 2022 Jul 1;64:372-89.

[109]   Qi Q, Tao F, Hu T, Anwer N, Liu A, Wei Y, Wang L, Nee AY. Enabling technologies and tools for digital twin. Journal of Manufacturing Systems. 2021 Jan 1;58:3-21.

[110]   Bao J, Guo D, Li J, Zhang J. The modelling and operations for the digital twin in the context of manufacturing. Enterprise Information Systems. 2019 Apr 21;13(4):534-56.

[111]   Tao F, Zhang H, Liu A, Nee AY. Digital twin in industry: State-of-the-art. IEEE Transactions on industrial informatics. 2018 Sep 30;15(4):2405-15.

[112]   VanDerHorn E, Mahadevan S. Digital Twin: Generalization, characterization and implementation. Decision support systems. 2021 Jun 1;145:113524.

[113]   Wu L, Leng J, Ju B. Digital twins-based smart design and control of ultra-precision machining: A review. Symmetry. 2021 Sep 16;13(9):1717.

[114]   Zhang P. Accuracy prediction model of an orifice-compensated aerostatic bearing. Precision Engineering. 2021 Nov 1;72:837-46.

[115]   Li Y, Zhou K, Zhang Z. A flow-difference feedback iteration method and its application to high-speed aerostatic journal bearings. Tribology International. 2015 Apr 1;84:132-41.

[116]   Cui H, Wang Y, Yang H, Zhou L, Li H, Wang W, Zhao C. Numerical analysis and experimental research on the angular stiffness of aerostatic bearings. Tribology International. 2018 Apr 1;120:166-78.

[117]   Wang C, Cheng K and Rakowski R. An experimental investigation on ultra-precision instrumented smart aerostatic bearing spindle applied to high speed micro-drilling, Journal of Manufacturing Processes, 31(1), 2018, 324-335.

[118]   Khaghani A and Cheng K. Investigation on multi-body dynamics based approach to the toolpath generation for ultraprecision machining of freeform surfaces, Proceedings of the IMechE, Part B: Journal of Engineering Manufacture, 234(3), 2020, 571-583.

[119]   Gao S, Cheng K and Ding H. Multiphysics-based design and analysis of the high-speed aerostatic spindle with application to micro-milling, Proceedings of the IMechE, Part J: Journal of Engineering Tribology, 230(7), 2016, pp. 852-871.

[120]   Shao Y, Adetoro M and Cheng K. Development of multiscale multiphysics-based modelling and simulations with the application to precision machining of aerofoil structures, Engineering Computations, 38(3), 2021, 1330-1349.

[121]   Sun X, Cheng K. Multi-scale simulation of the nano-metric cutting process. The International Journal of Advanced Manufacturing Technology. 2010 Apr;47:891-901.

[122]   Chapman WL, Bahill AT, Wymore AW. Engineering modeling and design. CRC Press; 1992 Sep 16.

[123]   Shao Y, Adetoro OB, Cheng K. Development of multiscale multiphysics-based modelling and simulations with the application to precision machining of

aerofoil structures. Engineering Computations. 2021 Jun 15;38(3):1330-49.

[124] Tadmor EB, Ortiz M, Phillips R. Quasicontinuum analysis of defects in solids. Philosophical magazine A. 1996 Jun 1;73(6):1529-63.

[125] Wood MA, Kittell DE, Yarrington CD, Thompson AP. Multiscale modeling of shock wave localization in porous energetic material. Physical Review B. 2018 Jan 30;97(1):014109.

[126] Gold K, Gaharwar AK, Jain A. Emerging trends in multiscale modeling of vascular pathophysiology: Organ-on-a-chip and 3D printing. Biomaterials. 2019 Mar 1;196:2-17.

[127] Kundalwal SI, Meguid SA. Multiscale modeling of regularly staggered carbon fibers embedded in nano-reinforced composites. European Journal of Mechanics-A/Solids. 2017 Jul 1;64:69-84.

[128] Web of Science Core Collection. Available online: www.webofknowledge.com. Accessed on 20 February 2021.

[129] Huo D, Cheng K, Wardle F. Design of a five-axis ultra-precision micro-milling machine—UltraMill. Part 1: holistic design approach, design considerations and specifications. The International Journal of Advanced Manufacturing Technology. 2010 Apr;47:867-77.

[130] Kritzinger W, Karner M, Traar G, Henjes J, Sihn W. Digital Twin in manufacturing: A categorical literature review and classification. Ifac-PapersOnline. 2018 Jan 1;51(11):1016-22.

[131] Sun X, Chen S, Cheng K. An analytic method calculation and analysis of the aerostatic guide way. J. Mach. Des. Manuf. 2005;1:40-2.

[132] Tao J. Method of calculate close double row orifice rectangular aerostatic slideways. Opt. Precis. Eng. 1997;5:55-60.

[133] Zheng T, Radhakrishnan S, Sarangan V. PMAC: an adaptive energy-efficient MAC protocol for wireless sensor networks. In19th IEEE international parallel and distributed processing symposium 2005 Apr 4 (pp. 8-pp). IEEE.

[134] Tao F, Zhang H, Liu A, Nee AY. Digital twin in industry: State-of-the-art. IEEE

Transactions on industrial informatics. 2018 Sep 30;15(4):2405-15.

[135]   Tao F, Sui F, Liu A, Qi Q, Zhang M, Song B, Guo Z, Lu SC, Nee AY. Digital twin-driven product design framework. International Journal of Production Research. 2019 Jun 18;57(12):3935-53.

[136]   Uhlemann TH, Lehmann C, Steinhilper R. The digital twin: Realizing the cyber-physical production system for industry 4.0. Procedia Cirp. 2017 Jan 1;61:335-40.

[137]   Tomiyama T, Lutters E, Stark R, Abramovici M. Development capabilities for smart products. CIRP Annals. 2019 Jan 1;68(2):727-50.

[138]   https://www.physikinstrumente.com/en/expertise/technology/electromagnetic-drives/magnetic-direct-drives. Accessed date: 14 March 2023.

[139]   https://www.acsmotioncontrol.com. Accessed date: 14 March 2023.s

[140]   Bourogaoui M, Sethom HB, Belkhodja IS. Speed/position sensor fault tolerant control in adjustable speed drives–A review. ISA transactions. 2016 Sep 1;64:269-84.

[141]   Gamazo-Real JC, Vázquez-Sánchez E, Gómez-Gil J. Position and speed control of brushless DC motors using sensorless techniques and application trends. sensors. 2010 Jul 19;10(7):6901-47.

[142]   Chen CS, Chen LY. Robust cross-coupling synchronous control by shaping position commands in multiaxes system. IEEE Transactions on Industrial Electronics. 2012 Jan 2;59(12):4761-73.

[143]   Koren Y, Lo CC. Variable-gain cross-coupling controller for contouring. CIRP annals. 1991 Jan 1;40(1):371-4.

[144]   Li H, Li S, Sun W, Wang L, Lv D. The optimum matching control and dynamic analysis for air suspension of multi-axle vehicles with anti-roll hydraulically interconnected system. Mechanical Systems and Signal Processing. 2020 May 1;139:106605.

[145]   Yang S, Ghasemi AH, Lu X, Okwudire CE. Pre-compensation of servo contour errors using a model predictive control framework. International Journal of

Machine Tools and Manufacture. 2015 Nov 1;98:50-60.

[146]   Ramesh R, Mannan MA, Poo AN. Tracking and contour error control in CNC servo systems. International Journal of Machine Tools and Manufacture. 2005 Mar 1;45(3):301-26.

[147]   Liu J, Wu Y, Fan L, Si Z, Jia Z. Current Hysteresis Control Design of Motorized Spindle Driven System Based on Semi-Physical Simulation Model. In2020 Chinese Control And Decision Conference (CCDC) 2020 Aug 22 (pp. 1110-1115). IEEE.

[148]   Kampker A, Stich V, Jussen P, Moser B, Kuntz J. Business models for industrial smart services–the example of a digital twin for a product-service-system for potato harvesting. Procedia Cirp. 2019 Jan 1;83:534-40.

[149]   Min Q, Lu Y, Liu Z, Su C, Wang B. Machine learning based digital twin framework for production optimization in petrochemical industry. International Journal of Information Management. 2019 Dec 1;49:502-19.

[150]   Stark R, Fresemann C, Lindow K. Development and operation of Digital Twins for technical systems and services. CIRP Annals. 2019 Jan 1;68(1):129-32.

[151]   Deloitte Insights. (2019). Industry 4.0 and the digital twin. https://www2.deloitte.com/insights/us/en/focus/industry-4-0/digital-twin-technology-smart-factory.html. Accessed 7 Apr. 2019.

[152]   Khaghani A, Cheng K. Investigation on multi-body dynamics based approach to the toolpath generation for ultraprecision machining of freeform surfaces. Proceedings of the Institution of Mechanical Engineers, Part B: Journal of Engineering Manufacture. 2020 Feb;234(3):571-83.

[153]   López J, Artés M, Alejandre I. Analysis of optical linear encoders' errors under vibration at different mounting conditions. Measurement. 2011 Oct 1;44(8):1367-80.

[154]   Niu Z, Jiao F, Cheng K. Investigation on innovative dynamic cutting force modelling in micro-milling and its experimental validation. Nanomanufacturing and Metrology. 2018 Jun;1:82-95.

[155] Rao P, Bukkapatnam S, Beyca O, Kong Z, Komanduri R. Real-time identification of incipient surface morphology variations in ultraprecision machining process. Journal of Manufacturing Science and Engineering. 2014 Apr 1;136(2):021008.

[156] Chen X. Monitoring and analysis of ultra-precision machining processes using acoustic emission. University of California, Berkeley; 1998.

[157] Fang FZ, Zhang XD, Weckenmann A, Zhang GX, Evans C. Manufacturing and measurement of freeform optics. CIRP Annals. 2013 Jan 1;62(2):823-46.

[158] Huerta-Carranza O, Avendaño-Alejo M, Díaz-Uribe R. Null screens to evaluate the shape of freeform surfaces: progressive addition lenses. Optics Express. 2021 Aug 16;29(17):27921-37.

[159] Ries H, Muschaweck J. Tailored freeform optical surfaces. JOSA A. 2002 Mar 1;19(3):590-5.

[160] Ott P. Optic design of head-up displays with freeform surfaces specified by NURBS. InOptical Design and Engineering III 2008 Sep 27 (Vol. 7100, pp. 339-350). SPIE.

[161] Park YD, Jang T. A study on the ultra precision machining of free-form molds for advanced head-up display device. Journal of the Korea Academia-Industrial cooperation Society. 2019;20(1):290-6.

[162] https://www.tecnotion.com/products/qtr-torque-105-series. Accessed 7 Apr. 2019.

Appendices

Appendix I

List of publications resulted from this research

1. Gou N, Cheng K, Huo D. Multiscale modelling and analysis for design and development of a high-precision aerostatic bearing slideway and its digital twin. Machines. 2021 Apr 25;9(5):85.

2. Gou N, Cheng K, Huo D. Investigation on an integrated approach to modelling and analysis of multi-axis aerostatic bearing stages for high precision performance. euspen's 22nd International Conference & Exhibition, Geneva, CH, May/June 2022.

3. Gou N, Liu S, Christopher D and Cheng K. Development of the digital twin of the ultraprecision diamond turning system and its application perspectives. Handbook of Digital Twins. CRC Press 2024. Accepted and under publication.

4. Gou N, Cheng K, Christopher D, Liu S and Huo D. Investigation on digital twin of the ultraprecision machining system for manufacturing freeform surfaced components. Advances in Mechanical Engineering. Under peer review.

5. Gou N, Cheng K, Huo D. Design and analysis methods for aerostatic bearings: the past, the present and the future. Proceedings of the Institution of Mechanical Engineers, Part J: Journal of Engineering Tribology. Under peer review.

Appendix II

Specifications of the TECNOTION QTR-A-105-17N frameless torque motor

	Parameter	Remarks	Symbol	Unit	QTR-A-105-17		
					N	Y	Z
Performance	Winding type				N	Y	Z
	Motortype max. voltage ph-ph	3-phase synchronous		$V_{ac\,rms}\,(V_{dc})$			
	Ultimate torque @ 20°C/s increase	magnet @ 25°C	T_u	Nm	2.9	3.3	3.3
	Peak torque @ 6°C/s increase	magnet @ 25°C	T_p	Nm	1.9	2.2	2.2
	Continuous torque	coil @ 100°C	T_c	Nm	1.4	1.4	1.4
	Maximum speed[3] @ 48 Volt	@ T_c	n_{max}	rpm	784	1761	3300
	Maximum speed @ max. voltage	@ T_c	n_{max}	rpm	6890	12286	16500
	Motor torque constant	up to I_c	K_t	Nm/A_{rms}	0.30	0.17	0.10
	Motor constant	coils @ 25°C	K_m	$(Nm)^2/W$	0.021	0.022	0.022
Electrical	Ultimate current	magnet @ 25°C	I_u	A_{rms}	13.8	28.2	48.8
	Peak current	magnet @ 25°C	I_p	A_{rms}	7.6	15.4	26.7
	Maximum continuous current[1]	coils @ 100°C	I_c	A_{rms}	4.6	8.5	14.7
	Back EMF phase-phase_peak		K_e	V/krpm	25	14	8
	Back EMF phase-phase_RMS		K_e	V/krpm	18	10	6
	Coil resistance per phase	coils @ 25°C ex. cable	R	Ω	1.38	0.43	0.14
	Coil induction per phase	$I < 0.6\,I_p$	L	mH	2.58	0.83	0.28
	Electrical time constant	coils @ 25°C	τ_e	ms	1.9	2.0	1.9
	Poles		N_{mgn}	nr	20	20	20
Thermal	Continuous power loss	coils @ 100°C	P_c	W	115	115	115
	Thermal resistance[2]	coils to mount. sfc.	R_{th}	°C/W	0.65	0.65	0.65
	Thermal time constant	up to 63% max. coiltemp.	τ_{th}	s	21	25	25
	Temperature cut-off / sensor						
Mechanical	Stator OD		OD_S	mm			
	Rotor ID		ID_R	mm			
	Motor height		H_{motor}	mm		17	
	Lamination stack height		H_{arm}	mm		8	
	Rotor inertia		J_R	$kg*m^2$		8.0E-05	
	Stator mass	excluding cables	M_S	g		299	
	Rotor mass		M_R	g		79	
	Total mass	excluding cables	M_T	g		378	
	Cable mass	all cables	m	g	63	90	90
	Cable type (power)	length 0.5 m	d	mm (AWG)	6.5 (20)	6.7 (14)	6.7 (14)
	Cable type (sensor)	length 0.5 m	d	mm (AWG)			

Appendix III

Specifications of the RENISHAW RESM20

Technical specifications

Measuring standard	RESM20: one-piece low profile stainless steel ring. Standard 'A' section with tapered internal diameter or low inertia 'B' section rings available Also available for partial rotation applications as REST20
Readhead size (LxHxW)	35 mm x 13.5 mm x 10 mm
Scale pitch	20 µm
Coefficient of thermal expansion at 20 °C	15.5 ±0.5 µm/m/°C
Ring outer diameter	52 mm to 550 mm. For larger custom sizes, contact Renishaw
Line count	8 192 to 86 400 (depending on ring size)
Reference mark	RESM20: single *IN-TRAC* reference mark ring REST20: two reference mark ring for partial rotation applications

Accuracy*
    Graduation accuracy
    System accuracy
	
	±3.97 to ±0.38 arc seconds (depending on ring diameter)
	±4.20 to ±0.40 arc seconds (depending on ring diameter)

Maximum speed
    Analogue
    Digital
	(See data sheet for details)
	3 673 rpm at -3 dB (on 52 mm RESM20)
	3 673 rpm (5 µm resolution TONiC on 52 mm RESM20)

Sub-Divisional Error (SDE)	Typically < ±30 nm
Dynamic signal control	Real time signal conditioning including Auto Gain Control (AGC) and Auto Offset Control (AOC) for optimised performance during operation

Incremental signals
    Analogue
    Digital
	(See data sheet for details of angular resolutions)
	1 Vpp (20 µm period)
	Resolutions from 5 µm to 1 nm

Electrical connection	0.5 m, 1 m, 1.5 m, 3 m, 5 m and 10 m cable lengths with mini connector (connects direct to TONiC interface)
Power supply	5 V ±10%, < 100 mA (analogue system), < 200 mA (digital systems) (unterminated)
Vibration (operating)	100 m/s² max @ 55 Hz to 2 000 Hz
Shock (non-operating)	1 000 m/s², 6 ms, ½ sine
Operating temperature (system)	0 °C to +70 °C
Sealing	Readhead: IP40 Interface: IP20

Appendix IV

Specifications of the ACS SPiiPlusCMhp

Specifications

Product (xx - BA or HP) (y - number of axes)	CMxxyA...	CMxxyB...	CMxxyC...
Number of built-in drives		1,2,3	
Motor voltage AC input [Vac]		85 - 265, single and 3 phase	
Control voltage input [Vdc]		24±10%	
Phase current Cont./Peak Sine amplitude [A]	5 / 10	10/20	15/30
Phase current Cont./Peak RMS [A]	3.6 / 7.1	7/14	10.6/21.2
Peak current time [sec]		1	
Max. output voltage [Vdc]		(Vac in) x1.41 x 97%	
Max. RMS input current 1-phase supply [A] 3-phase supply[A]	13	18	24
Min. load Inductance, at max. motor voltage [mH]		1	
Max. Heat dissipation per axis [W]	30	48	79
Weight [gram]		5750	
Dimensions [mm³]		324x249x120	

Example:CMBA3B24E21A1AWNANYY

Field	1	2	3	4	5	6	7	8	9	10	11	12	13	14	15	16	17
PN CM	ba	3	B	2	4	E	2	1	A	1	A	W	N	A	N	Y	Y

Ordering Options

Ordering Options	Field	Example User Selection	Values
Type	1	ba	ba-economical, hp-high performance
Number of built-in drives (85Vac-265Vac)	2	3	1,2,3
Current rating of built-in drives (cont/peak)	3	B	A- 5/10A, B- 10/20A, C- 15/30A
Sin-Cos encoder interface	4	2	0,1,2,3
Tot. no. of feedback channels	5	4	4
Absolute encoders type	6	E	U- All, N- None, E- EnDAT 2.1(digital)/2.2, S- Smart Abs, P- Panasonic, B- Biss-A/B/C, I-SSI
Number of Absolute encoders interface	7	2	0,1,2,3
XL SCAN (unit per scanner)	8	1	N- Non, 1,2,...,10(A), 11(B),12(C),13(D),14(E),15 (F),16(G)
Maximum number of axes	9	A	4 (included automatically FOC), 8, 16-A, B-32
3rd party EtherCAT servo drives	10	1	Up to the maximum number of axes (FOC) - number of internal drives
3rd party EtherCAT Step motor Drives)	11	A	Up to the maximum number of axes (FOC) - number of internal drives
ECAT 3rd party IO EtherCAT nodes	12	W	W- 32 (included automatically FOC), X- 64
G-Code, Flexible configuration, Both	13	N	N- None, G- G-code, F- Flexible configuration, T- Both
ServoBoost number of axes supported (HPversion only)	14	A	N- 0, A- 4, B- 8, C- 12, D- 16, E- 20, F- 24, G-28, H- 32
Input shaping	15	N	Y- Yes, N- No
Pulse-Dir for 4 axes or LC1 option installed	16	Y	N- No, Y- P/D, L- LC1
Low Voltage operation (17-85Vac or 24-120Vdc)	17	Y	Y- Yes, N- No

Servo
A standard comprehensive set of powerful algorithms to enhance accuracy, move & settle time, smooth velocity, stability and robustness.
• Advanced PIV cascaded structure
• Loop shaping filters • Gain Scheduling • Gantry MIMO control • Dual feedback / loop control •
Disturbance rejection control
Optional *ServoBoost* algorithm (CMhp only).

Drives
Type: digital current control with field oriented control and space vector modulation.
Current ripple frequency: 40 kHz
Current loop sampling rate: 20 kHz
Programmable Current loop bandwidth: up to 5 kHz
Commutation type: sinusoidal. Initiation with and without Hall sensors
Switching method: advanced unipolar PWM
Protection: Over voltage, Phase-to-phase short circuit, Short to ground, Over current, Over temperature, motor over temperature
Current sensing: CMBA: 12b ADC, CMHP: 16b ADC

Power Supplies
Motor Supply
Range: 85 to 265Vac, for 15/30A (cont./Peak)
current model: 130 to 265Vac
(Optional - Low Voltage 17-85Vac or 24-120Vdc)
Control Supply
24Vdc ± 10%, 4A
Motor Brake Supply
24Vdc ± 20%, 3A

Motor Types
Two- and three-phase permanent magnet synchronous (DC brushless/AC servo), DC brush, Voice coil, Two- and three-phase stepper (microstepping open or closed loop, loop)

Feedback
Incremental Digital Encoder: Four, A&B,I; Clk/Dir, IRS-422.
Max. rate: 40 million encoder counts/sec.,
Protection:Encoder error, not connected
Sin-Cos Analog Encoder (optional): Three. 1Vptp, differential
Multiplication factor: From x4, to-CMBA-x4,096, CMHP-x65,536
Maximum frequency: 250kHz
Automatic compensation of Offset, Phase and Amplitude
ADC used: CMBA: 12b, CMHP: 16b low S/N
Maximum acceleration: 10^8 million sine periods/sec².
Protection: Encoder error, not connected.
Hall inputs: Three sets of three per axis.
Single-ended, 5V, source, opto-isolated
Input current: <7mA
Absolute encoders (optional): EnDat2.1(Digital)/2.2, Tamagawa Smart-Abs, Panasonic, BiSS-A/B/C, SSI
5V feedback supply: Total current available for feedback devices: 1A

Pulse/Direction Interface (Optional)
Four pairs.
Type: RS-422. Up to 5 million pulse/sec.
Programmable pulse width
Range: 0.08 to 80 microseconds

Laser Interface (Optional)
Pulse differential output, RS422
Fault input, Opto-isolated, 2-terminal
Enable output, Opto-isolate, 2-terminal
Pulse frequency: 9Hz to 1.181Mhz
Pulse width: 6.67ns to 111ms
Duty cycle: 0 to 100%

Analog I/O
Inputs: Six ±10V, differential, 20kHz sampling rate.
The inputs can be used as feedback to the servo loops.

Digital I/O
Safety Inputs: Left + right limit per axis, E-stop
General Purpose Inputs: 8 Single-ended, 5Vdc (±10%) or 24Vdc (±20%), opto-isolated, sink/source,
Input current: 4-14mA
Registration MARK inputs: Four. RS422
Motor Brake Outputs: Three. 24V, 1A ,opto-isolated. Powered by the 24V Brake Supply
General Purpose Outputs: Eight. Single-ended, 5Vdc (±10%) or 24Vdc (±20%), opto-isolated, sink/source, Max. output current per output: 100mA, Max. total of 800 mA for all
Position Event Generator outputs (PEG):
Two PEG_Pulse and eight PEG_State, RS422
Can be used as GP outputs
HSSI channels: Two. RS422

Communication Channels
Serial ports: one RS-232. One RS-232/422.
Ethernet: TCP/IP 10/100Mbits/sec (10/100 BaseT)
EtherCAT: Two, In & Out, 100 Mbit/sec,
CoE and FoE protocols support

Motion Processor Unit (MPU)
Processor Type: Multi-core Intel Atom CPU (model depends on controller configuration)
EtherCAT Cycle Rate: 2kHz (contact ACS for higher rate options)
RAM: 1GB
Flash: 2GB

Certifications
CE: Yes
Electrical Safety: EN 60204
EMC: EN 61326-1
UL: 5/10A and 10/20A only (CSA Certification)
CSA standard C22.2 No 0, CSA standard C22.2 No 14, ANSI/UL508C

Environment
Operating: 0 to +40°C. Storage : -25 to +60°C

ACS MOTION CONTROL

Appendix V

MATLAB codes for the calculation and simulation of aerostatic bearing slideway static performance

```matlab
%%
% Constants
global VISC PA RHO
VISC = 0.00002; % viscosity of air in N*s/(m^2) 1.825E-5 @20C in literature
PA = 100000.0; % ambient pressure in N/m^2
RHO = 1.2; % kg/m^3 density of air at 20C at ambient. Note: RHO = 1.184@ 25C; RHO
= 1.22@ 15C


%%
% bearing design data $$$ will add these variables in an interface

global PS GAP0
global BLEN BWID NROW DJET NJET DO DP
global PType BType
PS = 5.5; % air supply pressure (Bar). It is gauge pressure
GAP0 = 10.0; % Bearing design clearance (um)
ECC = [0.2 0.4 0.6 0.8 1.0 1.2 1.4 1.6 1.8]; % deflection factor x

BLEN = 150;  % slide length (mm)
BWID = 80; % slide width (mm)
NROW = 2; % 1 for single and 2 for double rows, this program only model one or two
rows
DJET = 20; % DJET is the distance of jet row from bearing center (mm). It is zero
for single row by default
```

```matlab
NJET = 30; % Number of jets/row

DO = 60; % Orifice diameter (um)

PType = 1; % 1 for plain orifice and 2 for pocketed orifice

BType = 1; % 1 for single and 2 for opposed pad slide

DP = 800; % Pocket diameter (um)


% SI unit conversion

PS = PS*100000.0 + PA; % convert to N/m^2 and in absolute pressure

BLEN = 0.001 * BLEN; % convert to m

BWID = 0.001 * BWID; % convert to m

GAP0 = 0.000001 * GAP0; % convert to m

DJET = 0.001 * DJET; % convert to m

DO = 0.000001 * DO; % Convert to m

DP = 0.000001*DP; % convert to m


if PType == 1

    DP = DO;   % for plain orifice, disable DP

end


%%
% Define mesh size and adjust jet positions to fit mesh
IPAD = 24; % number of elements per orifice in length (I) direction, assign an
even number, e.g. 12 24 48
IMAX = IPAD*NJET; % number of elements in length (I) direction
JMAX = IMAX*BWID/BLEN/2.0; % number of elements in width (J) direction, half width
is modelled because of the symmetry about the center of the slide.
JMAX = round(JMAX); % JMAX must be an integer


IMAXP = IMAX+1; % number of nodes in length (I) direction
```

```matlab
JMAXP = JMAX+1; % number of nodes in width (J) direction

XINC = BLEN/IMAX; % element size (m) in X (Length, I) direction

YINC = XINC; % same element size in Y direction, so the modelled width may be

slightly different from the actual dimension

YINC1 = BWID/(2*JMAX); % see how much difference between YINC and YINC1


if abs(YINC-YINC1)/YINC >= 0.1

    fprintf ('sth wrong with element size in Y direction') % YINC1 is used to

check if there are large difference

    temp1 = (YINC-YINC1)/YINC;

end


% Assign orifice element numbers

global IJET   % IJET and JJET are the node index (position) of orifices

global JJET


% the following two ifs are for checking and correcting wrongly input DJET,

% assuming NROW is correct

if NROW == 1 && DJET ~= 0

    DJET = 0;

    fprintf('DJET is incorrect and has been reassigned as 0')

end

if NROW == 2 && DJET ==0

    DJET = BWID/4;

    fprintf('DJET is incorrect and has been reassigned as BWID/4')

end


IJET = zeros(1, NJET);

for I = 1:1:NJET
```

```
    IJET(I) = round(IPAD/2.0+1)+(I-1)*IPAD;

end

JJET = round(2.0*DJET/BWID*JMAX+1);


%%

% Initialization of pressure field across the film


global P1 % P1 is the node pressure matrix


% Initial guess at pressure field

PJET = 1; % Pressure under orifice (in bar^2, squared normalized Gauge pressure)

%Pressure distribution calculation

IterNo = 4000; % number of iterations in pressure distribution function

% no difference between 4000 and 6000, but 2000 is not good, so 4000 is used.


[P1] = PRESSR(IMAX,JMAX,PJET,IterNo);

% P1 is returned in the form of P1 = (p/pa)^2, i.e. squared normalized Gauge
pressure


Tol = 0.000002; % tolerance of flow rate comparison in the ELOAD function

% $$$ try other values


%%

% Flow rate and pressure field under no load condition:

% ECC factor = 1.0; Gap = GAP0


[FLOW, XLOAD, PFAC] = ELOAD(P1,IMAX,JMAX,XINC,YINC,GAP0,Tol);


% plot half bearing pressure distribution
```

```matlab
figure

X = (0:IMAX);

Y = (0:JMAX);

surf (Y, X, P1.^0.5*PFAC)

% P1. = P1.^0.5*PFAC; % update P1 if when plotting pressure distribution

title ('Bearing pressure (gauge pressure in bar) distribution')


% Calculate volume flow rate in liter/min @ supply pressure PS

% VFLOW = 2.0*PA*FLOW/RHO/PS*1000.0*60.0;

VFLOW = (PA/PS)*(FLOW/RHO)*1000*60;

% VFLOW: volume flow rate in liter/min @ PS - standard liter per minute (SLM)


if BType ==2

    VFLOW = VFLOW * 2;  % opposed pad slide

end


%%
% Bearing load-deflection characteristics for bearing gaps of
% ECC factor = 0.1, 0.2, 0.3, 0.4, 0.5, 0.6, 0.7, 0.8, 0.9 x design gap.


FLOWR = zeros(1, 9);

XLOADR = zeros(1, 9);

PFACR = zeros(1, 9);

VFLOWR = zeros (1,9);

GAP = zeros(1,9);


for I = 1:1:9

    GAP(I) = ECC(I)*GAP0; %0.2,0.4,0.6,0.8,1.0,1.2,1.4,1.6,1.8 x GAP0

end
```

190

```matlab
for I = 1:1:9

    [FLOWR(I), XLOADR(I), PFACR(I)] = ELOAD(P1,IMAX,JMAX,XINC,YINC,GAP(I),Tol);

    %VFLOWR(I) = 2.0*PA*FLOWR(I)/RHO/PS*1000.0*60.0;

    VFLOWR(I) = PA*FLOWR(I)/RHO/PS*1000.0*60.0;

    if BType ==2

        VFLOWR(I) = VFLOWR(I) * 2;

    % opposed pad slide,

    % $$$ when loaded, loaded and unloaded sides have different

    % air film thickness, hence different flow, VFLOWR is calculated on the

    % loaded sides, this will not be accurate.

    end

end


%%

% postprocessing

% plot bearing load-deflection characteristics


% Stiffness calculation for single acting thrust bearing

for I = 1:1:8

    STIFF(I) = (XLOADR(I)-XLOADR(I+1))/(GAP0*0.2*1E6);

end


% plot Load vs Gap

figure

plot(GAP.*1E6, XLOADR, '-o')

grid on

title ('Load (N) vs Gap (um)')
```

```
% plot Stiffness vs Gap

figure

plot(GAP(2:9)*1E6, STIFF,'-o')

grid on

title ('Stiffness (N/um) vs Gap(um)')


% plot Flow rate vs Gap

figure

plot(GAP.*1E6, VFLOWR, '-o')

grid on

title ('VFLOW rate at supply pressure (l/min) vs Gap (um)')


% plot PJET vs Gap

figure

plot(GAP.*1E6, PFACR, '-o')

grid on

title ('Pressure directly under the orifice (Bar) vs Gap (um)')


% plot Pressure distribution (Bar) at bearing Gap = 8um as an example

figure

X = (0:BLEN/IMAX:BLEN);

Y = (0:BWID/2/JMAX:BWID/2);

YY = [-fliplr(Y) Y];

PContour = [fliplr(P1.^0.5*PFACR(4)) P1.^0.5*PFACR(4)];

surf (YY, X, PContour)

title ('Pressure distribution (Bar) at bearing Gap = 8um')


%%

% solve Reynolds equation and obtain pressure distribution for the air film
```

```matlab
function [P1] = PRESSR(IMAX,JMAX,PJET,IterNo)

% --------------------------------------------------------------------------------

% solve Reynolds equation and obtain pressure distribution for the air film

% FDM form for slideway: P1(I, J) = (P1(IP1,J)+P1(IM1,J)+P1(I,JP1)+P1(I,JM1))/4.0;

% In the above XINC = YINC, if not delta X and delta Y must be included

% P1 is returned in the form P1 = (p/pa)^2, i.e. squared normalized Gauge pressure

% --------------------------------------------------------------------------------


IMAXP1 = IMAX +1;

JMAXP1 = JMAX +1;

global IJET

global JJET

global NJET


P1 = zeros(IMAXP1, JMAXP1); % P1 pressure matrix IMAXP1 by JMAXP1

for I = 1:1:IMAXP1

    for J = 1:1:JMAXP1

        P1(I, J) = PJET*(1 - (J-1)/(JMAX));

        % let centerline nodes pressure = 1; outer node pressure = 0

        if J<=JJET

            P1(I, J) = PJET;

            % pressure of nodes from jet to the centerline = PJET; if JJET

            % = 1, only the pressure on the centerline = PJET

        end

    end

end


%External boundary conditions for pressure field
```

```
for J = 1:1:JMAXP1

    P1(IMAXP1, J) = 0;

    P1(1, J) = 0;

    % both ends Pressure = 0 (gauge pressure)

end


for I = 1:1:IMAXP1

   P1(I, JMAXP1) = 0; % side end pressure  = 0(gauge pressure)

end


% Evaluate pressure field

% IterNo - Number of Iteration

for L = 1:1:IterNo

    for J = 1:1:JMAX %P1(I,JMAXP1)=0

        for I =2:1:IMAX % P1(IMAXP1, J) = 0 and P1(1, J) = 0

            % Values of neighbouring elements

            IM1 = I - 1;

            IP1 = I + 1;

            JM1 = J - 1;

            JP1 = J + 1;

            if JM1<1

                JM1 = 2; % boundary condition P1(I, 0) = P1 (I,2)is applied

            end

            %New iteration of pressure field

            IP = 0; % Orifice position or not? 1 means orifice position

            for K = 1:1:NJET

                if I == IJET(K)

                    IP =1;

                end
```

```matlab
            end

            if (J ~= JJET)||(IP == 0)% Exclude updating orifice positions

                P1(I, J) = (P1(IP1,J)+P1(IM1,J)+P1(I,JP1)+P1(I,JM1))/4.0;

                % finite difference form when XINC = YINC

            end

        end

    end

end

end


%%

% balance air flows and calculate total load


function [FLOW, XLOAD, PFAC] = ELOAD(P1,IMAX,JMAX,XINC,YINC,GAP,Tol)

% *************************************************************************

% Eload function first calculate mass flow rate of the air film using a P1

% and boundary (scaling factor PFAC = 1), then balances air flow across air film

% with air flow through jets (function is called), finally it calculates

% total load on one side of thrust plate or slideway bearings

% *************************************************************************


PFAC = 1.0;

% Pressure scaling factor, used to multiply pressure, P1^0.5 (not P1 as P1 is

pressure squared)

global PA RHO VISC

global PS

global NJET NROW IJET JJET


PS1 = PS/100000.0;
```

195

```matlab
% absolute pressure in bar or absolute normalized pressure, PS1 = PS/PA

PTEST = 0.999*(PS1-1.0);


% Mass flow through one side and one end of bearing

FLOWO = 0.0; %FLOWO is flow through two half sides (= one side)

FLOWI = 0.0; %FLOWI is flow through end (along length direction)


for J = 1:1:JMAX

    FLOWO = FLOWO + YINC*((P1(2,J)^0.5 - P1(1,J)^0.5)+(P1(IMAX,J)^0.5 -
P1(IMAX+1,J)^0.5))/XINC;

    % NB: (P1(I,J)^0.5 is non-squared, but still absolute and normalized pressure

end


for I = 2:1:IMAX

    FLOWI = FLOWI + XINC*(P1(I,JMAX)^0.5-P1(I,JMAX+1)^0.5)/YINC;

    % NB: index I could starts from 2

end


%Total mass flow through 2 sides and 2 ends

FLOWM = 2.0*PA*(FLOWO+FLOWI)*RHO*GAP^3/12.0/VISC;

% Multiplying PA, so it is absolute pressure in SI unit pascal in the

% calculation

% changed to /12.0

% x2.0 to include the whole bearing surface

% Unit of FLOWM is kg/s (mass flow rate)


tolerance = 1;

count = 0;

if NJET == 1
```

```matlab
    IJ = 1;

else

    IJ = IJET(NJET/2);

end


while tolerance >= Tol && PFAC < PTEST

    % FLOW = 2.0*PFAC*PA*(FLOWO+FLOWI)*RHO*GAP^3/24.0/VISC; % put it

    % outside so it is more efficient, replaced with the following

    FLOW = PFAC*FLOWM;

    % PFAC can be used to multiply flow rate as the pressure P1^0.5 used in

    % the calculation, not P1


    % Calculate air mass flow through jets

    FLOWT = FLOW/NJET/NROW; % mass flow per jet


    PJ = (P1(IJ,JJET)^0.5)*PFAC+1.0;

    % PJ is the orifice downstream pressure (absolute value in bar, or normalized

absolute pressure)

    % index = IJ = IJET(NJET/2), i.e. pressure at middle jet is used

    % $$$ may change other index numbers to see the difference


    [CFM]= ORFLOW(FLOWT,PJ,PS1,GAP);


    FLOWJ = CFM*NJET*NROW;

    % total mass flow rate through orifices and pocket curtains calculated

    % by ORFLOW


    PFAC = PFAC + 0.001*(FLOWJ-FLOW)/(FLOWJ+FLOW);

    % Instead of calculating mass flow rate again, the program
```

```matlab
        % updates the pressure scaling factor PFAC, then recalculate mass flow

        % rate using FLOW = FLOW * PFAC;


        tolerance = abs(FLOWJ-FLOW);

        count = count + 1;

    end


% Calculate thrust load over total bearing

XLOAD = 0.0;

for I = 1:1:IMAX

    for J = 1:1:JMAX

        AVP = 0.25*(P1(I,J)^0.5+P1(I+1,J)^0.5+P1(I,J+1)^0.5+P1(I+1,J+1)^0.5);

        % AVP is average normalized gauge pressure of an element

        AVLOAD = PFAC*PA*AVP*XINC*YINC;

        % AVLOAD is the load on that element, in Newtons

        XLOAD = XLOAD + AVLOAD;

    end

end

XLOAD = 2.0 * XLOAD; % unit in N, only half of the slide is modelled, hence times

2

end


%%

% calculates the mass flowrate of air through an orifice


function [CFM] = ORFLOW(FLOW1,POUT,PIN,GAP)

% ************************************************************************

% ORFLOW calculates the mass flowrate of air through an orifice

% It is not just about an orifice, it considered pocket edge loss effect
```

```matlab
% and calculate mass flow rate of air through an orifice and pocket in

% series

% ********************************************************************


% Define constants

global VISC DO DP

GAM = 1.4; % Gamma is the ratio of specific heats for air = 1.4

R = 287.0; % specific gas constant unit J /(kg.K)

T = 295; % 21.85 Celsius or using 293.5 K = 20C

FAC = (2.0*GAM/(R*T*(GAM-1.0)))^0.5; % FAC = 0.0091

DEL = 0.25*DO^2/DP/GAP; % ratio of orifice to pocket areas (curtain area)

E1 = 2.0/GAM;

E2 = (GAM+1.0)/GAM;


% Critical pressure ratios

PCRIT = (2.0/(1.0+GAM))^(GAM/(GAM-1.0)); % = 0.5283


PRATIO = POUT/PIN;

if PRATIO > 1.0

    PRATIO = 0.99999;

end


% Coefficient of discharge

DOM = 1000.0*DO;  % convert to mm

Cdc = 0.52 + 2.1*DOM - 3.0*DOM^2;

% Jet diameter should be in mm unit in the equation above

% Cdc is the discharge coefficient before adjustment


Cd = 0; % Cd is the coefficient of discharge
```

```
        %which is an empirical factor relating actual mass flow to

        %theoretical mass flow for an orifice

if PRATIO <= PCRIT % PCRIT = 0.5283

    Cd = Cdc;

    % Choked condition, hence no pressure recovery

    % also see Fig. 3 in Pink's 1979 paper; Cd = Cd*

end


if PRATIO > PCRIT

    Cd = Cdc/(1.174-0.327*PRATIO);

    % Eq[4.45] in Wardle's book

    % No choking condition, Correction of Cd with pressure ratio based on

recovered

    % conditions in pocket

end


Corf = 0;

% Mass flowrate

EK = 0.15 + 0.000225*2.0*FLOW1/(pi*DO*VISC); % EK entrance loss (pocket edge

loss)coefficient

% monitor EK!!!

Corf = (1.0/(1.0+DEL^2*Cd^2*EK))^0.5; %((1.0+DEL^2))is cancelled out in CFM

calculation

%Corf = ((1.0+DEL^2)/(1.0+DEL^2*Cd^2*EK))^0.5;

CFM = Corf*Cd*pi*DO^2*100000.0*PIN*FAC*(PRATIO^E1-PRATIO^E2)^0.5/4.0;

%CFM = Corf*Cd*pi*DO^2*(PIN-POUT)*FAC*100000.0/4.0;

% $$$ significant difference between using the above two equations in terms of

% Stiffness and VFlow and pressure distribution
```

```
if CFM < 0.0

    CFM = 0.0000001;

end

end
```